THE MECHANICS OF THE DRAWING OF POLYGONAL SECTIONS FROM ROUND AT ELEVATED TEMPERATURE

MUSTAFA ISA JORNAZ

Doctor of Philosophy

THE UNIVERSITY OF ASTON IN BIRMINGHAM

November 1990

1

THE UNIVERSITY OF ASTON IN BIRMINGHAM

THE MECHANICS OF THE DRAWING OF POLYGONAL SECTIONS FROM ROUND AT ELEVATED TEMPERATURE.

MUSTAFA ISA JORNAZ

Doctor of Philosophy

November 1990

Summary

Economic factors such as the rise in cost of raw materials, labour and power, are compelling manufacturers of cold-drawn polygonal sections, to seek new production routes which will enable the expansion in the varieties of metals used and the inclusion of difficult-to-draw materials. One such method generating considerable industrial interest is the drawing of polygonal sections from round at elevated temperature. The technique of drawing mild steel, medium carbon steel and boron steel wire into octagonal, hexagonal and square sections from round at up to 850 deg C and 50% reduction of area in one pass has been established.

The main objective was to provide a basic understanding of the process, with particular emphasis being placed on modelling using both experimental and theoretical considerations. Elevated temperature stress-strain data was obtained using a modified torsion testing machine. Data were used in the upper bound solution derived and solved numerically to predict drawing stress strain, strain-rate, temperature and flow stress distribution in the deforming zone for a range of variables.

The success of this warm working process will, of course, depend on the use of a satisfactory elevated temperature lubricant, an efficient cooling system, a suitable tool material having good wear and thermal shock resistance and an efficient die profile design which incorporates the principle of least work. The merits and demerits of die materials such as tungsten carbide, chromium carbide, Syalon and Stellite are discussed, principally from the standpoint of minimising drawing force and die wear.

Generally, the experimental and theoretical results were in good agreement, the drawing stress could be predicted within close limits and the process proved to be technically feasible.

Finite element analysis has been carried out on the various die geometries and die materials, to gain a greater understanding of the behaviour of these dies under the process of elevated temperature drawing, and to establish the temperature distribution and thermal distortion in the deforming zone, thus establishing the optimum die design and die material for the process.

It is now possible to predict, for the materials already tested,(i) the optimum drawing temperature range,(ii) the maximum possible reduction of area per pass, (iii) the optimum drawing die profiles and die materials,(iv) the most efficient lubricant in terms of reducing the drawing force and die wear.

Key Words :
> Section drawing
> Polygonal sections
> Difficult-to-draw
> Elevated temperature drawing
> Upper bound solution
> Finite element analysis

2

بِسْمِ اللهِ الرَّحْمٰنِ الرَّحِيمِ

In the name of Allah the Almighty, Most Merciful, and Compassionate

Dedication

To the memory of my father

ACKNOWLEDGEMENTS

The research described in this dissertation was carried out in the department of Mechanical and Production Engineering at the University of Aston in Birmigham.

I am grateful to my supervisor Dr. I. M. Cole who introduced me to the research and encouraged me by his valuable advice, guidance and continued enthusiastic support throughout the duration of the programme. My gratitude also extends to Mr. L. W. Crane for his advice given and interest shown in the research conducted.

I would like to thank:

Members of the technical staff in the Department of Mechanical and Production Engineering for their assistance, especially Messrs J. Foden, A. Evitts and M. Clark.

Acheson Colloids for the supply of lubricants, Mr R. Hemmingway of John Smith Wire for the supply of wire material. To Mr M. Antill.

Finally, I wish to express my deep appreciation to my mother, fiancee, brothers and sisters for their understanding, encouragement and continuous support throughout this work. My special thanks to my brother Kamel for his support and encouragement.

CONTENTS

Chapter One

Introduction and Literature Review

Chapter Two

Section Drawing

Chapter Three

Theoretical Analysis of the Drawing of Polygonal Sections from Round at Elevated Temperature

Chapter Four
Experimental Equipment and Draw Process Materials

Chapter Five
Instrumentation and Calibration of Measuring Equipment

Chapter Six

Stress-Strain Data

Chapter Seven

Experimental Technique, Procedure and Results

Chapter Eight

Finite Element Analysis of Polygonal Dies

Chapter Nine

Observations and Discussion of Results

Chapter Ten
Conclusions and Suggestions for Further Work

References

Appendices

LIST OF FIGURES

14

LIST OF TABLES

LIST OF PLATES

SYMBOLS

μ	Mean coefficient of friction
α	Die semi-cone angle
ΔV	Velocity discontinuities at the sliding surfaces
T_1	Predetermined body tractions
V	Volume of the deforming zone
ε_{ij}	Strain rate component
Γ	Surfaces of velocity discontinuities
S_t	Surface area subjected to predetermined body tractions
V_1	Velocity at entry and exit surfaces having predetermined body tractions
τ	Shear stress
p	Die pressure
β	Included angle of symmetric portion
N_s	Number of sides of the drawn section
A_r	Area ratio
t	Factor ($-1 \leq t \leq 1$) selected to optimise the inlet and outlet shear surfaces by minimisation of the plastic work
ρ, θ, Φ	General spherical co-ordinates
EqR_2	Radius of a circle enclosing outlet section
α_e	Equivalent die semi-angle, i.e semi-angle of a conical die which is equivalent to the section die for the same reduction of area
η	The relative lateral displacement of the assumed shape element at the outlet section referred to the inlet
ψ	Angle of deviation from the corresponding inclination angle θ of the material flow path, of an elemental triangle
θ	Inclination of the radius ρ to the wire axis
U_ρ, U_θ, U_ϕ	Velocities in ρ, θ and ϕ directions respectively
A	Cross-sectional area
$\rho_{1,2}$	Radial distance from the virtual apex to the centroid of the triangular element in the inlet and outlet section respectively
Y_m	Mean flow stress of a flow line
Y_f	Mean flow stress for calculating the total power of friction

Subscripts

1, 2	refer to entry and exit surfaces unless it is otherwise stated

17

Papers Published

In the course of the research, two relevant papers have been published. This thesis contains information from those papers. The papers are;

1)   Jornaz, M.I, Crane, L.W and Cole, I.M. The drawing of polygonal sections from round at elevated temperature. 28th M.T.D.R., Conf., (1990), 425-430.

2)   Jornaz, M.I and Cole, I.M. The effect of die design, die material and lubrication in elevated temperature section drawing from round. Proc. of the Int. Conf., on Developments in Forming Technology, Lisbon, Portugal, Sep 12 - 14 (1990)

CHAPTER ONE

INTRODUCTION & LITERATURE REVIEW

Chapter One

1.0 Introduction and Literature Review

1.1 Introduction

Hot working takes advantage of the decrease in flow stress at high temperature to reduce tool forces and, consequently, equipment size and power requirement. Symmetric and non-symmetric products made from steel alloys, stainless steels, aluminium alloys, copper alloys and other non-ferrous metals and their alloys are required for use in the electrical appliance, automobile, and other industries. Economic factors are compelling manufacturers of cold-drawn sections to seek new production routes which will enable the expansion in the varieties of metals used and the inclusion of materials which are difficult to draw because of their metallurgical structure or their property of rapid work hardening. Thus consideration is being given to elevated temperature section drawing from readily available standard round stock through a single die. Increasing demand for this process is activated by a continual increase in the price of rolled sections and a reduction in the range of sizes available. The lower cost of round stock material for this process is therefore becoming increasingly significant. This method will effectively reduce the costs involved in stocking a variety of items, in that only round bars will be stored in order to produce various sections, rather than storing various shapes to produce smaller shapes using conventional section-from-section drawing.

As an example, it is possible to warm-draw alloy steels at a temperature which is sufficient to reduce the yield stress to less than that of mild steel at normal temperature, thus high strength steels can be warm-drawn while only exerting the same tool loads as conventional mild steel drawing, furthermore the resultant product is in an annealed state.

The success of the warm working process will, of course, depend on the use of a satisfactory elevated temperature lubricant, a cooling system associated with a suitable tool material having hot-hardness characteristics, and an efficient die profile design which incorporates the principle of least work .

1.1.1 Objectives

- To provide a basic understanding of the mechanics of the drawing of polygonal sections from round at elevated temperature, in depth, both theoretically and experimentally. The theoretical approach includes three dimensional-modelling of the process and the establishing of temperature, flow stress, strain and strain-rate distribution in the deforming zone. The experimental programme comprises the use of three different workpiece materials, four die materials and five die geometries (three polygonal and two round die designs).

- To obtain elevated temperature stress-strain data for the test materials used, using hot torsion testing. Stress, strain, strain-rate and temperature will be related mathematically. This enables the flow stress distribution in the deformation zone to be calculated, after taking into consideration the temperature rise due to deformation and frictional work. Based on the flow stress distribution, a mean flow stress will calculated and used in the computer program developed to solve the upper bound solution and obtain a three dimensional-modelling of the process.

- To use finite element analysis of polygonal dies, to gain a greater understanding of the behaviour of the various die designs and die materials under the process of elevated temperature drawing, thus establishing the optimum die design and the die material to be used for the process.

1.2 Types of deformation

Deformation processes can be divided into five basic types, depending on the nature of the stress and strain acting during deformation. They are namely :-

1.2.1 Plane strain deformation.

1.2.2 Axisymmetric deformation.

1.2.3 Symmetric deformation.

1.2.4 Asymmetric deformation.

1.2.5 Plane stress deformation.

Asymmetric and plane stress deformations are not discussed further as they are considered to be beyond the scope of this project.

1.2.1 Plane strain deformation

Plane strain deformation is said to occur when all the deformation takes place in one plane. An example is the rolling of wide strip, where the straining in the direction of the roll axes is either zero or very small (little widening of the workpiece results). It is effectively restrained by the undeforming material on both sides of the roll gap and by roll friction.

1.2.2 Axisymmetric deformation

The conventional drawing of wire, rod and tube through a circular die is an example of this type of deformation, where the deformation occurs when all the straining is symmetrical about one axis.

1.2.3 Symmetric deformation

Symmetric deformation is said to occur when the state of stress at a given point is a mirror image of a similar point chosen about a symmetrical axis of the physical

configuration of the deformation zone. Direct section drawing is an example, where an axis of symmetry exists about diagonals and across flats.

1.3   Classification of drawing theories

1.3.1   Equilibrium approach

1.3.2   Slip line field

1.3.3   Upper bound solution

1.3.4   Energy approach

1.3.5   Visioplasticity

1.3.6   Finite element method

However, a comprehensive review is presented only for the equilibrium and the upper bound approaches which form the basis of the method which will be used to obtain solutions for the drawing of a polygonal section from round at elevated temperatures.

1.3.1   Equilibrium approach

The method is based on the equilibrium of forces, which is a lower bound approach, and predicts a lower estimate of the drawing force, since redundant work is neglected.

1.3.1.1   Axisymmetric wire drawing

Drawing theories based on the equilibrium of forces can be derived using either cartesian or polar co-ordinates. In these analyses the following assumptions are usually made.

(i)   constant friction

(ii)   no redundant work

(iii)   non work-hardening material, i.e. Y is constant

In 1927 Sachs[1,2] derived a theory which proved the most important among the early theories on wire drawing. He assumed that plane cross-sections of the workpiece remained plane as they passed through the die and that the stress distribution on such planes was uniform. Consequently, this method is known as the 'slab method '.

By considering the equilibrium of forces acting on an element and assuming the Tresca yield criterion, he derived the following expression for the drawing stress:-

$$\sigma_{x2} = \frac{Y(1+B)}{B} \left(1 - \left(\frac{D_2}{D_1}\right)^{2B} \right)$$

where

$B = \mu \cot \alpha$

Y = yield stress of material

D_1, D_2 are the diameters of the bar at the inlet and exit respectively.

This expression is generally known as the fundamental Sachs equation, and is regarded as an expression which combines simplicity with accuracy. Later Davis and Dokos[3] incorporated the strain-hardening effect into the Sachs analysis. They assumed that the strain-hardening effect of the material follows a linear relationship. However, Atkins and Caddell[4] have shown, using the power law, that for a practical range of parameters the error is about 8% when the mean yield stress is used instead of taking into account the strain-hardening relationship in the governing force-balance differential equations prior to integration. They also incorporated a redundant work factor into the above equation.

Johnson and Rowe[5] have given a general expression to account for redundant work in the drawing of cylindrical stock. Research workers Siebel[6] Korber and Eichinger[7] and MacLellan[8] refined and improved the drawing theory. Comprehensive reviews of

the work of the other investigators have been published by Wistreich[9,10] and MacLellan[8].

In 1957, Whitton[11] compared various drawing theories proposed by Sachs and van Horn[12] Korber and Eichinger[7], Siebel[6] Davis and Dokos[3] and Sachs with experimental data and stated that the deviation between theory and experimental results can be as much as $\pm 20\%$.

In 1955, Shield[13] analysed the plastic flow of metal in a converging conical channel using polar co-ordinates. The values predicted by Shield's equation under-estimates the drawing force, because the redundant shear at the entry and the exit of the die was neglected. This is of significance when the reduction of area is large and the die angle is large.

Avitzur[14,15] further considered the flow through a converging conical channel incorporating the redundant shear at the die entry and exit. His upper bound analysis was developed using a spherical co-ordinate system with the assumption of $\tau = mk$. Alexander[16], however, commented that the idea of a constant frictional stress (mk) at the die interface was incompatible with the accepted idea of Coulomb friction.

1.3.2   Slip line field solutions

The slip-line method is a powerful technique for solving complex plastic flow problems by establishing the maximum shear-line field. Its limitation is that certain restrictions are placed on the material and, strictly speaking, only plane strain problems can be solved. A full description is obtained from Johnson[17]. The following assumptions are made in using this technique:-

(i)   the work material is isotropic and remains so during deformation and the principal directions of the stress and strain rate coincide.

(ii)   the work material is rigid-plastic, i.e. elastic components of strain are neglected, and it deforms with constant flow stress.

(iii)   there is no change in the work material density during deformation (volume constancy).

(iv)   the deformation is plane strain.

In solving problems, it is the slip-line field, which consists of two orthogonal families of curves (the slip-lines) representing directions of maximum shear stress and maximum shear strain rate at each point in the plastic zone, which is treated as the unknown which has to be determined. Both stress equilibrium and flow equations are considered. These basic differential equations are hyperbolic and may then be solved by the method of characteristics [18,19]

1.3.3   Upper bound solution

In 1951, Prager and Hodge[20] proposed an upper bound theorem for a rigid-perfectly plastic material. It states that, " among all kinematically admissible strain rate fields, the actual one minimizes the expression mentioned below ". Drucker[21] extended the theorem to include the velocity discontinuities. With the additional assumptions that the material obeys von Mises yield criterion and the flow follows the Levy-Mises stress-strain relationship.

$$J^* = \frac{2}{\sqrt{3}} Y \int_V \sqrt{\frac{1}{2}\dot{\varepsilon}_{ij}\dot{\varepsilon}_{ij}}\ dV + \int_{S_r} \tau \left| \Delta v \right|\ dS - \int_{S_t} T_i\ V_i\ dS$$

The actual externally supplied power, J^*, is never higher than the value predicted by using the expression. In the case of wire drawing, the externally supplied power is

provided by the front pull. The first term computes the power of internal deformation over the volume of deformation and the second term expresses the shear power over the surface of velocity discontinuities including the boundary between the tool and the material. The last term covers power supplied by predetermined body tractions. Those tractions are, for example the back pull applied in wire drawing, or back and front tension in rolling.

Incorporating friction in the upper bound integral poses a problem. Coulomb friction could be allowed, when $\tau = \mu p$ where the tangential stress at any point is proportional to the pressure p, between the die and the workpiece. However, the inherent difficulty of obtaining the die pressure distribution is added to the complexity of the deformation zone. An indirect approach, the apparent strain method, has to be used to incorporate friction in the case of Coulomb friction. An alternative to this is to assume a constant shear stress $\tau = mk$, where $0 < m < 1$, where k is the yield stress in shear. The factor m takes a constant value for a given die and material under constant surface and temperature conditions. It is taken to be independent of velocity and it suffers from the disadvantage that the shear stress at the tools rarely bears a constant relationship to the yield stress in shear of the workpiece.

1.3.3.1   Plane (sheet) drawing

Hill[22], derived a similar upper bound theorem based on the maximum work-rate principle applied to plane-strain by a simple approximation to the slip-line analysis for wedge-shaped dies. Johnson and Mellor[23] further simplified the slip-lines by replacing them with the appropriate straight lines, in which the metal is subjected to velocity discontinuities along these lines but moves between them as a rigid body. The upper bound load so obtained will vary and depend on the sets of straight lines chosen. The best solution is the one which minimises the load. However, all plastic flow

energies are non-conservative and therefore the best upper bound solution is not necessarily the actual solution in a real case.

Kudo[24] introduced the concept of a unit rectangular region in plane-strain problems by using three different types of velocity fields in order to find a better upper bound solution. He considered a parallel, a centred face, and a rigid triangle velocity field and concluded that the rigid triangle velocity field lends itself best to the analysis of plane-strain forming processes in which deformation zones are bounded by straight lines.

In 1986, Avitzur and Pachla[25] presented an upper bound solution for the plane-strain problem. In their approach, the deformation region is divided into a finite number of rigid triangular bodies which slide with respect to one another. They analysed neighbouring rigid body zones in specific cases where the zones are (i) both in rotational motion, (ii) one in linear, the other in rotational motion and (iii) both in linear motion. They concluded that their analysis can be applied to such processes as sheet and strip drawing, extrusion, forging, rolling , etc, as well as to the investigation of failure flaws such as central burst, fir tree, and split ends.

1.3.3.2   Axisymmetric bar solution

In 1959, Alexander[26] extended the upper bound solution to represent the case of axial symmetry. He used the velocity field proposed by Johnson, but the deforming zone in this case is a single angular region which appears triangular in the plane of symmetry. Deformation was considered to occur by shearing at the boundaries in addition to the homogeneous deformation within the deforming zone.

In 1960, Kudo [27] extended his previous solution of plane strain to axisymmetric problems where the unit rectangular regions were cylindrical. Triangular velocity fields consisting of straight discontinuity lines in the plane of symmetry were then examined.

He considered the deforming energy of the material within the individual zones. Kobayashi[28] assumed curved surfaces as discontinuity surfaces for the admissible velocity fields which results in an improvement of the Kudo upper bound solutions for axisymmetric problems. However, the difference between his solution and Kudo's was too small for critical comparison.

Kobayashi and Thomsen[29] proposed that the velocity field be composed of an available number of separate triangles and assumed a constant value for the slope of the entry discontinuity. The solution was thus dependent on the initial choice of the slope. Thomsen et al[30] have extensively reviewed the earlier work of Kudo and others in their book. Pugh[31] analysed the hydrostatic extrusion of rod and included three different shapes of shear boundaries in his study, namely :

    (1)   plane transverse boundary

    (2)   conical boundary

    (3)   spherical boundary

Pugh compared the contribution of the redundant work with the extrusion pressure for the three different shear planes specified above. The graph in fig.1.1 shows that a plane transverse boundary provided the highest value for the upper bound solution when compared with the spherical, or conical shear boundary. Although a conical boundary gives a lower value than a spherical boundary, Pugh suggested that the latter seemed to be a more natural boundary for the conical flow in the die. He also declared that the redundant work contribution is independent of the type of metal and extrusion ratio and only depends on the angle of the die.

Avitzur[15] derived an upper bound solution in which he considered the deforming zone to be bounded by spherical shear surfaces with their centres at the virtual apex of

the die. The flow through the die was expressed by a kinematically admissible velocity field. The distinctive part of Avitzur's work is that he expressed the power of internal deformation as the homogeneous component multiplied by a factor greater than unity to account for relative shearing of the material in the deforming zone. Avitzur et al[32] used a triangular velocity field to predict the drawing stress for flow through converging dies.
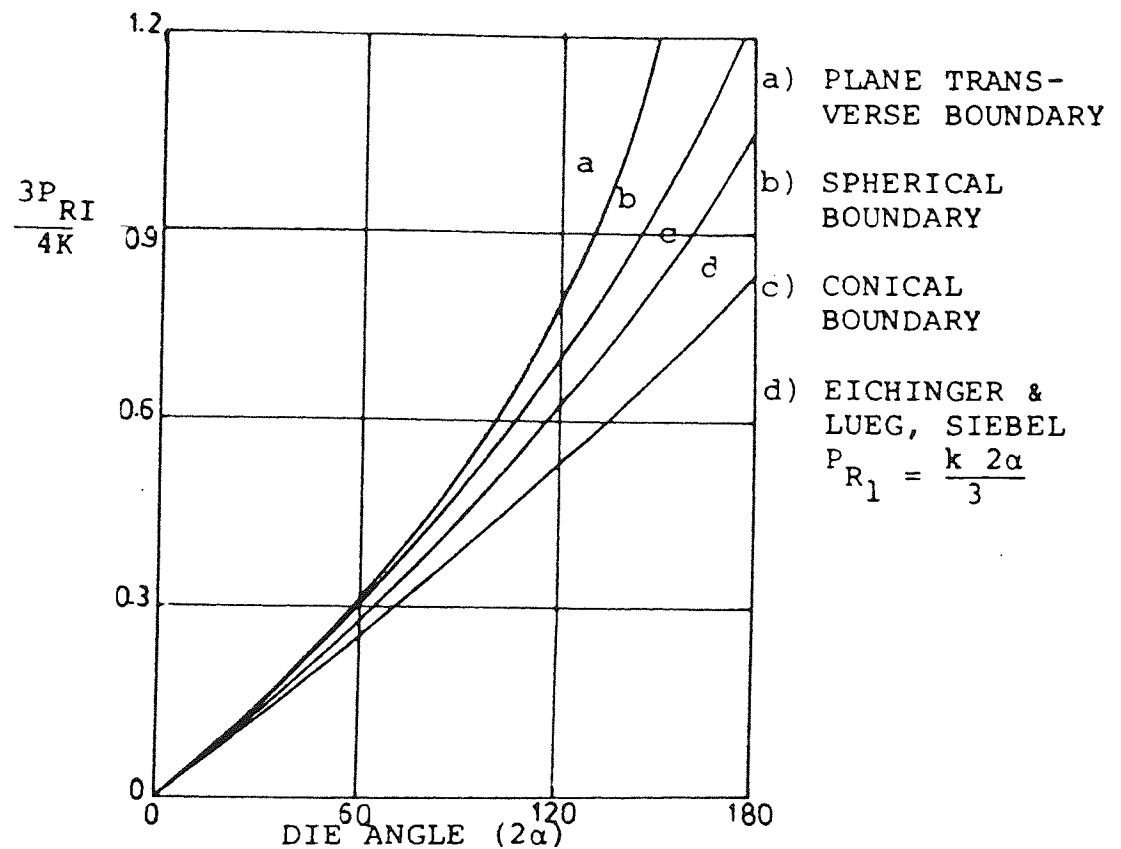
Fig. 1.1. Comparison of redundant work due to different shapes of boundary, after Pugh[31]

29

He compared the solution obtained by the spherical and triangular velocity fields and found that the solution predicted by the latter is higher than by the former. He concluded that, as the die semi-angle increases up to about 7°, the relative drawing stress decreases and then increases with continuing increase in the die semi-angle; this is for both velocity fields. The application of the Prager and Hodge upper bound theorem using spherical boundaries detailed by Avitzur[33].

1.3.4   Energy approach

The energy approach is generally used in complicated metal forming situations such as hydrostatic extrusion and forging, and is formulated on the assumption that the work expended in drawing consists of three energy components, namely ;

(i)   ideal loss-free (homogeneous) energy

(ii)   friction energy at the tool-workpiece interface

(iii)   redundant work

The work attributed to homogeneous and redundant deformation can be calculated from an assumed kinematically admissible velocity field. The work done in friction at the die workpiece interface is evaluated by means of equilibrium, either in a direct way by assuming the frictionless die pressure distribution[33] or indirectly by using the apparent strain method[34]. Avitzur[33] derived a solution for the drawing stress in wire drawing, based on the energy approach and assuming Coulomb friction.

1.3.5   Visioplasticity

Visioplasticity is a semi-analytical technique based on the examination of a velocity field developed incrementally within the deforming body which is obtained experimentally. This method of deriving the instantaneous motion of the particles making up the body is believed to have been developed by Thomsen et al[35,36,37].

1.3.6 Finite element method

The finite element was called as such by Clough (38) Early applications were in structural analysis, in which field the original developments were made . FE is a powerful technique for stress analysis. In recent years, the method has gained wide acceptance in solving metal deformation problems for plane strain and axisymmetric processes[39,40]. The conventional methods of metal forming analysis such as slip lines and upper bounds are not sufficient in a mixed elastic-plastic problems. The finite element technique is applied appropriately in such situations where elastic and plastic deformations are accounted for in separate regimes. The application has recently extended to metal working processes[41,42,43,44] to solve problems with irregular shaped boundaries and elastic-plastic conditions. In addition, the technique finds application in non-steady flow processes and is readily programmable to include realistic material properties such as strain hardening. Computer facilities will be required to solve even a relatively simple problem.

The basic process in finite element analysis is to divide the domain into pieces or elements, approximate the equations governing the problem for each element as a function of selected values, put all elements together, apply boundary conditions to some of the those selected values, and solve for such values.

1.4 Friction

Friction is an important parameter in metal forming processes, since it determines the surface temperature in high speed operations, and thus the life of the tools since it increases the forming loads. Of the numerous mathematical descriptions of friction, two are discussed here ; the Coulomb coefficient of friction and the constant shear factor.

1.4.1 Coulomb friction

If the tangential stress τ at any point on the surface is proportional to the normal pressure p between the two bodies and opposite to the direction of motion, then this state of friction is described by the Coulomb friction law.

$$\mu = \frac{\tau}{p}$$

The coefficient of friction μ is taken as a constant for a given die and material, for simplicity. It is also said to be independent of the velocity for the same reason.

1.4.2 Constant friction factor

The friction is expressed as a fraction of the shear yield stress, when one of the two bodies in contact is fully plastic

$$\tau = \frac{m\,Y}{\sqrt{3}}$$

The friction factor m is taken as a constant for a given die and material under constant surface and temperature conditions. It is also considered independent of velocity. The assumption of constant friction factor is preferred by some investigators because the computation of friction losses are easier[33]. However, as mentioned above, Alexander[26] commented on the idea of a constant frictional stress at the die interface as being incompatible with the accepted idea of Coulomb friction.

1.5 Determination of the Coefficient of Friction

1.5.1 Die rotation technique

A survey of friction in drawing was carried out by Rothman[45], indicating that die rotation techniques have been used industrially in wire drawing in order to improve die life and surface finish. Die life can be increased as a result of the even distribution of wear and through the reduction in drawing force which is achieved, but, because of the extra equipment and power needed the application of die rotation is very limited.

Linicus and Sachs[46] evaluated the mean coefficient of friction from the measured reduction in drawing load. Nishihara and Kakuzen[47] conducted a study on the rotating die technique and successfully evaluated the mean coefficient of friction for wire drawing by the measurement of the reduction in the drawing load and the torque. Sansome and Rothman[48] proposed a theory to explain the reduction in load when the die is rotated.

1.5.2   Split die technique

The measurement of the die separating force and the drawing force enables the mean coefficient of friction and the mean die pressure to be determined, this method was proposed by MacLellan[49] and applied subsequently by Wistreich[50] and MacLellan[51] for axisymmetric drawing. Lancaster and Rowe[52] used the plug technique in which two strips, separated by a flat bar, were drawn simultaneously. This eliminates the dependence of the mean coefficient of friction on the die angle.

Wistreich[50] clamped the die with a force greater than the expected splitting force. Gradually this pressure was released until the two haves of the die stared to separate. This clamping force is then almost equal to the separating force. The method was successful but cumbersome, and cannot be adopted for continuous measurement.

1.5.3   Split rotating die technique.

Basily and Sansome[53] developed this technique to determine the mean coefficient of friction and mean pressure in the cold drawing of polygonal bars from round stock. The design involved "finger tipped" split dies through which the bar was drawn, while a conical die rotated around the tips.

1.5.4 Redundant work estimation

Redundant work is defined as the work performed in the die in which the external constraint can cause appreciable internal distortion of the material in excess of that which is necessary for change in shape alone. It can be determined by superimposing the stress-strain curve of the drawn metal onto the basic curve of the undrawn metal. The area under the stress-strain curve swept by the curve of the drawn material when shifted to line up with it, gives a measure of the redundant work[54,55]. However, the method suffers from graphical errors inherent in curve fitting. Basily and Sansome[56], overcame this difficulty by expressing the stress-strain relationship of the material mathematically and obtaining the drawing parameters analytically. Thus, μ can be derived analytically in terms of the drawing stress σ_{xa}, flow stress σ_f of the drawn bar, reduction of area 'r', and the equivalent die semi-angle 'α' by

$$\mu = \frac{\left\{ \sigma_{xa} - k \left(\frac{e^{\left(\frac{\left(\ln\frac{\sigma_f}{k} \right)^{n+1}}{n} \right)}}{n+1} \right) \right\} \left(\frac{r}{r+1} \right)}{\left\{ \sigma_{xa} \ln\frac{1}{1-r} - \left(\frac{r}{1-r} \right) \left(k \left(\frac{e^{\left(\frac{\left(\ln\frac{\sigma_f}{k} \right)^{n+1}}{n} \right)}}{n+1} \right) - \sigma_{xa} \right) \right\} \cot \alpha}$$

The redundant work was deduced analytically from the drawing parameters. The method relied on the application of the apparent strain demonstrated by Thompson[57]. The accuracy of the results is therefore dependent on the theory, where the total work done consists of three components

$$W = W_h + W_r + W_f$$

W the total work done per unit volume or the drawing stress.

W_h the homogeneous work, which is derived from the stress-strain curve with the equivalent strain corresponding to the reduction of area.

W_f the component to overcome friction on the tool-workpiece interface and

W_r the redundant work.

The measurement of either W_r or W_f leads directly to the other, W_r is calculated from the displaced area under the curve of the undrawn metal over the master stress-strain curve or could be deduced analytically by the method used by Basily and Sansome[56].

1.6 Elevated temperature working of materials

Hot working takes advantage of the decrease in flow stress at high temperature to reduce tool forces and, consequently, equipment size and power requirement. When a metal is hot worked the conditions of deformation are such that the stock remains soft and ductile, work hardening takes place but it is balanced by the dynamic softening processes of recovery and recrystallisation. These processes, which are thermally activated, lead to a flow stress that depends on strain rate and temperature as well as on strain. Jonas et al[58] proposed that the lower limit of the temperature range suitable for hot working is taken as $0.6 \, T_m$, where T_m is the melting point of the metal in absolute. On the other hand, when metals are cold worked, strain hardening is not relieved and therefore the upper limit for this type of deformation can be taken as $0.3 \, T_m$. Warm working can therefore be defined as a shaping process in which the deformation temperature for the metal is $0.3 - 0.6 \, T_m$. In this temperature region a limited amount of recovery occurs, thus the degree of strain hardening that occurs is considerably less than when cold working.

According to the above definition, the warm-working temperature range for 0.11 % carbon steel would be 250 - 775°C. This agrees closely with the 200 - 800°C

temperature range which Hirschvogel[59], quoted as being suitable for the warm working of this steel. In practice, however, due to the occurrence of "strain-ageing", the lower limit of warm working for this material needs to be raised to 450°C. This then avoids, for normal strain rates, the rise in flow stress and reduction in ductility which occurs in this low temperature region[59,60].

1.6.1 Advantages of warm working

The major advantages of warm working over cold forming are the decrease in the flow stress and the lower strain-hardening rate which occur at elevated temperature. At these temperatures the flow stress is reduced and, furthermore, the resultant product is in an annealed state[61]. However, the temperature utilised for a low-carbon steel must be above 300°C before these advantages are noticed; this is shown in fig.1.2, as reported by Samanta[62]. Hawkins[63,64] presented a review of the warm working of steels and concluded that the mechanical properties resulting from extrusion at 660°C can give a strength increase of up to 60 % together with an improvement in toughness with no loss in ductility.

1.6.2 Effect of temperature on flow properties

At elevated temperatures, the rate of strain hardening falls rapidly in most metals, with an increase in temperature. The temperature dependence of flow stress is closely related to its strain rate dependence. Decreasing the strain rate has the same effect on flow stress as raising the temperature. A number of investigations have been made of the effectiveness of increases in temperature in reducing the flow stress of steels up to 700°C [65]. It is these data, produced and converted into design charts, which enable the calculation of maximum press loads and punch stresses to be made for commercial forming operations. These charts include the variables of steel composition, die angle, billet length-to-diameter ratio, temperature and extrusion ratio. Similar charts have been produced by Yuasa[66], which enable the maximum die pressure for forward extrusion,

or the maximum punch pressure for backward extrusion, to be determined for any of twelve different steels at temperature from 400 - 1000°C, for reductions of area of 40, 60 or 80 %.

Of notable interest are the very early historic high-speed tension tests of Nadai and Manjoine[67] whose results showed that there was an initial fall in the ultimate tensile strength of stainless steel at temperatures slightly above ambient and then a continuous decrease with further temperature increase.

1.6.3   Effect of strain-rate on flow properties

The rate at which strain is applied to a specimen can have an important influence on the flow stress, where an increase in the strain rate increases tensile strength. Moreover, the strain rate dependence of strength increases with increasing temperature. The yield stress and flow stress at lower plastic strains are more dependent on strain rate than the tensile strength. High rates of strain cause a definite yield point to appear in tests on low-carbon steel which do not show a yield point under ordinary rates of loading.

Flow stress measurements were carried out using compression testing by Samanta[62] and by Osakada et al.[68]. The strain during deformation has a significant effect on the relationships between stress and temperature. As the strain-rate increases the resistance to deformation increases. As the temperature increases the resistance to deformation decreases. Similar effects were also observed by Alder and Philips [69] when studying the strain rate temperature effects on compression of aluminium with 40% reduction fig.1.3. Cook[70] reported the same effects in the compression testing of various steels at temperatures of 900 - 1200 °C and strain rates of 1.5 /s to 100 /s. Osakada et al observed that a minimum in the stress-temperature curve of mild steel occurred at near room temperature at low strain, but at high deformation speeds the minimum appeared at a temperature of about 400 °C.
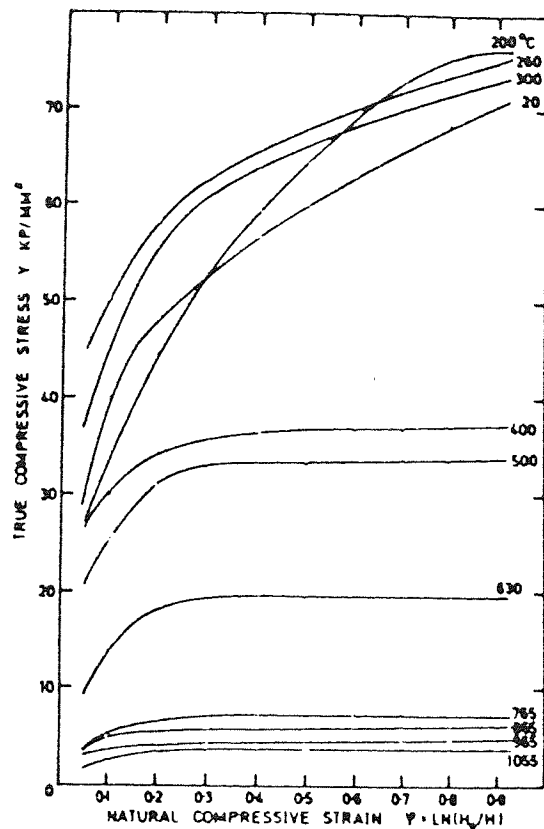
Fig. 1.2. Effect of temperature on the stress-strain relationships for a low carbon steel after Samanta[62].
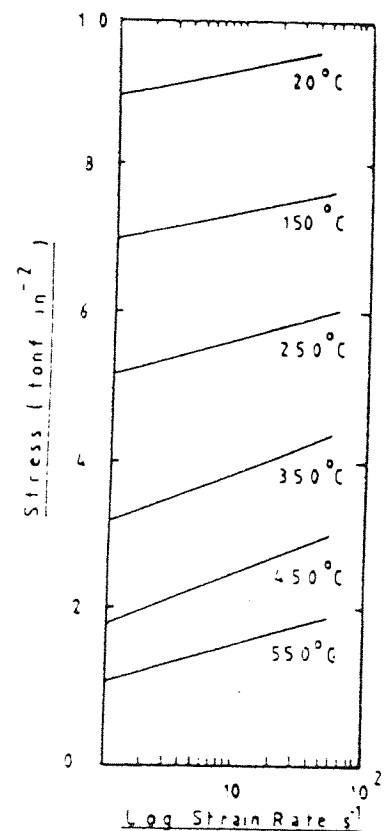
Fig.1.3.   Effect of strain rate required to compress aluminium to 40% reduction at various temperatures after Alder and Phillips [69].

Manjoine[71] performed tension tests at elevated temperatures up to 600°C and also found that a strain-ageing occurs in mild steel, and that this range extends from about 50 - 250°C when a slow strain rate of 0.00085 /s was applied. When the strain-rate was raised to 300 /s, the strain-ageing region moved to higher temperatures, in the range of about 350 - 550°C. This is clearly shown in fig.1.4.

Doravielu and Gopinathan[72], reported on the effects of temperature on the flow stress of 1.5% C, 11.2% Cr steel at a strain rate of 10 /s. They noted that there were two temperature ranges where the flow stress increased as the temperature increased due to the strain-ageing effect and phase transformation; 150 - 200°C and 800 - 900°C.

Thomason et al[73], used a plane-strain cam plastometer to test nine different steels at strain rates of 3 - 52 /s, to a natural strain of 2.3, at temperatures of 20 - 600°C. They concluded that it is possible to obtain an immediate indication of the pre-heat temperature needed to reduce the tool loads for alloy steels to an acceptable level, as illustrated in fig.1.5. Since the extrusion or drawing loads for a wide range of En 2A mild steel components give an acceptable tool life under cold working conditions, it should be possible to warm extrude any of the alloy steels if the pre-heat temperature is sufficient to bring their mean equivalent yield stress below the value for En 2A mild steel at room temperature; i.e. below the line A-A in fig.1.5. The results suggest, therefore, that any one of the range of medium-carbon and alloy steels could be warm-worked with acceptable tool pressure, if the pre-heat temperature is in excess of 550°C. They concluded that the pearlitic alloy steel shows relatively low ductility for pre-heat temperatures approaching 600 °C. These steels show a large reduction in yield stress combined with an increase in ductility; the effects are thought to be the result of the accelerated spheroidization of the lamellar carbides, which is achieved normally at lower temperatures, when the alloy steels have received a long and extensive spheroidizing treatment[74].
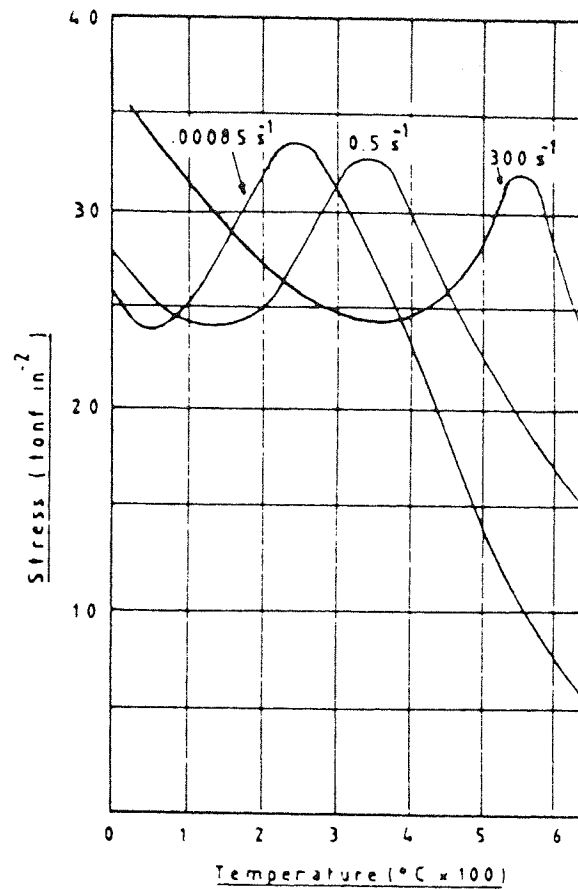
Fig.1.4.Ultimate stress of mild steel at various temperatures and strain-rates after Manjoine[71].
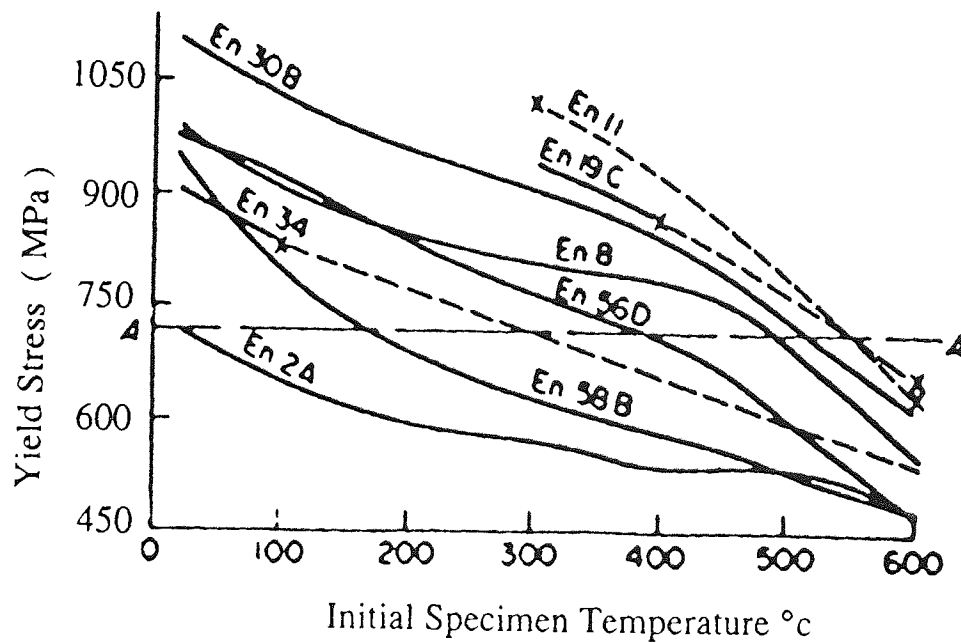
Fig.1.5. 'Adiabatic' mean equivalent yield stress at an equivalent strain of 2.66 for various steels after Thomason et al[73]

The Belgian cold forging group[75], carried out tests at strain rates of 3.5 and 20 /s, on six steels of plain-carbon and low-alloy composition, at temperatures of up to 800°C and strains of up to 50%. From their data, the reduction in flow stress, when compared with room-temperature values and at a strain of 50 %, have been plotted for the six steels at test temperatures of 500, 600, 700 and 800°C, as shown in fig.1.6. The conclusion was that, by raising the temperature, maximum loads may be reduced by 30, 45, 60 and 65% respectively at the four test temperatures.

1.6.4   Concluding remarks

A considerable number of investigations have shown that the decrease in flow stress which occurs when steels are warm worked, which emphasis the considerable effect of strain rate and temperature on the flow stress[76]. However, as already mentioned, the generalisations that the flow stress increases as the strain rate increases cannot always work and as the temperature increases the flow stress decreases, since the combined effect of strain rate and temperature must be considered together. However, changes in strain rate during deformation can cause similar effects to change in temperature. An increase in strain rate gives less time for thermally activated events; consequently, it is equivalent to a reduction in the temperature of deformation.

Fewer measurements have been made of the accompanying improvement in ductility. Manjoine and Nadai[67] reported how the ductilities of mild and stainless steel varied when tensile tested over a range of strain rates at temperatures of up to 1000°C. Later work by Dean[77], also reported on the variation of the tensile ductility of mild steel with temperature. In general, these results showed that it was necessary for the test temperature to exceed 600°C before considerable improvements over the room temperature tensile ductility could be achieved.

In their earlier work, Macgregor and Fisher[78] showed that the effect of true-strain rate on ductility, strength, or modulus of strain hardening is not known until the temperature is specified. Increased strain rate may bring higher or lower strength and greater or less ductility.
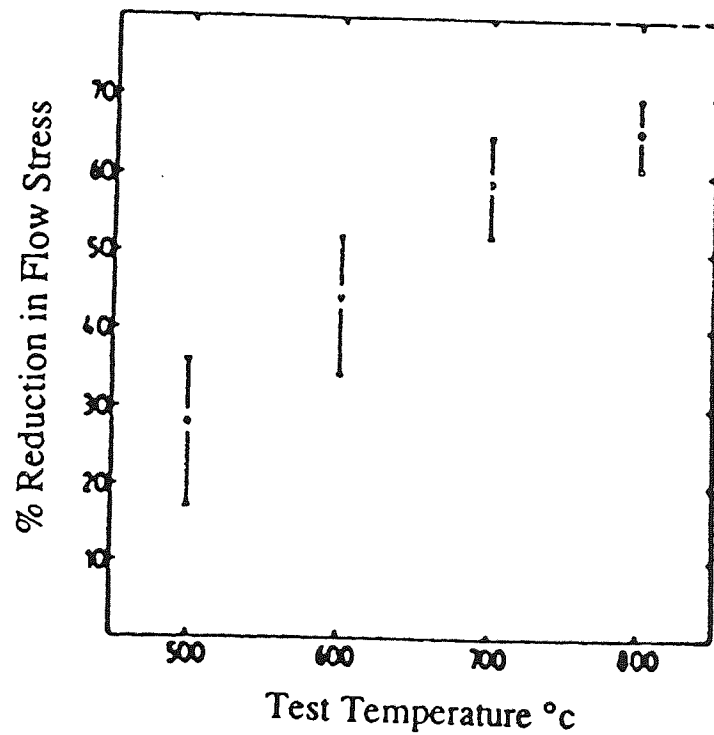
Fig. 1.6. Percentage reduction in flow stress, compared with that at room temperature, for a strain of 50% at warm-forming temperatures after[75].

1.7 Stress-strain data at elevated temperature

In metal forming processes, such as elevated temperature drawing, a basic understanding of the plastic behaviour of the metals and alloys at various temperatures and strain rates is required. It is therefore important to obtain flow curves at different temperatures and strain rates in order to solve metal-forming problems by numerical analysis methods. Stress-strain data used for this work are presented in Chapter 6.

In elevated temperature forming, the flow stress is a function of true strain ε, strain rate $\dot{\varepsilon}$, and temperature.

$$\sigma = f\left(\varepsilon, \dot{\varepsilon}, T\right)$$

When stress-strain behaviour is examined over a range of strain rate and temperature, it becomes cumbersome to report the results as complete series of stress-strain curves, i.e. the flow stress in terms of true strain at various temperatures and strain rates. More commonly, a few typical curves are shown and characteristic values of flow stress are reported as a function of temperature and strain rate.

Attempts have been made by many investigators to fit mathematical equations to the stress-strain curves at different temperatures and strain rates in order to predict the properties of the material during deformation. The required stress-strain data must be obtained from experimental investigations carried out at the temperatures and strain rates that actually exist during the forming operation for each material. The collection of stress-strain data over a range of operating conditions can be very difficult, mainly due to the limitations of the type of tests, the equipment used to conduct the test and also the difficulty in matching the exact prevailing deformation conditions which occur in the process with those in laboratory testing.

1.7.1 Measurement of flow stress

Stress-strain behaviour under conditions appropriate to hot working can be measured in tension, compression or torsion, each method having advantages and limitations.

1.7.1.1 Tension tests

The tension test is one of the simplest tests used to obtain stress-strain data and has been performed over a range of strain rates up to 10^3 /s[67] but many researchers have found that it has limited use. When using a constant cross-head speed, the true strain rate decreases slightly during homogeneous deformation and then increases rapidly as necking occurs. This increase in strain rate during necking results in an anomalous rise in the flow stress. Hence the only useful data obtained are the data recorded up to strains less than those prevailing during the onset of necking, which varies from 0.2 - 0.3 for steels[79].

1.7.1.2 Compression tests

Compression testing does not suffer the same strain limitation. Tests have been performed to a true strain of 0.7 or more using cam plastometer giving constant true strain rates in the range 0.1 - 300 /s, for the axisymmetric compression of cylindrical specimens[68,69].

1.7.1.3 Torsion tests

Torsion of solid cylindrical specimens is an increasingly popular method of hot-workability testing, since high strains can be attained at constant surface strain rate and quantitative measures of both flow stress and ductility can be obtained. The advantages and disadvantages of torsion and compression testing are considered elsewhere[79,80], and will not be dealt with here.

Singer and Evans[81] described a technique for the rapid measurement of high-temperature flow stress which uses a relatively simple machine and allows determinations to be made very rapidly. The method relies on the simultaneous indentation of a hot surface by two projectiles with hemispherical ends. The projectiles impact with velocities which are approximately in the ratio of 2:1 and the individual impact velocity, together with the diameter of the indentations, are measured accurately. A series of tests has been conducted on aluminium alloys at strain rates of up to 530 /s. From the knowledge of the above quantities, the effective flow stress and strain rate sensitivity have been calculated. They claimed that the results produced reasonable assessments of strength when compared with results obtained by cam-plastometer compression testing.

1.7.2 Flow stress strain-rate temperature relations

A great amount of work has already been done in trying to correlate stress-strain curves by mathematical relationships. The most common relationship used to correlate data at constant temperature is the semi-logarithmic formula proposed by Ludwik[82], the form of the equation being

$$\sigma = \sigma_0 + B \ln \varepsilon \quad \text{---------------- (i)}$$

where B and σ_0 are constants.

Alder and Philips[69], in their work on copper, aluminium and steel were best able to summarize their results in the strain rate range 1- 40 /s by the following power law;

$$\sigma = \sigma_0 \, \varepsilon^n \quad \text{------------------ (ii)}$$

where σ_0 and n are constants.

They also pointed out that if flow-stress data are obtained over a relatively narrow range of strain rate, less than two orders of magnitude, it can be difficult to distinguish whether equation (i) or (ii) best fits the results at different temperatures.

Hodierne[83], fitted results obtained by torsion on mild steel at temperatures from 30 - 700°C and a strain rate of $10\text{-}10^3$ /s to the power law. Johnson and Mellor[84] found that the power law provided a slightly better interpretation of their results than did the semi-logarithmic law. Samanta[85] found that the semi-logarithmic law fits the stress-strain data of tool steel at hot working temperatures reasonably well. Cook[70] reported for more complex alloys that either equation may be entirely satisfactory.

To correlate data at different temperatures Zener and Holloman (86), proposed that ;

$$\sigma = f\left\{ \dot{\varepsilon}, \exp \frac{Q}{RT} \right\}$$

where

ε = strain rate

Q = activation energy for diffusion of the metal

R = universal gas constant

T = absolute temperature

The development predicts that if the strain rate to produce a given stress at a given temperature is plotted on a logarithmic scale against $1/T$, a straight line should result with a slope of (- Q/R).

Correlations of this type are very useful in relating temperature and strain effects. However, such correlations may break down if applied over too large a range of temperatures. In order to accommodate data better, and for some theoretical reasons, a modification to the equation been suggested by Jonas, Sellers and Tegart [87];

$$\dot{\varepsilon} = A \left[\sinh\left(\alpha\, \sigma\right)\right]^{n'} \exp\left(\frac{-Q}{R\,T}\right)$$

where

A, α ,and n' are constants which are independent of temperature and stress.

The activation energy Q can be obtained from a plot of $\dot{\varepsilon}$, at α constant sinh as, against 1/T.

MacGregor and Fisher[78] reported the results of tension tests for which the true strain rate was kept constant by varying the rate of head motion, these tests were conducted at the temperature range of -70 to 665°C and the range of true strain rates 50×10^{-6} to 50 /s on SAE 1020 steels, SAE 1045 steel, and a brass. A single variable called the velocity-modified temperature is used to represent the combined influence of true strain and testing temperature i.e. for a given material, instead of having the flow stress as a function of temperature, strain, and strain rate, it is a function of the strain and modified temperature only. The expression given is;

$$T_m = T \left(1 - K \ln\frac{\dot{\varepsilon}}{\varepsilon_o} \right)$$

where

T = testing temperature in degrees absolute

ε_o = a base strain rate (constant)

$\dot{\varepsilon}$ = true strain rate

K = material constant

It should be possible for a given choice of ε_o to select a value of K so that when stress is plotted versus T_m, a smooth curve will result. In their investigations, the constant ε_o is taken as 10×10^{-6} /s, the value of K selected to obtain a smooth curve

was 0.018 which is chosen by trial and error. MacGregor and Fisher[88], verified that the velocity-modified temperature is equally applicable to tension tests conducted at both slow and rapid rates, up to 0.5 /s, over a range of temperatures and found it to give satisfactory correlation.

Inoue[89], as reported by Nakayama[90], has applied the concept of velocity-modified temperature to tension data of several steels at temperatures ranging from 830 - 1230°C and at strain rates of 0.8-75 /s. Inoue found satisfactory correlation by use of the velocity-modified temperature T_m. More recently Loh[91], has applied the velocity-modified temperature concept in her work on the mechanics of drawing wire at elevated temperature. The formula was modified to take into consideration the temperature rise ΔT that occurs in the compression tests. Thus, T_m is expressed as:

$$T_m = \left(T + \Delta T \right) \left(1 - K \ln\frac{\dot{\varepsilon}}{\varepsilon_o} \right)$$

and conclusion drawn was that the velocity-modified temperature concept does not relate well at higher values of T_m, thus giving lower flow stresses. Oxley[92] presented a paper which reviewed the attempts that have been made to include strain rate effects on the flow stress of the work material and concluded that, in order to obtain meaningful results, account must also be taken of the temperature of the material being deformed. The power law relationship presented is

$$\sigma = \sigma_1 \varepsilon^n$$

where σ and ε are the uniaxial flow stress and strain, and σ_1 and n are material constants which define the stress-strain curve for given values of strain rate and temperature. By using the flow stress results obtained by Oyane at al[93] from high speed compression tests with a strain rate of 450 /s and temperature range of

0 -1100°C, he found that, for the given values of strain rate and temperature, the above power law gave a good fit with those experimental results.

Oxley applied the concepts of velocity-modified temperature in order to extrapolate the results to the higher strain rates in machining and to relate σ_1 and n to strain rate and temperature in a convenient manner, finding a good fit to a single curve which gave some support to the use of T_m. He also used the Oyane et al results to obtain values of σ_1 and n for 0.16% carbon steel, as shown in fig.1.7.
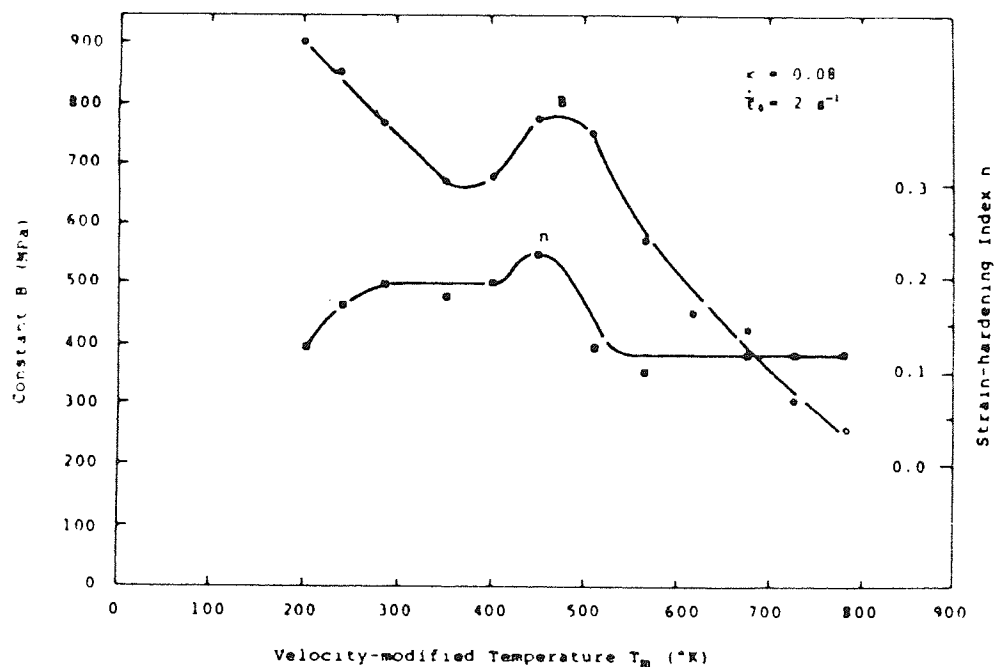
Fig.1.7. Relationship between B, n and Tm, based on the experimental data of Oyane et al[93]

1.8 Temperature distribution in the deforming zone

During deformation the work done in the material, i.e. the essential deformation and redundant work, is mostly transformed into heat, which is manifested as a rise in temperature and, as a result, varying the thermo-mechanical behaviour of the material; friction losses also raise the temperature at the die-workpiece interface. Therefore, the influence of temperature change on the material behaviour and, hence, on the forming load, must be taken into account in the process modelling of metal forming.

1.8.1 Calculation of plastic deformation and heat distribution

During drawing, heat is generated by deformation in the material and by friction at the die-workpiece interface. Heat is transported with the drawn material and conduction takes place simultaneously.

The process modelling includes the division of the deformation zone into many small deformation steps which are continuously updated. In this way the material flow, the stress and the strain fields are determined step-by-step from the beginning to the end of the deforming process. This is achieved by using data obtained by elevated temperature stress-strain analysis at various strain rates, thus simulating the behaviour of materials at conditions which might be experienced during the actual deformation process.

In addition, the calculation of the power of deformation, heat generation and heat transfer will be analysed in each time increment to obtain the temperature distribution, and then material behaviour is updated due to the just - predicted field of temperature, therefore the flow stress distribution in the deformation zone can be established. The process will be repeated to the end of the deforming zone.

Total temperature increase of each element will be obtained from the heat balance :

$$\Delta = \Delta Q'D - \Delta Q'h$$

with

$$\Delta Q'D = \Delta Q'd + \Delta Q'f$$

where

$\Delta Q'd$ = heat due to the dissipated forming energy

$\Delta Q'f$ = heat due to the dissipated friction

$\Delta Q'h$ = heat transferred over the element

1.8.2   Temperature prediction in drawing

Siebel and Kobitzsch[94] were the pioneers in analysing the temperature in wire drawing, and made the following assumptions.

(i)   the temperature increase due to deformation is uniform across a section.

(ii)   the temperature distribution due to friction is parabolic in the vicinity of the tool-workpiece interface.

(iii) there is no heat flow in the axial direction.

(iv)   only 20% of the generated friction heat flows into the die while the other 80% remains in the workpiece.

Kopp[95] in his work on rod drawing , which is a slower process, indicated that nearly half of the friction heat remains in the drawn material while the other half flows into the die. The amount of heat remaining in the drawn wire depends mainly upon the speed of drawing, thermal conductivities of the wire and die materials, and the insulating properties of the lubricant.

Ranger [96] measured the temperature at the external surface of a tungsten carbide die insert and calculated the interface temperatures by means of an electrical analogue technique. Ranger's work illustrated the difficulties involved in determining

temperatures in wire drawing dies. Thus a theoretical approach to establish the temperature distribution in the deformation zone would be advantageous.

Altan[97] used a numerical method for calculating temperature in drawing, and stated that approximately 90% of the mechanical energy involved in the process is transformed into heat. Perfect contact at the tool-workpiece interface is assumed for heat transfer purposes, and the friction shear stress is assumed to be 0.05 times the flow stress of the wire, whereas friction at the die land, which contributes to temperature increase, was neglected, which is probably the reason for obtaining slightly lower values of the temperature predicted than those obtained by Ranger[96]. Altan concluded that the large temperature gradient in the die shows that external cooling of the die is an extremely inefficient way of cooling, and the best method is to cool the wire between reductions.

1.8.3   Calculation of heat generation

The friction losses and forming energy are transformed into heat. The temperature increase during a time interval Δt is calculated using the following :

The temperature increase due to friction is given by ;

$$\Delta_\theta = \frac{m\ \sigma\ A\ v\ \Delta t}{V\ J\ c\ \rho\ \sqrt{3}}$$

where

Δt = time interval

v = velocity at the interface

A = surface area at the interface

V = volume of the friction element divided into two equal halves on the workpiece and tool side.

52

c , ρ = specific heat capacities and densities of the workpiece and tool material respectively.

J = conversion factor between mechanical and thermal energies.

The temperature increase ΔT due to deformation is given by ;

$$\Delta T = \frac{\sigma \; \dot{\varepsilon} \; \Delta t}{J \; c \rho}$$

where

σ = flow stress of the drawn material

$\dot{\varepsilon}$ = effective strain rate

c = specific heat of drawn material

ρ = specific weight (density) of the drawn material

1.8.4   Calculation of heat transfer

By solving the heat conduction difference equation, the temperature change in an element after conduction during time interval Δt can be calculated. In a similar way to the calculation of heat generation, the drawn material and the die will be divided into a grid system, in order to derive the difference equations of conduction and to calculate the local temperature changes; the temperature increase and heat transfer will be calculated for each grid point. Heat transfer due to convection and conduction will not be considered in the theoretical analysis because their contribution is small, especially at high speeds, and to reduce computing time.

The time increment Δt of the heat calculation could be different from the time increment of the plastic deformation. In order to increase the accuracy of the heat calculation, a small time increment might be chosen for this calculation. Thus the time increment of plastic deformation is divided into many time increments in order to predict the

temperature field. Usually the temperature calculations are done by finite element analysis and the upper bound technique is most common for determining flow patterns. Sometimes flow patterns are determined experimentally.

Heat transfer due to convection appears mainly on the free boundaries of the workpiece and tool. The heat flow through these boundary surfaces is given by :

$$q = \alpha_1 (T_s - T_b)$$

where

q = heat flow

T_s = surrounding temperature

T_b = boundary surface temperature

α_1= average heat transfer coefficient, the heat transfer coefficient is related to the surface conditions and the surrounding medium.

The importance of temperature calculations during a metal forming process has been recognised for a long time. Until recently the majority of the work has been based on procedures that uncouple the problem of heat transfer from the metal deformation problem.

Several research workers used the approach of determining the flow characteristics of the problem either experimentally or by calculation, and then of using these calculations for the calculation of heat generation. Among these is the work of Johnson and Kudo[98] on hot rolling and extrusion; no account of roll distortion, radiation losses, conduction losses to dies or rolls, and variation of yield stress with temperature is considered in their calculations. Tay et al[99] concerning metal forming processes; in general, take account of the dependence of the material flow stress on temperature, the thermal properties are assumed constant, to reduce computing time.

Another approach uses Bishop's[100] numerical method, in which heat generation and transportation is considered to occur instantaneously for each time increment, followed by an interval in which conduction takes place as for a stationary medium. Bishop's solution, however, is for the special case of the plane-strain extrusion of an ideal plastic material, where the velocity and strain rate distributions are determined from slip line theory.

The new temperature distribution is used to calculate flow characteristics, which in turn will originate the instantaneous heat generation and transportation for the next step. This approach is represented by the work of Altan and Kobayashi[101] on extrusion, Lahoti and Altan[102] on compression and torsion, and Lahoti et al[103] on selected metal forming processes.

Avitzur[104] assumed the process to be adiabatic when he analysed metal flow through conical converging dies. The work of internal deformation, redundant work, and friction losses, are assumed to convert into heat. Material properties (strength, and specific heat) are considered as variables. He proposed an alternative scheme for the approximation of flow strength as a function of temperature, effective strain, and effective strain-rate values, to compensate for the fact that formulation or tabulation of these variables are not well studied and published data is scarce, as follows;

" For a strain-hardening material a typical steel was studied, obeying the following strength equation:

$$\sigma_o \ (kgf/cm^2) = \left(1 - \frac{T}{1520}\right)\left(2500 + 250 \tan^{-1}\phi\right)$$

$$= 250 \left(1 - \frac{T}{1520}\right)\left(10 + \tan^{-1}\phi\right)$$

55

Where the results obtained should be considered valid only below the recrystallization temperature T < 1100°C. At these temperatures steel is considered non-strain rate sensitive, $\tan^{-1}\phi$ is measured in degrees and ϕ is the strain".

Two points to consider from the above analysis;

- it claims that the recrystallization temperature for typical steel is above 1100°C, where, in fact recrystallization temperature for a low carbon steel starts from 538°C (Chapter 6).

- at such temperatures steel is considered non-strain rate sensitive .

In the stress-strain data obtained by torsion testing (Chapter 6), up to the temperature of 400 - 500°C there is no significant effect of strain-rate on the flow stress i.e. at these temperatures steel might be considered as non-strain rate sensitive, but as the temperature increased over 500°C, it is clearly shown that steel at these temperatures is strain-rate sensitive. The data obtained are converted into mathematical expressions and used in the theoretical analysis, to obtain flow stress, strain, strain rate and temperature distribution in the deforming zone. Temperature rise due to deformation and friction work are calculated assuming adiabatic deformation in order to simplify calculations. All work done was assumed to degenerate to heat.

CHAPTER TWO

SECTION DRAWING

Chapter Two

2.0   Section Drawing

2.1   Introduction

There are two types of section drawing, namely: symmetric drawing and direct drawing. In the symmetric drawing of section, a section profile is drawn from an original section of the same profile. This is the usual method adopted in industry for the manufacture of section rods. The direct drawing of section involves the drawing of a section from a round profile.

2.2   Symmetric drawing and extrusion of section rods

In 1975 Juneja and Prakash[105], derived an upper bound solution for the drawing of polygonal sections, i.e. the drawing of section from section. They obtained a velocity field for the deforming metal similar to that of Avitzur[33], by assuming spherical inlet and exit shear surfaces. To account for redundant work, they further assumed that the zone of plastic deformation is enclosed by two cylindrical surfaces of velocity discontinuity, at entry to and exit from the pyramidal portion of the die. This assumption was not appropriate because the shape of the deformation zone changes with friction and reduction. They concluded that the drawing load for the symmetric drawing of section rod is higher than that for the corresponding axisymmetric drawing. This drawing load decreases rapidly to that of the axisymmetric solution derived by Avitzur as the number of sides of the section increases.

In 1979 Prakash and Khan[106], presented a generalised expression for the spherical flow field generated by the plastic flow of metal through a converging die of regular polygonal cross-section. The surfaces of velocity discontinuity are assumed to be

57

exponential cylindrical surfaces, and they optimised the solution by successive approximations with respect to the shape of the deforming zone to obtain the lowest upper bound value of the working stress.

2.3   Direct drawing and extrusion of section rods

In 1976 Basily[53] and Basily and Sansome[107] derived numerical upper and lower bound solutions for the drawing of regular polygonal bars from round stock in a single pass. In the upper bound solution, based on an energy approach and the apparent strain method,the velocity field was obtained from a deformation pattern constructed by conformal mapping of elemental areas between the inlet and exit shear planes.

In the 1978 paper by Yang and Lee[108], a method is proposed for the extrusion of section through curved dies by conformal transformation, they formulated kinematically admissible velocity fields in the extrusion of billets with generalised cross-sections where similarity in cross-section is maintained throughout the deformation.

In 1979 Boer et al[109] a theoretical approach is presented for the analysis of the direct drawing of square section rod with various corner radii from round bar, as the first step towards the study of more complicated shape drawing. An optimising factor was found which gives the minimum value of the upper bound solution, obtained using a co-ordinate transformation. In their analysis, the kinematic boundary condition is not satisfied at the exit plane of the die.

In 1975 Nagpal and Altan[110] analysed three-dimensional metal flow with the use of dual stream functions, applied to the cold extrusion of A1 1100 from round billet to an ellipse-shaped product. Plane strain flow of an incompressible material can be represented by a single stream function, another single stream function represents the velocity field in axisymmetric flow. The use of stream function makes the method

58

difficult to use with other, more complicated, shapes. In 1979, Yang et al(111) obtained an analytical expression for the analysis of the three-dimensional extrusion of arbitrarily-shaped sections from round billets through continuous dies by utilizing external conformal mapping of sections to construct a continuous die surface and thus to design an optimal die for the process.

In 1980 Hoshino and Cunasekera(112) presented an upper bound solution for the extrusion of square section from round billet through converging dies. The geometry of the die chosen for the analysis is constructed by an envelope of straight lines drawn from points on the perimeter of the circular entry section to corresponding points on the square exit shape. In 1982 the same authors(113) presented an upper bound solution for the extrusion or drawing of polygonal sections through straight converging dies.

In 1981, Kiuchi et al(114) investigated analytically the extrusion and drawing of rods, bars and wires with various kinds of non-symmetric cross-section. They presented a generalized simulation technique based on the upper bound theory for various cross-sections. By using this method, energy requirements, extrusion pressures, drawing stresses, optimal die length and dimensions of the dead zone are successfully calculated regarding the process from round, square and rectangular billets into rods, bars and wire with square, rectangular, hexagonal, L-type, T-type, H-type and flower-type. They concluded that it is possible to make systematic investigations into those processes or to predict optimum dimensions of the die and working conditions necessary for the required product.

In the Kiuchi et al investigations, the fact that symmetric and non-symmetric section drawing is an extremely limited operation in which it has a minimum as well as a maximum achievable reduction of area per pass (see table in Appendix A1), and that in practice a material can only be drawn to a limited reduction of area before the drawing

stress equals the maximum tensile stress of the material and tensile failure will take place, is totally ignored. For example, in the drawing of round from round when the coefficient of friction is zero the maximum reduction of area achievable is 63.3%. When considering a square section, the minimum and the maximum achievable reductions of area are 36.34% and 63.3% respectively. The maximum reduction of area achieved in the present work was 50% when producing a square from round in one pass and at 80°C, (Jornaz et al[115]). The effect of different materials is not expressed; for instance, some examples where given with a reduction of area of 75% and obviously, with single pass drawing, this is impossible. Other examples mention 73% reduction of area from round to hexagonal shape; again this is impossible for single pass drawing and may only be true for the extrusion process. To conclude, this paper does not give the correct representation for section drawing, since most of the examples apply to extrusion but not to section drawing. There is no mention of the type of material used in the theoretical analysis; or that could be used with the analysis, certainly this will effect the reduction of area achieved in any drawing process. Finally, only very few sections can be drawn from round to the required shape successfully in a single pass, and these will not include the L-type, H-type, T-type and flower type cross-sections. These will require a very large reduction of area, and thus tensile failure will take place; for example a minimum of 58.65% reduction of area needed to produce a triangular section from round in a single pass and that is almost an impossibility judging from the problems experienced with square sections. No attempt is made to make quantitative comparisons of predicted with experimentally measured forces. The author feels that Kiuchi et al added 'Drawing' to the heading of their published work without studying the limitations of the drawing process as compared to the extrusion one, when it is applied to the symmetric and non-symmetric production of sections from round in a single pass.

In the same work Kiuchi et al claimed that, as regards the extrusion from a round billet into a square bar, the extrusion pressure obtained by them is distinctly lower than that obtained by Avitzur et al[109] and further added that this means that the analytical method developed in their study can give quite resonable results and is better than the method developed by Avitzur et al . The author feels that what Kiuchi et al claim is of questionable scientific significance, because in their work, they compared the results obtained by Avitzur et al[109] concerning the direct drawing of square section from round bar with their results concerning the extrusion from round billets into round bars and square bars; this comparison is presented in fig.5 in their work.

Drawing and extruding of metals are two different processes in that the state of stress in the extrusion process consists of three compressive stresses, whereas, in the drawing operation, it consists of two compressive and one tensile stresses. Furthermore the drawing process is a more limited one in terms of the reduction of area achievable; this limitation is further magnified when dealing with the direct drawing of sections from round in a single pass due to the tensile failure that takes place when the drawing stress 'pulling' exceeds the tensile stress of the drawn material. On the other hand, this problem is non-existent in the extrusion process, where the deforming force is a 'pushing' one. To conclude, the author feels that this comparison does not present a realistic or scientific result because both processes are different in many ways.

In 1984 Kiuchi[116] presented an upper-bound solution by assuming axial and rotational velocity fields, the analyses are also based on the assumption of constant axial velocity either over the whole cross-section or along the radial direction, when applying this investigation into non-symmetric extrusion and or drawing of rods, bars and tubular products with various cross-sections. In this work Kiuchi has generalised the process by including extrusion, drawing of rods, bars and tubular products but these processes have different limitations as explained earlier and this leads to questions

61

which cannot be answered because most of these theoretical or semi-theoretical methods lack experimental back-up, in that many parameters are not fully studied e.g. the materials used and the limitations of reduction of area achieved especially when drawing complicated shapes.

Recently, in 1985, Gunasekera and Hoshino[117], developed an upper bound solution for the analysis of the extrusion of polygonal sections through streamlined dies. They concluded that the streamlined die is superior to the straight converging die from the aspect of reducing the forming stress, and that the forming stress required through the streamlined die closely follows the pattern of the axisymmetric case with the increase in the number of sides of a regular polygonal section.

In 1986, Han et al[118] derived a kinematically admissible velocity field for a generalised three-dimensional flow. The analysis takes into account the effect of product shape complexity, lubrication and reduction of area on extrusion pressure. Computation is carried out for work-hardening materials such as aluminium and steel; for a computational example, extrusion of clover sections from round billets is chosen.

In 1990, Chitkara et al[119] used a CAD/CAM bilinear representation of the die surface to obtain a generalised upper bound solution for three-dimensional extrusion of shaped sections from round. They concluded by claiming that the theory presented was in good agreement with the experimental results, but that improvements, however, can be made to the theory with respect to the variation in the axial-velocity of the extruded material inside the deformation zone.

2.4 The drawing of polygonal tube

In 1980, Karyawasam and Sansome[120] used the minimum energy approach to solve the problem of drawing square section tube directly from round section tube. The bore and outer periphery are both square and the drawn tube wall is of uniform thickness.

In 1981, Muriuki and Sansome[121] investigated the direct drawing of circular section tube to a tube whose outer periphery is changed to any regular polygonal while the bore remains circular. In 1985, Kiuchi and Kimura[122] presented a computer simulation of the extrusion and drawing of tubular products having square cross-section with round inner holes.

2.5 Limitations of cold drawing theories, techniques and conventional section drawing.

- Most of the theories of cold metal working operations assume that the work material is deformed with constant flow stress. It is assumed generally that the deformed metal is not subject to strain hardening and the effect of strain-rate is not considered. Temperature changes in the deformation zone are not taken into account, thus the changes in material properties due to temperature distribution, are neglected, but it must be borne in mind that temperatures reach to between 200-300 °C in cold drawing.

- The variation of flow stress for steel as a function of temperature is very complex, no adequate information can be found in the literature covering a range of temperatures, strains, strain-rates and materials. Data used for this work is presented in Chapter six.

- When a material has been put into a highly strained condition by drawing, it loses its ductility to such a degree that it is not practical to submit it to further

63

drawing and it becomes necessary to restore the grains to the original form by annealing. This process is sometimes used between drawing operations (inter-stage annealing) and is sometimes carried out two or three times for a complete job.

-    Due to technological advancements, materials of better quality are required and frequently these are more difficult to form into the required shape because of their metallurgical structure or their property of rapid work hardening.

-    Most cold drawing operations have to be followed by heat treatment to obtain the desirable mechanical properties for a workpiece material, i.e an extra cost is added to the process.

-    There is a limited range of sizes and variety of rolled sections obtainable, and the high cost of stocking these varieties of sizes and shapes as compared to the lower cost of round stock makes the drawing of sections from sections a limited process as compared with polygonal drawing from round.

-    The continual increase in the cost of manufacturing rolled polygonal sections compels manufacturers to seek better techniques for producing polygonal sections to remain competitive. Such a technique is the drawing of polygonal drawing from round at elevated temperature

The current work helps to overcome the combined limitations of cold drawing theories and techniques and the conventional section-to-section drawing in a way that any polygonal section can be produced from round at a increased reduction of area and at the same time a heat treating operation is carried out while the material is being drawn. Furthermore, in elevated temperature drawing, the flow stress is a function of true

strain, strain-rate and temperature, therefore the effect of temperature on the flow stress is considered in the development of the process modelling to predict the drawing stress, temperature distribution and other data for a range of variables. The plastic behaviour of the materials used at various temperatures and strain-rates are presented in (Chapter 6).

Elevated temperature drawing has not been widely employed for several reasons; it is difficult to change traditional methods of manufacture, the flow of information has been restricted, and some techniques are considered to be confidential. However, there are powerful technological and commercial advantages associated with elevated temperature drawing, which may be listed as; (i) metals which are difficult to cold draw, or cannot be drawn, can be drawn more easily, (ii) a greater reduction of area per pass is possible, (iii) the reduction of repeated annealing, pickling and lubrication operations, (iv) minimisation of handling costs, metal losses, surface decarburisation and (v) shortening of the production route.

2.6   Finite element approach applied to the drawing and extrusion of square from round

In 1978, Webster and Davis[123] developed a three-dimensional finite element computer program to combine the finite element technique with the upper bound theory to provide a means for analysing metal forming problems in which there are many parametric effects.

In 1985 Boer and Webster [124] presented a comparison between the direct upper bound solution and the finite element approach to round-to-square drawing. They obtained a kinematically admissible velocity field in the deforming region and then obtained a solution for the minimum power for the first method. In the second method they used the finite element approach, where the deforming region is subdivided into small

elements and the velocities are calculated at each node with the condition of minimising the power required. They concluded that, when the relative drawing stress is plotted against the semi-cone angle of the die, the agreement is fairly good.

The advantages of the direct upper bound solution are the possibility of incorporating friction and of calculating a whole range of die angles in a very short computer time (two minutes). The disadvantages are in the inflexibility of the solution. For any other shape the velocity field has to be calculated or to be found by some empirical method and converted into mathematical expressions.

The advantages of the finite element approach are mainly in its great flexibility to adapt to almost any shape. But a new mesh has to be generated for every shape, and this is a very time-consuming process.

The shape of the die passage through which an entirely circular wire-rod transforms to a regular section is complex fig. 2.1. The associated flow is irregular and therefore a velocity field is derived from a conformally mapped deformation pattern.
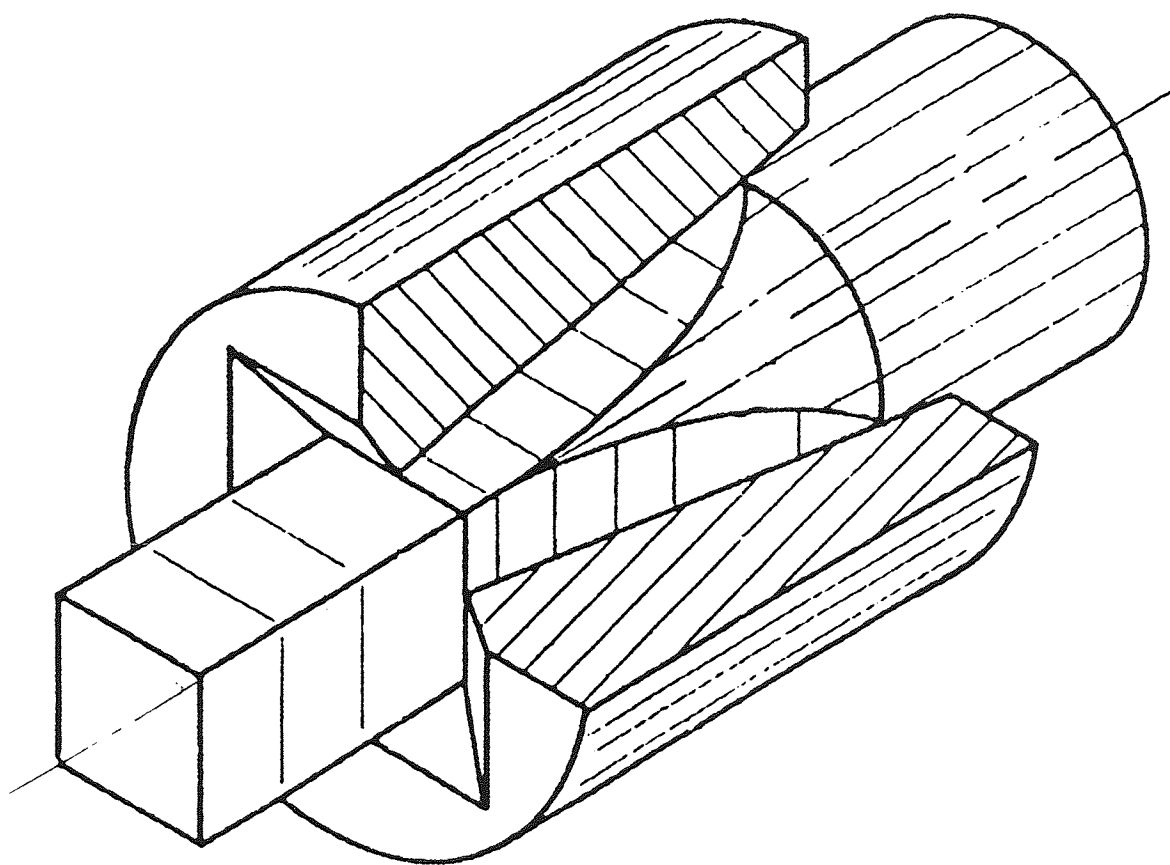
Fig. 2.1. The direct drawing of polygonal sections from round.

2.7 Construction of the deformation pattern

In the direct drawing of polygonal sections, the transformation of rod-wire from round to a section is irregular and, therefore, the associated velocity fields are difficult to analyse. Material flow is irregular and therefore a velocity field will be derived from a conformally mapped deformation pattern. The deformation pattern will be obtained by dividing the circular inlet section of the undrawn wire into triangular elements and it will be assumed that they will be transformed into corresponding triangular elements at the exit section. see fig.2.2.

Basily and Sansome[107] obtained the velocity field from a deformation pattern constructed by conformal mapping of elemental areas between the inlet and exit shear planes. They used the following:-

(i)   the exit section was bounded by hyperbolic curves i.e. the exit plane was divided into bands by a set of (N-1) hyperbolic curves of which the focal distance was adjusted to suit the curvature at the corner.

(ii)   conformally mapping elements, then the local axes (x,y) are transformed to global axes (X,Y), which coincide with the entry section; this is done by both rotation and transformation of the local axis to the global one.

Using the above technique, some numerical errors will take place, arising from ;

(i)   the area omitted at the end of the symmetrical section; this area is inclosed between the hyperbolic curves and the sharp edges of the section, see fig.2.3.

(ii)   errors caused by fitting straight-sided triangular elements to the assumed hyperbolic curves.
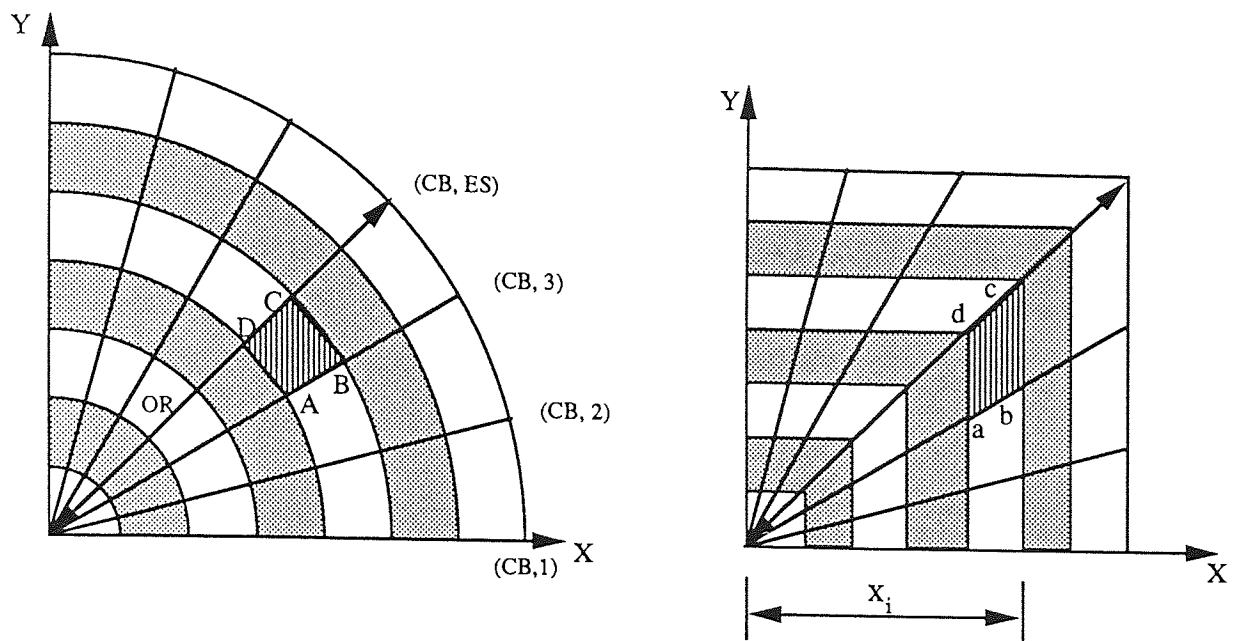
Fig.2.2. Conformal mapping of elemental areas of the inlet and outlet planes.
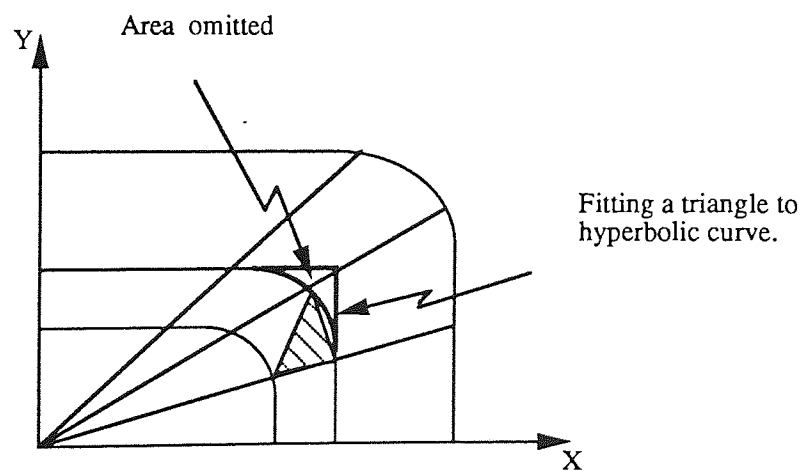
Fig.2.3. Area bounded by two hyperbolic curves on the outlet plane after Basily (107)

The same technique used by Basily and Sansome for conformally mapping the deforming elements will be used, with the following modifications in order to minimise numerical errors and to simplify the analysis:-

(i)   the exit section will be assumed to be bounded by straight lines, i.e. the symmetrical section will be divided by straight lines, thus equations of straight lines will be used instead of equations of hyperbola in the calculations of the positions of the unknown-nodal co-ordinates.

(ii)   conformally mapping elements with reference to a fixed global axis, from the initial stages, will eliminate the process of rotation and transformation of every local axis to the global one.

The deforming pattern will be obtained by dividing the inlet circular section area into (BC - 1), equally spaced bands. These will be subdivided into (ES - 1), equi-spaced sectors, the element area (ABCD) which, in turn divided into two triangles, a large triangle ΔL (ABC) and a small triangle ΔS (CDA), both of known area. These triangles were assumed to be transformed into corresponding triangular elements (abc) and (cda) at the exit section as shown in fig.2.4.

Assuming a constant reduction of area, the area of the corresponding area of any triangle on the exit plane is determined. For example, the area of the large triangle could be defined by the co-ordinates (x_1,y_1), (x_2,y_2) and (x_3,y_3) of which (x_3,y_3) lies on the straight line ST_1, and could be determined by considering the known area of the triangle and the two known points (x_1,y_1) and (x_2,y_2), if the start is to begin from an axis of symmetry i.e., cross-flat length, the co-ordinate (x_4,y_4) relating to the corresponding smaller triangle which lies on the straight line ST could be determined by considering the known area of this triangle together with the know point (x_1,y_1) and the height (x_2-x_1). The procedure continues until the whole area is built up. For greater

accuracy, the total number of co-ordinate points along the x-axis, i.e. number of circular inlet bands and the number of points in the circumferential direction (the division of band area into sectors) should be as many as the computer time allows.

Since the centroids of both entry and exit triangles refer to the same fixed datum, and it was assumed that the flow of the deforming material travels along the vector joining the centroids of corresponding triangles, the angle of twist and inclination with respect to the workpiece axis can be obtained and a velocity model for each element can be found.

The analysis of triangular elemental areas, obtained by conformal mapping, between the inlet and the outlet shear planes, bears close resemblance to the finite element method, where both methods deal with finite elements and combine the effect of entire elements to give a complete solution. The procedure is illustrated mathematically as follows;

Assuming that the circular inlet bar is divided into (CB - 1) equal bands.

$$\text{The thickness of a circular band} \quad T = \frac{R_1}{(CB - 1)}$$

$$\text{Area of a designated section at the inlet plane} \quad \delta A_i = \frac{\pi \, Ur_{(i)}^2}{2 \, N_S}$$

$$\text{The equivalent area corresponding to the above area at the exit plane} \quad \delta A_o = \frac{\pi \, Ur_{(i)}^2}{2 \, N_S \, A_r}$$

Where R_1 is the inlet bar radius.

$$Ur_{(i)} = I.T \quad \text{and} \quad I = 1 \text{ to } (CB\text{-}1).$$

A_r is the ratio of inlet and outlet area of the bar being drawn.
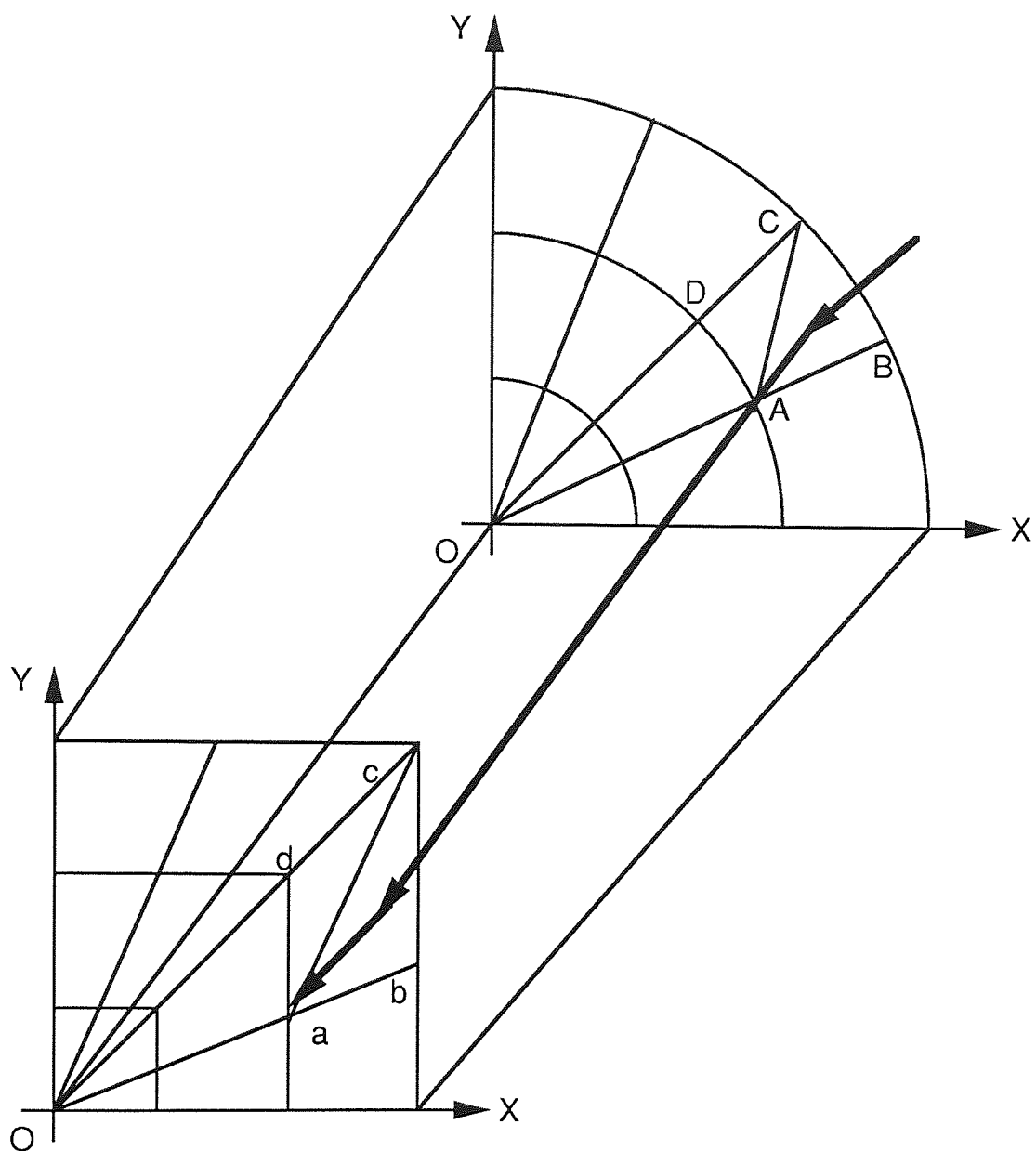
Fig.2.4. Conformal mapping of elements with reference to a fixed global axis.

Assuming that there was no transfer of material between adjacent sections within a regular polygonal section, then the distance X_i along the datum at the exit plane is determined from the known equivalent area of triangular section

$$\frac{1}{2} \cdot X_i \cdot X_i \ \tan\beta \ = \ \frac{\pi \ Ur^2_{(i)}}{2 \ N_s \ A_r}$$

$$\therefore \quad X_i = \pm \sqrt{\frac{2 \cdot \pi \ Ur^2_{(i)}}{2 \ N_s \ A_r \ \tan\beta}} \tag{2.1}$$

only the positive sign was chosen since the axes were taken as shown in fig.2.5. Hence, the co-ordinates at point H and J were evaluated as

$$H_{(x1,y1)} = (\ X_i \ , \ 0 \ )$$
$$J_{(x2,y2)} \ = (\ X_i \ , \ 0 \ )$$

Dividing the area of the inlet section to (ES-1) equal sectors, the area of each elemental area, say ABCD, fig.2.5a, is given by

$$\frac{\text{area of band}}{\text{number of sectors}}$$

$$\delta A_s = \frac{\pi \ Ur^2_{(i)}}{2 \ N_s \ (ES - 1)}$$

The elemental area of each sector, say ABCD is divided into a large ABC and a small triangle ADC. If the angle subtended at the centre is $d\theta$ and the radial increment $T = dR$, where $Ur_{(i)} = R$; then

73
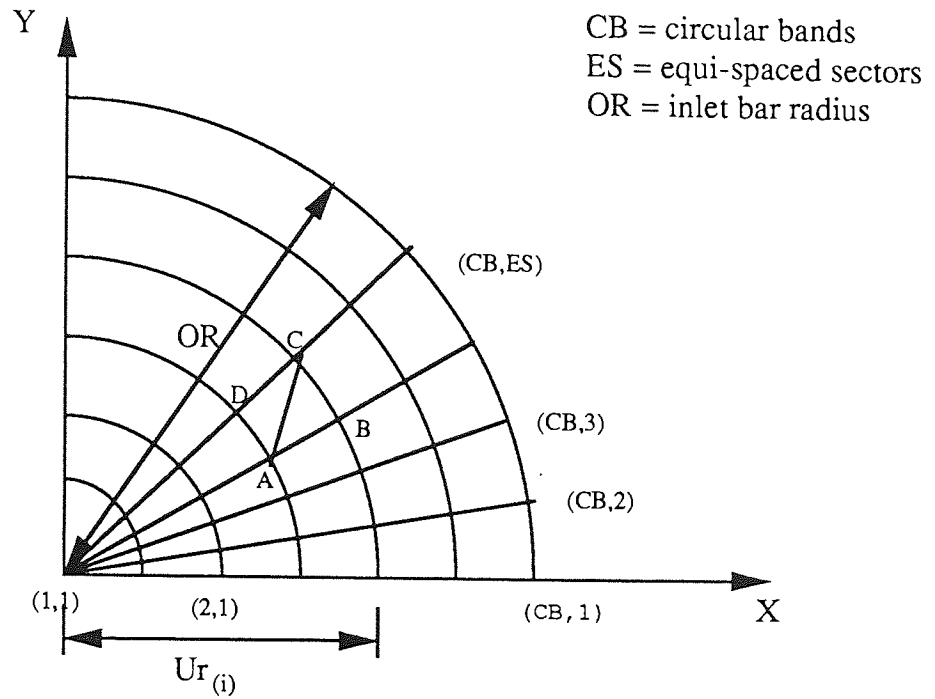
fig.2.5 a. Dividing the entry plane into (CB-1),(ES-1) sectors each sector
is further sub-divided into a small and a large triangle.
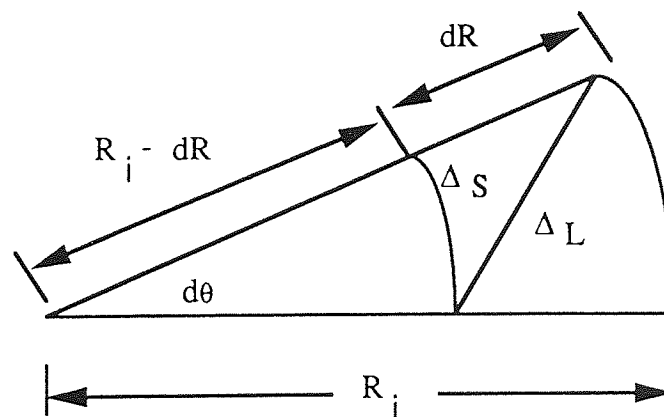
Fig.2.5 b . Division of a sector block into a large and
small triangle at the inlet plane.

74

Area of large triangle ABC $\Delta_L = 1/2.\ dR.\ R_i\ d\theta$

Area of small triangle ADC $\Delta_S = 1/2.\ dR.\ (R_i - dR)\ d\theta$

$$\Delta_L + \Delta_S = ABCD \tag{2.2}$$

$$\frac{\Delta_L}{\Delta_S} = \frac{R_i}{(R_i - dR)} \tag{2.3}$$

Solving equations (2.2), (2.3) and for the area ABCD, the general expressions for the areas of the large and small triangles are:

$$\Delta_L = \delta A_S \left(\frac{R_i}{2R_i - dR} \right) \qquad \text{where } dR = T$$

ie $$\Delta_L = \delta A_S \left(\frac{R_i}{2R_i - T} \right) \tag{2.4}$$

$$\Delta_S = \delta A_S \left(\frac{R_i - T}{2R_i - T} \right) \tag{2.5}$$

Each triangle at the entry plane is transformed into a corresponding triangle at the exit section, with the constant reduction of area A_r

$$\Delta'_L = \frac{\Delta_L}{A_r} \qquad \& \qquad \Delta'_S = \frac{\Delta_S}{A_r}$$

Since the co-ordinates of the points H and J were evaluated, the unknown co-ordinate $K(X_3,Y_3)$ for the first triangle to be conformally mapped was found as follows

By considering the geometry of fig.2.6. Since area Δ'_L is known

$$\therefore \quad \Delta'_L = \frac{1}{2} (X_2 - X_1)(Y_3 - Y_2)$$

75

$$\therefore \qquad Y_3 = \frac{2 \, \Delta'_L}{X_2 - X_1} + Y_2 \qquad\qquad (2.6)$$

and $X_3 = X$

Since the first sector includes only a large triangle, the co-ordinates of the small triangle are equal to zero.

For subsequent sectors; point(X_4, Y_4), is calculated from the known area Δ'_S

$$\Delta'_S = \frac{1}{2} \, (X_2 - X_1)(Y_4 - Y_1)$$

$$Y_4 = \frac{2 \, \Delta'_S}{X_2 - X_1} + Y_1 \qquad\qquad (2.7)$$

and $\quad X_4 = X_1$

The above procedure of the conformal mapping of elemental areas was therefore repeated for each circular band at the inlet circular section until the complete area at the inlet was built up.

Since the triangular elemental areas at both the inlet and outlet planes were referred to the same directional axis(X,Y), the co-ordinates of the centroids of such elemental triangles were given by

For a large triangle (inlet plane)

$$LX_{1(i,j)} = \frac{LX_{1(i,j)} + LX_{1(i+1,j+1)} + LX_{1(i+1,j)}}{3}$$

$$LY_{1(i,j)} = \frac{LY_{1(i,j)} + LY_{1(i+1,j+1)} + LY_{1(i+1,j)}}{3}$$
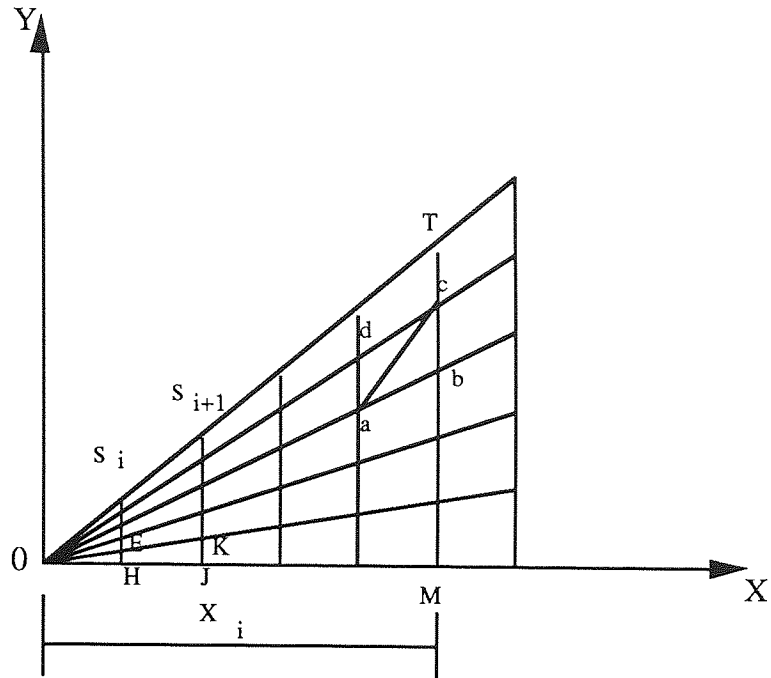
Fig.2.6 a. Conformal mapping of elemental areas of the outer plane.
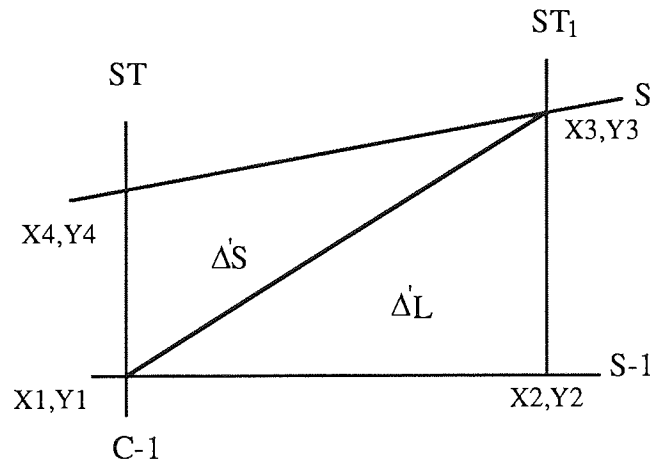
Fig.2.6 b. Division of a sector block into a large triangle
and a small triangle at the exit plane.

77

For a small triangle (inlet plane)

$$MX_{1(i,j)} = \frac{MX_{1(i,j)} + MX_{1(i+1,j+1)} + MX_{1(i,j+1)}}{3}$$

$$MY_{1(i,j)} = \frac{MY_{1(i,j)} + MY_{1(i+1,j+1)} + MY_{1(i,j+1)}}{3}$$

For large triangles (outlet plane)

$$LX_{2(i,j)} = \frac{LX_{2(i,j)} + LX_{2(i+1,j+1)} + LX_{2(i+1,j)}}{3}$$

$$LY_{2(i,j)} = \frac{LY_{2(i,j)} + LY_{2(i+1,j+1)} + LY_{2(i+1,j)}}{3}$$

For small triangles (outlet plane)

$$MX_{2(i,j)} = \frac{MX_{2(i,j)} + MX_{2(i+1,j+1)} + MX_{2(i,j+1)}}{3}$$

$$MY_{2(i,j)} = \frac{MY_{2(i,j)} + MY_{2(i+1,j+1)} + MY_{2(i,j+1)}}{3}$$

2.8 Material flow path parameters

A triangular element at the die entry is assumed to shear at an elemental surface inclined at an angle (t θ) where $-1 \leq t \leq 1$ to the die axis. The position of the element is defined by a general spherical surface (ρ, θ, ϕ) with the centre at the virtual apex of the equivalent die cone. The parameter t is used to optimise the shear surface by minimising the total shear work.

Similarly, a general pyramidical shear surface is defined at the exit of the deforming zone and the parameter t optimises the geometry of the surface. If the centroid of a triangular element at the entry is (x_1, y_1) and the centroid of its corresponding transformed triangular element at the exit is (x_2, y_2), then the vector joining the two centroids defines the flow.

The flow path parameters such as θ, η and ψ for a triangular element are determined from the geometry of fig.2.7. δ_1 is the horizontal distance that an element, with its centroid, travels after shearing at the assumed discontinuity boundary, measured to the entry plane. δ_2 is the horizontal distance which the particle travels after shear at the assumed pyramidical discontinuity boundary, measured to the exit plane.

The equivalent die semi-angle of the direct drawing of polygonal sections was defined as the die semi-angle of the corresponding conical die for the axisymmetric drawing Appendix (A1) which gives the same area reduction and the same die length, and its exit diameter is given by

$$D_e = \sqrt{\frac{4 A_{sc}}{\pi}}$$

where A_{sc} is the area of the drawn section

The length of the flow path D_T for each element, and the relative angular deflections η and ψ as the element flows through the deforming zone are determined from the geometry of fig.2.7.

$$R_1 = \sqrt{X_1^2 + Y_1^2}$$

$$R_2 = \sqrt{X_2^2 + Y_2^2}$$

Radius of shear

$$\rho_1 = \frac{\text{length of die} * R_1}{\cos\alpha_e * (R_1 - EqR_2)} \tag{2.8}$$

The die length of a die semi-cone angle α_e is therefore given by

$$L = \frac{R_1 - EqR_2}{\tan\alpha_e} \tag{2.9}$$

$$\delta_1 = \rho_1 (\cos\theta_1 - \cos\alpha_e) \tag{2.10}$$

The inclination ρ, to the axis is given by

$$\theta_1 = \sin^{-1}\left\{\frac{R_1}{\rho_1}\right\} \tag{2.11}$$

at entry

$$\phi_1 = \tan^{-1}\left(\frac{X_1}{Y_1}\right) \tag{2.12}$$
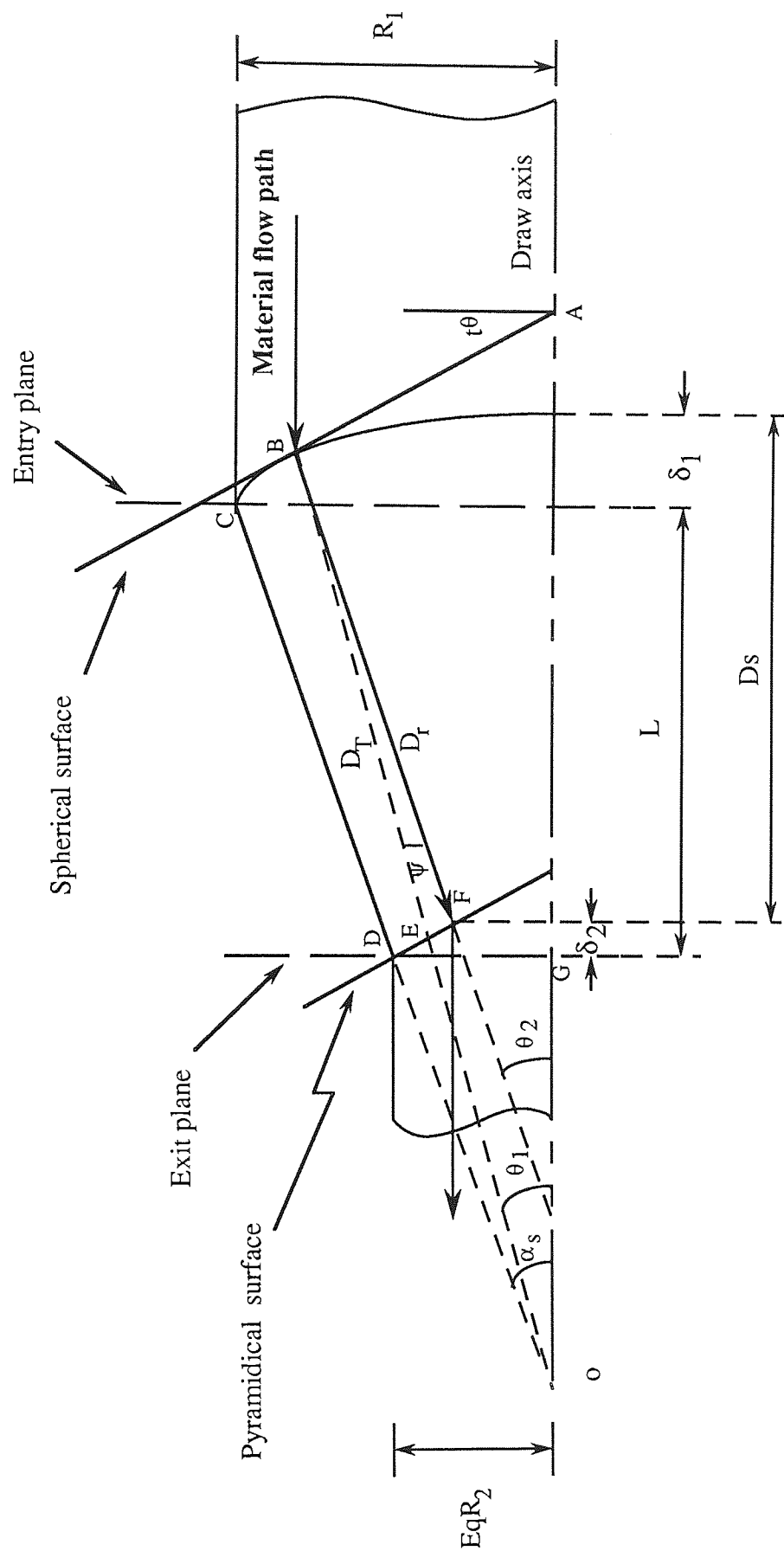
Fig.2.7. The assumed shear surface and flow path parameters.

at exit

$$\phi_2 = \tan^{-1}\left(\frac{X_2}{Y_2}\right) \tag{2.13}$$

where

$$\phi_2 = \begin{cases} \tan^{-1}\left(\frac{X_2}{Y_2}\right) & \text{FOR } \phi_2 \leq \beta \\ 2\beta - \tan^{-1}\left(\frac{X_2}{Y_2}\right) & \text{FOR } \phi_2 > \beta \end{cases}$$

$$DA = \rho_1 (1 - \cos \alpha_e)$$

$$\delta_2 = DA * \frac{\left(\dfrac{\text{Diagonal length of die}}{2 \cos \phi_2} - R_2\right)}{R_2} \tag{2.14}$$

From fig.2.7, the total horizontal distance covered by the particle in the deforming zone is

$$D_s = L + \delta_1 - \delta_2 \tag{2.15}$$

The total travel of the element of area is therefore given by

$$D_T = \sqrt{(X_1 - X_2)^2 + (Y_1 - Y_2)^2 + D_s^2} \tag{2.16}$$

82

The angle of twist ' lateral displacement ', η, for the same triangular element is given by;

$$\eta = \tan^{-1}\left\{\frac{EqR_2 \sin\omega}{D_r}\right\} \qquad (2.17)$$

where

$$\omega = \tan^{-1}\frac{X_1}{Y_1} - \tan^{-1}\frac{X_2}{Y_2} \qquad (2.18)$$

$$D_r = \sqrt{(R_1 - EqR_2\cos\omega)^2 + D_s^2} \qquad (2.19)$$

The angle of inclination ' deviation ' ψ, from the corresponding angle θ, for any elemental area is given by;

$$\psi = \theta_2 \text{ (at exit)} - \theta_1 \text{ (at entry)} \qquad (2.20)$$

$$\theta_2 = \tan^{-1}\left\{\frac{R_1 - EqR_2\cos\omega}{D_S}\right\} \qquad (2.21)$$

Therefore

$$\psi = \tan^{-1}\left(\frac{R_1 - EqR_2\cos\omega}{D_S}\right) - \sin^{-1}\left(\frac{R_1}{\rho_1}\right) \qquad (2.22)$$

83

Having found the material flow path parameters i.e. ρ, θ, η, ψ, D_t, D_s. The corresponding associated velocity field was computed, using the above known flow parameters.

CHAPTER THREE

THEORETICAL ANALYSIS

Chapter Three

3.0 Theoretical Analysis of the Drawing of Polygonal Sections from Round at Elevated Temperatures

3.1 Introduction

An upper-bound solution was developed and solved numerically with the aid of the specially written computer programs in 'Matlab' computer language, discussed in section (3.2.11), to predict the drawing stress, temperature and flow stress distributions and other data for a range of variables. The prime objectives of the theoretical solution were : to model the process numerically, i.e. a study of the process variables, comparison of the validity of the solutions with the experimental results and a proposition for a technological approach to the design of optimised section drawing tools and other parameters for industrial application.

The upper-bound method is a very practical technique for determining the velocity, strain rate and strain distributions in the deforming metal. This method considers a velocity field that satisfies the incompressibilty of metals and the velocity boundary conditions. Since the deformation of rod-wire from round to a section is irregular and, therefore the associated velocity fields are difficult to analyse, a velocity field is derived from a comformally mapped deformation pattern. This method is described in detail in section 2.7.

Based on this velocity field, the deformation, shear and friction energies are computed to give the total forming load. In order to obtain the variation of flow stress as a function of strain, strain rate and temperature within the deforming material, a grid pattern was constructed. Initially, a kinematically admissible velocity field was selected. At each subsequent step, new values of velocity fields, strains, temperature and the

corresponding values of the flow stress were calculated at the nodal point. This method is described in detail in section 3.2.

The value of the forming load calculated is higher than the actual load required by the process and, therefore, it represents an upper-bound to the actual forming load. Thus the lower this upper-bound load, the better is the prediction. The considered velocity field includes a parameter which varies the shape of the inlet and outlet shear surfaces and the overall work was minimised by varying this parameter.

3.2 The upper bound solution

In the upper bound solution, the minimum energy required to deform the metal is calculated. The material is assumed to shear as it crosses the shear surfaces at the inlet and outlet regions of the deforming zone. If a velocity field is assumed and the deforming material obeys the von Mises yield criterion and the Levy-Mises flow rule, the upper bound solution, discussed in section (1.4.2) indicates that the actual strain rate is the one which minimises the expression

$$ J^* = \frac{2}{\sqrt{3}} Y \int_V \sqrt{\frac{1}{2}\dot{\varepsilon}_{ij}\dot{\varepsilon}_{ij}} \; dV + \int_{S_r} \tau \left| \Delta v \right| \; dS - \int_{S_t} T_i \, V_i \, dS $$

3.2.3 Velocity field

The working region of a pass is divided into a number of zones distinguished by the fact that particle velocity in each of them is continuous. Different velocity distributions may exist in adjacent zones but discontinuity may occur only in the tangential components of velocity along the actual zone interfaces and the tool material boundaries. Discontinuities, of course, imply the presence of shear, and the existence of velocity distributions in each zone indicates the presence of plastic strain and, consequently, dissipation of energy.

Within the die, the velocity of a particle is expressed three-dimensionally by the spherical system of co-ordinates, $\overset{\circ}{U} = \overset{\circ}{U} (\overset{\circ}{U}_\rho, \overset{\circ}{U}_\theta, \overset{\circ}{U}_\phi)$ and changes as the deformation proceeds. The flow of the metal was assumed to be in the direction of the vector joining the centroids of the corresponding triangles at the exit and the entry plane. Therefore the magnitude and the direction of the resultant velocity $\overset{\circ}{U}_{\rho, \theta, \phi}$ are governed by the co-ordinates of the particular set of corresponding triangular elements chosen, fig.3.1.

There is, generally, no means of determining the shape or exact position of the different boundaries stated earlier. The surfaces normally assumed are plane, spherical or conical[31]. However, since the deformation mode of the problem is complex, a streamline on entry to the deformation zone is assumed to shear at a surface inclined at an angle (tθ) to the drawing axis. The position of the particle is defined on the spherical surface (ρ,θ,ϕ) . The parameter t, where $-1 \leq t \leq 1$, is used to optimise the shear surface by minimising the shear work. Similarly, a general pyramidical shear surface is defined at the exit from the deformation zone and the parameter t is used to optimise the geometry of the surface.

From the calculated material flow parameters, (see Chapter two), and the flow path, the velocity field and, therefore, the strain rates are established.

If V_1 is the velocity of an element before shear and $\overset{\circ}{U} = \overset{\circ}{U} (\overset{\circ}{U}_\rho, \overset{\circ}{U}_\theta, \overset{\circ}{U}_\phi)$ is the velocity after shear, then, to satisfy the continuity of flow at the entry shear surface, the normal velocity components on each side of the inlet shear surface must be equal.
i.e.

$$V_1 \cos(t\theta) = \overset{\cdot}{U} \cos\psi \, \cos\eta \, \cos(\theta - t\theta)$$

Fig.3.1. The flow model of the direct drawing of polyogonal sections.

$$\therefore \quad \dot{U} = V_1 \frac{\cos(t\theta)}{\cos\psi \, \cos\eta \, \cos(\theta - t\theta)} \tag{3.1}$$

Assuming a linear convergence of the deformation passage with an equivalent die semi-angle α_e, the virtual apex is the centre of the spherical co-ordinate system (ρ, θ, ϕ). (equivalent semi-angle is discussed in Appendix A1). The cross-sectional area of the material at any radius ρ is given by,

$$A = \pi \left(\rho \sin\alpha_e \right)^2 \tag{3.2}$$

since

$$V = \frac{A_2}{A_1} V_1$$

Therefore, the velocity of an element at any radial distance ρ is given by :-

$$\dot{U} = V_1 \left(\frac{\rho_1}{\rho}\right)^2 \frac{\cos(t\theta)}{\cos\psi \, \cos\eta \, \cos(\theta - t\theta)} \tag{3.3}$$

Resolving the velocity vector into its three principal polar components, namely $\dot{U}_\rho$, $\dot{U}_\theta$, $\dot{U}_\phi$ as shown in fig.3.1.

$$\dot{U}_\rho = \dot{U} \cos\eta \, \cos\psi \tag{3.4}$$

$$\dot{U}_\theta = \dot{U} \cos\eta \, \sin\psi \tag{3.5}$$

$$\dot{U}_\phi = \dot{U} \sin\eta \tag{3.6}$$

substituting equation (3.3) in equation (3.4), (3.5) and (3.6), gives

$$\dot{U}_\rho = V_1 \left(\frac{\rho_1}{\rho}\right)^2 \frac{\cos(t\theta)}{\cos(\theta - t\theta)} \tag{3.7}$$

$$\dot{U}_\theta = V_1 \left(\frac{\rho_1}{\rho}\right)^2 \frac{\cos(t\theta)}{\cos(\theta - t\theta)} \tan\psi \tag{3.8}$$

$$\dot{U}_\phi = V_1 \left(\frac{\rho_1}{\rho}\right)^2 \frac{\cos(t\theta)}{\cos(\theta - t\theta) \cos\psi} \tan\eta \tag{3.9}$$

Similarly, maintaining continuity at the exit shear surface where $\rho = \rho_2$, the exit velocity can be obtained from;

$$V_2 \cos(t\theta) = \left(\dot{U}_\rho\right)_2 \cos(\theta - t\theta) \tag{3.10}$$

substituting equation (3.7) in equation (3.10) gives

$$V_2 \cos(t\theta) = V_1 \left(\frac{\rho_1}{\rho_2}\right)^2 \frac{\cos(t\theta)}{\cos(\theta - t\theta)} \cos(\theta - t\theta)$$

$$\therefore \qquad V_2 = V_1 \left(\frac{\rho_1}{\rho_2}\right)^2$$

$$= V_1 A_r \tag{3.11}$$

The above relation can also be obtained directly from volume constancy.

3.2.4 Strain rates

Using the general spherical polar co-ordinates (ρ, θ, ϕ) and the previously derived velocity field $\dot{U}_\rho$, $\dot{U}_\theta$, $\dot{U}_\phi$ the strain rate components are given by

$$\dot{\varepsilon}_\rho = \frac{\delta \dot{U}_\rho}{\delta \rho} \tag{3.12}$$

$$\dot\varepsilon_\theta = \frac{1}{\rho}\frac{\delta \dot U_\theta}{\delta\theta} + \frac{\dot U_\rho}{\rho} \tag{3.13}$$

$$\dot\varepsilon_\phi = \frac{1}{\rho\sin\theta}\frac{\delta \dot U_\phi}{\delta\phi} + \frac{\dot U_\rho}{\rho} + \frac{\dot U_\theta}{\rho}\cot\theta \tag{3.14}$$

$$\dot\gamma_{\rho\theta} = \frac{1}{2}\left(\frac{\delta \dot U_\theta}{\delta\rho} - \frac{\dot U_\theta}{\rho} + \frac{1}{\rho}\frac{\delta \dot U_\rho}{\delta\theta}\right) \tag{3.15}$$

$$\dot\gamma_{\theta\phi} = \frac{1}{2}\left(\frac{1}{\rho\sin\theta}\frac{\delta \dot U_\theta}{\delta\phi} + \frac{1}{\rho}\frac{\delta \dot U_\phi}{\delta\theta} - \frac{\cot\theta}{\rho}\dot U_\phi\right) \tag{3.16}$$

$$\dot\gamma_{\theta\phi} = \frac{1}{2}\left(\frac{\delta \dot U_\phi}{\delta\rho} - \frac{\dot U_\phi}{\rho} + \frac{1}{\rho\sin\theta}\frac{\delta \dot U_\rho}{\delta\phi}\right) \tag{3.17}$$

Substituting the various derivatives of the velocity component equations (3.7), (3.8) and (3.9) in equations (3.12) to (3.17), the corresponding strain rate will then be obtained. The proofs of the following derivations are shown in appendix (A2).

$$\dot\varepsilon_\rho = -2\,V_1\frac{\rho_1^{\,2}}{\rho^3}\frac{\cos(t\theta)}{\cos(\theta - t\theta)} \tag{3.18}$$

$$\dot\varepsilon_\theta = V_1\frac{\rho_1^{\,2}}{\rho^3}\frac{\cos(t\theta)}{\cos(\theta - t\theta)}\left\{1 + \tan\psi\Big((1-t)\tan(\theta - t\theta) - t\tan(t\theta)\Big)\right\} \tag{3.19}$$

$$\dot\varepsilon_\phi = V_1\frac{\rho_1^{\,2}}{\rho^3}\frac{\cos(t\theta)}{\cos(\theta - t\theta)}\Big(1 + \tan\psi\cot\theta\Big) \tag{3.20}$$

$$\dot{\gamma}_{\rho\theta} = \frac{V_1}{2} \frac{\rho_1^2}{\rho^3} \frac{\cos(t\theta)}{\cos(\theta - t\theta)} \Big((1-t)\tan(\theta - t\theta) - 3\tan\psi - t\tan(t\theta)\Big) \tag{3.21}$$

$$\dot{\gamma}_{\theta\phi} = \frac{V_1}{2} \frac{\rho_1^2}{\rho^3} \frac{\cos(t\theta)\ \tan\eta}{\cos(\theta - t\theta)\ \cos\psi} \Big((1-t)\tan(\theta - t\theta) - t\tan(t\theta) - \cot\theta\Big) \tag{3.22}$$

$$\dot{\gamma}_{\phi\rho} = \frac{-3V_1}{2} \frac{\rho_1^2}{\rho^3} \frac{\cos(t\theta)\ \tan\eta}{\cos(\theta - t\theta)\ \cos\psi} \tag{3.23}$$

3.2.5 Effective strain rate

The effective strain rate is an acceptable measure of the combined effect of the components of strain rates and is expressed as

$$\dot{\bar{\varepsilon}} = \frac{2}{\sqrt{3}} \sqrt{\frac{1}{2} \dot{\varepsilon}_{ij} \dot{\varepsilon}_{ij}}$$

$$= \sqrt{\frac{2}{3}\left\{ \dot{\varepsilon}_\rho^2 + \dot{\varepsilon}_\theta^2 + \dot{\varepsilon}_\phi^2 + 2\left(\dot{\gamma}_{\rho\theta}^2 + \dot{\gamma}_{\theta\phi}^2 + \dot{\gamma}_{\phi\rho}^2\right)\right\}}$$

substituting equations (3.18) to (3.23) into the above equation gives

$$\dot{\bar{\varepsilon}} = \frac{V_1}{\sqrt{3}} \frac{\rho_1^2}{\rho^3} \frac{\cos(t\theta)}{\cos(\theta - t\theta)} \sqrt{J} \tag{3.24}$$

where

$$J = \left\{ \begin{array}{l} 2\left(4 + \Big(1+\tan\psi\big((1-t)\tan(\theta -t\theta) - t\tan(t\theta)\big)\Big)^2 + \big(1+\tan\psi\cot\theta\big)^2\right) \\[2mm] + \Big((1-t)\tan(\theta-t\theta) - 3\tan\psi - t\tan(t\theta)\Big)^2 + \Big((1-t)\tan(\theta -t\theta) - t\tan(t\theta) - \cot\theta\Big)^2 \\[2mm] \hspace{4cm} - 3\tan^2\eta\ \sec^2\psi \end{array} \right\}$$

92

3.2.6 Effective mean strain

For a particular flow line in the deformation zone, the radial velocity is given by

$$\dot{U} = V_1 \left(\frac{\rho_1}{\rho}\right)^2 \frac{\cos(t\theta)}{\cos\eta \cos\psi \cos(\theta - t\theta)}$$

The time taken for a particle to move a small radial distance $d\rho$ is taken as dt, and is given by

$$dt = \frac{d\rho}{\dot{U}} \tag{3.25}$$

The effective mean strain $\bar{\varepsilon} = \displaystyle\int_0^t \dot{\varepsilon}\, dt$

substituting equations (3.24) and (3.25) into the above expression gives

$$\bar{\varepsilon} = \frac{1}{\sqrt{3}} \int_\rho^{\rho_1} \frac{1}{\rho} \left(\sqrt{J}\ \cos\eta\ \cos\psi\right) d\rho$$

$$\therefore\ \bar{\varepsilon} = \frac{1}{\sqrt{3}} \ln\frac{\rho_1}{\rho} \left(\sqrt{J}\ \cos\eta\ \cos\psi\right) \tag{3.26}$$

3.2.7 Internal power of deformation

The internal power required to deform a unit volume of material can be expressed in terms of the derived strain rate components and is given by:

$$\dot{W}_1 = \frac{Y_m}{\sqrt{3}} \sqrt{2\left(\dot{\varepsilon}_\rho^2 + \dot{\varepsilon}_\theta^2 + \dot{\varepsilon}_\phi^2 + 2\left(\dot{\gamma}_{\rho\theta}^2 + \dot{\gamma}_{\theta\phi}^2 + \dot{\gamma}_{\phi\rho}^2\right)\right)}$$

Therefore the expression for the total internal power of deformation becomes,

$$P_1 = \int_v \dot{W}_1\ dv = Y_m \int \dot{\bar{\varepsilon}}\ dv$$

$$= \frac{Y_m}{\sqrt{3}} \int_v V_1 \frac{\rho_1^2}{\rho^3} \frac{\cos(t\theta)}{\cos(\theta - t\theta)} \sqrt{J} \; dv \tag{3.27}$$

The elemental spherical volume $\quad dv = \rho^2 \sin\theta \, d\rho \, d\theta \, d\phi$ $\tag{3.28}$

substituting equation (3.28) in equation (3.27) gives

$$P_1 = \frac{Y_m}{\sqrt{3}} v_1 \rho_1^2 \int_{\theta=0}^{\alpha_e} \int_{\phi=0}^{2\pi} \int_{\rho_2}^{\rho_1} \frac{1}{\rho^3} \frac{\cos(t\theta)}{\cos(\theta - t\theta)} \sqrt{J} \; \rho^2 \sin\theta \; d\theta \, d\phi \, d\rho$$

$$= \frac{Y_m}{\sqrt{3}} v_1 \rho_1^2 \ln\!\left(\frac{\rho_1}{\rho_2}\right) \int_{\theta=0}^{\alpha_e} \int_{\phi=0}^{2\pi} \frac{\cos(t\theta)}{\cos(\theta - t\theta)} \sqrt{J} \; \sin\theta \, d\theta \, d\phi \tag{3.29}$$

since

$$\rho_1 = \frac{D_1}{2 \sin\alpha_e} \qquad \text{and} \qquad \rho_2 = \frac{D_2}{2 \sin\alpha_e} \tag{3.30}$$

substituting equation (3.30) into equation (3.29) gives

$$P_1 = \frac{Y_m v_1 D_1^2}{4\sqrt{3} \sin^2\alpha_e} \ln\!\left(\frac{D_1}{D_2}\right) \int_0^{\alpha_e} \int_0^{2\pi} \frac{\cos(t\theta)}{\cos(\theta - t\theta)} \sqrt{J} \; \sin\theta \, d\theta \, d\phi \tag{3.31}$$

The elemental spherical surface area at entry $\quad dA_1 = \rho_1^2 \sin\theta \, d\theta \, d\phi$

Equation (3.31) can be re-arranged to give:

$$P_1 = \frac{Y_m v_1 D_1^2}{4\sqrt{3}\,\sin^2\alpha_e}\,\ln\!\left(\frac{D_1}{D_2}\right)\int_0^{\alpha_\bullet}\int_0^{2\pi}\frac{\cos(t\theta)}{\cos(\theta - t\theta)}\,\sqrt{J}\,\frac{dA_1}{\rho_1^2} \qquad (3.32)$$

since

$$\rho_1 = \frac{R_1}{\sin\alpha_e}$$

substitute for $\rho 1$ in equation (3.32) gives:

$$P_1 = \frac{Y_m v_1 D_1^2}{4\sqrt{3}\,R_1^2}\,\ln\!\left(\frac{D_1}{D_2}\right)\int_0^{\alpha_\bullet}\int_0^{2\pi}\frac{\cos(t\theta)}{\cos(\theta - t\theta)}\,\sqrt{J}\,dA_1 \qquad (3.33)$$

Equation (3.33) can be written as

$$P_1 = Y_m\,V_1\,D_1^2\,\ln\!\left(\frac{D_1}{D_2}\right) f(s)$$

where

$$f(s) = \frac{1}{4\sqrt{3}\,R_1^2}\int_0^{\alpha_\bullet}\int_0^{2\pi}\frac{\cos(t\theta)}{\cos(\theta - t\theta)}\,\sqrt{J}\,dA_1 \qquad (3.34)$$

f(s) is the shape transformation factor since it is a function of α, t and the shape of the section rod. It cannot be further simplified, so it is evaluated numerically for a section rod having Ns number of sides, and is given by:

$$f(s) = \frac{Ns}{4\sqrt{3}\,R_1^2}\sum_{i=1}^{N}\sum_{j=1}^{M}\frac{\cos(t\theta)}{\cos(\theta - t\theta)}\,\sqrt{J}\,dA_1 \qquad (3.35)$$

3.2.8 Power losses in shearing the material

It was assumed that the shearing of material occurs at both the inlet and the outlet shear surfaces, causing velocity discontinuities in the material. A particle travels parallel to the drawing axis before shear at entry with a velocity V_1 but, after shearing, its velocity is defined by $\dot{U}$ ($\dot{U}_\rho$, $\dot{U}_\theta$, $\dot{U}_\phi$). Therefore, the worked material has been subjected to a velocity discontinuity, fig. 3.2, tangential to the shear boundary. The resultant velocity of the tangential components on both sides of the shear surface gives the velocity discontinuity.

The velocity discontinuities for the shear surfaces Γ_1 and Γ_2 are Δv_1 and Δv_2 respectively. In order for a particle to change direction the work material has been subjected to a velocity discontinuity Δv tangential to the shear boundary. The resultant velocity of the tangential components on both sides of the shear surface gives the velocity discontinuity, fig.3.3.

For the inlet shear surface

Resultant velocity component $\dot{U}_r$ tangential to the shear surface and the $\rho - \theta$ plane, $\dot{U}_\phi$, component of velocity normal to $\rho - \theta$ plane.

$$\Delta v_1 = \sqrt{\dot{U}_r^2 + \dot{U}_\phi^2}$$

where

$$\dot{U}_r = -V_1 \sin t\theta + \dot{U}_\theta \cos(\theta - t\theta) + \dot{U}_\rho \sin (\theta - t\theta)$$

Therefore

$$\Delta v_1 = \sqrt{ \dot{U}_\phi + (-V_1 \sin t\theta + \dot{U}_\theta \cos(\theta - t\theta) + \dot{U}_\rho \sin (\theta - t\theta))^2 }$$

Substituting for $\dot{U}_\phi$, $\dot{U}_\theta$ and $\dot{U}_\rho$ derived in equations (3.7), (3.8) and (3.9), gives

$$\Delta v_1 = V_1 \left[\left(\frac{\cos\theta}{\cos(\theta - t\theta)} \quad \frac{\tan\eta}{\cos\psi} \right)^2 + \left\{ -\sin\theta + \cos\theta \tan\psi + \cos\theta \tan(\theta - t\theta) \right\}^2 \right]^{1/2} \quad (3.36)$$

For the exit shear surface

Similarly for the outlet shear surface, the velocity before shear is ($\mathring{U}_\rho, \mathring{U}_\theta, \mathring{U}_\phi$) but, after shear, the particle travels parallel to the drawing axis with a velocity V_2. From the volume constancy i.e. equation (3.11) the resultant tangential velocity is

$$\Delta v_2 = \Delta v_1 \left(\frac{\rho_1}{\rho_2} \right)^2 \quad (3.37)$$

Thus the power consumed along these surfaces is given by:

$$P = \int_{\Gamma_1 \Gamma_2} \tau \left| \Delta v_s \right| \, ds \qquad = \int_{\Gamma_1} \tau \left| \Delta v \right| \, dA_1 + \int_{\Gamma_2} \tau \left| \Delta v \right| \, dA_2$$

since the von Mises yield criterion was assumed, $\tau = \dfrac{Y_m}{\sqrt{3}}$

The rate of work dissipation at the entry and exit shear surfaces is given by ;

$$\dot{w}_1 = \frac{Y_m}{\sqrt{3}} \int_{\Gamma_1} \left| \Delta v_s \right| \frac{dA_1}{\cos\theta} \quad (3.38)$$

$$\dot{w}_2 = \frac{Y_m}{\sqrt{3}} \int_{\Gamma_2} \left| \Delta v_1 \right| \left(\frac{\rho_1}{\rho_2} \right)^2 \frac{dA_1}{\cos\theta} \left(\frac{\rho_2}{\rho_1} \right)^2$$

$$= \frac{Y_m}{\sqrt{3}} \int_{\Gamma_2} \left| \Delta v_1 \right| \frac{dA_1}{\cos\theta} \quad (3.39)$$

Fig.3.2. A diagram showing the velocity discontinuity in the deformation zone

The total power to shear the material at the inlet and outlet shear surfaces is

$$\dot{w}_T = \dot{w}_1 + \dot{w}_2$$

$$= \frac{2}{\sqrt{3}} Y_m \int_{r_1} \Delta v_1 \frac{dA_1}{\cos\theta}$$

$$= \frac{2}{\sqrt{3}} Y_m V_1 R(s) \qquad\qquad (3.40)$$

where

$$R(s) = \int \left[\left(\frac{\cos\theta}{\cos(\theta - t\theta)} \frac{\tan\eta}{\cos\psi} \right)^2 + \left\{ -\sin\theta + \cos\theta \tan\psi + \cos\theta \tan(\theta - t\theta) \right\}^2 \right]^{1/2} \frac{dA_1}{\cos\theta}$$

This equation is expressed in terms of the associated conformally mapped elemental areas as follows;

$$= N_s \sum_{i=1}^{N} \sum_{j=1}^{M} \left[\left(\frac{\cos\theta}{\cos(\theta - t\theta)} \frac{\tan\eta}{\cos\psi} \right)^2 + \left\{ -\sin\theta + \cos\theta \tan\psi + \cos\theta \tan(\theta - t\theta) \right\}^2 \right]^{1/2} \frac{dA_1}{\cos\theta}$$

$$(3.41)$$

Since t is an arbitrary parameter, values of $-1 \leq t \leq 1$ will be used to select the value which gives an optimum shear surface for the given drawing conditions.
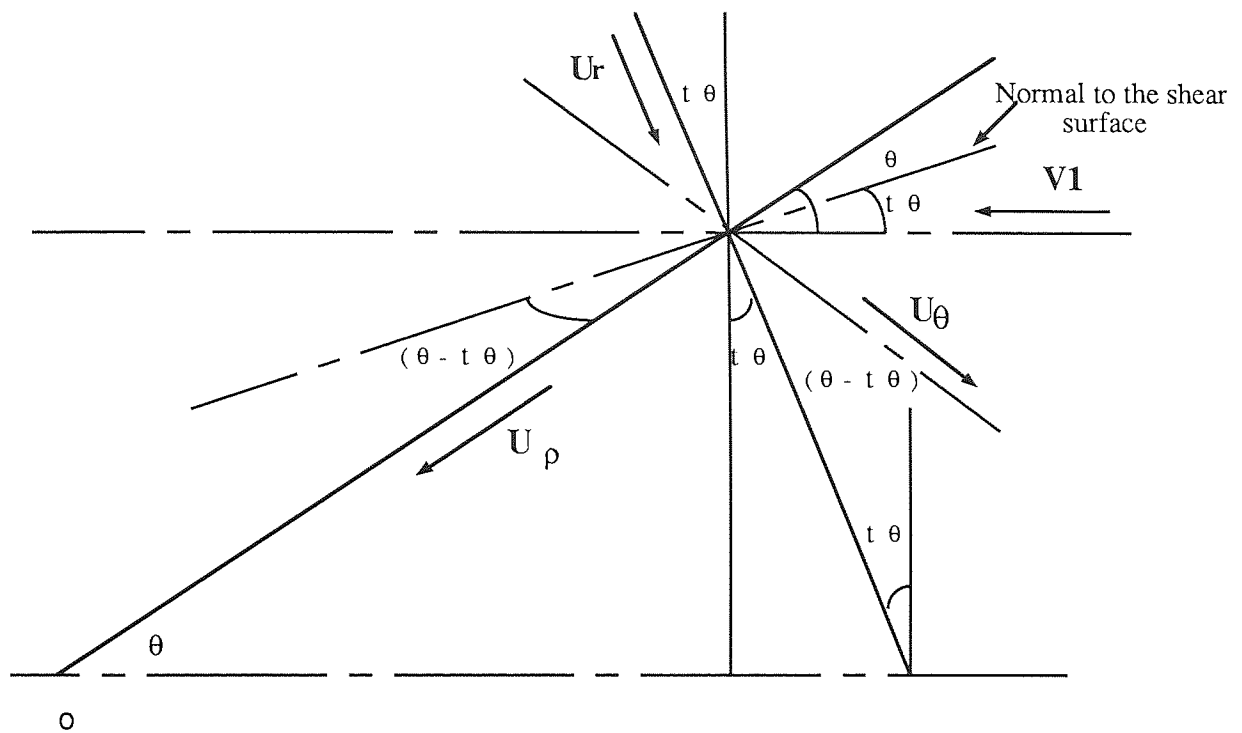
a) The flow model showing the resultant velocity compound (Ur) tangential to the shear surface.
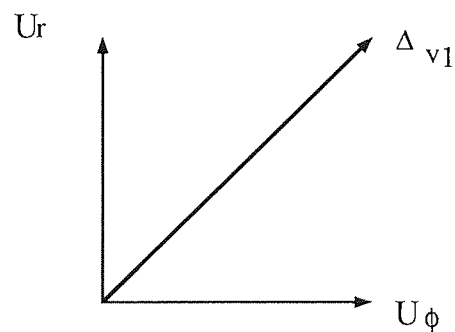
b) U_ϕ Velocity component normal to thre shear surface

Fig.3.3 . Flow model diagram showing velocity discontinuity of an element at the entry shear surface

3.2.9 Power Losses in Friction

Surface Γ_3

Assuming the condition of constant friction, where the shear stress of the material τ is given by :

$$\tau = \frac{m \sigma_o}{\sqrt{3}} \qquad \text{where } 0 \leq m \leq 1$$

the power required to overcome friction which occurs between the die and the workpiece is given by:

$$\dot{W}_f = \int \tau \left| \Delta v_f \right| ds_f \tag{3.42}$$

For a particular flow line in the deformation zone, the radial velocity is given by equation (3.3)

$$\Delta v_f = V_1 \left(\frac{\rho_1}{\rho} \right)^2 \frac{\cos(t\theta)}{\cos\eta \ \cos\psi \ \cos(\theta - t\theta)}$$

substituting the respective values into equation (3.42)

$$\dot{W}_f = \int_{\rho_2}^{\rho_1} \frac{m \, Y_f}{\sqrt{3}} V_1 \left(\frac{\rho_1}{\rho} \right)^2 \frac{\cos(t\theta)}{\cos\eta \ \cos\psi \ \cos(\theta - t\theta)} \ dA_f \tag{3.43}$$

where

dA_f is the area of an element of the contact surface from fig.3.4 .

$dA = d\rho \ dx$

$x = \rho \tan\psi \quad = \rho \sin\alpha \ \tan\phi$

hence

$dx = \rho \sin\alpha \ \sec^2\phi \ d\phi$

$\therefore \quad dA = \rho \sin\alpha \ \sec^2\phi \ d\phi \ d\rho$

101

substituting for dA_f in equation (3.43)

$$\dot{W}_f = \int_{\rho_2}^{\rho_1} \int_0^\beta \frac{m\, Y_f}{\sqrt{3}}\, V_1 \left(\frac{\rho_1}{\rho}\right)^2 \frac{\cos(t\theta)}{\cos\eta\ \cos\psi\ \cos(\theta - t\theta)}\, \rho\, \sin\alpha\, \sec^2\phi\, d\phi\, d\rho$$

$$\dot{W}_f = \frac{m\, Y_f}{\sqrt{3}}\, V_1\, \rho_1^2\, \ln\left(\frac{\rho_1}{\rho_2}\right) \frac{\cos(t\theta)}{\cos\eta\ \cos\psi\ \cos(\theta - t\theta)}\, \sin\alpha\, \tan\frac{\pi}{N}$$

since

$$\rho_1 = \frac{R_1}{\sin\alpha_e}$$

$$\therefore\quad \dot{W}_f = \frac{m\, Y_f}{\sqrt{3}}\, V_1\, \frac{R_1^2}{\sin\alpha_e}\, \ln\left(\frac{R_1}{R_2}\right)\, R(t)\, \tan\left(\frac{\pi}{N}\right) \tag{3.44}$$

where

$$R(t) = \frac{\cos(t\theta)}{\cos\eta\ \cos\psi\ \cos(\theta - t\theta)}$$

Surface $\Gamma 4$

The power loss due to friction in land portion of the die along surface of discontinuity $\Gamma 4$ for constant friction factor is given by:

$$\dot{W}_{f_L} = \frac{m\, Y_f}{\sqrt{3}}\, v_2\, EqR_2\, L\, N_s \tan\beta \tag{3.45}$$

Where

L = Length of land portion.

Geometrical relationships are explained in Appendix (A1).

102
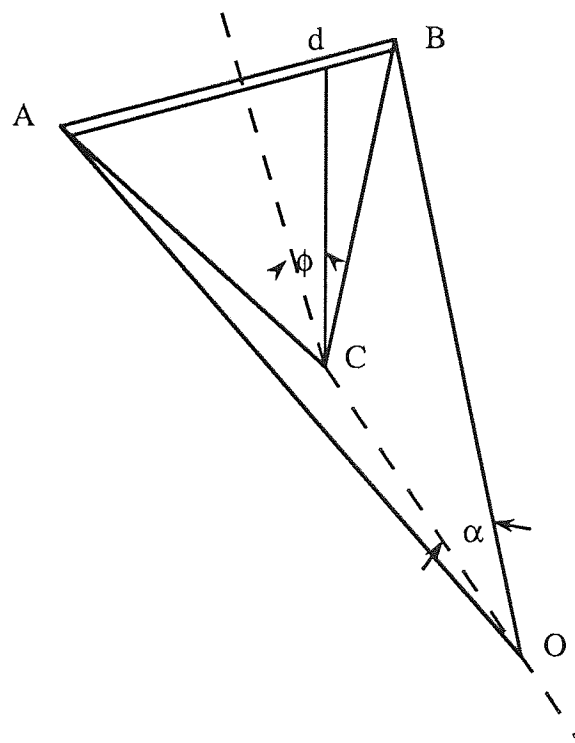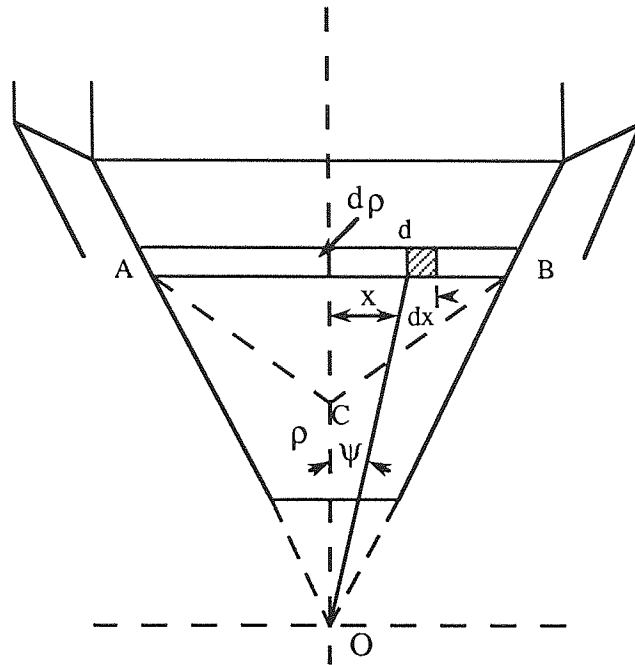
Fig. 3.4. Geometry of an element at the die-material interface.

3.2.10 Flow stress and temperature distributions in the deformation zone

The method used is a practical technique for determining the velocity field from the flow path which is found from conformally mapping the deformation zone. Strain rates are determined from the appropriate velocity gradients and, by integrating these strain rates with respect to time, the strains along the flow lines are determined.

In metal forming processes, such as elevated temperature section drawing, a basic understanding of the plastic behaviour of the tested metals at various temperatures and strain rates is required. It is therefore important to obtain flow curves in order to solve metal forming problems by numerical methods, If these calculations are carried out manually they are extremely time-consuming and, for this reason, a computer program in Matlab has been developed, see Appendix (A3). The stress-strain data used in the theoretical analysis can be found in Chapter 6.

It was assumed that adiabatic conditions prevail and that the work of internal deformation, shear losses, and redundant work are converted into heat and that the flow stress of the work material will be a function of strain, strain rate and temperature and is represented by;

$$\sigma_o = f\left(T, \varepsilon, \dot{\varepsilon}\right)$$

It is assumed that, for a given strain rate and temperature, the flow stress and strain can be related by the well known empirical equation

$$\sigma = B\,\varepsilon^n \qquad\qquad\qquad (3.46)$$

where B and n are constants which define the stress-strain curves and can be obtained from plotting log strain against log stress for the given values of strain rate and temperature.

The velocity-modified temperature is a single variable which is used to represent the opposing effects of strain rate and temperature in a single parameter, see section (1.7.2). It has been demonstrated that velocity-modified temperature is a useful parameter for collating flow stress data at high strain rates and over a wide range of strain rates and temperatures and it is defined as

$$T_{mod} = T \left(1 - k \ln \frac{\dot{\varepsilon}}{\dot{\varepsilon}_o} \right) \tag{3.47}$$

It is possible, for a given choice of $\dot{\varepsilon}_o$, to select a value of k so that, when stress is plotted against T_m, a smooth curve will result. In some cases $\dot{\varepsilon}_o$ was taken as 1 or 2 /s, the values of k selected to obtain a smooth curve were 0.08 / 0.09 for steel, these values being obtained by trial and error.

The values of B and n are plotted against velocity-modified temperature. For given values of strain rate and temperature, the flow stress can now be found in the following way; the strain rate and temperature values are substituted in equation (3.47) to give T_m and the corresponding values of B and n found from the curves (represented mathematically). These are then used together with the strain in equation (3.46) to give the flow stress. However, since full stress-strain data at elevated temperatures are obtained experimentally, the complete data are stored in the shape of polynomials and used directly to obtain the mathematical modelling required for this process. However should this technique prove to be negative, the former would be used.

105

To establish the temperature rise due to deformation and friction, the deformation zone is subdivided into several regions and, for each individual region, the process is assumed temporarily to be isothermal. Initially, a kinematically admissible velocity field was selected: at each subsequent step, new values of the velocity field, strains, strain rates, temperature and the corresponding values of the flow stress which change accordingly, were calculated. The temperature rise due to plastic and frictional work in each region is determined by successive approximations, and, step by step, the procedure is repeated for the next region in the line until the entire deformation zone is covered.

For the purpose of these calculations, the deforming zone, i.e. the distance between the inlet and outlet surfaces, was divided three-dimensionally, making used of the already available division of the inlet and outlet sections into sectors and triangles as shown in fig.3.5.

Calculations of Heat Generation

3.2.10.1 Temperature increase due to deformation work

When a particle travels from nodal position 1 to nodal position 2 along a flow line in fig(3.5), work is done and this work will be dissipated as heat. The temperature rise due deformation work refrred to in section (1.83) at the nodal position 2 is given as:

$$\Delta T_{d_2} = \frac{\sigma \, \dot{\varepsilon} \, \Delta t}{J \, c \, \rho} \tag{3.48}$$

this can be written as

$$\Delta T_{d_2} = \frac{\sigma \, \Delta \bar{\varepsilon}}{J \, c \, \rho}$$

where

$$\sigma = \frac{1}{2}\left(\sigma_{node1} + \sigma_{node2}\right)$$

$\overline{\Delta\varepsilon} = \dot{\varepsilon}\,\Delta t$ is the effective strain generated during time interval Δt

= equivalent mean strain between the nodal positions 1 and 2

Therefore the change in temperature in the deforming zone is given by:

$$\Delta T = \frac{\int_{\varepsilon_1}^{\varepsilon_2} \sigma \, d\varepsilon}{J \quad c \quad \rho}$$

with all the mechanical work being assumed to be converted into heat and the specific heat and density of the material assumed to be independent of temperature.

3.2.10.2 Temperature rise due to frictional work

The temperature increase due to friction between workpiece and die can be written as:

$$\Delta T_{f_2} = \frac{m \, \sigma \, v \, A \, \Delta t}{\sqrt{3}\, J \, c \, \rho \, V} \tag{3.49}$$

It is assumed that each arc Na represents a surface of a sphere

elemental spherical volume $dv = \rho^2 \sin\theta \, d\theta \, d\phi \, d\rho$

$\therefore$ volume of a sphere $= \int_{\rho_2}^{\rho_1} \rho^2 \sin\theta \, d\theta \, d\phi \, d\rho$

$\therefore$ $V = \int_{\rho_2}^{\rho_1} 2\,\pi\left(\cos\theta(2) - \cos\theta(1)\right) \rho^2 \, d\rho$

$= 2\,\pi\left(\frac{\cos\theta(2) - \cos\theta(1)}{3}\right) \rho_{(1)}^3 - \rho_{(2)}^3$

107
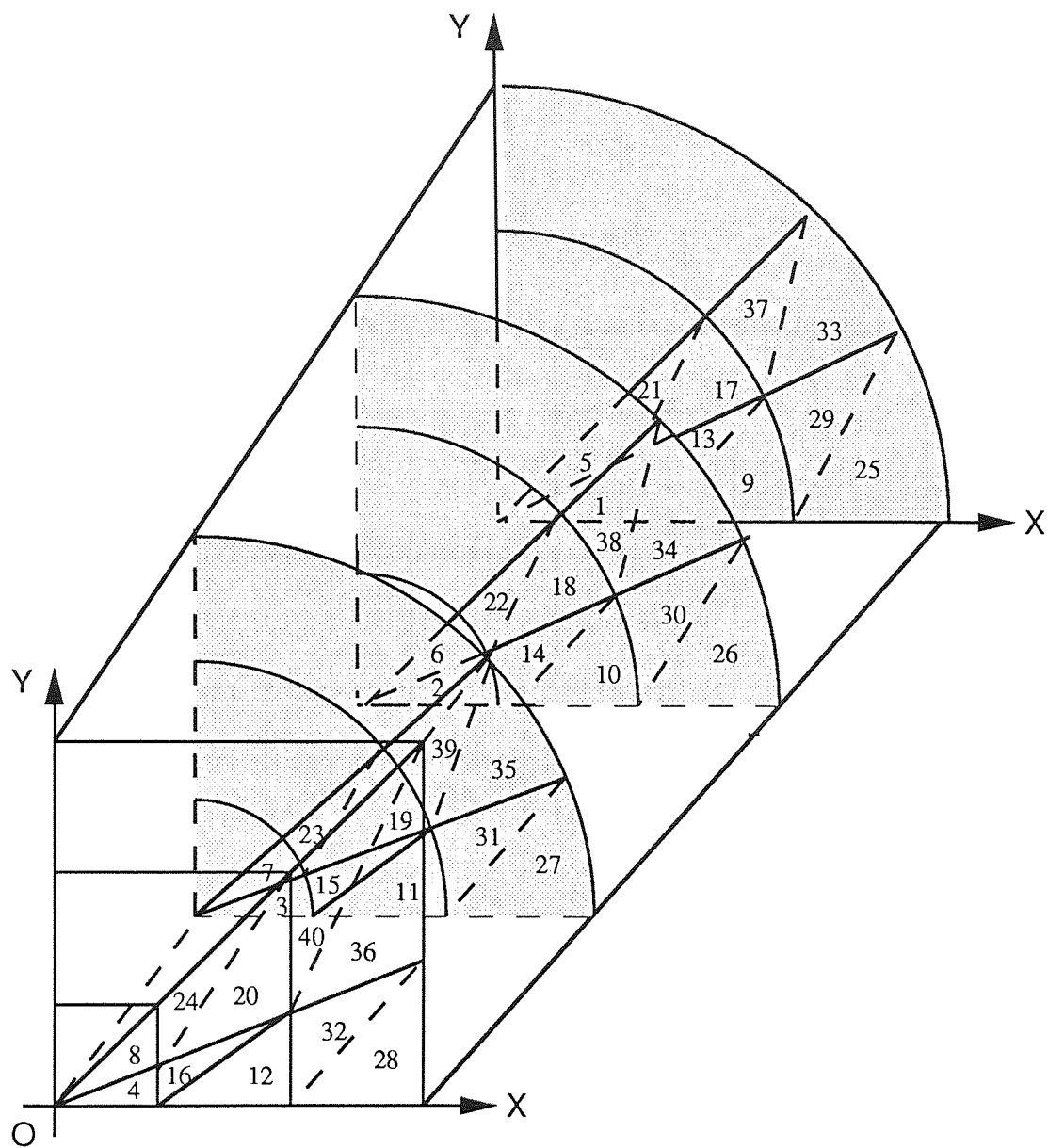
Fig. 3.5. The division of the deformation zone for computation purposes

dA = an element of the contact surface (section 3.2.9 , fig.3.4.)

$$= \rho \sin\alpha \sec^2\phi \, d\phi \, d\rho$$

$$\therefore \quad A = \int_0^{\frac{\pi}{N}} \int_{\rho_2}^{\rho_1} \rho \sin\alpha \sec^2\phi \, d\phi \, d\rho$$

$$= \left(\rho_{(1)}^2 - \rho_{(2)}^2 \right) \frac{\sin\alpha \, \tan^\pi\!/_N}{2}$$

During a time interval Δt a particle moves a small radial distance $\Delta\rho$; the velocity is given by:

$$v = \frac{\Delta\rho}{\Delta t}$$

Substitute for V, A and v in equation (3.49)

$$\Delta T_{f_2} = \frac{m \, \sigma \dfrac{\Delta\rho}{\Delta t} \sin\alpha \, \tan\dfrac{\pi}{N} \left(\dfrac{\rho_{(1)}^2 - \rho_{(2)}^2}{2} \right) \Delta t}{\sqrt{3} \, J \, c \, \rho \, 2\pi \dfrac{\left(\cos\theta(2) - \cos\theta(1) \right)}{3} \left(\rho_{(1)}^3 - \rho_{(2)}^3 \right)}$$

since $\quad \Delta\rho = \rho_{(1)} - \rho_{(2)}$

where (1) and (2) represent two points successively in the deformation zone. Therefore,

$$\Delta T_{f_2} = \frac{3 \, m \, \sigma \, \sin\alpha \, \tan\dfrac{\pi}{N} \left(\rho_{(1)}^2 - \rho_{(2)}^2 \right) \left(\rho_{(1)} - \rho_{(2)} \right)}{4\pi \sqrt{3} \, J \, c \, \rho \left(\cos\theta(2) - \cos\theta(1) \right) \left(\rho_{(1)}^3 - \rho_{(2)}^3 \right)} \qquad (3.50)$$

3.2.10.3 Mean yield stress calculation

Having established the flow stress and equivalent strain distribution in the deforming zone, the mean yield stress $Y_{m(J)}$ for a particular flow line can be found by plotting the flow stress against equivalent strain for a certain flow line, and the area under the curve

can be integrated numerically. Thus the mean yield stress for a particular flow line is given by:

$$Y_m = \frac{1}{\varepsilon_1 - \varepsilon_0} \int_{\varepsilon_0}^{\varepsilon_1} \bar{\sigma} \, d\bar{\varepsilon}$$

$$Y_{m\,(J)} = \frac{\displaystyle\int_{\bar{\varepsilon}_{(1,J)}}^{\bar{\varepsilon}_{(J)}} \bar{\sigma}_{(I,J)} \, d\bar{\varepsilon}_{(I,J)}}{\bar{\varepsilon}_{(J)} - \bar{\varepsilon}_{(1,J)}}$$

(3.51)

ε_1 = Effective mean strain at shear surface Γ_2

ε_0 = Effective mean strain at shear surface (Γ_1 = zero)

Therefore mean yield stress for the deformation zone, is given by:

$$Y_d = \frac{\displaystyle\int_{\bar{\varepsilon}_{T(J)}}^{\bar{\varepsilon}_{T(1)}} Y_{m\,(J)} \, d\bar{\varepsilon}_{T\,(J)}}{\bar{\varepsilon}_{T\,(1)} - \bar{\varepsilon}_{T\,(J)}}$$

(3.52)

Equations (3.51) and (3.52) were integrated numerically. The value of the mean yield stress Y_f at the outer surface of the die was obtained in the same way using the outer surface of the deforming zone, where friction takes place.

3.2.11 The process modelling programs

A computer program was developed to solve equations 3.24, 3.26, 3.35, 3.41, 3.44, 3.48, 3.50, 3.51, and 3.52 numerically. The detailed computer program is given in Appendix (A3).

3.2.11.1 The computer program

The flow chart for the computer program shown in fig.3.6. consists of :

- input of various parameters and constants.
- the main program including major and minor 'for' loops.
- three "data" programmes.
- three sub-programmes.
- print-out statements of results.

The main purpose of the computer program is to obtain the following

- the conformal mapping of the deformation zone.
- calculation of the flow path parameters.
- the optimisation of the entry and exit shear surfaces.
- calculation of the theoretical effective mean strain and the effective mean strain-rate.
- establishing the temperature distribution in the deforming zone.
- using stress-strain data at elevated temperature to obtain the flow stress distribution in the deformation zone.
- estimation of the internal power of deformation.
- estimation of power losses due to the shearing at the entry and exit planes.
- estimation of power losses due to friction between workpiece-tool interface.
- finally, the tabulation of the total power of deformation, mean drawing stress, and other variables such as reduction of area, speed of drawing, die semi-cone angle, coefficient of friction, and the drawing temperature, as well as strain, strain-rate, and temperature distribution in a three dimensionally deforming zone.

The complete program is presented in Appendix (A3). Table 3.1 presents a sample of results obtained for various parameters.

Fig.3.6. The layout of the computer program for a 3D process modelling.

Flowchart:

START
↓
Input dimensions, speed, geometry of pass , reduction of area , shape parameters and other constants.
↓
Divide the entry cross-section into equal bands
↓
For K = 1 : CB - 1
↓
Division of band area into sectors
↓
Division of sectors into a small and large triangles
↓
Refering areas of triangles into outlet section
↓
For K = 1 : CB
↓
Establish the x and y co-ordinates along across flat lengths
↓
2

Second column:

2
↓
For K = 2 : CB
↓
Establish the co-ordinates along diagonal length
↓
For i = 2 : CB
For j = 2 : ES
↓
Mapping the deformation zone
↓
For i = 2 : CB
For j = 2 : ES
↓
Calculation of the centroid of the triangles at outlet
↓
Calculation of the centroid of the triangles at inlet
↓
3

```
        ( 3 )                                    ( 4 )
          │                                        │
          ▼                                        ▼
┌──────────────────────┐              ╭─────────────────────────╮
│   Input the drawing   │      ┌──────┤   For ii = 1 : increment │
│     temperature       │      │      ╰─────────────────────────╯
└──────────────────────┘    ( 8 )                 │
          │                                        ▼
          ▼                           ┌─────────────────────────┐
╭──────────────────────╮             │ Division of the deformation│
│  For  EQ = 2 : 1 : 20 │             │  zone into a grid system  │
│                       │──┐          └─────────────────────────┘
│  For FR = 0 : 0.1 : 0.3│  │                      │
╰──────────────────────╯ ( 6 )                     ▼
          │                           ┌─────────────────────────┐
          ▼                           │    Calculation of the    │
╭──────────────────────╮             │  effective strain-rate &  │
│    For  i = 3 : CB    │             │    effective strain       │
│                       │             └─────────────────────────┘
│    For  j = 2 : ES    │                          │
╰──────────────────────╯                          ▼
          │                           ┌─────────────────────────┐
          ▼                           │   Calculation of the flow │
┌──────────────────────┐             │         stress           │
│ Generate  equivalent  die │         └─────────────────────────┘
│ semi angle and coefficent │                     │
│       of friction        │                      ▼
└──────────────────────┘             ┌─────────────────────────┐
          │                           │ Calculation of temperature│
          ▼                           │  rise due to deformation  │
┌──────────────────────┐             └─────────────────────────┘
│   Computation of the  │                          │
│     velocity field    │                          ▼        Yes   ┌──────────────┐
└──────────────────────┘                       ◇ is ◇──────────→│ Calculation of│
          │                                   i = CB-1           │ temperature rise│
          ▼                                       ◇              │ due to frictional│
┌──────────────────────┐                          │              │     work      │
│   Optimisation of the │                          ▼              └──────────────┘
│  inlet and outlet shear│                    ╭─────────╮               │
│      surfaces         │                     │  Δ T_f  │               │
└──────────────────────┘                      ╰─────────╯               │
          │                                        │                     │
          ▼                                        ▼                     │
╭──────────────────────╮             ┌─────────────────────────┐
│    For i = 3 : CB     │             │   New temperature        │
│                       │──┐          │  TT = T + Δ T_f + Δ T_d  │
│    For j = 2 : ES     │  │          └─────────────────────────┘
╰──────────────────────╯ ( 7 )                     │
          │                                        ▼
          ▼                                     ( 5 )
        ( 4 )
```

$$\text{For } EQ = 2 : 1 : 20$$
$$\text{For } FR = 0 : 0.1 : 0.3$$
$$\text{For } i = 3 : CB$$
$$\text{For } j = 2 : ES$$
$$\text{is } i = CB-1$$
$$\Delta T_f$$
$$TT = T + \Delta T_f + \Delta T_d$$

```
            ( 5 )
              │
              ▼
   ┌─────────────────────┐
   │  Calculation of the new │
   │      flow stress        │
   └─────────────────────┘
              │
              │
   ┌─────────────────────┐
( 8 )│  New temperature NT = TT │
  ▲  │   for next nodal point   │
  │  └─────────────────────┘
  └──────────┤
              │
   ┌─────────────────────┐
( 7 )│  Set temperature for a new │
  ▲  │   line in the grid system  │
  │  └─────────────────────┘
  └──────────┤
              │
   ┌─────────────────────┐
   │  Computation of internal │
   │   power of deformation   │
   └─────────────────────┘
              │
   ┌─────────────────────┐
   │  Computation of frictional │
   │     and shear powers       │
   └─────────────────────┘
              │
( 6 )┌─────────────────────┐
  ▲  │  Computation of the mean │
  │  │      draw stress         │
  └──└─────────────────────┘
              │
   ┌─────────────────────┐
   │   Tabulation of results  │
   └─────────────────────┘
              │
              ▼
        ╭───────────╮
        │           │
        │    END    │
        │           │
        ╰───────────╯
```

Test results

Test material   : Mild steel   Test temperature   : 20 deg C

Test speed   : 6 m/s   Coefficent of friction : 0.05

Section   : Square   Reduction of area   : 36.34 %

Die semi-angle :12

Nodal position	Temperature deg. C	Effective strain rate	Effective mean strain	Flow stress N/mm^2
1	20	0	0	-
2	95	1	0.9	599
3	258	1.3	1.85	582
4	429	1.6	2.9	517
5	20	0	0	-
6	95	1	0.9	599
7	259	1.3	1.86	581
8	430	1.6	2.9	516
9	20	0	0	-
10	48	0.43	0.38	524
11	112	0.53	0.79	587
12	186	0.68	1.23	559
13	20	0	0	-
14	55	0.52	0.46	545
15	136	0.65	0.96	587
16	226	0.83	1.5	595
17	20	0	0	-
18	48	0.43	0.38	524
19	113	0.54	0.79	587
20	187	0.69	1.24	558
21	20	0	0	-
22	55	0.52	0.47	545
23	37	0.66	0.97	587
24	227	0.84	1.5	594
25	20	0	0	-
26	39	0.29	0.26	488
27	80	0.37	0.54	582
28	131	0.47	0.85	589
29	20	0	0	-
30	40	0.33	0.29	489
31	87	0.41	0.6	572
32	143	0.52	0.94	584
33	20	0	0	-
34	39	0.29	0.26	489
35	81	0.37	0.55	582
36	133	0.47	0.86	588
37	20	0	0	-
38	41	0.33	0.29	489
39	88	0.41	0.61	572
40	144	0.52	0.95	583

Drawing stress : 440 N/mm^2   Ym = 421 N/mm^2
                                     Yf = 553 N/mm^2

Table. 3.1. Tabulated results of the three dimensional modelling

116

CHAPTER FOUR

EXPERIMENTAL EQUIPMENT AND DRAW PROCESS MATERIALS

Chapter Four

4.0 Experimental Equipment and Draw Process Materials

4.1 Experimental equipment

      3.1.1 The bull block

      3.1.2 Die-holder assembly

      3.1.3 Induction heating equipment

      3.1.4 The lubricator assembly

      3.1.5 Wire and die cooling system

4.1.1 Horizontal bull block

The drawing machine used is a horizontal bull-block, which has a 450 mm diameter steel drum with a 450 mm long working surface, mounted in a fabricated steel frame. The drum is supported on a steel shaft which is mounted horizontally and supported by heavy-duty bearing and driven through an enclosed wormgear, Plate 4.1. Attached to the bull-block is a traversing table which is mounted on the guides and is driven by a lead screw to give approximately 4 mm traverse per revolution of the drum. The steel traversing table was extended and used for mounting the straightening rolls, the lubricator, and the air wipe assemblies, the heating coil and the die holder. In order to prevent the traverse table from bending, a support, which is mounted on a wheel arrangement, is fitted to the end of the table to facilitate its movement with respect to the lead screw. The set-up of the equipment used in the laboratory is shown diagrammaticaly in fig.4.1, and Plate 4.2

The block was designed for drawing speeds of up to 146 m/min, which were selected by means of a four-speed gear box, and is described in detail by Winsper[125].
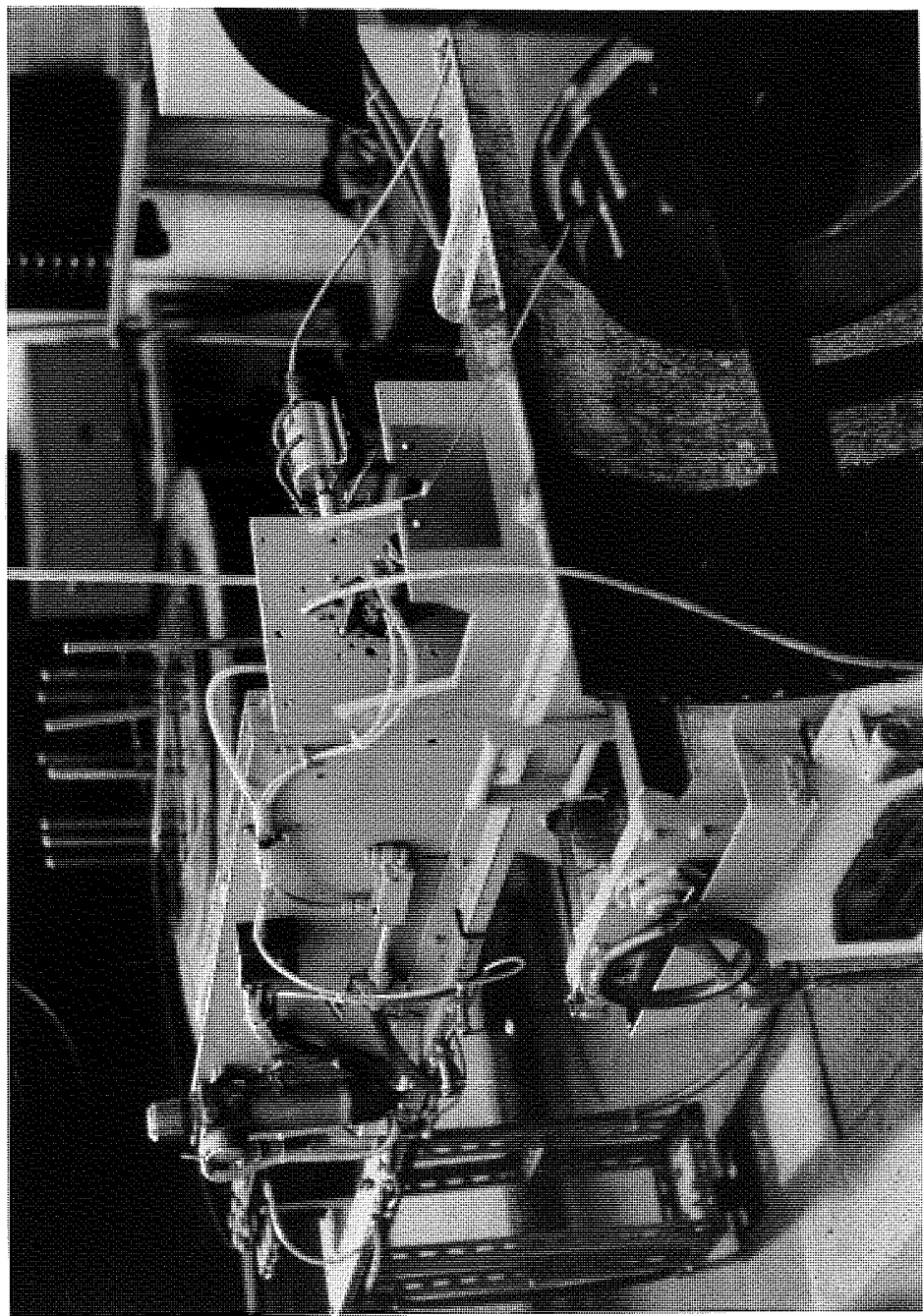
Plate 4.1. The Horizontal Bull Block
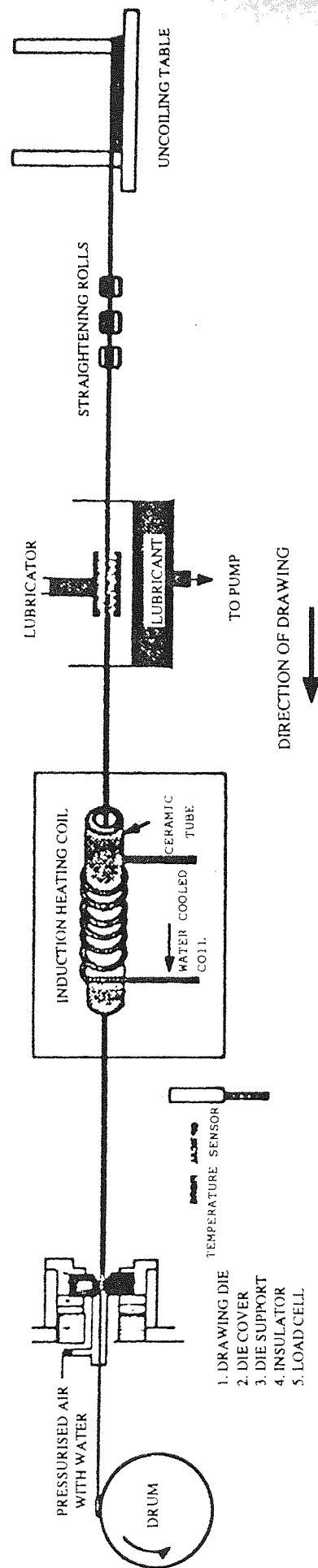
Fig. 4.1. Schematic diagram showing the layout of the equipment

UNCOILING TABLE

STRAIGHTENING ROLLS

LUBRICATOR

LUBRICANT

TO PUMP

DIRECTION OF DRAWING

INDUCTION HEATING COIL

CERAMIC TUBE

WATER COOLED COIL.

TEMPERATURE SENSOR

PRESSURISED AIR WITH WATER

DRUM

1. DRAWING DIE
2. DIE COVER
3. DIE SUPPORT
4. INSULATOR
5. LOAD CELL

119
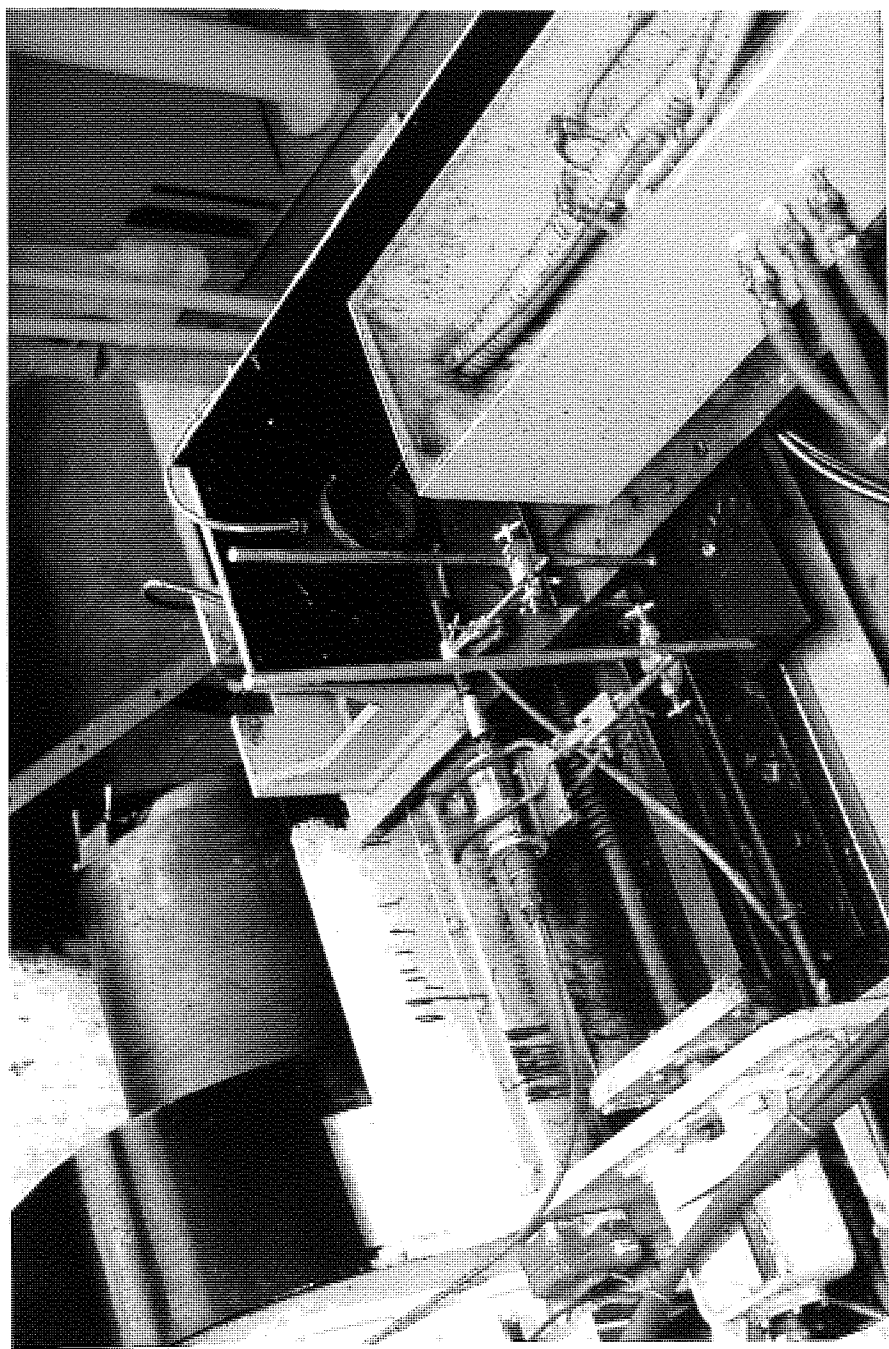
Plate 4.2. The Layout of the Equipment

120

The drum shaft is driven through a variable speed gear and a four speed gear box by a 11.2 kW squirrel cage induction motor. Gripping jaws are supplied for gripping wire up to 9.5 mm in diameter.

4.1.2 Induction heating

A solid state 20 TQ 50 generator which has an output of 20 kW at a nominal frequency of 50 kHz, manufactured by Radyne Ltd, is used, Plate 4.3. Matching load procedures are shown in Appendix (A4). The reasons for choosing induction heating for the research were:

- health and safety are improved since there are no explosive gaseous mixtures needing elaborate precautions, no noxious fumes, and no risk of burns from furnace casing.

- the time spent in heating the workpiece is much shorter than that spent in a radiant heater or a lead bath. As a result, the time available for scaling is reduced. Such scaling results in scrap and the accelerated wear of dies.

- since there are no combustion products in the heating region, the fast heating produces clean bars, virtually free of oxidation and decarburisation.

- the accurate temperature control, coupled with absence of scale, results in longer die life.

- since induction heating is rapid, it fits well into automated production lines.

- the rapid start allows the heater to be switched off for die changes, speed alterations, production hold-ups and for meal breaks, thus saving energy. The equivalent furnace takes a longer time to reach working temperature and is normally left running during breaks etc.
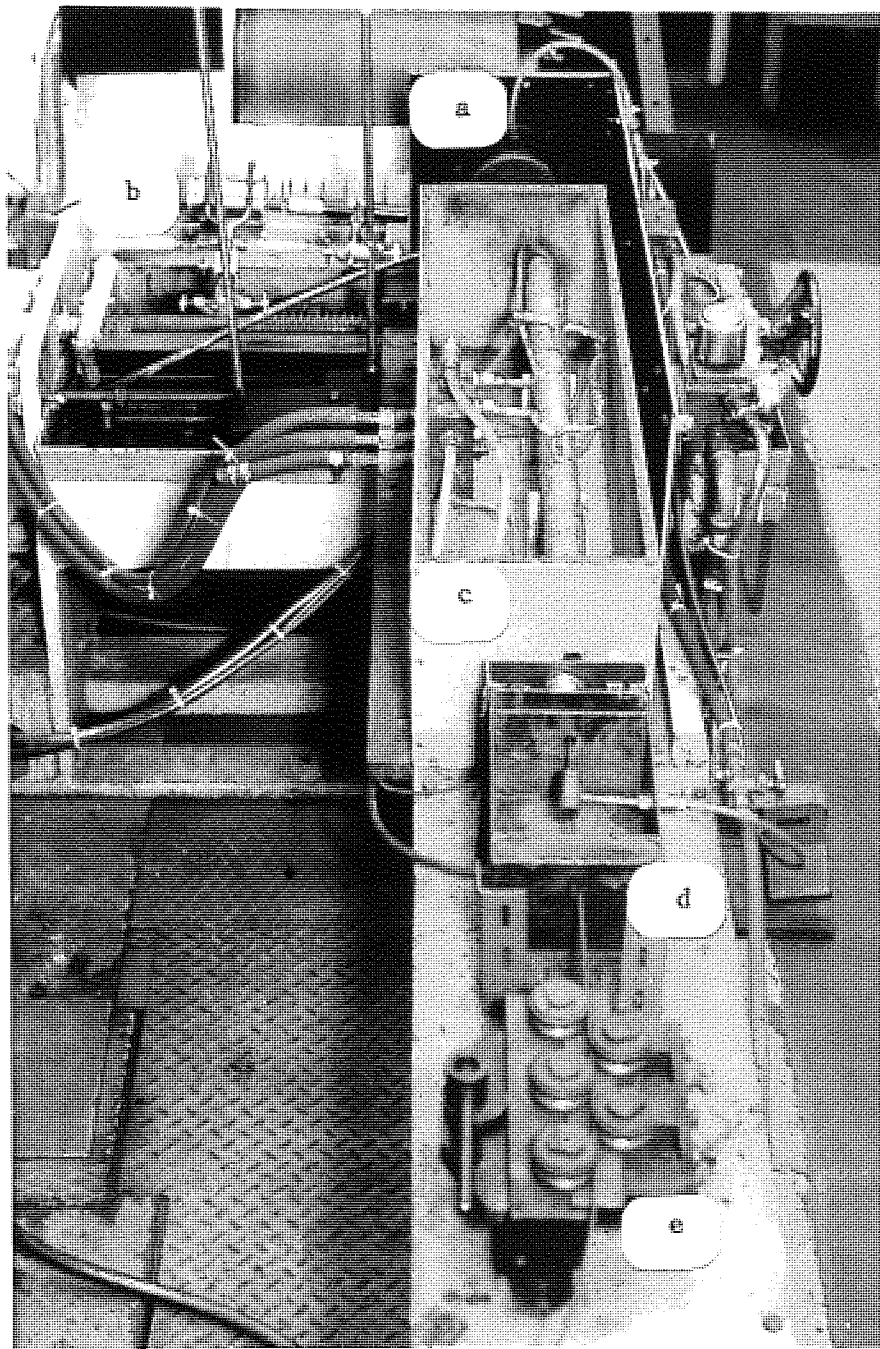
Plate 4.3. Details of the Equipment

a) Die Holder

b) Infra-red Detector

c) Induction Heater Coil

d) Lubricator and Air wipe

e) Straightening Rolls

4.1.3 Die-holder assembly

A schematic drawing of the die-holder assembly is shown in fig.4.2; it is basically made up of five components.

1   die-holder

2   die-holder cover

3   die support

4   insulator (Sindanyo)

5   loadcell

The main purpose of the die holder is to support the loadcell so that the drawing force could be measured. It was designed by Loh[91], so that it could be mounted into a block which is welded at right angles to the steel traversing table. The die is held in position by the use of a three-pin supporting system, these pins situated at 60°, 120°, and 180° so that they provide a strong support to the die. The die support is fitted with an 'O' ring around it is circumference to prevent the die cooling water from penetrating into the loadcell. A semi-circular tube is welded on to the die support to drain away the water from the wire cooling system. Most of the parts and the 'O' rings had to be changed because they allowed cooling water to penetrate to the load cell, then covered in silicone grease to reduce the friction between the various parts and also as a protection against water. The die-holder cover was screwed to the die-holder to hold the die in position, it also had two 'O' rings to prevent cooling water reaching the hot wire before it entered the die. The loadcell was placed against the welded block, behind a disc of Sindanyo acting as a heat insulator from the hot drawing die, and to maintain the temperature of the strain gauges fitted in the loadcell at an acceptable level in order to obtain a reasonable accuracy when measuring the drawing load.
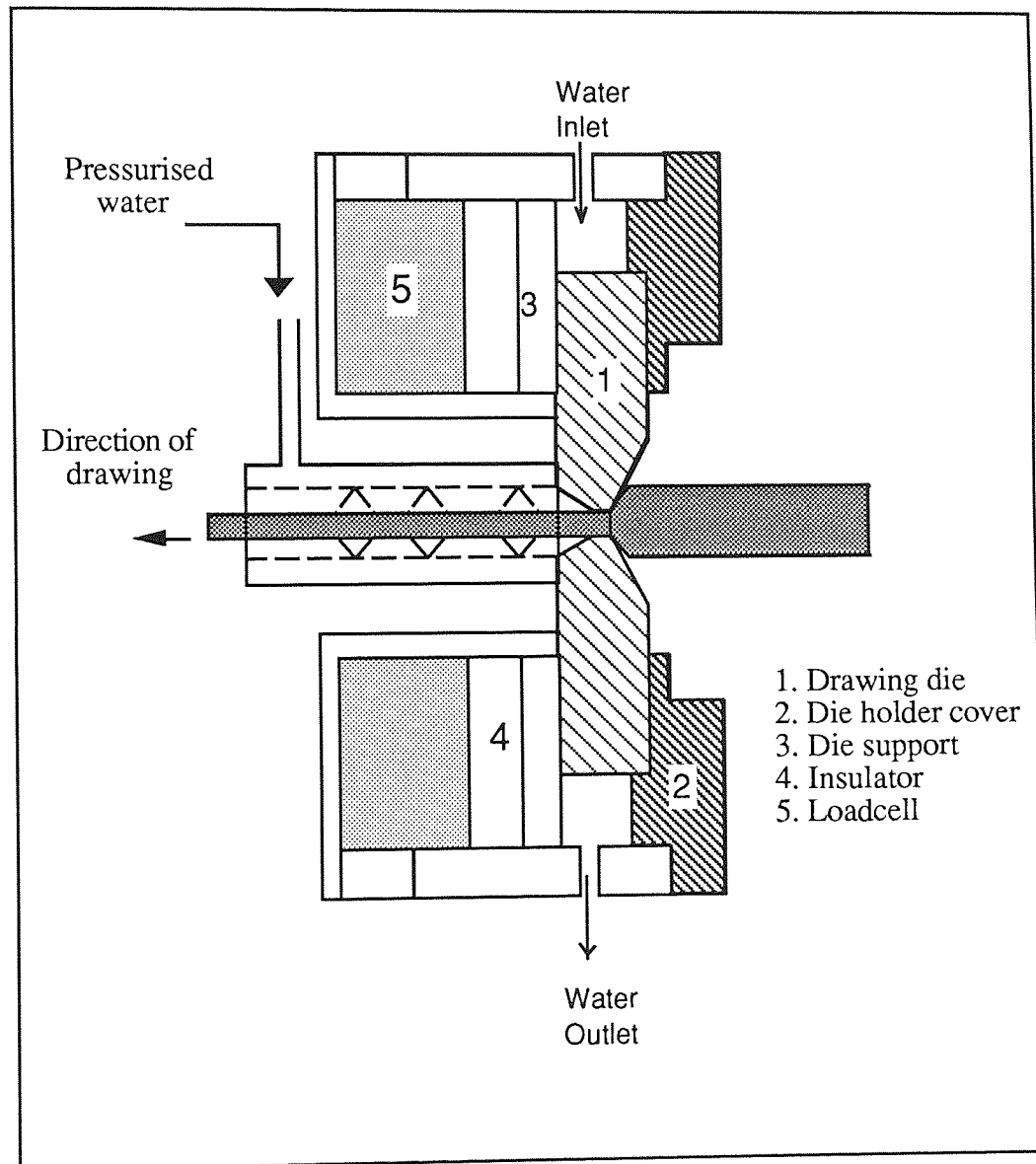
Fig.4.2. Schematic diagram of the drawing die holder

4.1.4 Lubricator assembly

The most successful method of lubrication is by spraying the lubricant on to the wire; this provides an even, continuous coating of the graphite-based lubricant. The lubricant mixture is pumped into the spray arrangement, then flows over the wire. The thickness of the coating depends up on the speed of the wire or the flow rate of the lubricant. Thus, the flow of lubricant is controlled by a valve before it reaches the spraying system. The excess lubricant is collected in a steel container, from where it is recirculated. The use of a gear pump in the system ensures good mixing of the lubricant mixture used in the testing. The lubrication assembly used is show in fig.4.3.

4.1.5 Wire and die cooling assembly

An essential part of the process of hot wire drawing is the cooling of the drawn wire, particularly when drawing at the higher temperatures and reductions of area when the strength of the drawn wire drops, and local necking, followed by rupture of the wire, occurs.

A direct cooling system which employs spray jets is used. Water is introduced on to the wire immediately it leaves the drawing die, where the temperature is highest, and only left in contact for a short time. It is important that the cooling water is prevented from splashing into the die, causing sudden cooling and quenching, which will result in thermal stresses being set up in the die and even if a high thermal shock resistance material is used, cracks will appear. The cooling water is prevented from reaching the die by the use of an air jet which will ensure that excess water is kept away from the die.

The system employed fig.4.4, consisting of a spray of water atomised by compressed air at approximately 276 kN/m^2 and an air regulator to control the compressed air, which is delivered to an air and water mixer. This fine, high pressure spray quenches

the drawn wire, increasing its strength and rendering it easier to handle; compressed air alone is used to drive excess water away from the die during elevated temperature drawing. Cooling of the die assembly is achieved by water which is fed into the top of the die holder and circulates round the drawing die before draining away from the bottom of it, as shown on the die holder diagram fig.4.2.
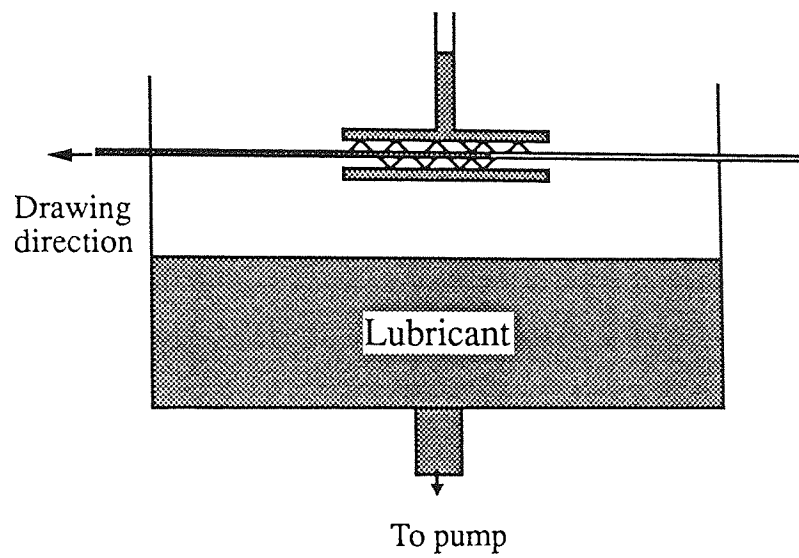
Fig.4.3. The lubricating assembly
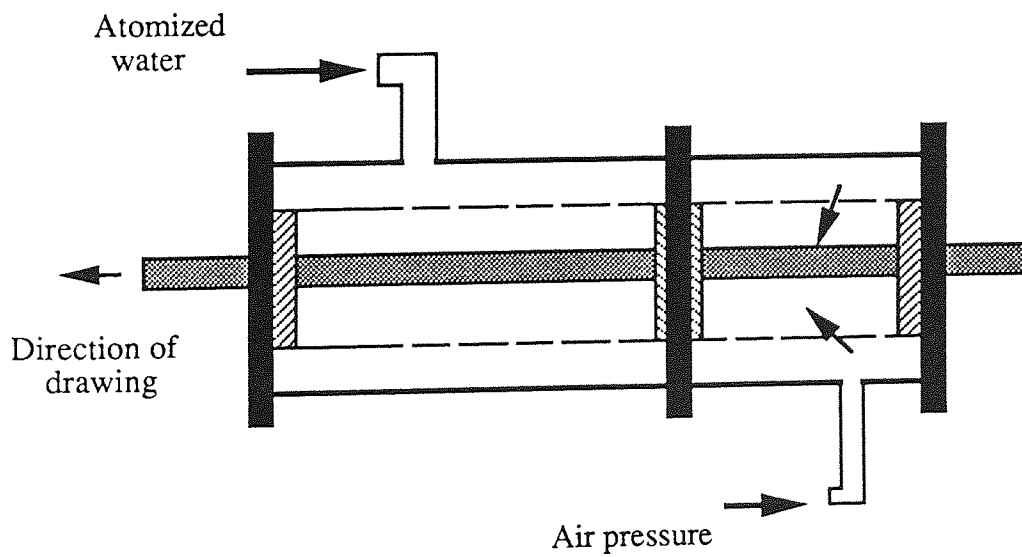
Fig.4.4. Diagram of the cooling system

4.2 Draw process materials

Each metal forming process is different, presenting many parameters and problems to study, including the shape of the product produced. Some of these parameters are variables of product material, forming temperature, lubrication and forming speed, making it difficult to select materials for particular processes. This, unfortunately, often means that each tool design and material has to be proved and tested for each process, forming condition and geometry.

In commercial production, the most important qualities required from a metal forming tool are wear resistance for long life and resistance to both cyclic and suddenly applied loads. Unfortunately, the resistance to abrasive wear, the most predominant wear mechanism in metal forming, and the resistance to fast fracture and fatigue are incompatible for most materials. The other significant properties of a tool material are those associated with its surface and ability to transfer heat.

Quite clearly, it is difficult to specify particular tool materials for individual processes, workpiece and forming conditions. To prove and design a tool and tool material for a particular application requires, at present, specific knowledge of the process and its traditions, and a time-consuming design and trial period.

However, the rapid growth in technology, especially in the computer field led to the establishment of specially orientated packages that can be used to perform different tasks with a high grade of accuracy. Packages such as Finite Element Method (FEM) can be used to test and verify different materials for different purposes in a relatively short time with no time wasted in trial and error techniques. The finite element analysis of polygonal dies at elevated temperatures is presented in Chapter eight.

4.2.1 Selection of die materials

The selection of die materials for metal forming processes is extremely important. This is due to the fact that different materials have different life time. Therefore, the die should be carefully made from a well chosen material to provide an adequate die life at an acceptable cost. However, there are three factors commonly considered as criteria whenever a die material is selected. These factors are the process, type of die loading and the mechanical properties of the die material.

There are several factors that effect die conditions and bring about a need for a replacement. These reasons include changes in dimensions and deterioration of the surface finish which are both caused by die wear, breakdown of lubricant, and by the thermal fatigue, which takes place on the surface of the die during the hot forming process. This thermal fatigue is created from cyclic yielding of the die surface due to the contact with the hot forming material which causes the surface layers to expand and because of the very steep temperature gradients, the surface layers are subject to compressive stresses. At high temperatures, these compressive stresses may cause the surface layers to deform. The tension will be created after the die surface cools down, and the stress reversal occurrs. After repeated cycling in this way, fatigue will cause the formation of a crack pattern and, finally, breakage or cracking which is caused by the overloading of the die and the high stress concentration.

4.2.2 Drawing dies

In section drawing, which is a steady state process of the reduction of a continuous workpiece through a shaped orifice, the tool material has to resist wear, heat build-up and fatigue at the entry angle. Variables such as workpiece material, lubricant, forming temperature, drawing speed, product and die geometry, make it difficult to generalise and optimise die materials for any forming process. The die materials used include chromium carbide, which is commonly used for extrusion tooling and forging dies

129

because its toughness and ductility give resistance to fracture, higher wear resistance and hot hardness[126], together with tungsten carbide, Stellite and Syalon, which is a member of the ceramic family and essentially consists of aluminium nitride, alumina and silicon nitride, chemical and mechanical properties for these materials are presented in Appendix (A4). Different die geometries are also used; these include die designs used by Basily and Sansome[53], conventional section drawing dies and others designed for this present work. These designs are illustrated in more details in Chapter eight and technical drawings are shown in Appendix (A4).

4.2.3 Test materials

The preliminary trials were carried out with mild steel, since it has excellent workability, a relatively low work hardening rate and is readily available since it is relatively inexpensive. The choice is in line with the previous research on the mechanics of drawing bars from round. Therefore, for comparisons to be drawn, mild steel is selected as the experimental metal. Another important point is the limitation of section drawing i.e. minimum and maximum reduction of area achievable. Thus, when the drawing procedures and limitations are understood for mild steel, the more difficult-to-draw materials are introduced. Boron steel and medium carbon steel were introduced in the second stage of the research in order to study further the limitations of section drawing and the advantages of elevated temperature drawing when dealing with relatively difficult to draw materials. The chemical compositions of the materials used are shown in Table 4.1.

4.2.4 Lubricants

Lubrication is a very important aspect of metal working processes, especially when the processes are being conducted at elevated temperature. In all metal working operations, the workpiece is constrained to flow in the required manner by the configuration of the tooling and frictional forces are generated at the interface between the workpiece and the

tooling. In some operations, the generation of friction forces is necessary for the process to work successfully e.g. rolling and Conform process. In other processes, frictional forces are a hindrance and result in large deformation forces, high tool stresses, inadequate flow and, frequently, poor surface finish. Under these conditions, a lubricant is necessary in order to reduce the effects of friction at the workpiece-tool interface. Lubrication is much more critical when the workpiece is being deformed at elevated temperatures.

Conventional liquid lubricants are not usually suitable at high temperature since they become thermally unstable and increasingly volatile. Most oils and greases show considerable oxidative or thermal degradation in the range 260 - 320°C. It is therefore necessary to look for other forms of lubricant for temperatures above 300°C.

4.2.4.1 Lubricant requirements

In the selection of materials for possible use as metal working lubricants in the temperature range 300 - 800°C, the following requirements should be considered:-

- the lubricant should be stable, unaffected by temperature, oxidation, repeated exposure to high pressure and the minor contamination which is normally unavoidable in industrial practice.

- it should not be corrosive to the product or the tooling.

- the possibility of removing the lubricant film without much difficulty after drawing, in order not to interfere with subsequent finishing operations such as painting, annealing, welding, and electro-deposition.

- ability to reduce the drawing force and die wear.

- it should be non-toxic and non-flammable.

- the cost of the lubricant should be compatible with its function. Where the cost of the raw material is low the cost of lubricant should be low.

Tests were conducted on different graphite-based lubricants supplied by Acheson Colloids Ltd including; Dag 2543, MolyDag 709 (which is used with a quick drying agent such as toluene) and MolyDag 15 details of the lubricants used are presented in appendix (A4).

MATERIAL	CONSTITUENTS										
	C	S	Si	P	Mn	Ni	Cr	Al	B	Mo	Ti
Mild steel	0.07	0.021	0.02	0.012	0.3	-	0.02	0.05	-	-	-
Boron steel	0.19	0.013	0.23	0.014	0.96	0.017	0.2	0.04	0.003	0.004	0.038
Medium carbon steel	0.37	0.022	0.19	0.014	0.69	0.01	0.03	-	-	-	-

Table 4.1. Chemical compositions of mild steel, boron steel and medium carbon steel

CHAPTER FIVE

INSTRUMENTATION AND CALIBRATION
OF MEASURING EQUIPMENT

Chapter Five

5.0 Instrumentation and Calibration of Measuring Equipment

5.1 Data collection and analysis used previously

5.1.1 Ultraviolet recorder

In an ultraviolet (uv) recorder, the amplified signal voltage deflects a miniature mirror galvanometer, which directs a beam of ultraviolet light on to moving light-sensitive paper to produce a trace of the signal variation with time. The uv recorder is generally a multi-channel system with up to one input channel per centimetre of paper width. Recorders with 6,12, and 20 channels are the most common. A grid is put on to the paper by fixed light beams within the recorder to assist in the analysis of the traces. Because of the exposure time required for the light-sensitive paper, the uv recorder as an on-line method of display is restricted to low frequency tests.

5.1.2 Storage of data

The trace produced can be retained as a permanent record of the test and for post-processing purposes. However, since there is a gradual degradation of the trace caused by continual exposure to daylight, the trace should be chemically fixed for permanence. The reduction of the trace into a form suitable for post-processing must be manual, the acquisition of any detailed information is tedious and requires good on-site documentation.

5.2 Installation of new instrumentation system

```
Elements of Data
Acquisition and Analysis
Systems

[ Data Capture      [ Data Analysis       [ Data Presentation
       &                   &                      &
   Control ]           Formatting ]           Management ]

Data Acquisition    Signal processing      Graphs

Analogue, Digital,  Simulation/ Loops      File I/O

   Counters         Formatting             Displays

                                           Data Logging
```
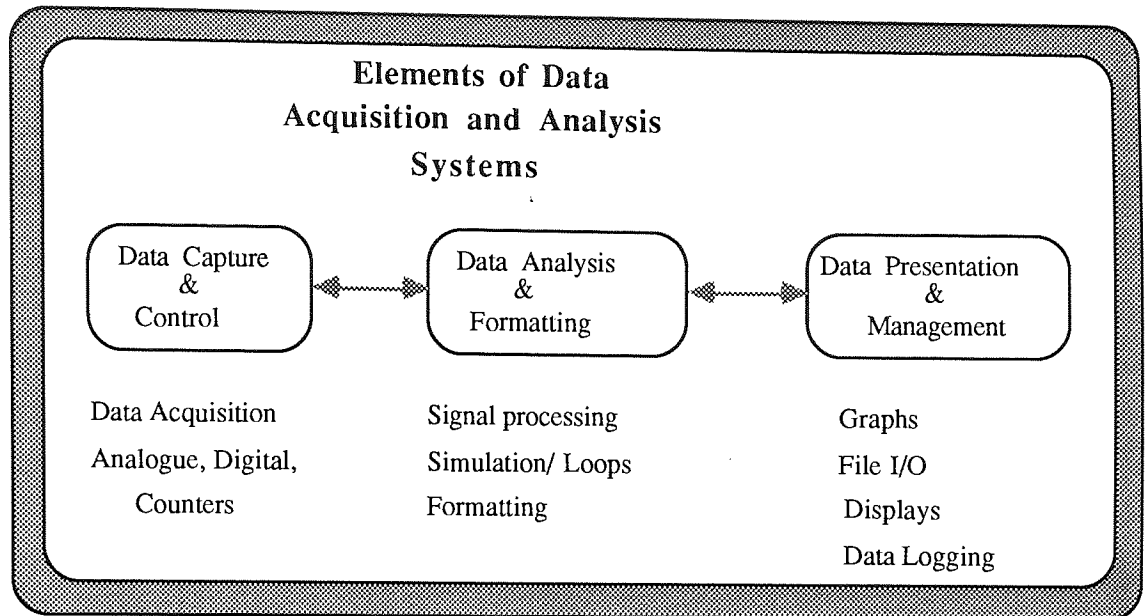
The following three components make up a complete data acquisition and analysis system.

- Data Capture and Control

- Data Analysis and Formatting

- Data Presentation and Management

A typical application involves acquiring the data, formatting and analysing the data, and presenting or saving the data for later use. It is important to chose carefully the type of sensors required, the conditioning module that matches the output of that sensor and the hardware required to capture the output of the signal-conditioning module; this could be an amplifier, a comparator, filter, potential dividers etc. Once the signal reaches the personal computer, the rest of the application is totally dependent on the software developed.

5.2.1 Data collection

There are two options for capturing data with micro computers. The first is to use an analogue-to-digital converter (A/D) board or chip that is installed inside the computer. The signals to be captured are connected to the A/D converter and a software program performs the capture operation. The program configures the A/D converter then acquires the data. The second option uses instruments. The instrument normally has an interface board that enables data and command transfer from or to some controller. The personal computer must have a similar interface to communicate with the instrument; the signals are connected to the instrument. The software program sends commands through the interface bus to the instrument to perform an acquisition. When the acquisition operation is complete, the instrument is instructed to send the captured data to the computer over the interface bus. The software program controls the instrument through the interface bus, while the instrument performs the data acquisition.

5.2.2 Interfacing

Data Capture Hardware
General Block Diagram

Full Block	
Sensors	Conditioning Modules
Option 1	Option 2
	Computer
	A/D Converter
Instrument	
Interface Board	Interface Board
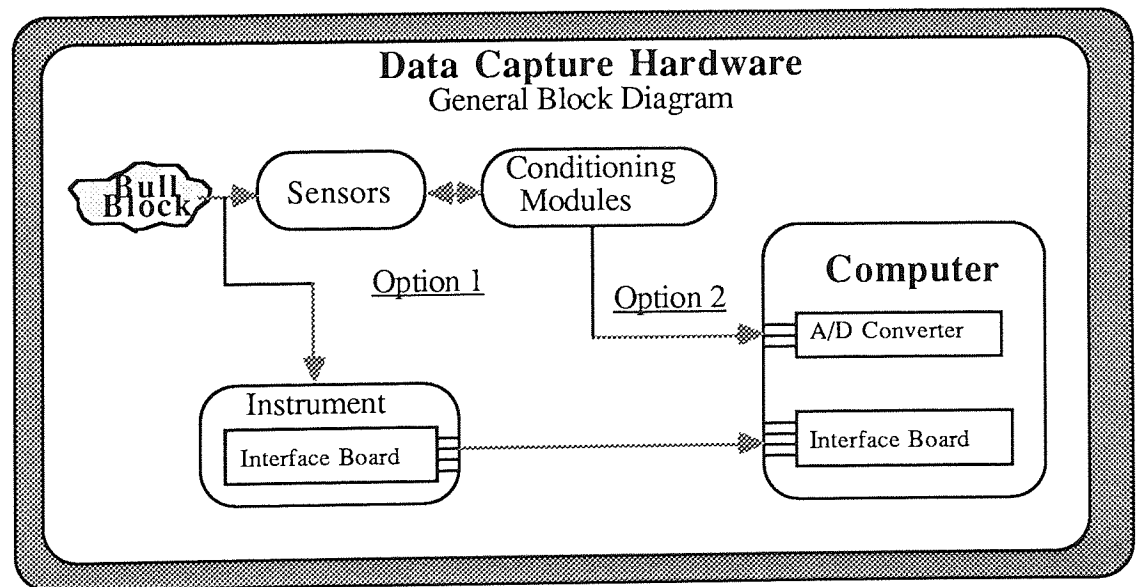
The above is a general block diagram of the data capture process. The final objectives is to monitor an experimental "physical phenomenon". The phenomenon is translated into

electrical signals through sensors. The electrical signal from the sensor is conditioned by a conditioning module. The signal from the conditioning module is captured using either A/D converter or instruments.

The second option was selected because, the BBC micro computer has two useful facilities, the A/D converter and the User port. The presence of these two facilities makes it suitable for a wide range of serious tasks such as controlling experiments and other machinery, and making measurements automatically. The BBC micro is ideally suited to this sort of application; its graphics capabilities can be put to good use for displaying either results or the current state of the equipment being controlled; the high speed calculating power of the Basic computer language can be used to process the measurements, and even the sound generator can be used to draw attention to an abnormal condition. The difficulty with the A/D converter lies in the electronics that should be connected to it rather than the programs which will be written afterwards.

5.2.3 Analogue to digital converter (A/D)

A/D Parameters

- Sampling rate

- Resolution

- Range

- Accuracy
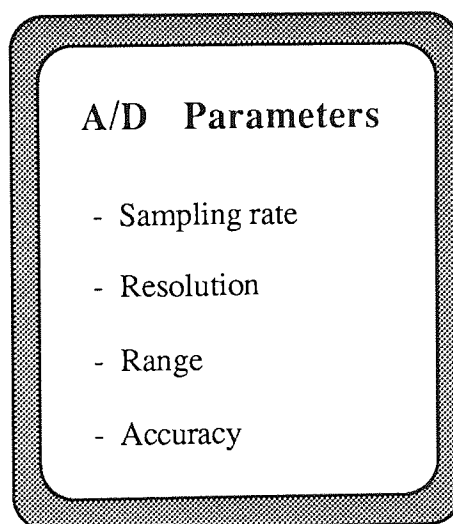
The sampling rate determines how often conversions take place. Resolution is the number of bits which the A/D converter uses to represent the analogue signal. In the BBC micro, the converter forms a 12 bit representation of the signal; the converter is

said to have 12 bit resolution. The larger the resolution, the larger the number of divisions the range is broken into and, therefore, the smaller the voltage change detected. Range refers to the minimum and maximum levels that the A/D converter can quantize. The BBC has a range of 0 to 1.8 V, and will produce a corresponding number in the range 0 to 65520. The accuracy of an A/D converter determines how closely a measured value represents the actual value. The accuracy depends upon the resolution and range.

The BBC micro (model B) is equipped with an A/D converter a (μ pd 7002) which is a four channel 12-bit converter. This means that it can select any one of four inputs to convert. A 12-bit number lies in the range 0 to 4095 and this indicates how finely the A/D converter divides up its input range. This means that the smallest voltage change that can be detected is $V_{max}/4095$ or roughly 0.02% of the maximum reading.

The A/D converter in the BBC micro takes 10 ms per conversion, this limits the sort of application that it can perform. If the four channels are in use and each channel is treated in turn, any one channel is read every 40 ms. This is fast enough for position measurement, temperature, and speed measurements etc.

5.2.3.1 Analogue to digital technology

A/D Techology	
A 3 Bit A/D converter	Input Range: 0 to 1.8 v
Input Range	3 Bit Equivalent
0.000 - 0.224v	000
0.225 - 0.449v	001
0.450 - 0.674v	010
0.675 - 0.899v	011
0.900 - 1.124v	100
1.125 - 1.349v	101
1.350 - 1.574v	110
1.575 - 1.799v	111

For simplicity, an example of a three bit A/D converter is considered. Three bits result in eight different levels. The signal range is then divided into eight different segments and each segment is assigned a binary value. Any voltage reading within a given segment is assigned that binary value. In this example, any voltage reading between 0.450 and 0.674 V is assigned the binary value 010. Thus the A/D converter forms a binary representation of the voltage signal depending on the range of the input voltage. The BBC converter has 4095 levels and is thus able to detect very small voltage changes, as indicated earlier.

5.3 Simulation of working conditions

It is of paramount importance to simulate the working conditions before any major instrumentation changes take place that involve the simulation of four input voltages to be connected to the four A/D converter channels, available with the BBC micro. The advantages of such an undertaking are the simulation and anticipation of any problems before any connection is made to the measuring devices. This includes checking the

range of voltages that the A/D converter accepts and the corresponding number obtained for any conversion. As an example, the A/D converter accepts the range 0 to 1.8 V and will produce a corresponding number in the range 0 to 65520. But in actual testing it only produces a range of 0 to 63250 for a maximum of 1.8 V. This is a very important point to notice, because this figure will be used to convert the values back to voltages and then to m/min, degrees, and N/mm^2.

To simulate the system, full use is made of the voltage reference available with the BBC micro. The V_{ref} is used to supply a maximum of 1.8V, thus the A/D converter will not be damaged in the case of malfunction. Four potentiometers, resistance 100kΩ, 10 turns each, are connected in parallel to the V_{ref} (1.8V) and zero. A digital voltmeter was used to check the input signal to the potentiometers. The value obtained depended on the adjustable turns, i.e. 10 turns maximum, zero turns 0 voltage. The output from the potentiometers is then connected to the BBC's A/D converter, and four inputs into the converter are available which can be adjusted as desired. The circuit diagram is shown in fig.5.1.

The major problem encountered when connecting transducers to an A/D converter is getting the voltage range of the output of the transducer into the range which is required by the A/D converter .

The problem of reducing a large range of voltages is easily solved using a voltage divider, fig.5.2. A small capacitor is used to remove any spurious signals (its exact value being unimportant). If the maximum voltage input is V_{in} then the maximum output V_{out} to the A/D converter is given by

$$V_{out} = R2 . V_{in} / (R1 + R2)$$
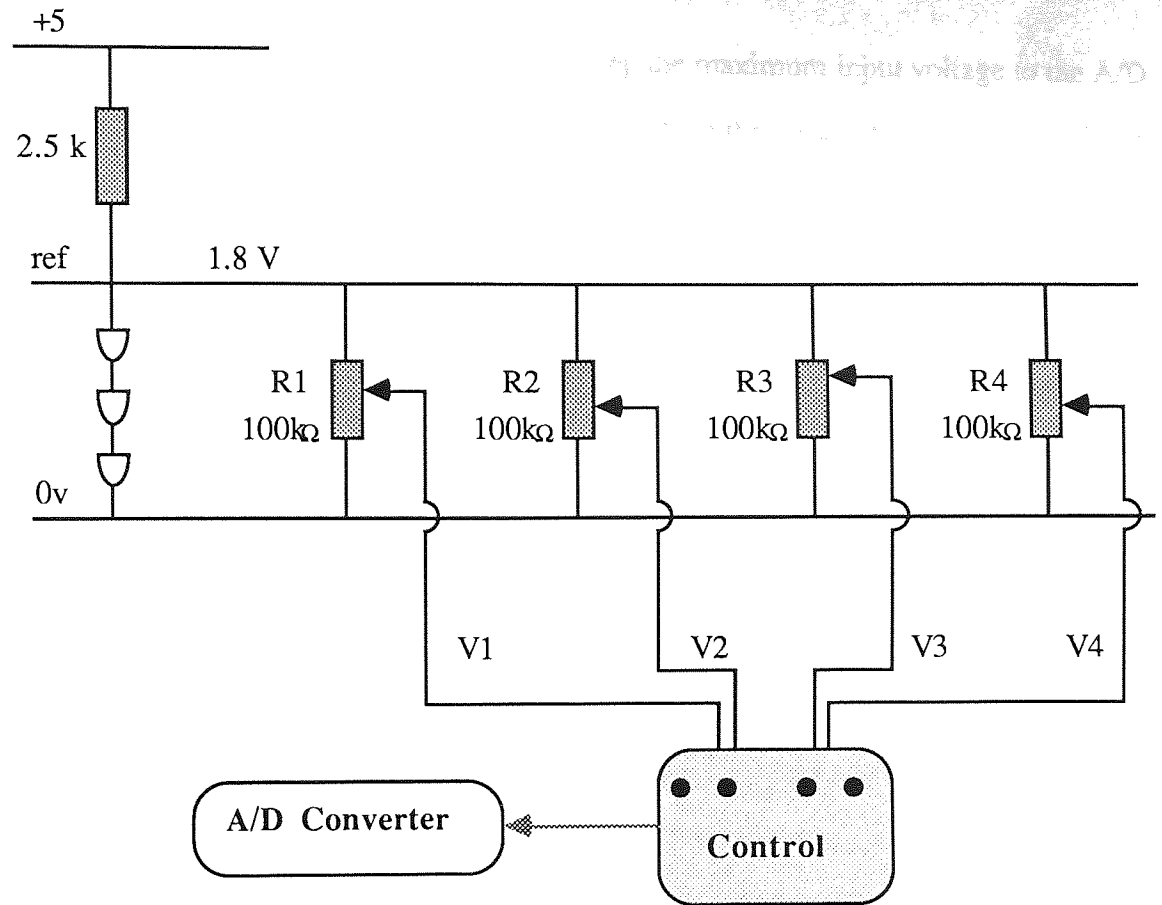
Fig.5.1. Circuit diagram for the Simulation of working conditions
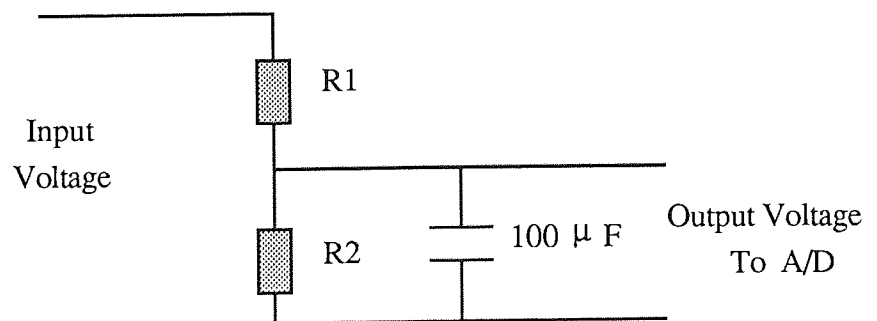
Fig.5.2. Circuit diagram of a voltage divider

Obviously, R1 and R2 should be chosen to keep the maximum input voltage to the A/D converter lower than V_{ref} to avoid any damage. Also the value of (R1+ R2) should be kept large to avoid taking too much current from the transducer, (R1+ R2) should be large compared with the impedance of the transducer.

5.4 Instrumentation and calibration of measuring equipment

The experimental investigation of the drawing of metals at elevated temperatures involves the measurement of the following parameters

5.4.1 drawing force

5.4.2 drawing speed

5.4.3 drawing temperature

5.4.1 Measurement of drawing load

5.4.1.1 The loadcell

The die loadcell formed from a continuous ring which strained in terms of bending and torsion when subjected to an axial thrust. The bending stress and the strain distribution and the stiffness of this type of loadcell is discussed elsewhere in detail by Basily and Sansome[53].

The active strain gauges were bonded at the position of maximum bending moment derived from stress analysis. Dummy gauges were bonded also on both the outside and the inside surfaces of the ring at the positions of zero bending moment, the dummy gauges compensated both for the temperature and any distortion caused by axial thrust. The arrangement of the gauges, as shown in fig.5.3, compensated for any offset load.

The loadcell designed for a maximum axial load of 20 kN, consisted of a continuous square cross-section. On one side were four integral supports equally spaced and on the other side were an equivalent number of the equi-spaced supports in positions at half the pitch. The ring was thus formed from a continuous series of circumferentially shaped beams which strained in terms of bending and shear when subjected to an axial thrust. One set of the sectoral supports was bolted to the thrust block and the other set to the die holder plate. Care was taken to ensure that the presence of threads did not affect the stress distribution at the points at which the strain gauges were bonded.

The loadcell used by Loh[91] could not be used because it suffered from noise interferences, instability, and drift. Therefore the loadcell was re-gauged and re-wired using a 350 ohm rather than 120 ohm gauge because the higher resistance is preferable in reducing the heat generation rate by a factor of three (for the same applied voltage across the gauge). Higher gauge resistance is also advantageous in decreasing lead wire effects, and spurious signals caused by lead wire resistance changes with temperature fluctuations. Similarly, the signal-to-noise ratio can be improved with high resistance gauges (by using higher voltages).

Bridge supply 12.5 Volts

Gauge Resistance is 350 Ω
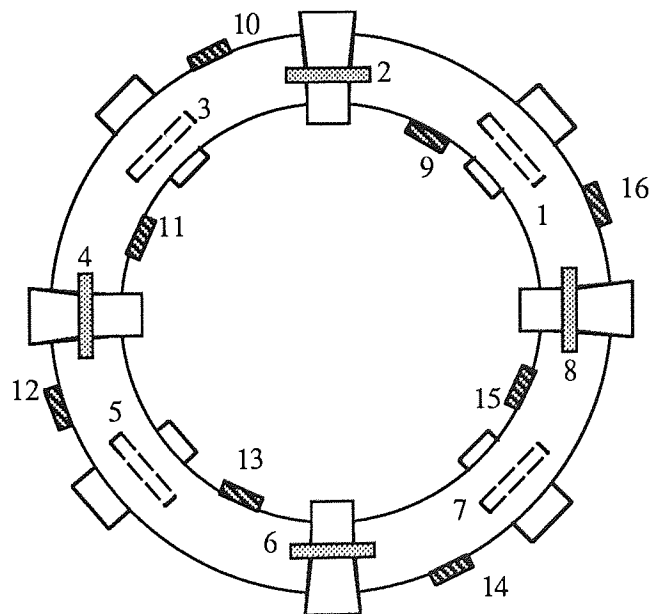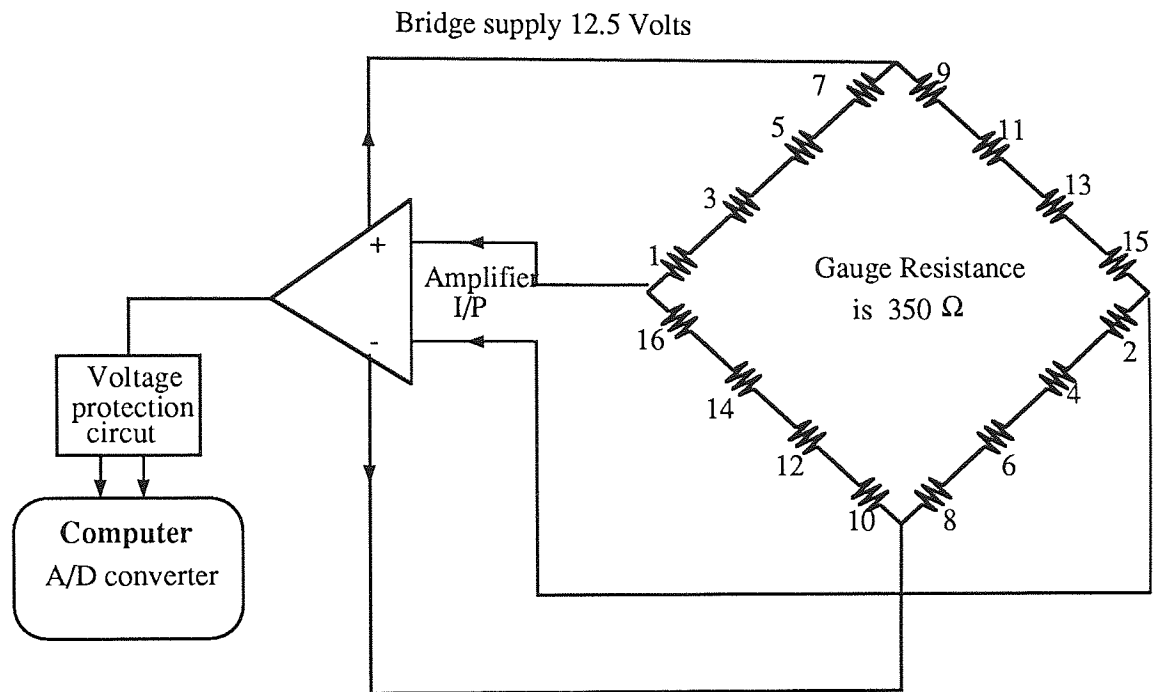
Fig.5.3 Circuit diagram of the loadcell

5.4.1.2 The effect of temperature on the loadcell

During preliminary experimental work, three thermocouples were attached to the loadcell casing using a quick-set adhesive and the temperature was monitored during actual testing. The rise in temperature was only in the order of 10-15°C, at the highest temperature used. The increase is small, because the die cooling water is allowed to overflow and cool the loadcell. Nevertheless, this slight temperature increase affects the strain gauge output because all electrical conductors have a temperature coefficient of resistance, which means that a strain gauge made from these materials will undergo a change in resistivity with temperature. In a bonded resistance strain gauge there is an additional effect producing a change resistance with temperature. When a gauge is bonded to a test material which has an expansion coefficient different from that of the gauge material, a change in temperature will produce a strain in the gauge and, hence, a resistance change due to the difference in expansion. This is clearly noticeable as an off-set from the origin. When the loadcell is warmed up with no load applied, then loading takes place, the change in load will be a continuation from the off-set position, and thus introducing a shift in the readings. The amount of shift is represented by a reading on a digital voltmeter, after the applied load is released; this reading should be approximately zero in the case were the effect of temperature is not experienced.

The combination of these changes of resistance which occur is interpreted as a mechanical strain and is referred to as temperature induced apparent strain. This is apparently a serious potential source of error in the practice of load measurement with strain gauges.

Some of the material used in strain gauges is processed by heat treatment to adjust the basic temperature coefficient of resistance to compensate for the resistance change due to the differential expansion effect on various materials. These are referred to as self-

temperature-compensated gauges. This is the type used in this research, however, even this type is effected by even a slight change of temperature.

The problem of the temperature effect on the loadcell is dealt with in these ways:

- calibration of loadcell under the same temperature conditions, i.e. raising the temperature while loading.
- fitting protective covers and insulators around the loadcell.

5.4.1.3 Calibrating the loadcell

Calibration of the loadcell was conducted by compression between the platens in a 500 kN Instron compression machine. The loadcell was calibrated with four different load ranges to accommodate the different loads achieved at different areas of reductions. Readings were taken for both an increasing and a decreasing load. The load ranges are : 0-2 kN, 0-5 kN, 0-10 kN, and 0-20 kN. The calibration graphs are shown in Appendix (A5).

5.4.2 Measurement of drawing speed

The rotational speed of the drum was measured by using a tachometer giving 20.8 V per 1000 rev/min, attached to the worm shaft of the motor. The calibration graph is shown in Appendix (A5).

5.4.3 Measurement of the drawing temperature

5.4.3.1 Infra-red thermal monitor

The temperature of the wire before entering the drawing die was measured by the Vanzetti infra-red thermal monitor. It is a non-contact temperature-measuring system making use of the infra-red radiation which is received from the target. The principle feature of this system is the use of a flexible optical bundle which permits the

observation of targets in remote or inaccessible places. The system consists of an optical detector head assembly with an optical fibre bundle and a connecting cable, and an electronic chassis with controls and with a digital display. The detector head assembly contains an infra-red detector, a radiation chopper assembly with electronic driver, and a pre-amplifier.

Alignment of the fibre assembly lens cell with the wire is performed by " black illuminating " the fibre assembly using a light source. Calibration of the infra-red thermal monitor is carried out using a calibration source which is used for checking the energy-collecting ability of the thermal monitor optical system and the accuracy and repeatability of the entire system.

Two sets of optical fibre bundles termed " low " and " high "optical fibres were used to accommodate the range of temperatures used 100 - 800°C . The ranges covered were 80 - 350°C and 300 - 1000°C, respectively. Each type of fibre assembly has its own calibration voltage, and the correct data is used with each assembly. The optical fibre bundle detects the amount of radiation from a " spot " of fixed dimension focussed within the wire. For the low optical fibre the diameter of the spot size is 3.2 mm, for the high optical fibre a rectangular spot size of 1.4 mm x 4.2 mm is used. For best focus, the working distance is 127 mm.

5.4.3.2 Calibration of the infra-red thermal monitor

The calibration source box was used to calibrate the two optical fibre bundles. A resistance heating unit was used to heat the wire for the calibration of the thermal monitor. The wire sample was heated to the maximum temperature required. The spot of the optical fibre focussed on the heated wire, this was possible by using a light source which illuminated the spot. At the higher temperatures the wire tends to sag and therefore there is a necessity to check the focussing of the spot and to adjust if required.

The temperature was decreased in steps of 100°C and the optical fibre sensor was changed when the appropriate range limit was reached. The calibration curves are shown in Appendix (A5).

5.4.3.3 The resistance heating unit

The circuit diagram of the resistance heating unit is shown in fig.5.4. All the electrical wiring used in the circuitry was twisted together in order to nullify any electromagnetic current pick-up. Three turns of cable were wound round the transformer to give low voltage secondary windings.

5.4.3.4 Emissivity calibration

Before the thermal monitor could be used in the experiments, the emissivity calibration was carried out for the temperature range of 100°-800°C in steps of 100°C. Representative wire samples from each of the materials tested were used for the emissivity trails. The wire samples were heated to the required temperatures by using the a.c. resistance heating unit referred to earlier. A chromel-alumel thermocouple was used to measure the surface temperature of the representative wire sample. The end of the thermocouple was formed into a small bead by gas welding, and was attached to the surface of the sample to give good thermal contact.

The calibration of the emissivity was as follows:-

- the wire sample was coated with the same lubricant as that used in the drawing tests.
- the spot of the optical fibre was focussed very close to the junction of the wire sample and thermocouple, thus ensuring similar thermal conditions.
- the wire was heated by an a.c resistance heating and the temperatures adjusted by a voltage regulator.
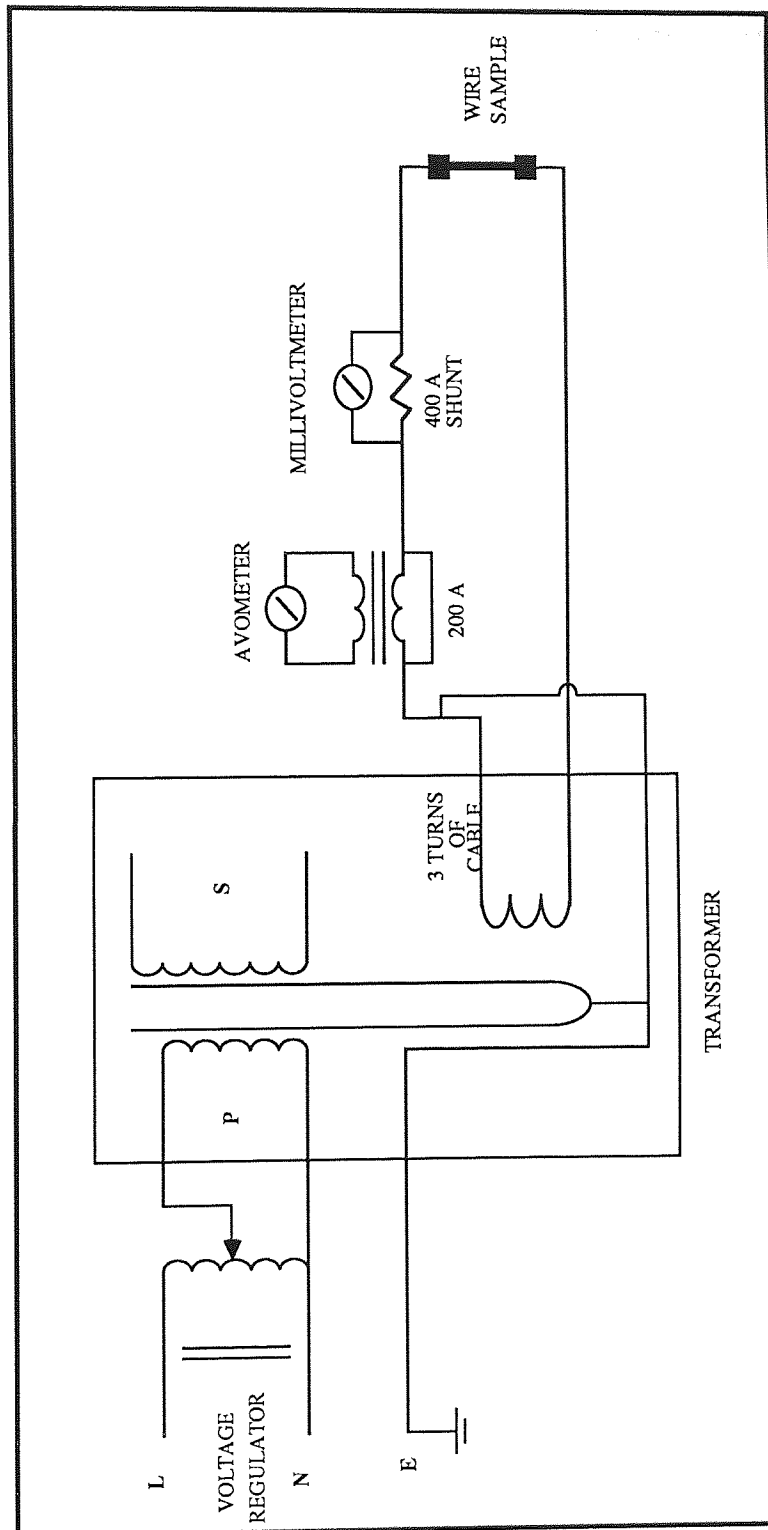
Fig.5.4. Circuit diagram of the resistance heating unit

when the temperature reached its steady-state condition, the emissivity was adjusted so that the temperature indicated by the thermocouple and the infra-red thermal monitor agreed to within 2°C.

The emissivity values of the materials used to date are shown in table 5.1.

	Temperature deg C	Emissivity Value		
		mild steel	boron steel	medium carbon steel
low optical fibre	100	0.90	0.93	0.95
	200	0.90	0.91	0.91
	300	0.86	0.88	0.91
high optical fiber	400	0.86	0.88	0.91
	500	0.82	0.83	0.80
	600	0.80	0.76	0.76
	700	0.75	0.72	0.72
	800	0.70	0.70	0.70

Table 5. 1. Emissivity values for mild steel, boron steel and medium carbon steel.

5.5 Instrumentation and conditioning modules

5.5.1 Loadcell

- an amplifier was used to amplify the output of the loadcell and to supply a constant voltage of 12.5 V to the Wheatstone bridge.

- a filter was used, when the signal from the loadcell suffered from " pick-up " noise, and to suppress any background electrical noise such as noise from the induction motor which is used to drive the bull block and noise from the induction heater.

- a voltage protection circuit was used to protect the computer built in A/D converter which has a range of 0-1.8 V; the converter will be damaged if the signal exceeds 1.8 V. Its circuit diagram consists of :-

(1)   operational amplifier, called the voltage follower circuit which has a unity gain with a high impedance of 2 MΩ, thus preventing the circuit from overloading. Comparator, set at 1.8 V, comparing the V_{in} signal with that received from a potentiometer, and trips whenever a discrepancy arises.

(2)   electronic switch " diode "; whenever a discrepancy takes place this cuts out and the voltage switches to zero.

(3)   potentiometer, which is pre-set at 1.8 V.

The input signal is compared with a signal received from a pre-set potentiometer. If its less than 1.8 V, the electronic switch will be set at open and the signal is transferred to the A/D converter to be processed, but if the signal exceeds 1.8 V the comparator switches to zero and the electronic switch gives a zero reading, thus ensuring that any signal received by the A/D converter will be ≤ 1.8 V. A 10kΩ resistor was used to prevent short-circuiting. The circuit diagram is shown in fig.5.5. The output voltage of the loadcell was displayed on an oscilloscope and a digital voltmeter. This assisted in

151

easing the balancing of the Wheatstone bridge and checking on the noise affecting the load measurements.
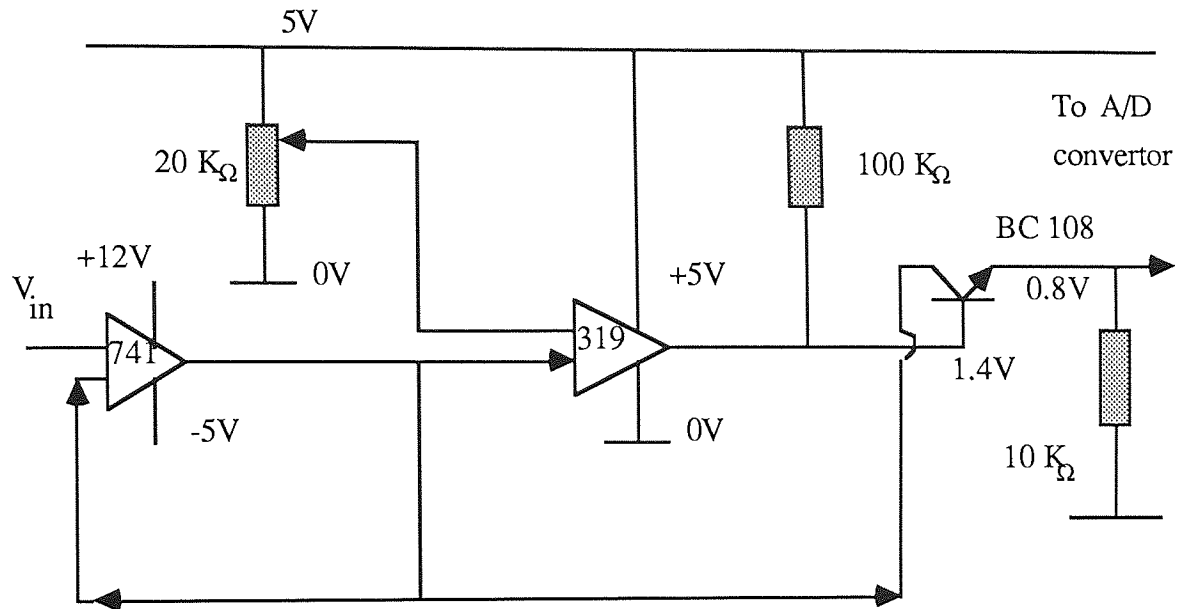
Fig.5.5. Voltage protection circuit

5.5.2 Tachometer

The voltage output from the tachometer was sufficiently high to be passed directly to the A/D converter, eliminating the use of amplifiers ;

- a capacitor of 500 μF was connected across the tachometer to reduce the noise made by its brushes.

- a voltage protection circuit was used, to make sure that the A/D converter would not be damaged if the speed was increased accidentally.

- a filter was used to suppress any " electronic noise ".

5.5.3 Thermal monitor

The temperature is indicated in digital form on the electronic chassis. This temperature corresponds to a linear output voltage of 1 mV/°C. The output was fed into the A/D converter, since the maximum temperature achieved could only be 1000°C i.e. 1.0 V, and that is well within the working range of the converter.

The output voltage of the loadcell, tachometer, and the thermal monitor were displayed on the computer screen before the beginning of any testing. These readouts assisted in the checking, adjusting and balancing of signals prior to the commencement of tests.

5.6 Data Acquisition and Analysis

Data Acquisition & Analysis System

Section Drawing

Bull Block → Loadcell / Tachometer / Thermal monitor → Computer / A/D Board → Operator
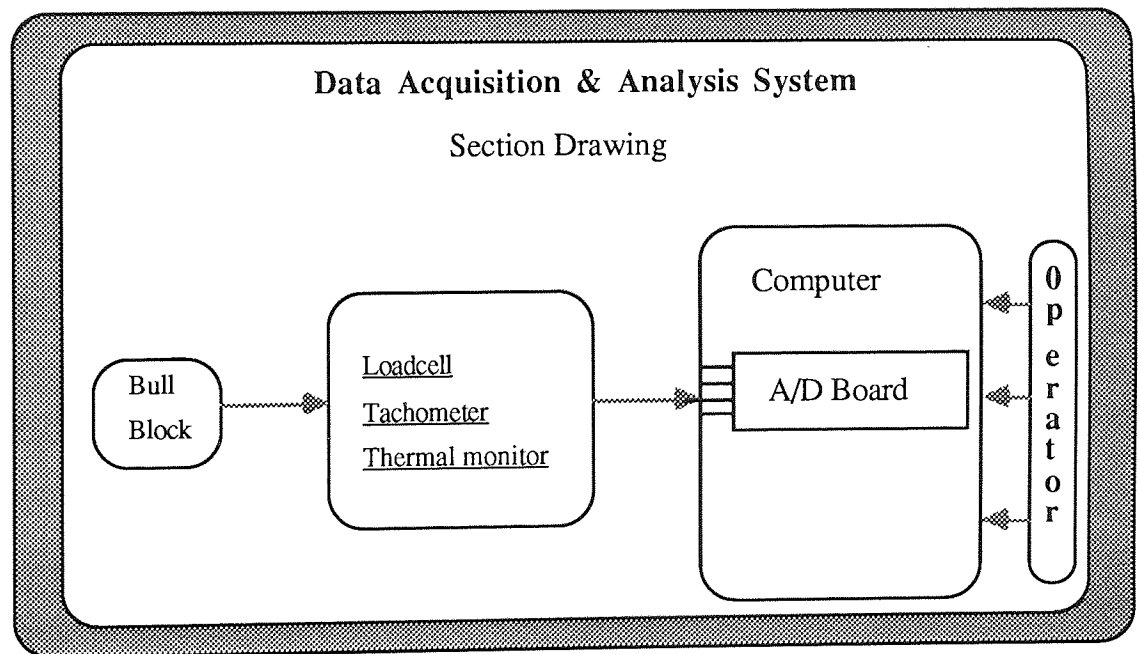
The output of the instruments and conditioning modules which are used to measure the voltage generated by the loadcell, tachometer, and thermal monitor, are connected to the A/D converter. In the computer program developed, a subroutine is used to capture data from these channels. These data are in the form of several readings from multiple

153

channels at a set rate. The output of these subroutines is passed to other subroutines to be formatted, analysed and displayed, i.e. the conversion of the three voltage readings into drawing stress, drawing speed, and drawing temperature. The layout of the flow chart used for real-time data acquisition and analysis is shown in fig. 5.6.

A straightforward approach is used for data capture which includes a timed " for " loop. which executes that function for the desired number of times. The speed of execution is timed so that the three measurements are spread out over the duration of the test and not simply made as quickly as possible. While the test is performed, the three parameters are displayed on the visual display unit so that the user monitors the whole process.

The next step is to analyse the data. For many applications the data acquisition is done in real time and the analysis is done later. Two versions of the application were developed, one that analyses in real time and the other that accesses a data base to analyse stored results. The application uses the captured test data to analyse and present the results. The data are passed to the maximum, minimum, and average functions from the analysis library to compute the minimum, maximum, and average of the three measured variables.

When this application executes, it captures the data at the set rate, scales the data and analyses it, and finally displays the results. A sample of test results and the computer program developed are presented in Appendix (A3).
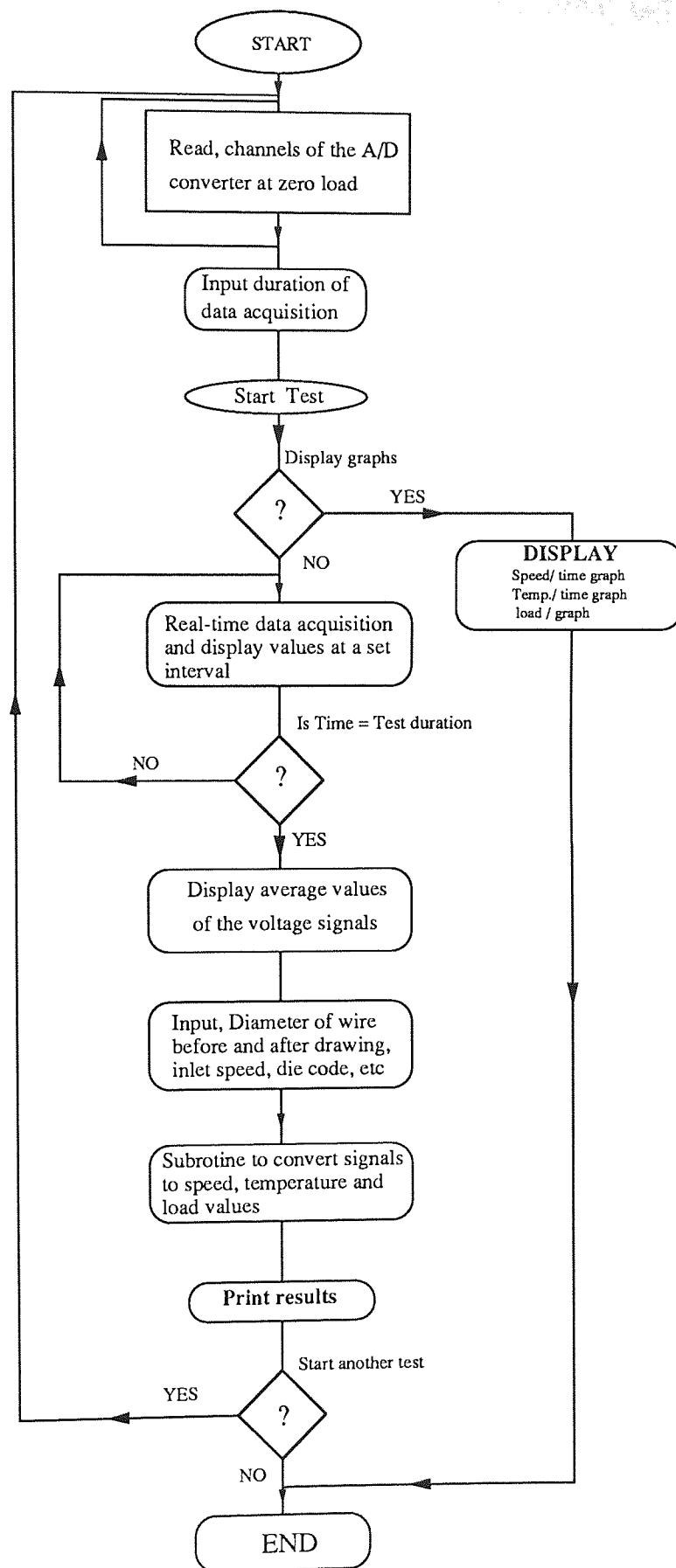
Fig. 5.6 The layout of the flow chart used for real-time
data acquisition and analysis

155

CHAPTER SIX

STRESS-STRAIN DATA

Chapter Six

6.0 Stress-Strain Data

6.1 Introduction

The fluctuations of flow stress for steel as a function of temperature is very complex; no adequate information can be found in the literature covering a range of temperatures, strains, strain-rates and materials. The present experimental tests were carried out with materials for which there were insufficient stress-strain data.

Stress-strain data was generated in the temperature range 20 - 800°C, for mild steel, medium carbon steel and boron steel, with three strain-rate values. The data obtained are represented by mathematical polynomials and fed into the theoretical computations to establish temperature and flow stress distributions and other data for a range of variables.

The results show that below 500°C both the strain-rate and temperature had a small effect on the flow stress but above 500°C, when there is sufficient energy to activate the internal stress relieving mechanisms of dynamic recrystallization, increasing temperature causes a large reduction in flow stress and increasing strain-rate causes the flow stress to increase. In addition it was found that increasing the temperature from room temperature to 400°C causes the strain where the material undergoes to failure to be reduced by 50%, but from 400 - 800°C the strain to failure increases until it reaches the original value of tests at normal temperature.

Stress-strain behaviour under conditions appropriate to hot working can be measured in tension, compression or torsion, each method having advantages and limitations, see section (1.7.1).

156

Tensile tests are of limited use to a true strain of 0.3 before necking occurs. The necking causes a complex stress state and locally raises the strain-rate. The advantages of tensile tests prevails in the simple calculations of stress from normal tensile tests. Special techniques have to be used to obtain a constant strain-rate.

Compression tests do not suffer the same strain limitation, were higher strains can be achieved. However, friction between the specimen and the anvils causes barrelling to occur. Loh[91] conducted compression tests on a cam plastometer, the tests were discontinued because problems were experienced with the experimental equipment, technique and specimen size, and finally she decided on using the limited published data after interpolating the stress in terms of the carbon content, i.e. expressing the interpolated value to that of the 0.16% plain carbon steel as a ratio.

Torsion of solid cylindrical specimens is an increasingly popular method of hot workability testing, since high strains can be attained at constant surface strain-rate and quantitative measures of both flow stress and ductility can be obtained. It is capable of producing strains of up to 20, however most existing torsion machines have an upper strain-rate limit of $\dot{\varepsilon} = 10$ /s, though this could be extended by using specimens of smaller gauge-length. In the present work, the length of the specimen is controlled by the size of the furnace used, thus it was not possible to increase the strain-rate any further.

The torsion test has been used for forty years as a method of assessment of hot workability as well as a method of study of micro-structure. It has certain advantages for particular purposes.

- Torsional shear tests can give more representative values for the plasticity of a material than is obtainable in tension or compression tests, because no

157

attenuation, like that of the necking in tension, takes place and, with a suitable test piece, the instability and friction effects of compression testing are avoided.

On the other hand there are certain disadvantages;

- Analysis of results is often relatively difficult, either because of the presence of a stress gradient in torsion or of bending in direct shear.

By stress gradient it is meant that the induced shear stress normal to the torsion axis is not uniform and varies from a maximum at the outer surface to zero at the axis. Many different methods have been devised to overcome these difficulties. Probably most use is made of hollow cylindrical test pieces in an effort to keep the stress differences between the inner and outer surface small, but buckling becomes a progressively greater difficulty as the wall thickness is reduced and length is increased.

Torsion tests were chosen for this work for of the following reasons.

- the limitations of the tensile test referred to earlier

- the difficulties and limitations encountered by Loh[91] when she tried to use compression testing namely, the friction effect, availability of a machine and problems with the technique, referred to earlier.

- the availability of a cold torsion machine at the University, which was modified in order to carry out tests at elevated temperatures.

- the availability of computer packages such as Cricket graph with various curve-fitting subroutines to help in interpreting the results obtained, and finally

- data obtained by tensile and compression tests were used in many theoretical analyses with some limitations at certain temperatures or strains, i.e. the need to use torsion data in the analysis to establish the accuracy and limitations of data obtained by torsion testing.

All graphs obtained are represented mathematically by polynomials using the aforementioned computer packages, and fed into the computer programs developed in order to solve the upper-bound solution numerically.

6.2 Testing machine

The layout of the equipment used for the torsion testing at elevated temperature is shown in fig.6.1, the machine used is an Avery testing machine equipped with four scales for the torque measurement, they range from 170-1700 Nm, four speeds of rotation are obtained, and these are 90, 30, 10 and 3.5 deg/min.

6.2.1 Torque measurement

A displacement transducer is fitted to the machine to replace the torque dial, in order that a more accurate result is obtained and more important a signal which could be fed into an analogue-to-digital converter; this enables the use of a computer to read and record the instantaneous torque readings. The displacement of the static chuck is proportional to the torque applied, this displacement is picked up by a system of mechanical linkage which connects to a dial which registers the torque being applied to the static chuck and hence to the sample. The reading on the dial is directly proportional to the displacement of the last mechanical link. By placing a displacement transducer on this link a direct correlation between displacement of the bar and torque can be obtained, the signal from the transducer is fed into a computer equipped with an A/D converter, this enables the continuous reading of the torque values, with the help of a computer program written for this purpose.

6.2.2 Angle of twist measurement

The torsion machine has no built-in method of measuring the angle of twist which a sample undergoes during testing. Normal methods of measuring twist, such as marking the sample or the use of electronic type microscope vernier, reflective mirrors, etc are
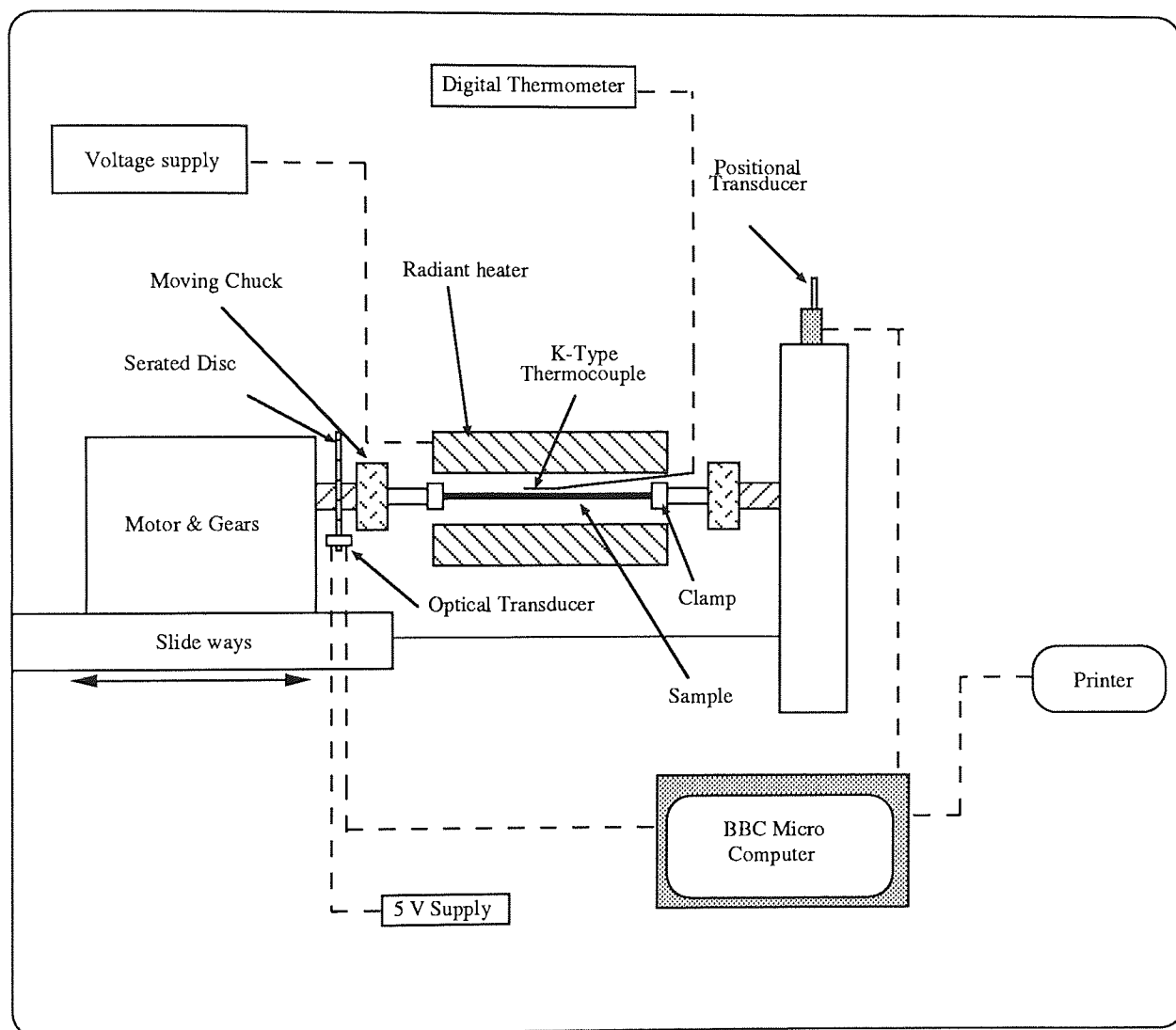
Fig. 6.1. Schematic diagram of experimental equipment

160

impractical, because of the presence of the furnace and the need to obtain an instantaneous torque verses angle of twist readings. To achieve this, a thin disc with 180 slots was machined and located behind the rotating chuck fig.6.1. An optical transducer which gives a reading each time a slot comes into view i.e. gives a reading every 2°. The readings is fed into a computer equipped with an A/D converter, which counts the number of slots and keeps a total of the angle the moving chuck has rotated through. A supply of 5V, 0.5A from a stabilised power supply was fed to the transducer. Depending on the time interval used in the computer program, torque and angle of twist measurements were taken and retained for further processing.

6.2.3 Temperature measurements

The temperature was read by a K-type thermocouple, (Cr-Ni, Al-Ni). This type of thermocouple gives readings accurate to one degree over a range of 20 - 1000°C. The voltage from the thermocouple is fed into a digital unit which converts the voltage readings into a temperature which is displayed on a digital readout.

6.2.4 Heating the sample

A small radiant heater is used to heat the specimen to the required temperature. It was chosen because it was small in size to accommodate the specimens. The temperature is controlled by altering the voltage supply to the heater using a variable voltage supply.

6.2.5 Clamps and specimens

Specimens size and clamps are shown in Appendix (A4) The clamps are made from En8c which has similar properties to En8, they were austentised at 850°C for 1.5 hours and then oil quenched, followed by annealing at 560°C for two hours and air cooled. The heat treatment was carried out to harden the clamps particularly the internal screw thread.

6.3 Data transformation

The results obtained from the computer were in the form of torque (M) against angle of twist, a sample of the graphs are shown in fig.6.2. The results in this form are of a little use and are therefore transformed to shear stress, shear strain using the Fields and Backofen equation.

$$\tau = \frac{1}{2 \pi r^3} \left(3M + \gamma \frac{dM}{d\gamma} + \dot{\gamma} \frac{dM}{d\dot{\gamma}} \right) \tag{6.1}$$

$$\gamma = \frac{r}{l_o} \psi \qquad \& \qquad \dot{\gamma} = \frac{r}{l_o} \dot{\psi} \tag{6.2}$$

r = radius of the specimen ψ = angle of twist in radians

γ = shear strain $\dot{\gamma}$ = shear strain rate

lo = gauge length of the specimen $\dot{\psi}$ = angular velocity

The term $\gamma \, dM/d\gamma$ has to be determined by graphical differentiation of the torque curve, and $\dot{\gamma} \, dM/d\dot{\gamma}$ is obtained from the results of several experiments at different strain rates. A double logarithmic plot of M against $\dot{\gamma}$ gives curves that very often can be assumed to be straight lines. The following expression applies

$$M = M_o \left(\frac{\dot{\gamma}}{\dot{\gamma}_o} \right)^n \tag{6.3}$$

Mo = constant

$\dot{\gamma}_o$ = constant

n = slope

By differentiation

$$\dot{\gamma} \frac{dM}{d\dot{\gamma}} = n M$$

and substitution

$$\tau = \frac{M}{2 \pi r^3} \left(3 + \frac{\gamma}{M} \cdot \frac{dM}{d\gamma} + n \right)$$

The term $\gamma \, dM/d\gamma$ is often ignored because otherwise the analysis of the experimental results becomes too tedious i.e.

$$\tau = \frac{M}{2 \pi r^3} \left(3 + m + n \right)$$

where m and n are the slopes of curves of ln M versus ln γ and ln M verses ln $\dot{\gamma}$, respectively, and m is taken as zero. This gives the more usual expression

$$\tau = \frac{M}{2 \pi r^3} \left(3 + n \right) \tag{6.4}$$

when investigations are not carried out at different speeds the n values are ignored and, the analysis then gives;

$$\tau = \frac{3 M}{2 \pi r^3} \tag{6.5}$$

equation (6.5) gives an underestimation of the shear stress, at large strains this usually amounts to less than 10%. In the present work equation (6.4) is used to obtain the shear stress value from the torque versus angle of twist for various values of n, but when these values are negative equation (6.5) is used instead. Values of n obtained for the three materials tested are shown in table (6.1).

The shear stress, strain and strain-rates determined from the torsion test have to be converted to the equivalent uniaxial values. According to the shear stress hypothesis;

$$\sigma_f = 2\,\tau \quad , \quad \phi = \frac{\gamma}{2} \quad , \quad \dot{\phi} = \frac{\dot{\gamma}}{2} \tag{6.6}$$

and, from the shear strain energy criterion

$$\sigma_f = \sqrt{3}\,\tau \quad , \quad \phi = \frac{\gamma}{\sqrt{3}} \quad , \quad \dot{\phi} = \frac{\dot{\gamma}}{\sqrt{3}} \tag{6.7}$$

where σ_f is the flow stress

6.3.1 Sample transformation

A sample transformation of results obtained by testing boron steel samples at three different speeds are presented in this section, the results obtained from the graphs of fig.6.2.The tests are carried out at three rates of twist and these are, 90, 30, and 10 deg/min. Equation (6.4) is used to transform torque values into shear stress as follows;

$$\tau = \frac{M}{2\,\pi\,r^3}\,(3 + m + n)$$

where m is assumed to be zero and n is found from the gradient of the steady state value of the logarithmic plot of torque verses strain-rate plotted at a constant angle. From fig.6.2. the steady state region of the graph is noted in relation to the angle of twist. For each temperature and angle of twist, the torque is read from the three graphs representing the three rates of twist. A plot of the natural log of this value against the natural log of the strain-rate at the chosen angle of twist is performed. A straight line is plotted and a value of n was found. The curves used to find n are each plotted with three different sets of angle of twist values to give an averaging effect. The temperature of 800°C is chosen for this example. Fig.6.3. shows a sample of these graphs used to find the values of n, the angles of twist chosen for this example are 1000°, 2000° and 2500°.

Using equation(6.2), shear strain-rate is used instead of strain-rate, since only the gradient is required and the transformation will not effect the gradient of the line.

$$\gamma = \frac{r}{l_o} \psi \qquad \& \qquad \dot{\gamma} = \frac{r}{l_o} \dot{\psi} \qquad\qquad (6.2)$$

where $r = 3$ mm $\& l_o = 76.2$ mm

the following conversion is obtained;

Rate of twist deg/min	Angular velocity $\dot{\psi}$	Shear strain-rate $\dot{\gamma}$	$\ln \dot{\gamma}$
90	0.0262	$1.03 * 10^{-3}$	-6.88
30	$8.723 * 10^{-3}$	$3.435 * 10^{-3}$	-7.98
10	$2.908 * 10^{-3}$	$1.145 * 10^{-3}$	-9.07

The value of the torque and angle of twist at the shear strain-rates obtained represented as follows

Angle of twist	1000		2000		2500	
$\ln \dot{\gamma}$	M	ln M	M	lnM	M	lnM
-6.88	2.016	0.701	1.969	0.678	2.015	0.701
-7.98	1.420	0.351	1.466	0.383	1.420	0.351
-9.07	1.191	0.175	1.237	0.213	1.232	0.208

From fig.6.3. three values are obtained for n, in all cases the average value is used for the data transformation, for this example the average value for n is 0.225. Using equations (6.4), (6.6) and (6.7), the transformation from torque to shear stress is as follows;

165

$$\tau = \frac{M}{2 \pi r^3} \, (3 + n) \tag{6.4}$$

$$\sigma_f = 2 \tau \qquad \text{or} \qquad \sigma_f = \sqrt{3} \, \tau$$

An average value is used to convert the shear stress into flow stress by using

$$\sigma_f = \frac{2 + \sqrt{3}}{2} \, \tau$$

$$= \frac{1.87 \, M}{2 \, \pi r^3} \, (3 + n) \qquad \text{where} \quad r = 3 \text{ mm}$$

$$\sigma_f = 11 \times 10^6 \, M \, (3 + n) \tag{6.8}$$

For this example $n = 0.225$

$$\sigma_f = 35.5 \times 10^6 \, M$$

The transformation from angle of twist to shear strain is given by equation (6.2), and the transformation from shear strain to normal strain is given by;

$$\varepsilon = \frac{\gamma}{\sqrt{3}} \qquad \text{or} \qquad \varepsilon = \frac{\gamma}{2} \tag{6.9}$$

An average of the two values is used as follows

$$\gamma = \frac{r}{l_o} \, \psi \qquad \text{where} \quad l_o = 76.2 \text{ mm}$$

$$\gamma = 6.87 \times 10^{-4} \, \psi$$

$$\varepsilon = \frac{\left(\dfrac{\gamma}{2} + \dfrac{\gamma}{\sqrt{3}} \right)}{2}$$

$$\therefore \qquad \varepsilon = 3.7 \times 10^{-4} \, \psi \qquad\qquad\qquad (6.10)$$

Equations (6.8) and (6.10) are used to transform all experimental results into flow stress, strain curves. Figs.6.4 - 6.12.

If the rates of twist are converted to shear strain-rate using equation (6.2), and converting this value of shear strain-rate to normal strain-rate by using

$$\dot{\varepsilon} = \frac{\dot{\gamma}}{2} \qquad \text{or} \qquad \dot{\varepsilon} = \frac{\dot{\gamma}}{2}$$

i.e. an average of

$$\dot{\varepsilon} = \frac{\left(\dfrac{\dot{\gamma}}{2} + \dfrac{\dot{\gamma}}{\sqrt{3}} \right)}{2} \qquad\qquad\qquad (6.11)$$

Using the γ obtained earlier for the rate of twist of 90, 30, and 10 deg/min and using equation (6.11), then strain-rates in s^{-1} obtained are as follows;

	$\dot{\gamma}$	$\dot{\varepsilon}$
90	10.3×10^{-4}	5.55×10^{-4}
30	3.435×10^{-4}	1.85×10^{-4}
10	1.145×10^{-4}	0.62×10^{-4}

6.4 Discussion of results

Studying the flow stress, strain curves given in figs.6.4 - 6.12, a number of observations can be made, these are;

- when experiments performed at low temperatures, the curves are closely spaced. This is because the stress-relieving mechanisms do not have enough energy to activate them, therefore strain-rate has little effect upon the results of the flow stress.

- at higher temperatures, 500°C and above, the curves begin to loose their shape and fluctuations occur in the flow stress.

- in general, higher strain-rates give higher flow stresses but in some cases this is not always so, due to the combined effect of temperature and strain-rate on the flow stress. Increasing temperature will cause the flow stress to decrease, while increasing the strain-rate causes the flow stress to increase. The effect of these two factors combined does not have a linear effect, so in some instances the lower strain-rate will give a higher flow stress than the higher strain-rate.

- comparing the flow stress with the temperature, for all materials tested, the flow stress falls slightly as the temperature is raised from 20 - 200°C, then the flow stress rises to its higher value at 400°C. Above 400°C a significant drop in the flow stress is obtained. At 800°C the value of flow stress is less than 10% of the value of flow stress for the samples tested at normal temperature.

- the values of strain, drops significantly, by approximately 50%, as the temperature increases from 20 - 400°C. As the temperature increases, the values of strain start to rise again and at 800°C the strain is approximately the same as it was for the samples tested at normal temperature.

6.5 Conclusions

Using a specimen of fixed geometry and applying the Fields and Backofen equation to the results from a torsion test is a relatively simple method of determining the flow stress of materials. The graphs of figs.6.4 - 6.12, show that increasing the temperature from 20 to 400°C gives a slight decrease and then an increase in flow stress and a

168

significant reduction in strain, (approximately 50%). Above 400°C the flow stress falls sharply with increasing temperature, at 800°C it is less than 10% of it is value for samples tested at normal temperature. Above 400°C the strain increases with temperature until 800°C, then the strain values are approximately the same as those for tests carried out at normal temperatures. This decrease in flow stress and increase in strain at high temperatures is caused by dynamic recrystallisation which is a thermally activated at above 500°C for steel.

The effect of strain-rate on the flow stress and strain is small below 400°C, but above this temperature the effect is significant because the strain-rate at higher temperatures dictates how long the material has to recrystallise and relieve the internal stresses.

To conclude, all graphs of figs.6.4 - 6.12, will be mathematically transformed into polynomials and fed into the computer programs developed, as discussed in Chapter three, in order to enable the estimation of flow stress and its distribution in the deforming zone. The effect of strain-rate will be considered for results of 500°C and above, since the effect of strain-rate below 500°C is negligible. Test results above 500°C will be re-plotted, taking into consideration the opposing effect of strain-rate and temperature by using, the velocity modified temperature expression figs 6.16 - 6.18 discussed in Chapter one.

$$T_m = T \left(1 - k \ln \frac{\dot{\varepsilon}}{\dot{\varepsilon}_o} \right)$$

Graphs of Tm versus flow stress for various strains and strain-rates are presented in figs. 6.13 - 6.15. These graphs are represented mathematically by polynomials and are fed into the computer program discused earlier.

Temperature	MATERIAL		
	Boron steel	Medium carbon steel	Mild steel
20	0.0086	0.0026	-0.0247
100	0.0701	-0.0019	0.0773
200	-0.028	-0..0509	-0.1174
300	-0.0173	-0.0598	-0.0575
400	0.020	0.0061	-0.0061
500	0.1757	0.0081	-0.0303
600	0.4095	-0.1209	0.0148
700	0.2446	0.160	-0.3059
800	0.2249	0.157	0.3021

Table.6.1. values of n for the three materials tested.
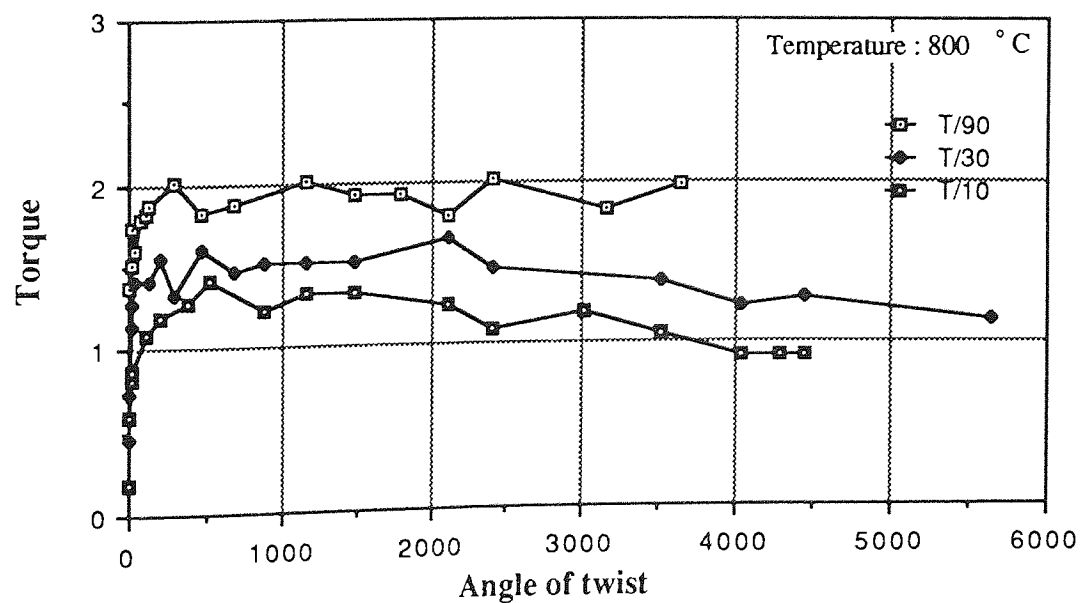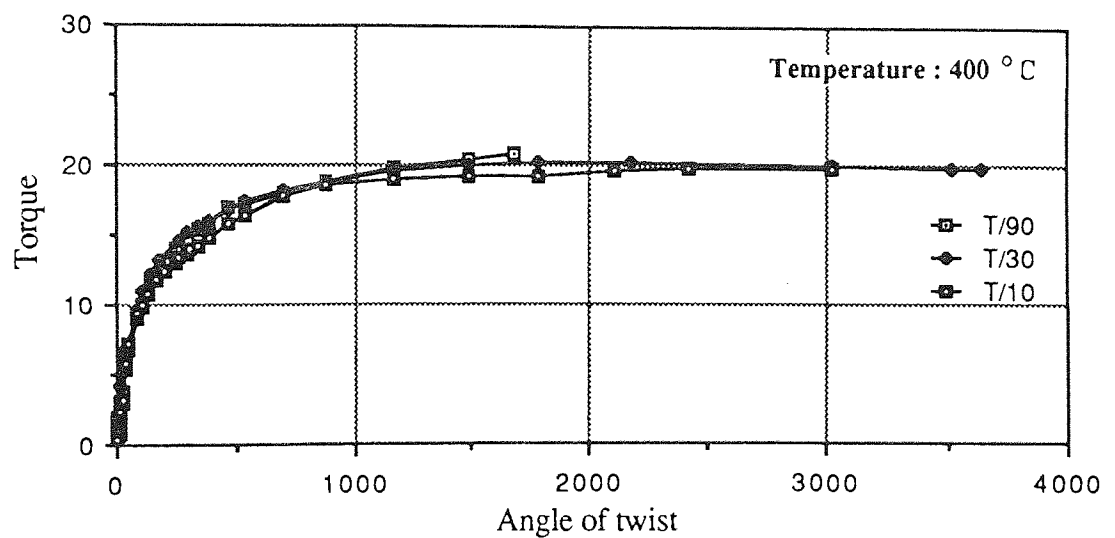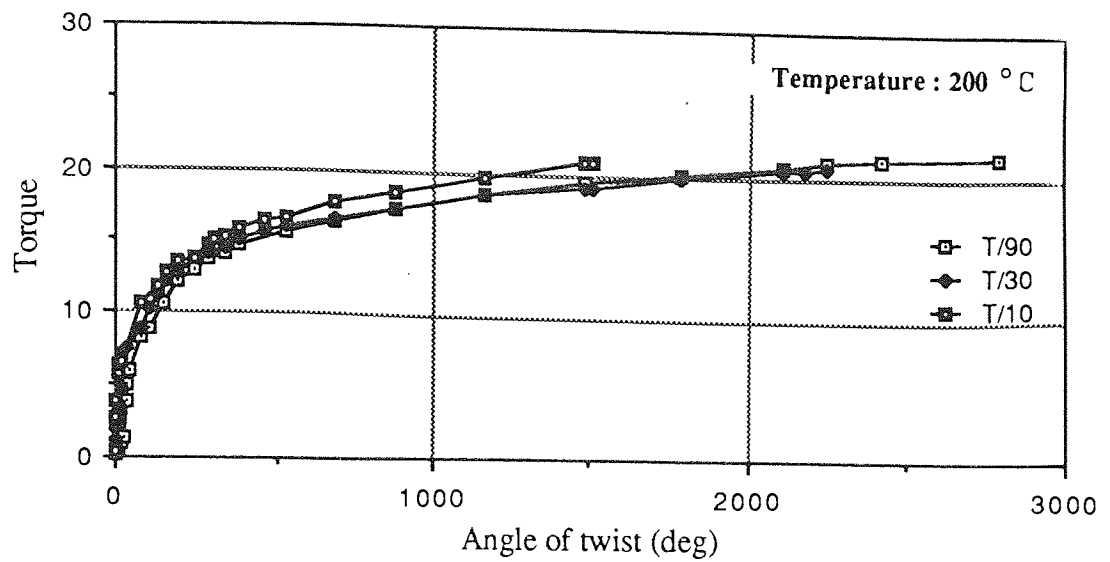
Fig.6.2. Graph of Torque versus angle of twist for boron steel.
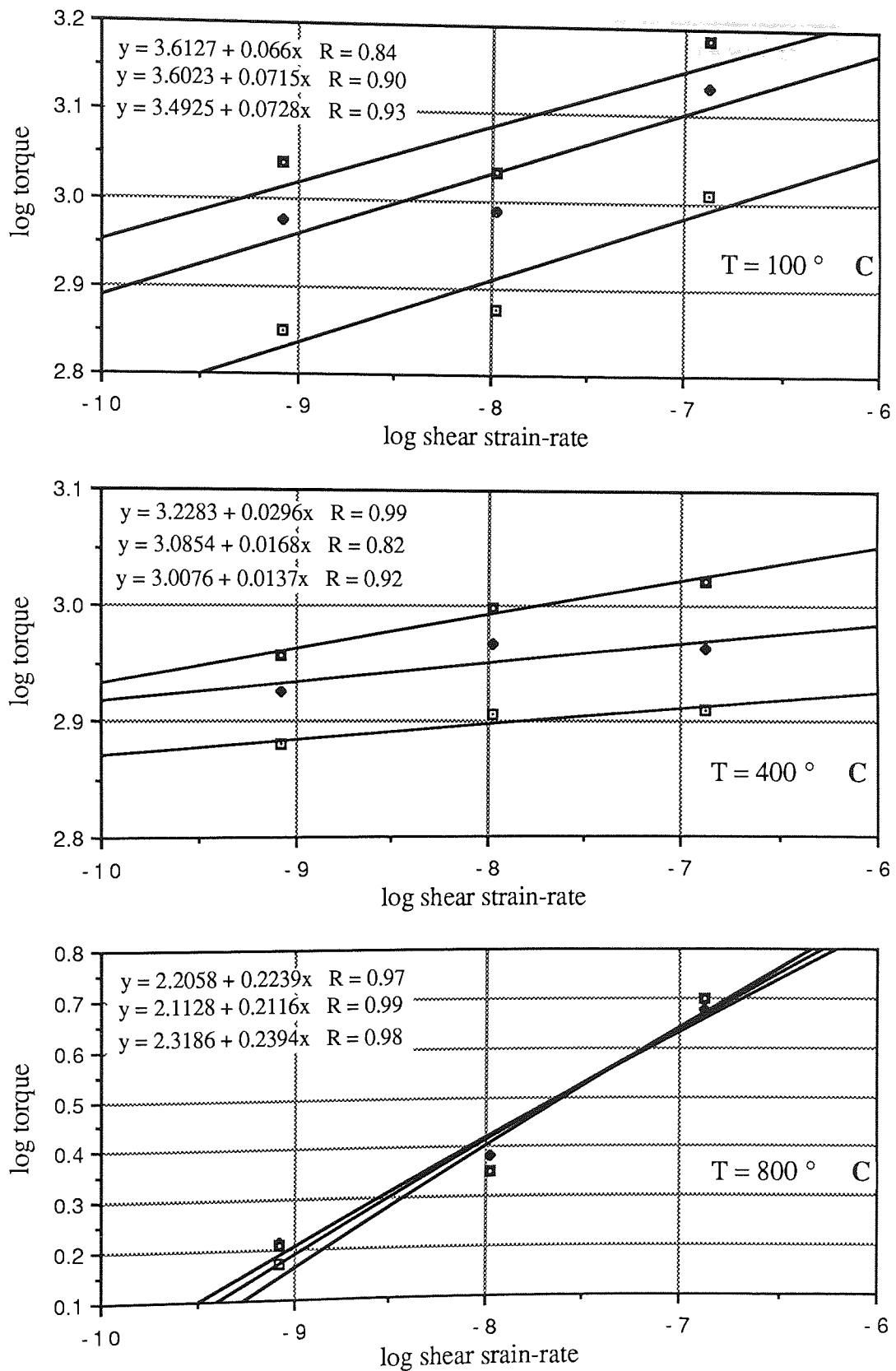
Fig.6.3. Graphs of log torque against log shear strain-rate to find the value of n.
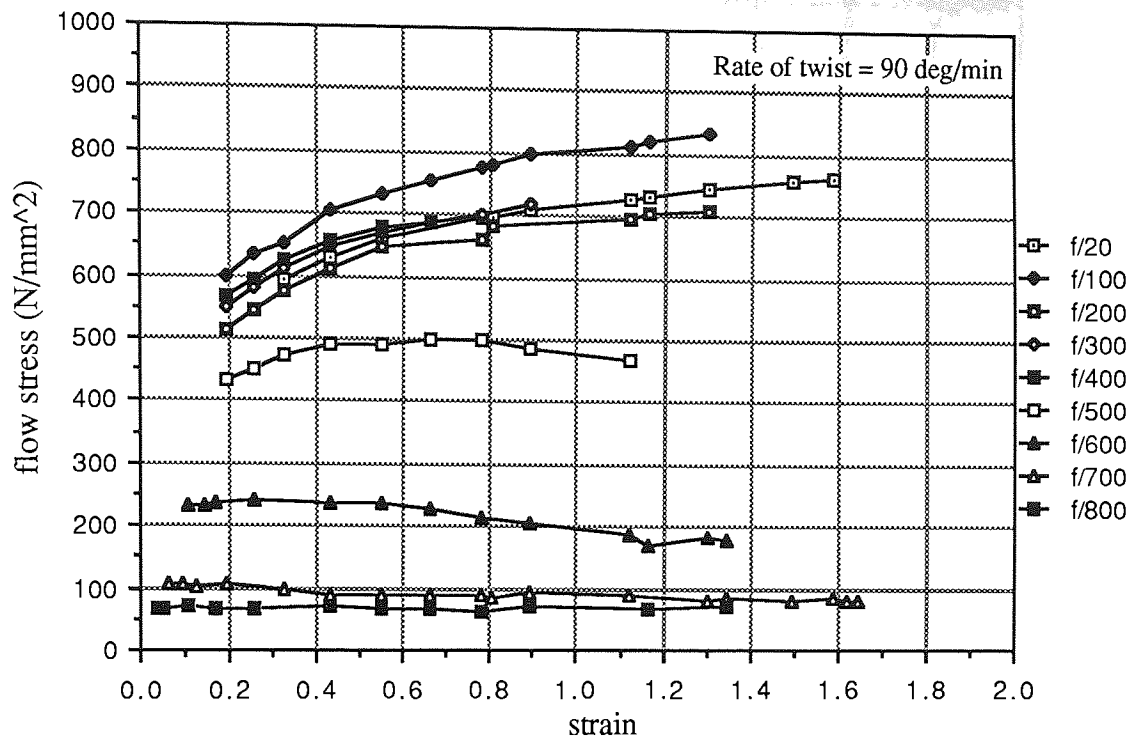
Fig.6.4. Effect of temperature on the flow stress/strain for boron steel
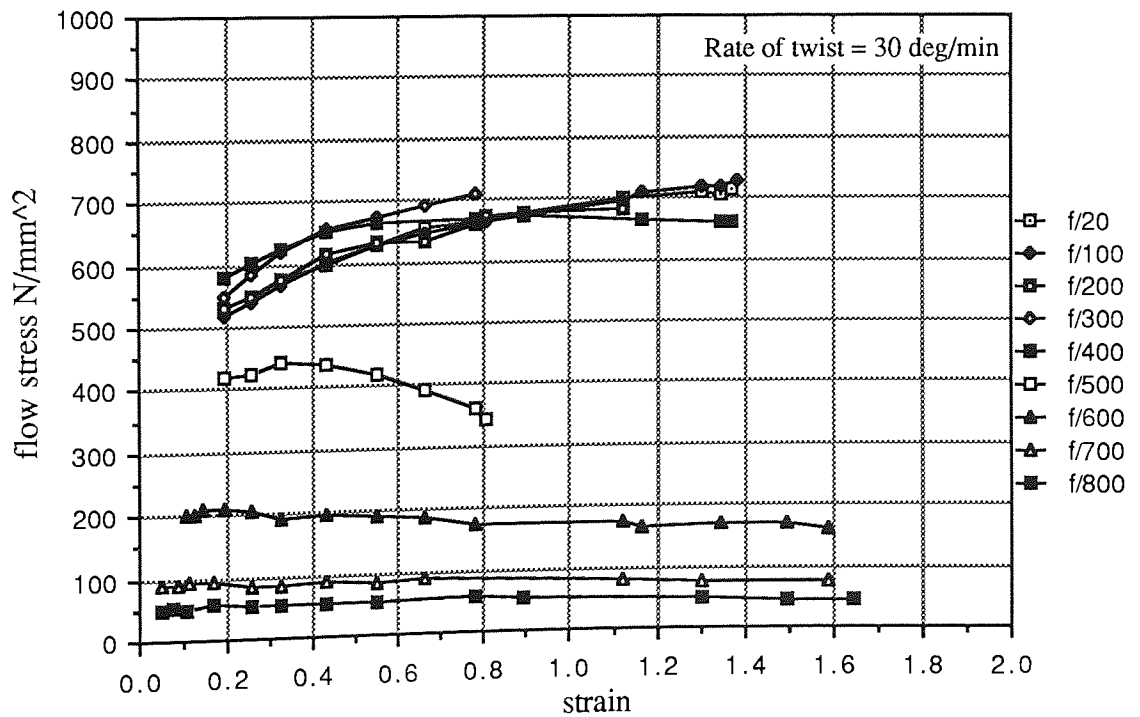
Fig.6.5. Effect of temperature on the flow stress/strain for boron steel
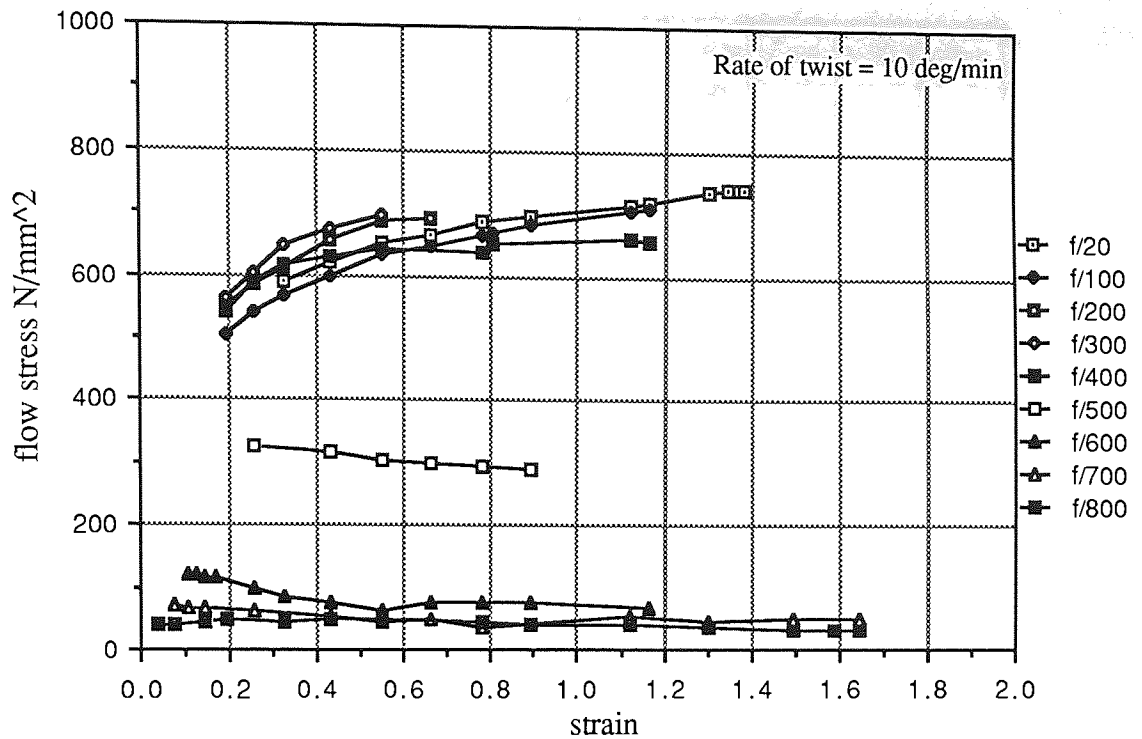
Fig.6.6. Effect of temperature on the flow stress/strain for boron steel
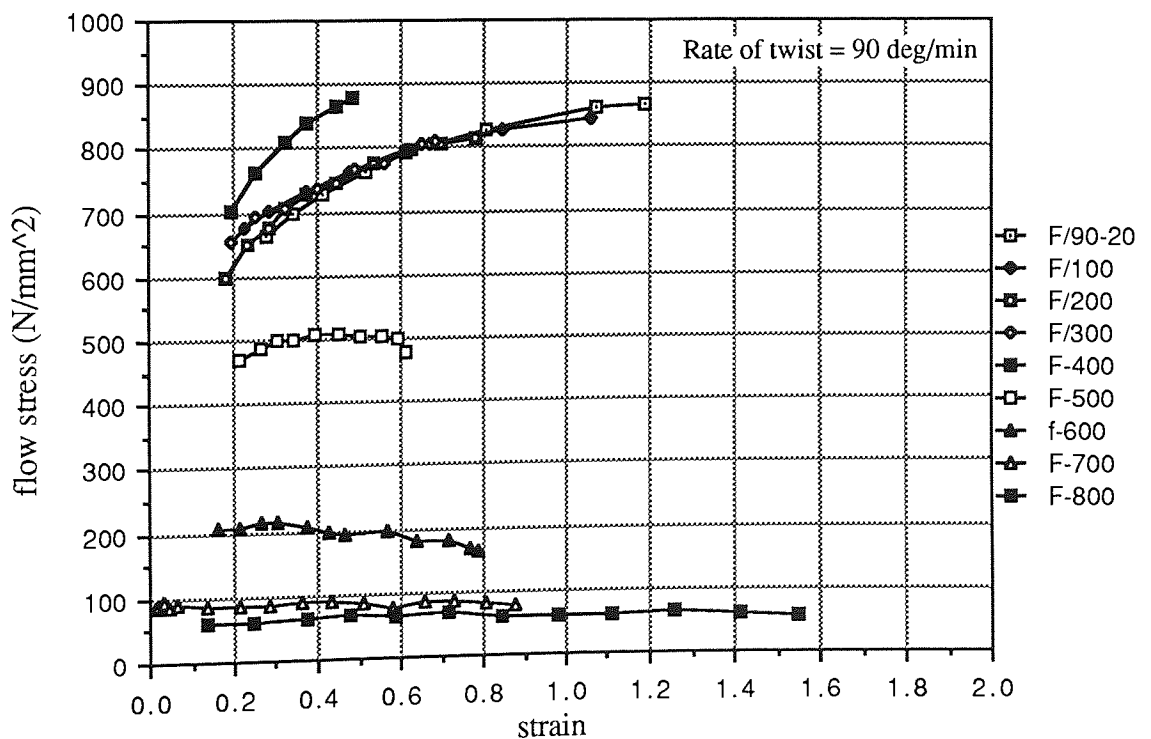
Fig.6.7. Effect of temperature on the flow stress/strain for medium carbon steel

174
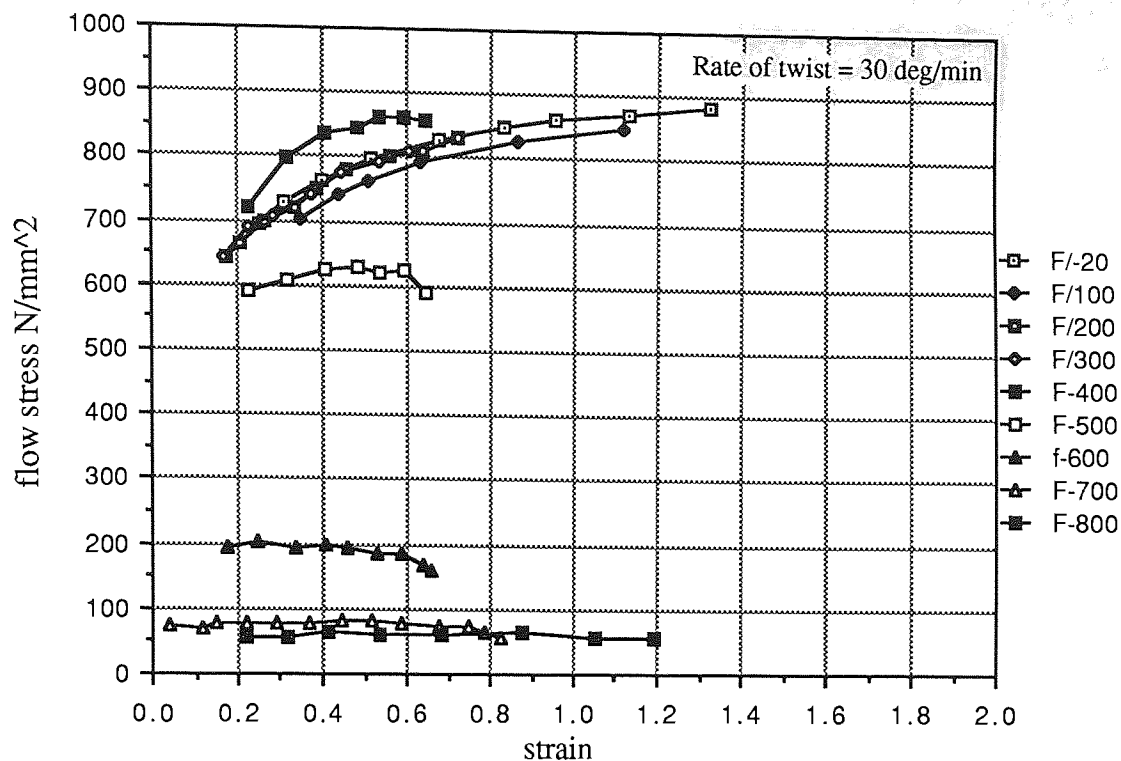
Fig.6.8. Effect of temperature on the flow stress/strain for medium carbon steel
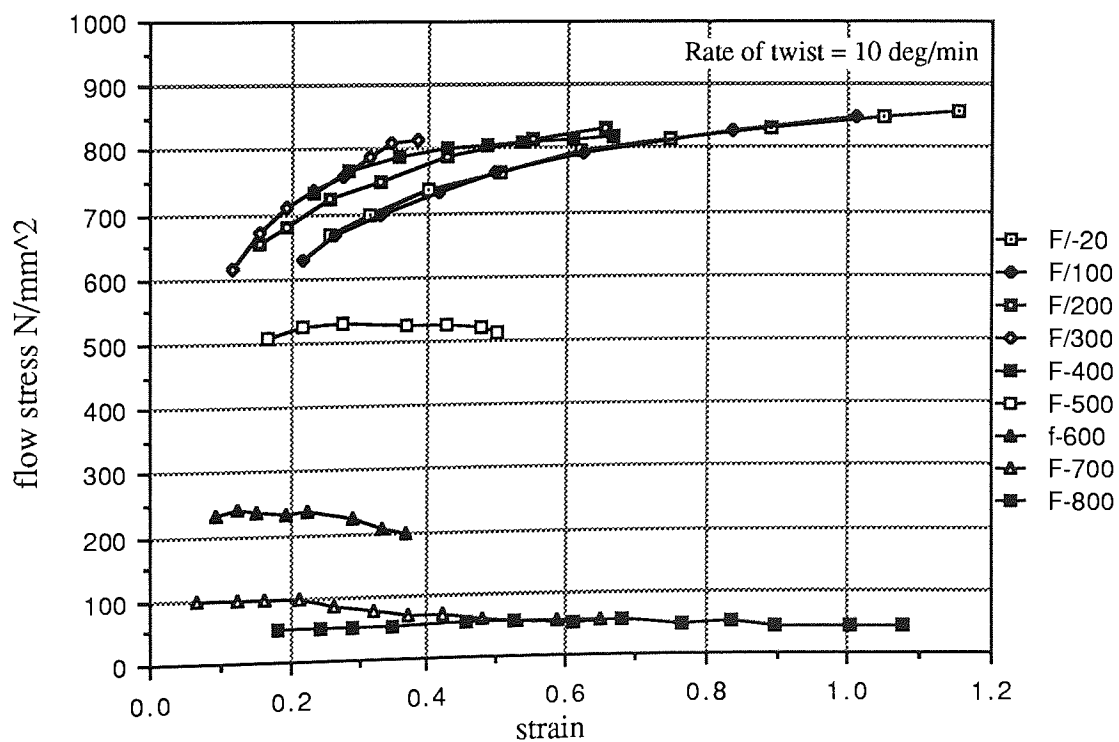
Fig.6.9. Effect of temperature on the flow stress/strain for medium carbon steel
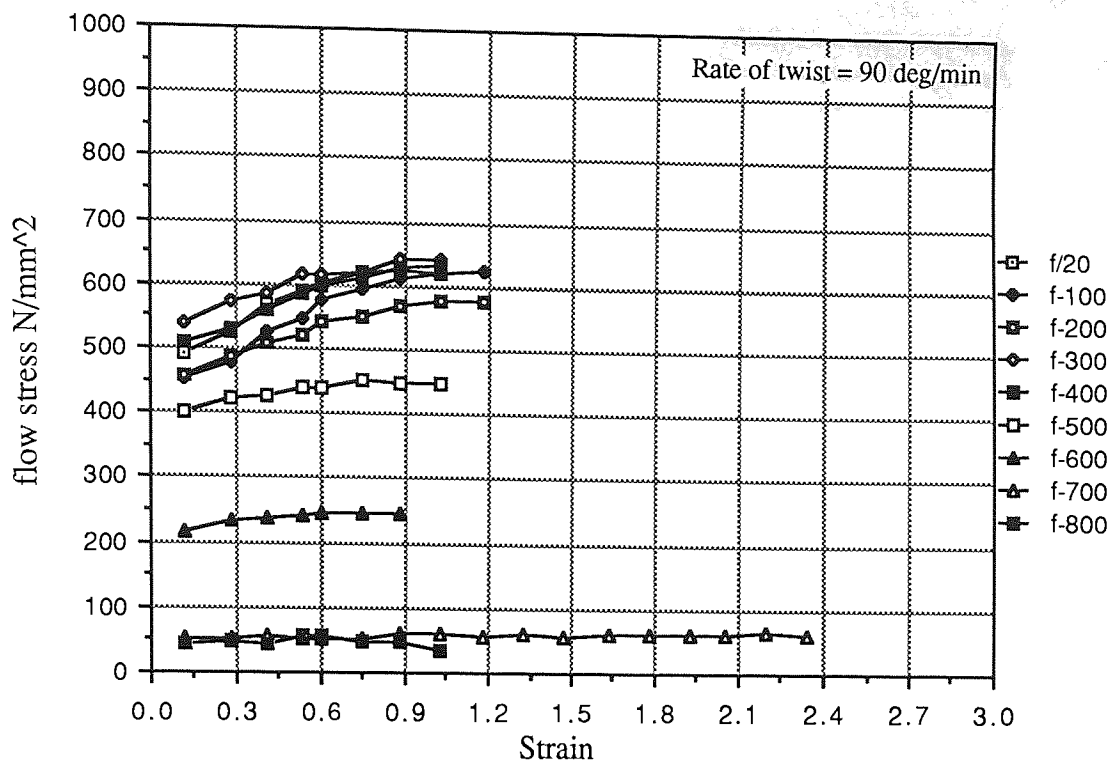
Fig.6.10. Effect of temperature on the flow stress/strain for mild steel.
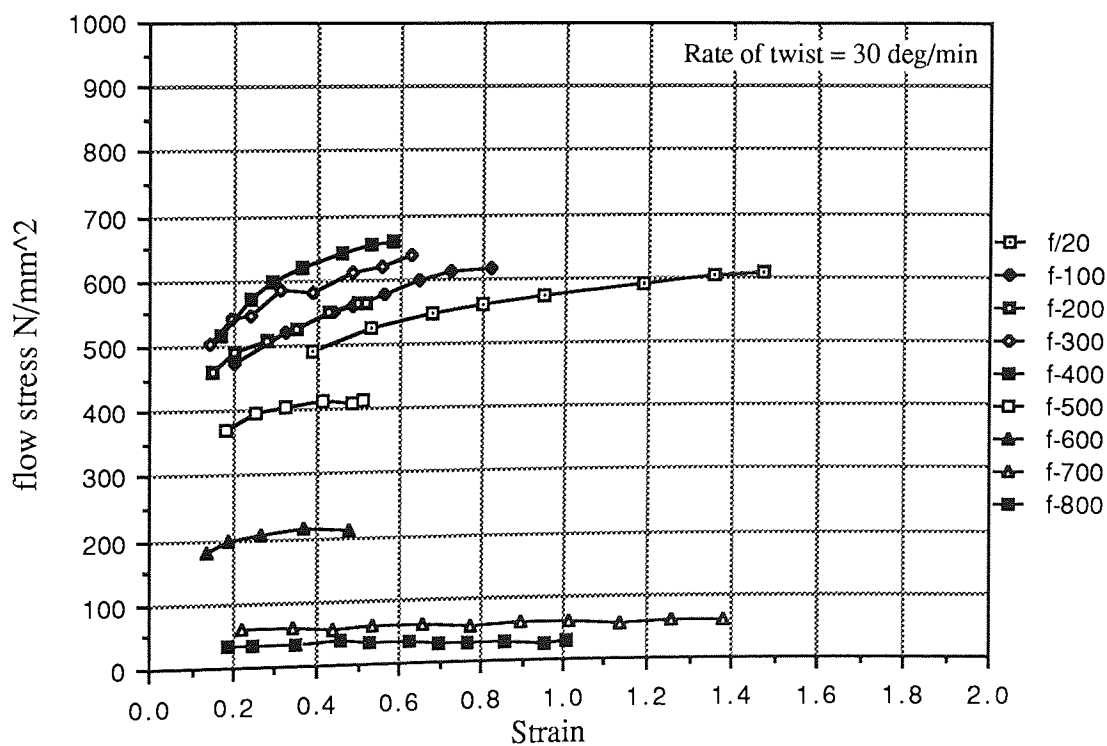
Fig.6.11. Effect of temperature on the flow stress/strain for mild steel.

176
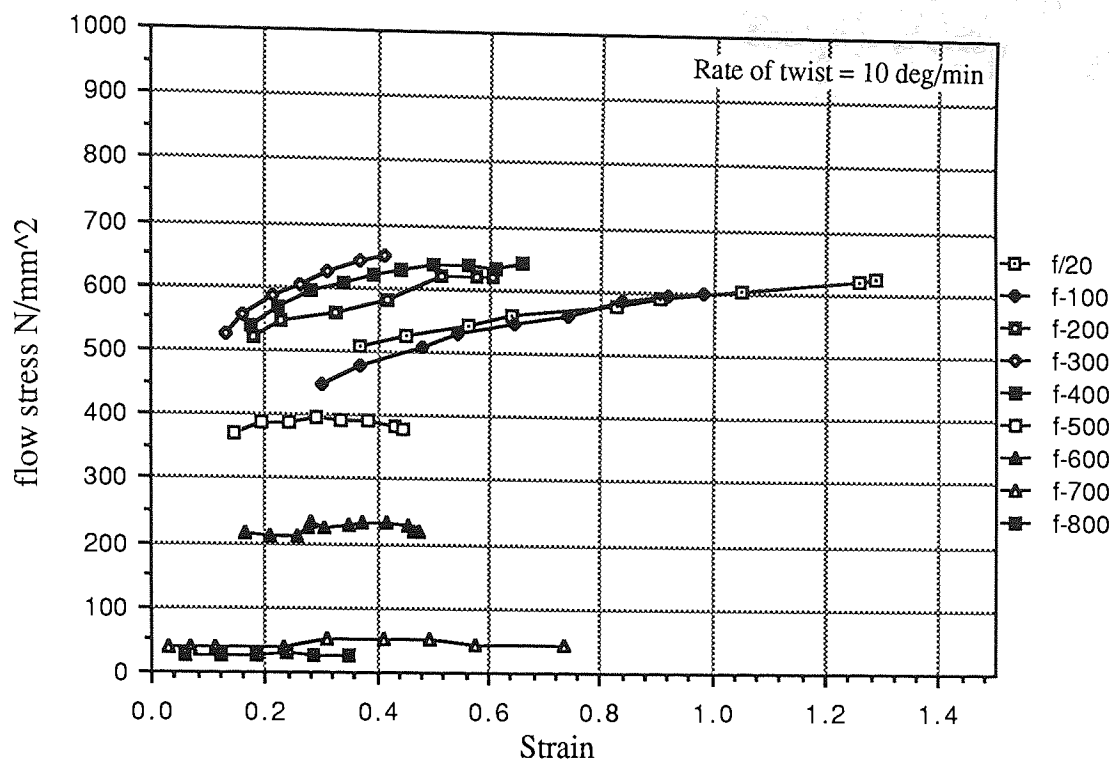
Fig.6.12. Effect of temperature on the flow stress/strain for mild steel.
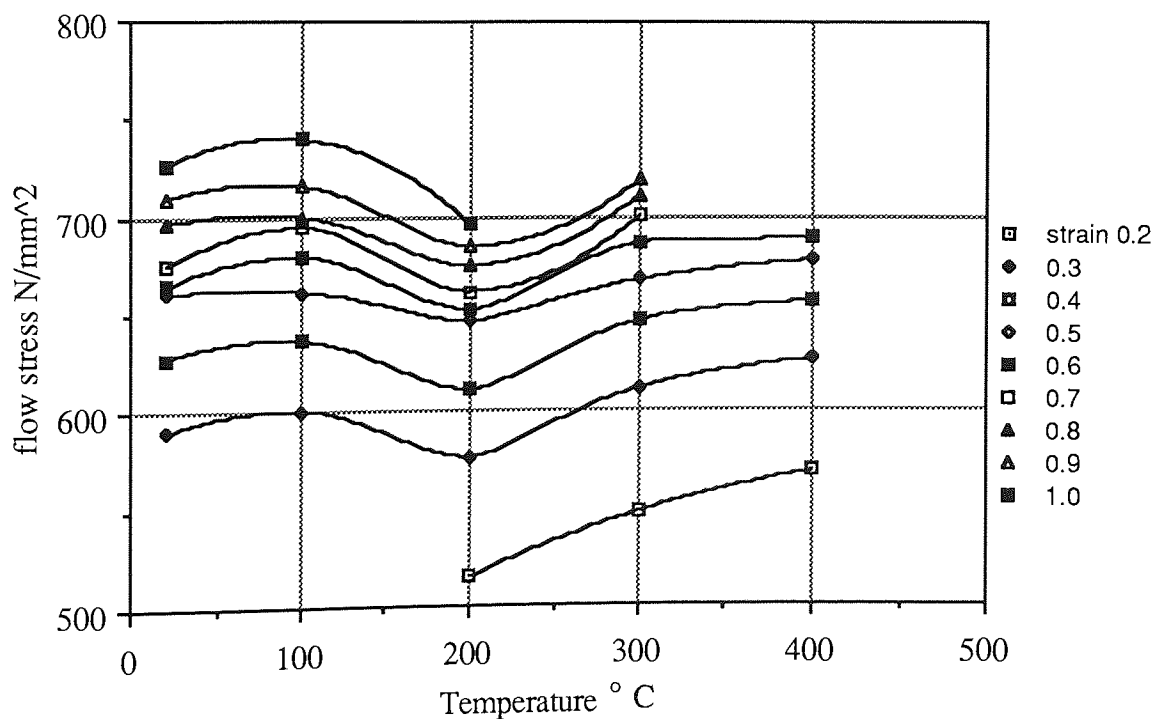
Fig.6.13. Flow stress as a function of the strain and temperature for boron steel.
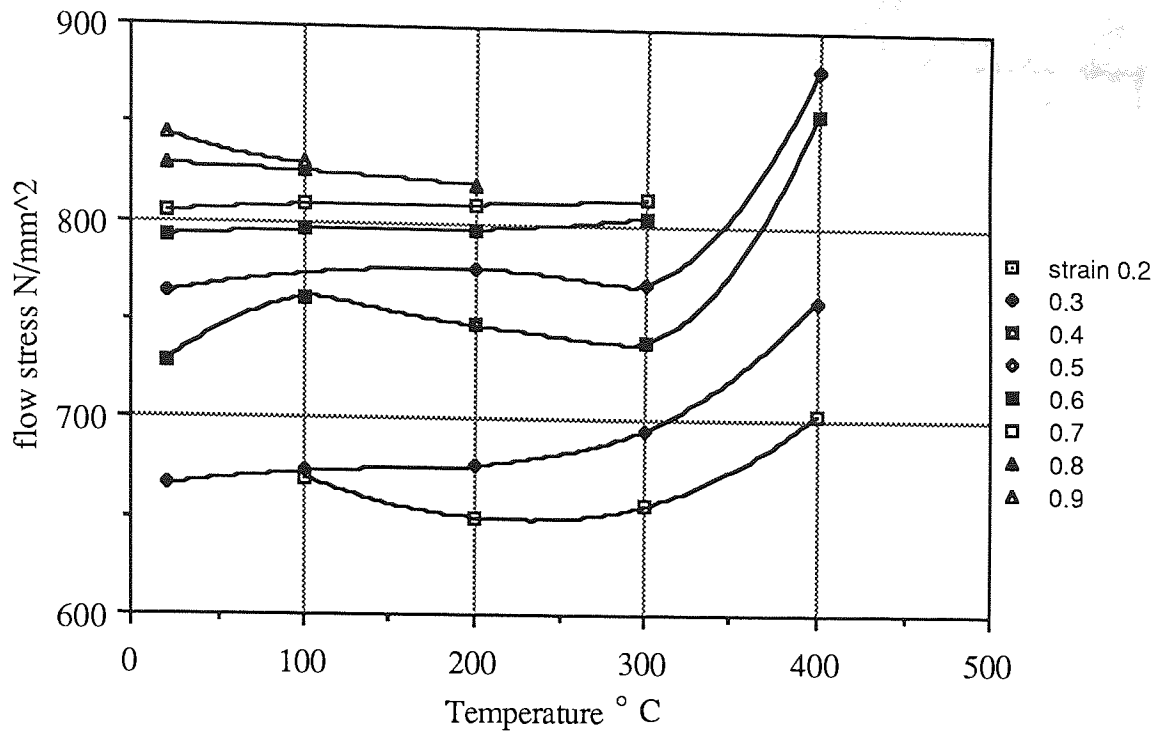
Fig.6.14. Flow stress as a function of the strain and temperature for medium carbon steel.
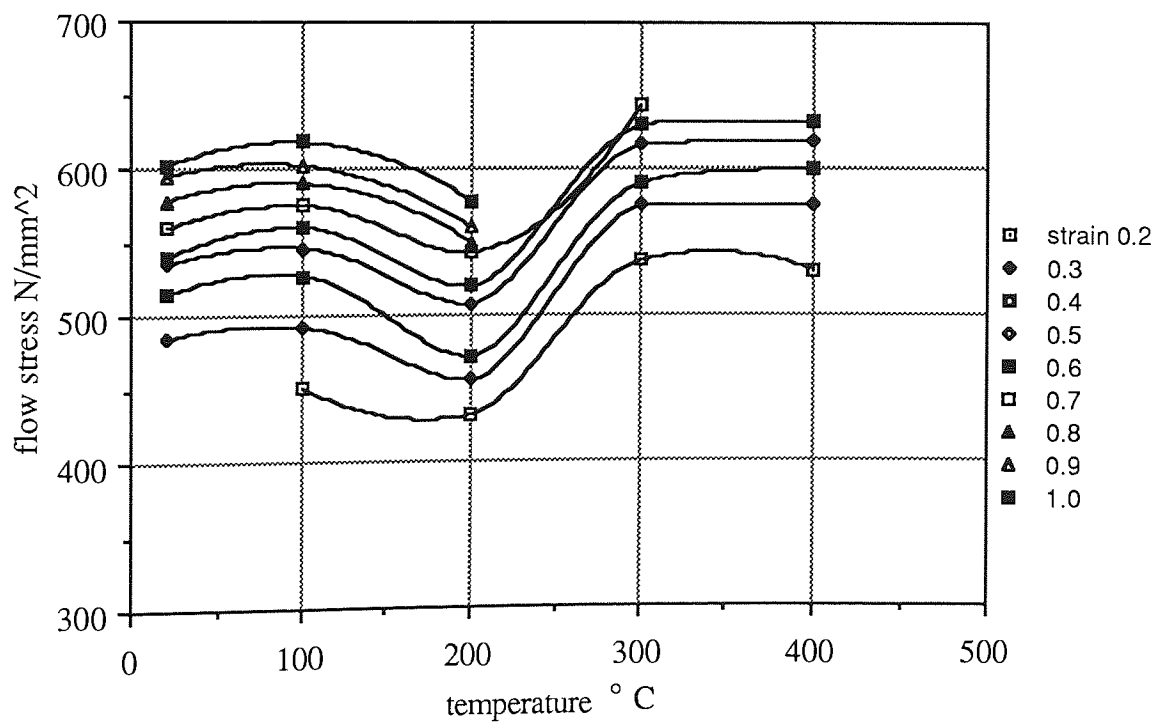
Fig.6.15. Flow stress as a function of the strain and temperature for mild steel.
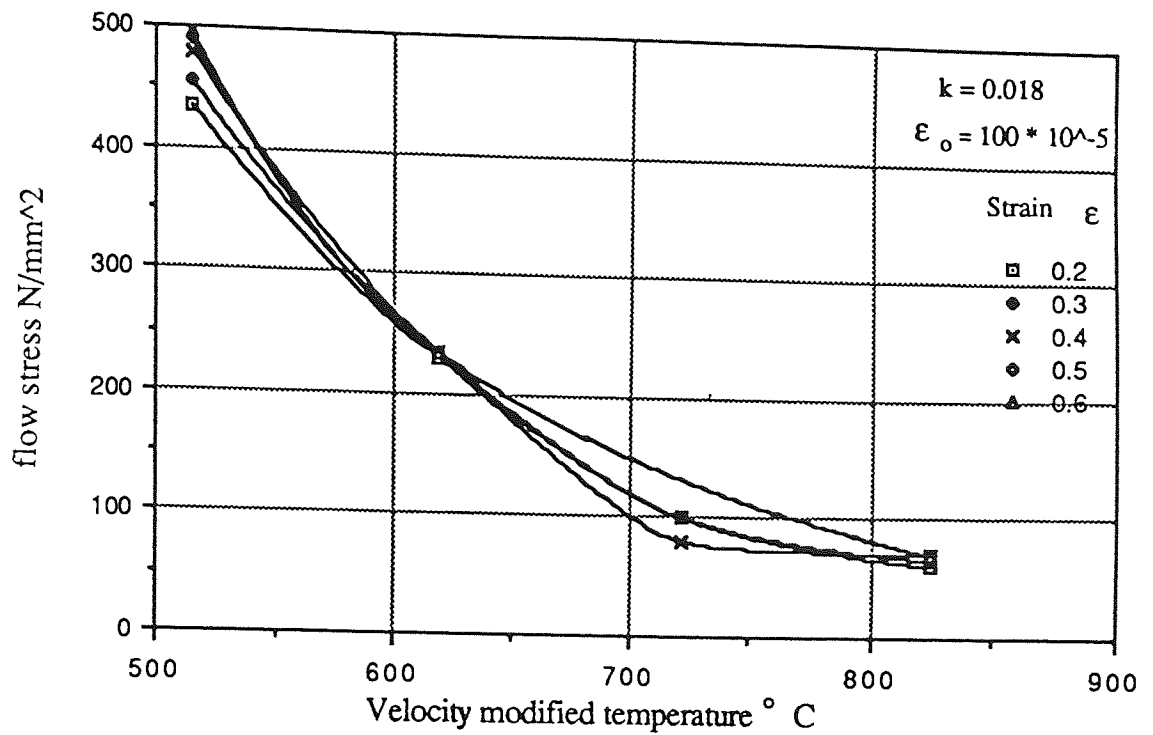
Fig.6.16. Flow stress as a function of strain and velocity-modified temperature for boron steel.
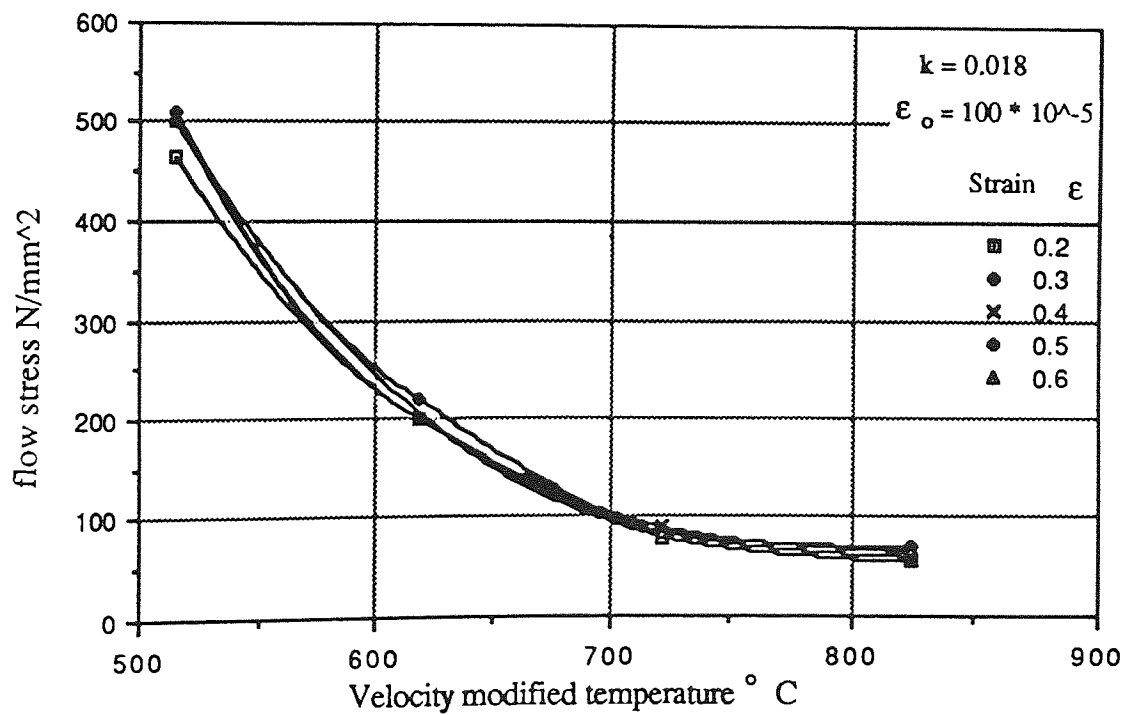
Fig.6.17. Flow stress as a function of strain and velocity-modified temperature for medium carbon steel
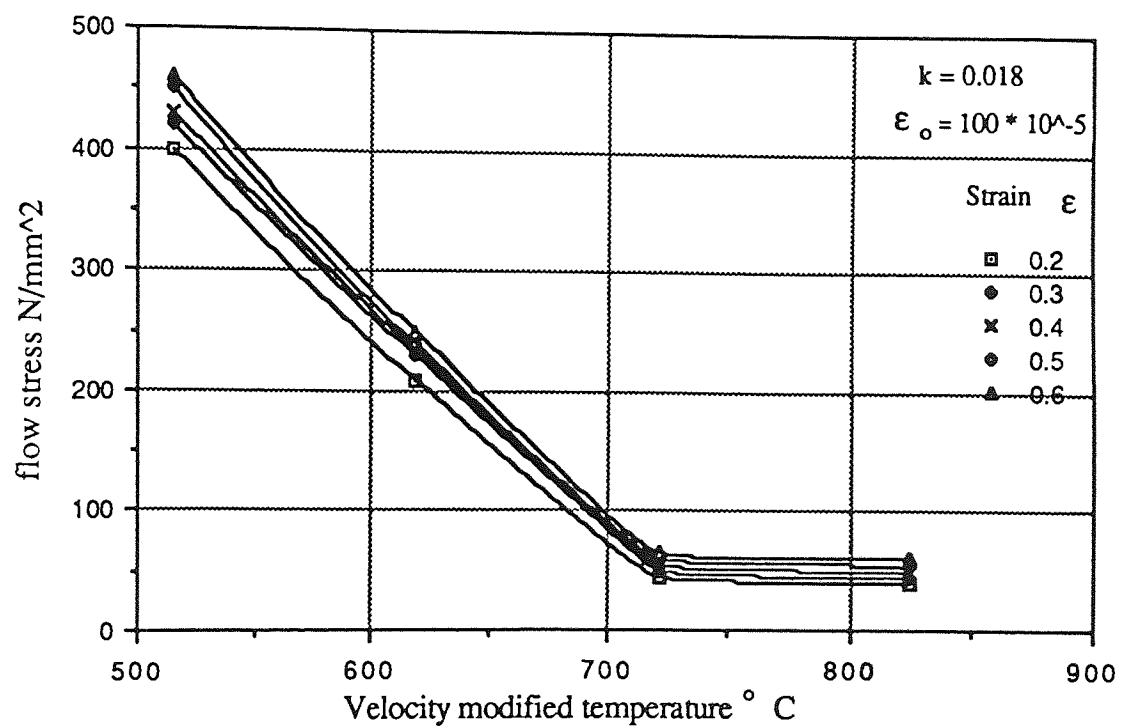
Fig.6.18. Flow stress as a function of strain and velocity-modified temperature for mild steel

CHAPTER SEVEN

EXPERIMENTAL TECHNIQUE, PROCEDURE AND RESULTS

Chapter Seven

7.0 Experimental Technique, Procedure and Results

7.1 Introduction

The experimental investigation for the polygonal section drawing from round at elevated temperatures was divided into four series of tests, the preliminary trials, final tests, metallographic examinations and mechanical testing of samples drawn at different temperatures and reductions of areas. The objectives of the preliminary trials were not only to gain familiarity with the machine and instrumentation, but also to establish a procedure and to study the optimum die geometry needed to produce a successful shape with the least work done. The main body of tests was to investigate the validity of the theory of polygonal drawing from round at elevated temperatures, developed in Chapter three, to predict the drawing stresses at elevated temperatures. Metallographic and mechanical examination of samples drawn at different temperatures and reductions of area, to study the effect of varying these parameters on the microstructure and the mechanical properties of the drawn samples.

7.2 Preliminary preparation

- The wire was initially swaged, using a rotary swager, to enable the wire to be threaded through the die. It was swaged down to different diameters depending on the degree of reduction of area and the toughness of the workpiece material used. In some tests, the wire was swaged five different times to different diameters to provide, at the start of the drawing operation, a gradual transformation from round to the particular section produced. When the final swage had been reached, the workpiece materials had sufficient strength to pull the undrawn wire through the die, achieving a high reduction of area without breaking taking place.

181

- preparing the lubricant mixture; a fixed proportion of two volumes of soap solution was added to one volume lubricant, and stored in a large drum to be used throughout the testing to ensure uniformity of lubricant. A quick drying solvent such as Toluene is sometimes mixed with a number of the lubricants used in the preliminary trials which were conducted to decide on the type of lubricant to be used for the main tests. Before each test, the lubricant was thoroughly mixed and some poured into the lubricator.

- the drawing die to be used was cleaned ultrasonically in the proprietary agent Inhibisol and examined, before being mounted in the die holder.

- at this stage, with everything in position, it is not necessary to check the loadcell supply voltage, because the voltage is fixed at 12.5 V, which is the maximum for the amplifier used. The computer program was loaded into the disc drive and run, to display an initial reading of various quantities existing on the A/D converter channels before testing takes place. A check of the various instruments used was then made, to make sure that they all function well. Bridge balancing is carried out by the software, which uses an offset value to account for and re-balance the different values obtained.

7.3 The drawing technique

The wire sample was threaded through the roller straightener, lubricator, induction coil and into the drawing die. The swaged end was pushed through the die and gripped in the jaw of the bull block. The undrawn wire held between the die and roller straightener had been straightened. This enabled better alignment of the wire in the induction coil and lubricator, and the focussing of the optical fibre. The optical fibre was focussed on the wire using a light source and it was then re-connected to the thermal monitor. The water supply was turned on, to cool the die during testing. Atomised water was switched on to cool the wire as it leaves the die. The lubricator pump was switched on to mix the lubricant.

Before the start of the drawing tests, all the equipment was switched on for warming up and stablising, these include, "the induction heater, amplifier, computer, and compressors" then set to the correct requirements. The bull block was started, the wire was allowed to run for several turns of the swift, and then stopped in order to check that the infra-red detector was correctly focussed on the wire, the bull block was then re-started, followed immediately by the induction heater, which was already set at the approximate desired temperature. When the desired temperature was reached, the computer was set to capture data for a specified time interval. The induction heater was switched off and the wire was allowed to run for two turns at ambient temperature, then the bull block was stopped. The drawn wire was marked using marker tape. The emissivity value and power input were adjusted for the next desired temperature. A print out of the average values of speed, temperature, and load are available at this stage. By the input of relevant information a complete test result is obtained immediately, a sample test result is shown in Appendix (A3).

The drawn wire was cut off, labelled and stored for further mechanical testing and metallographic examinations.

7.4 Experimental and theoretical results

The following section represents some of the experimental results carried out using various test piece materials, die geometries, die materials and lubricants; these are represented by figs.7.1-7.24. Theoretical results obtained are represented by figs.7.25 - 7.73 and Tables 7.1 - 7.5.
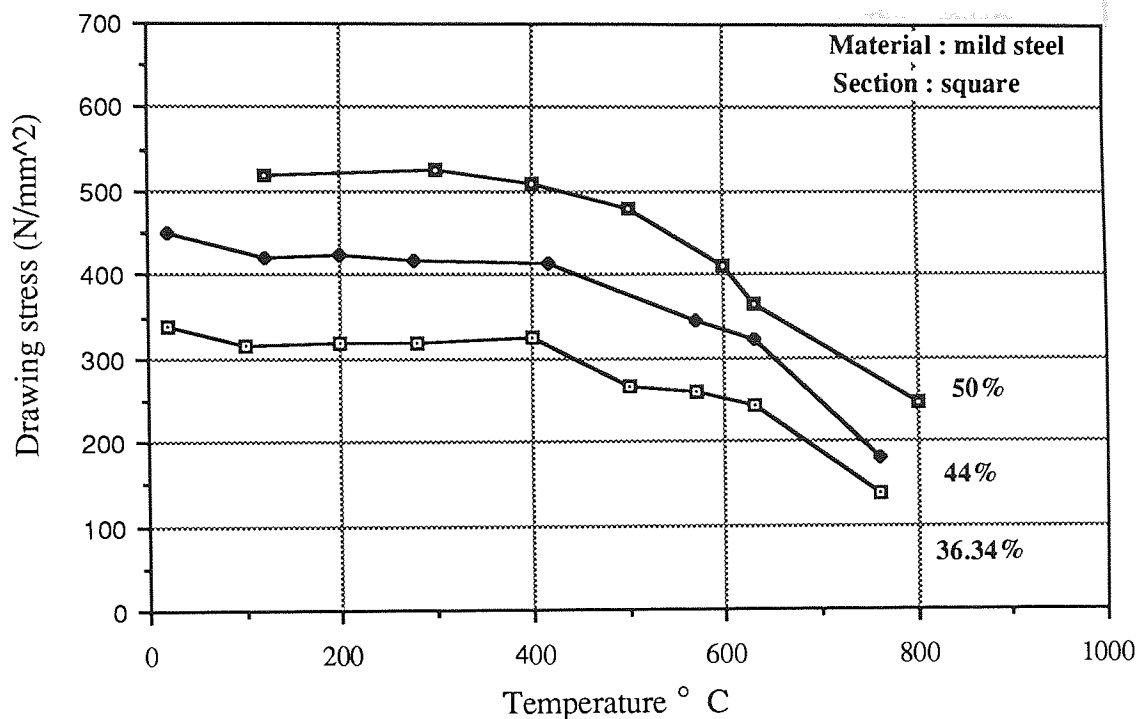
Fig.7.1. Variation of experimental drawing stress with temperature and reduction of area using the modified die design.
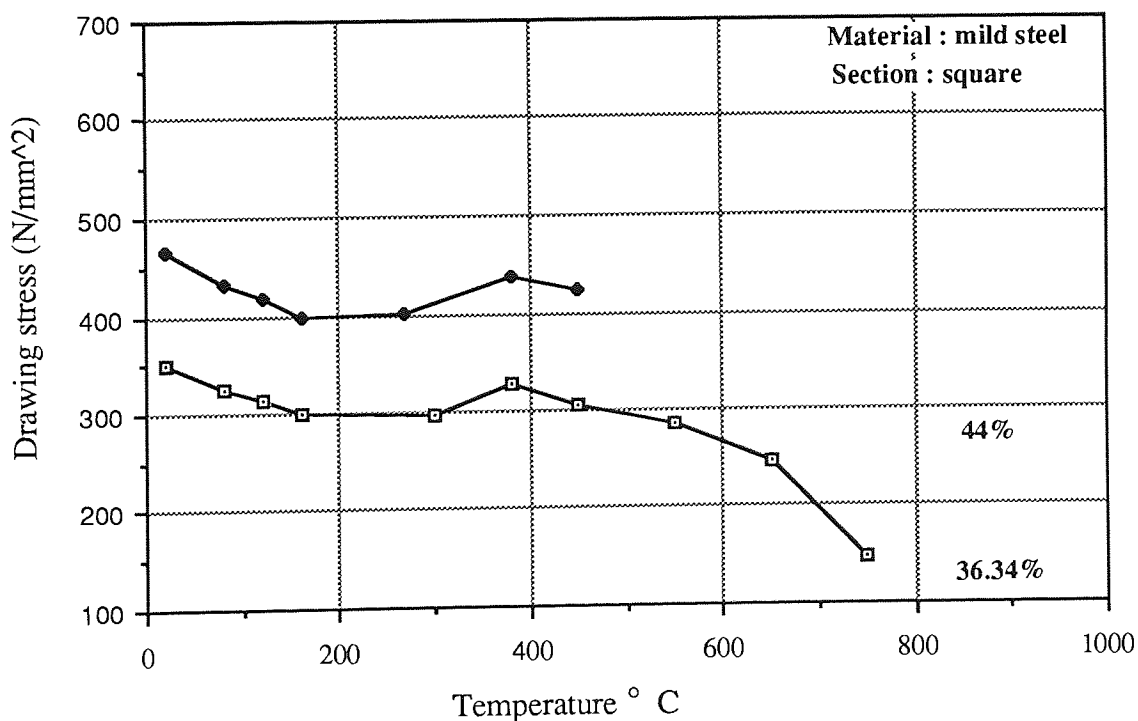
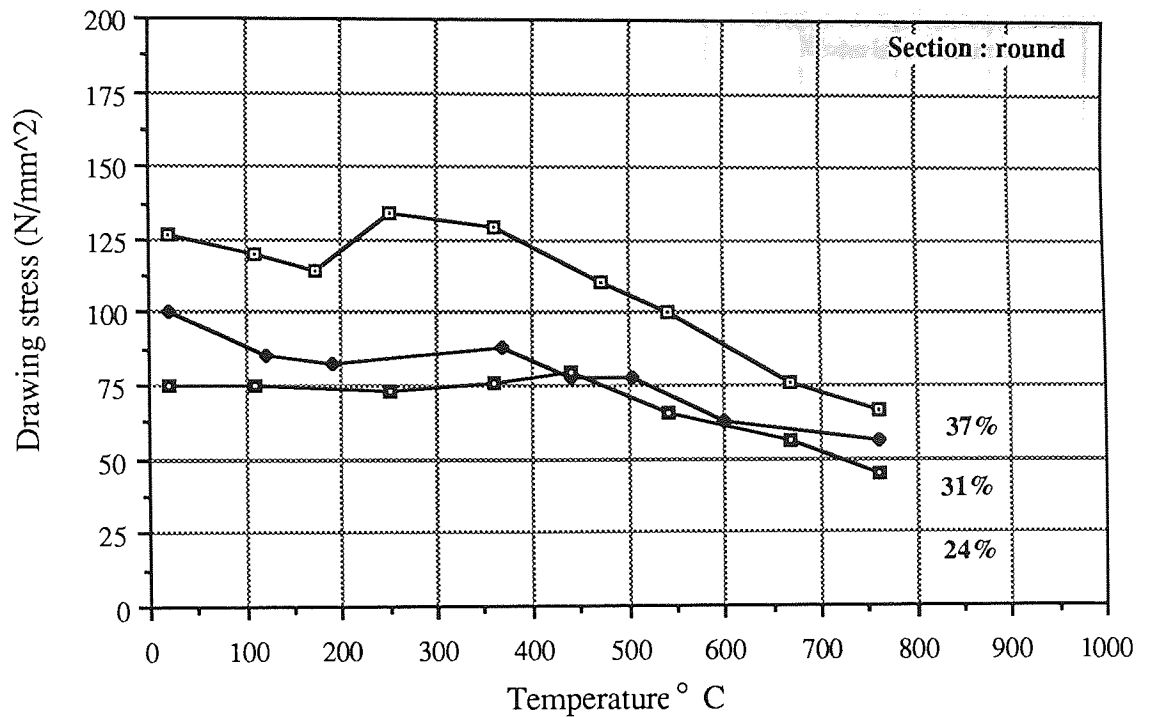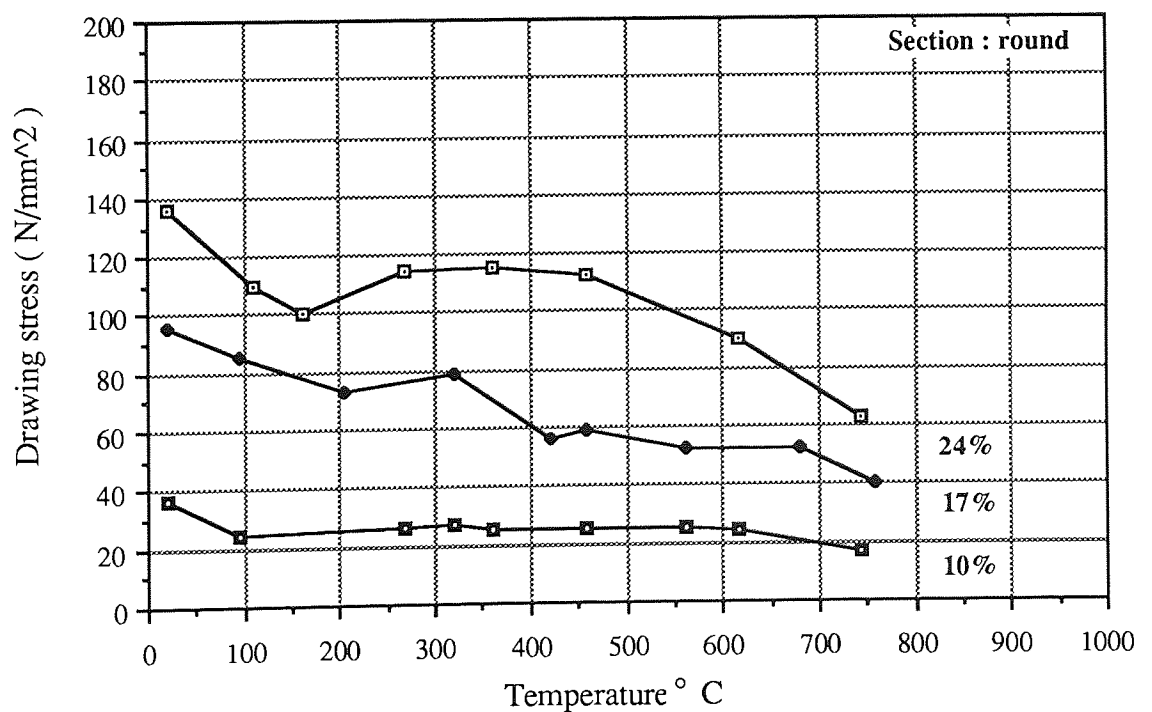Fig.7.2. Variation of experimental drawing stress with temperature and reduction of area using die designed by Basily.

184
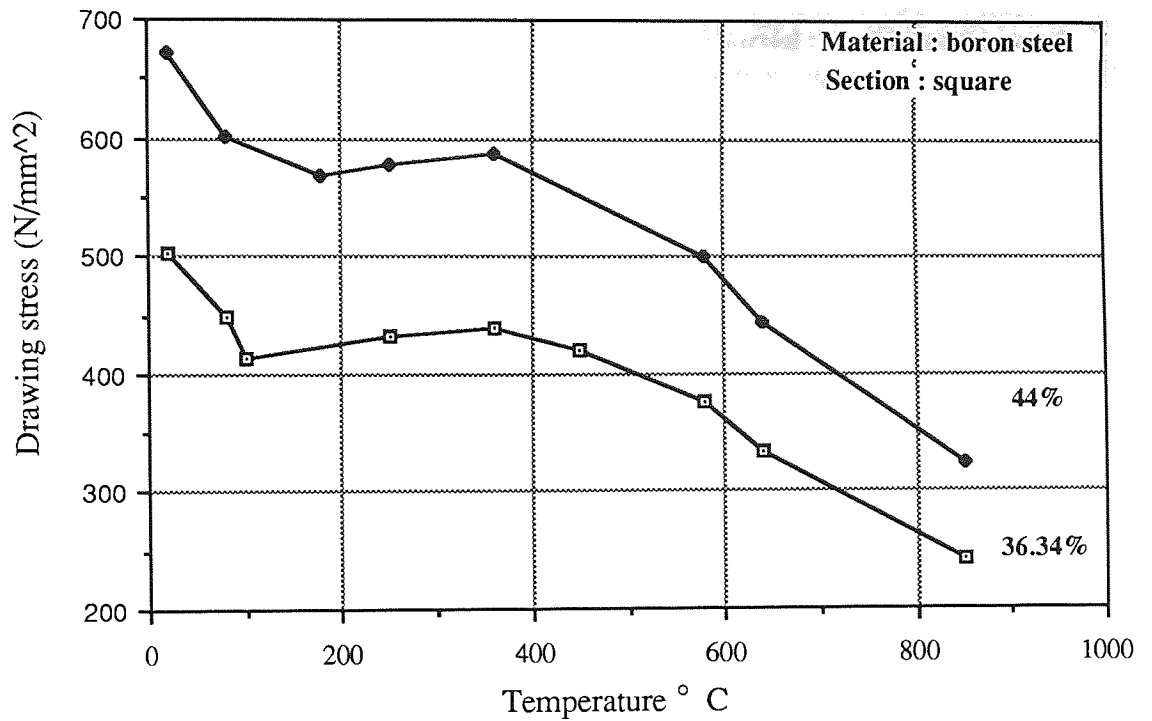
Fig.7.3. Variation of experimental drawing stress with temperature and reduction of area using the modified die design.
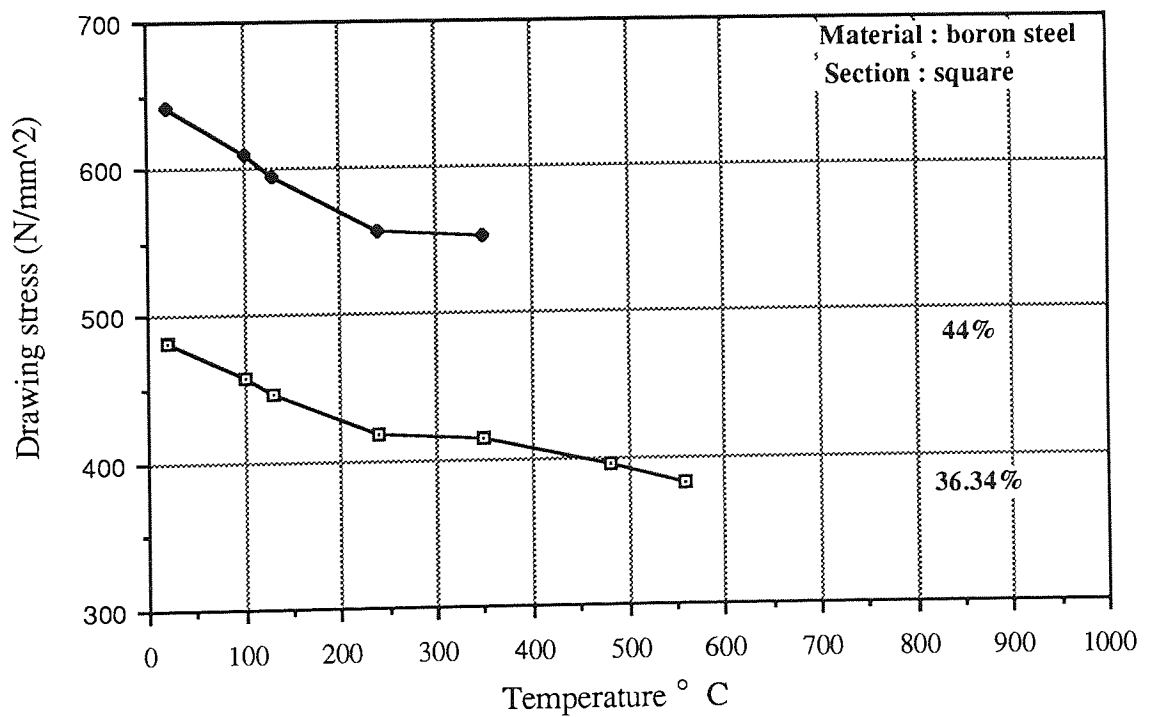
Fig.7.4. Variation of experimental drawing stress with temperature and reduction of area using die designed by Basily.

185
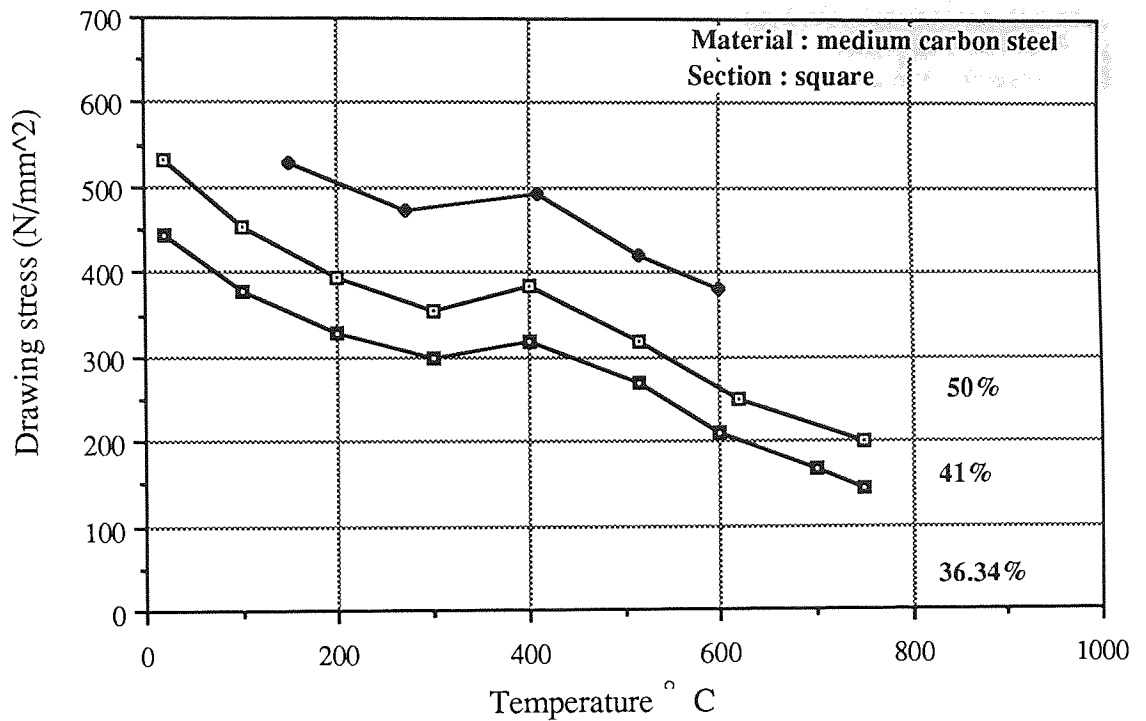
Fig.7.5. Variation of experimental drawing stress with temperature and reduction of area using the modified die design.
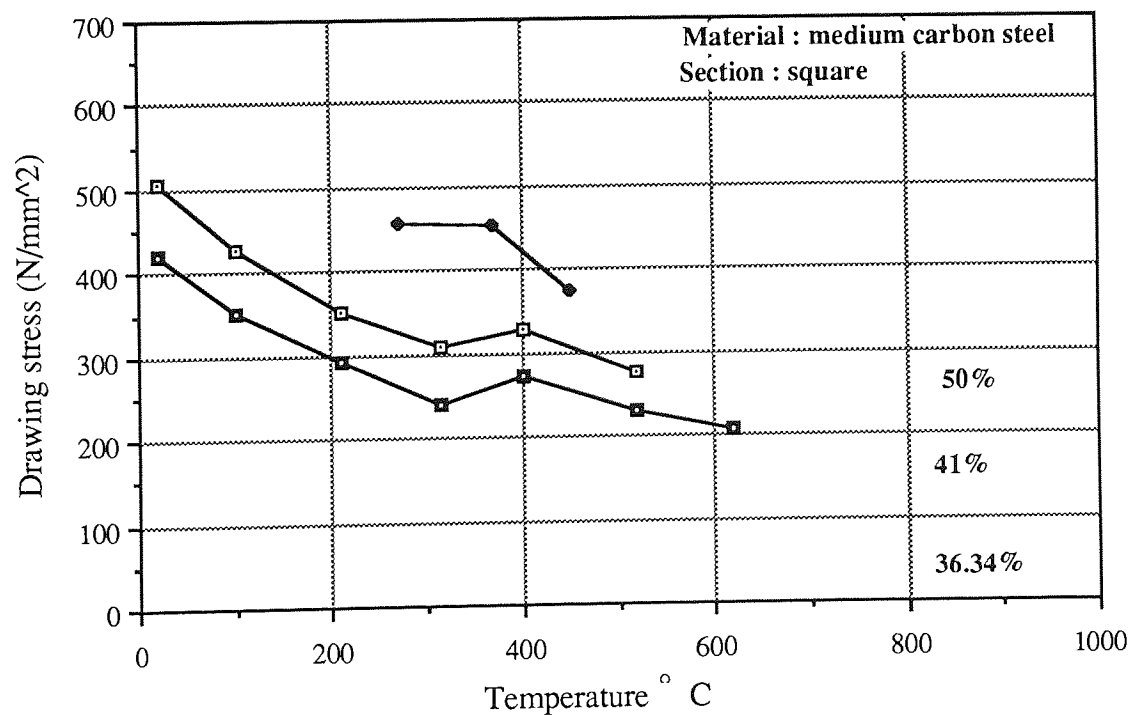
Fig.7.6. Variation of experimental drawing stress with temperature and reduction of area using die designed by Basily.

186
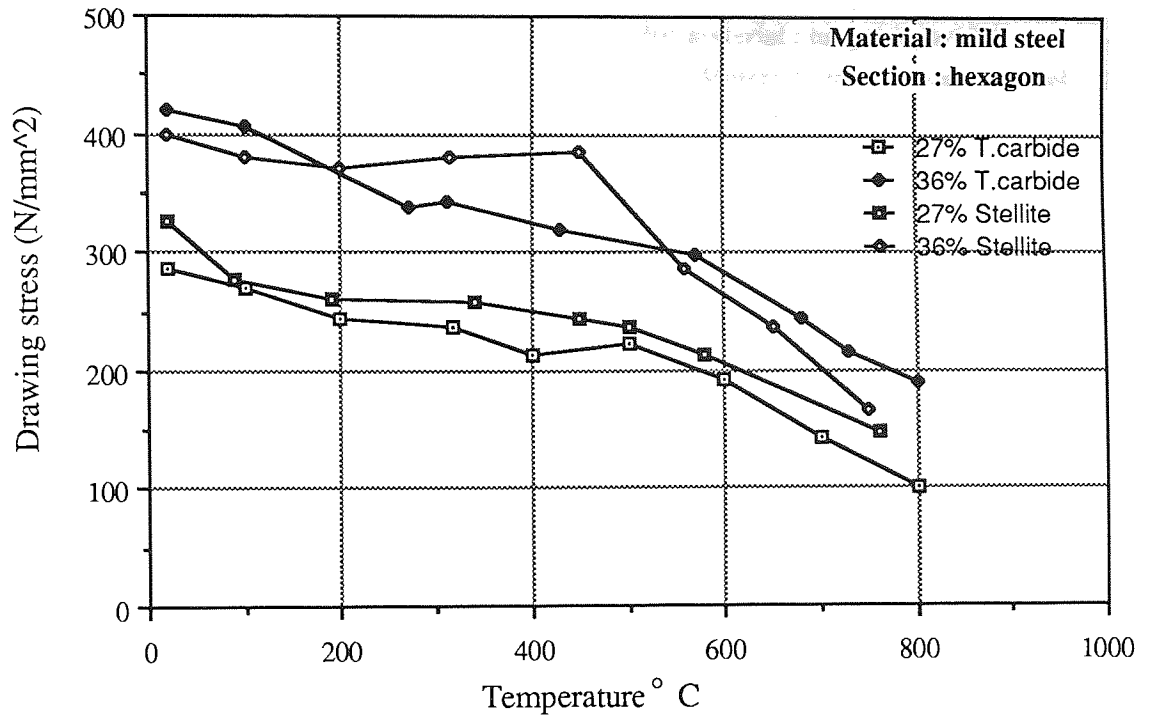
Fig.7.7. Variation of experimental drawing stress with temperature and reduction of area using tungsten carbide and Stellite as die materials.
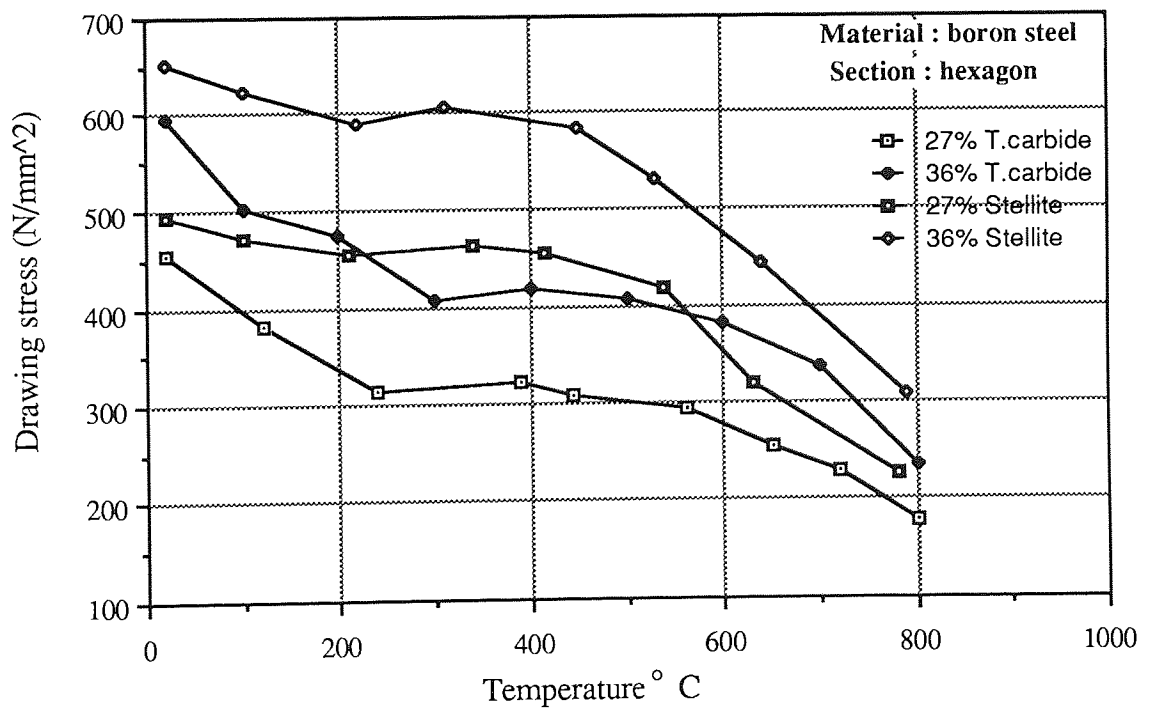
Fig.7.8. Variation of experimental drawing stress with temperature and reduction of area using tungsten carbide and Stellite as die materials.
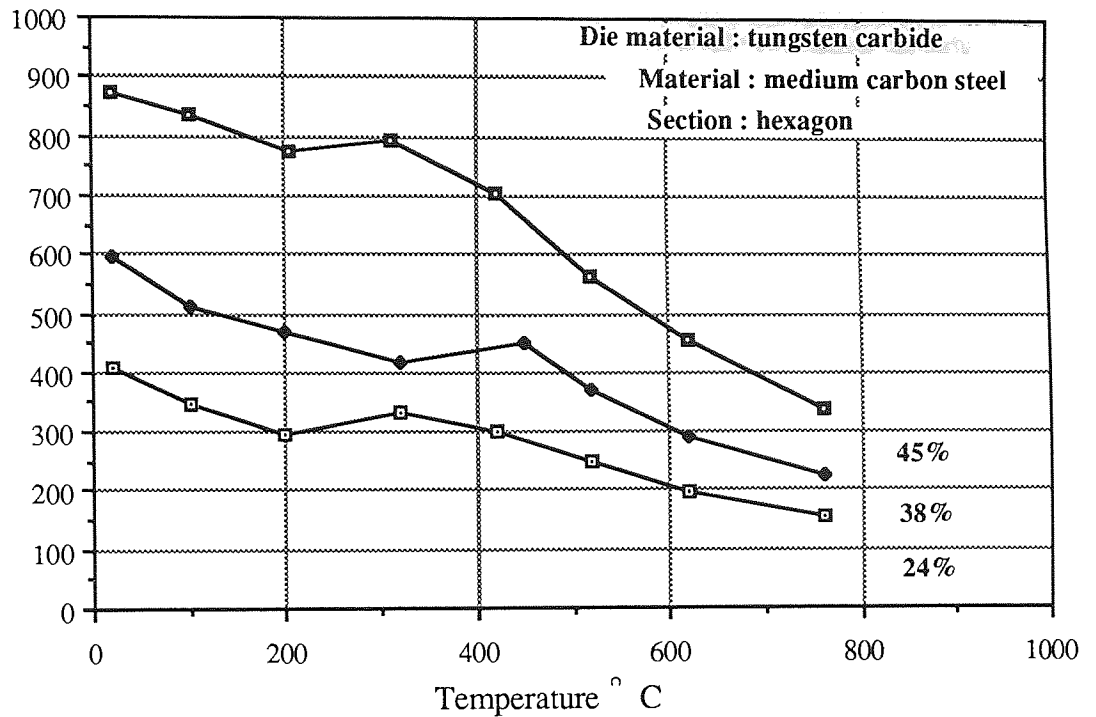
Fig.7.9. Variation of experimental drawing stress with temperature and reduction of area using the modified die design.
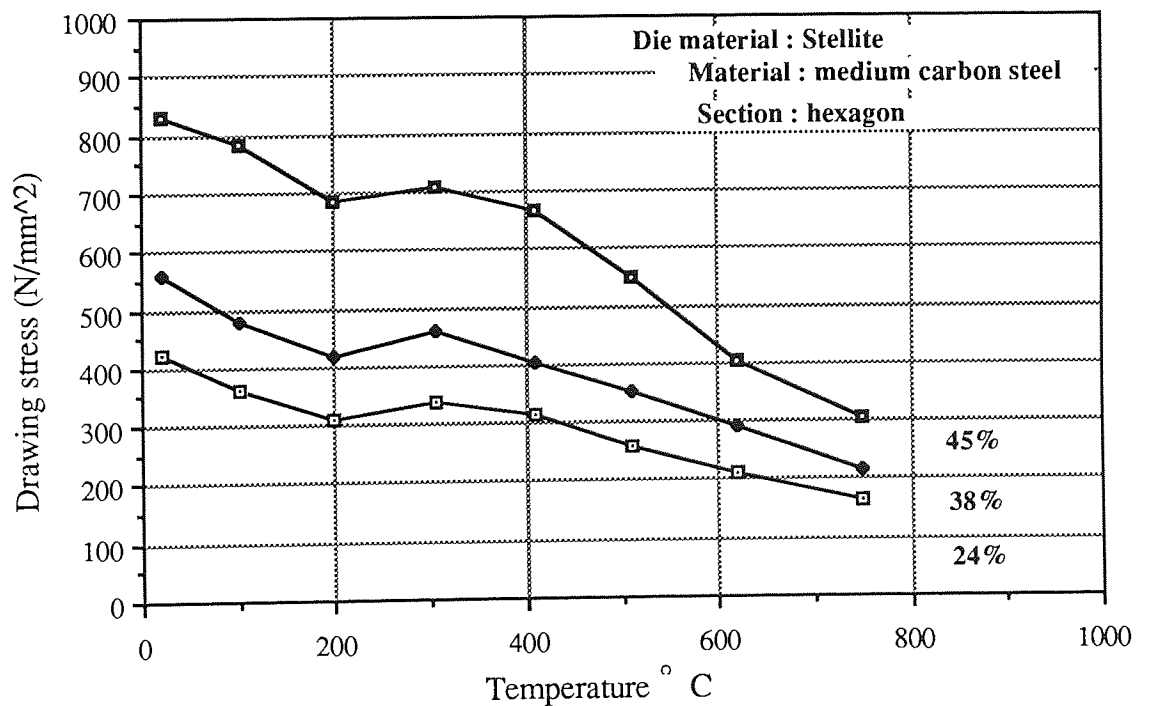
Fig.7.10. Variation of experimental drawing stress with temperature and reduction of area using the modified die design.

188
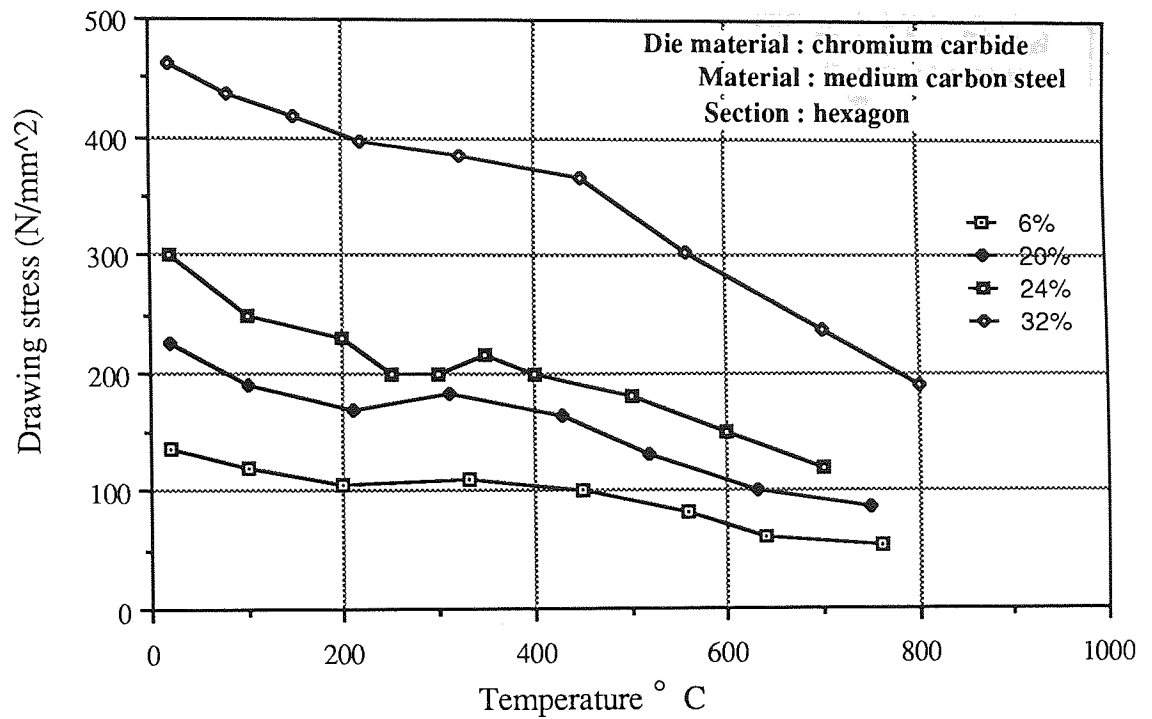
Fig.7.11. Variation of experimental drawing stress with temperature and reduction of area using the designed die.
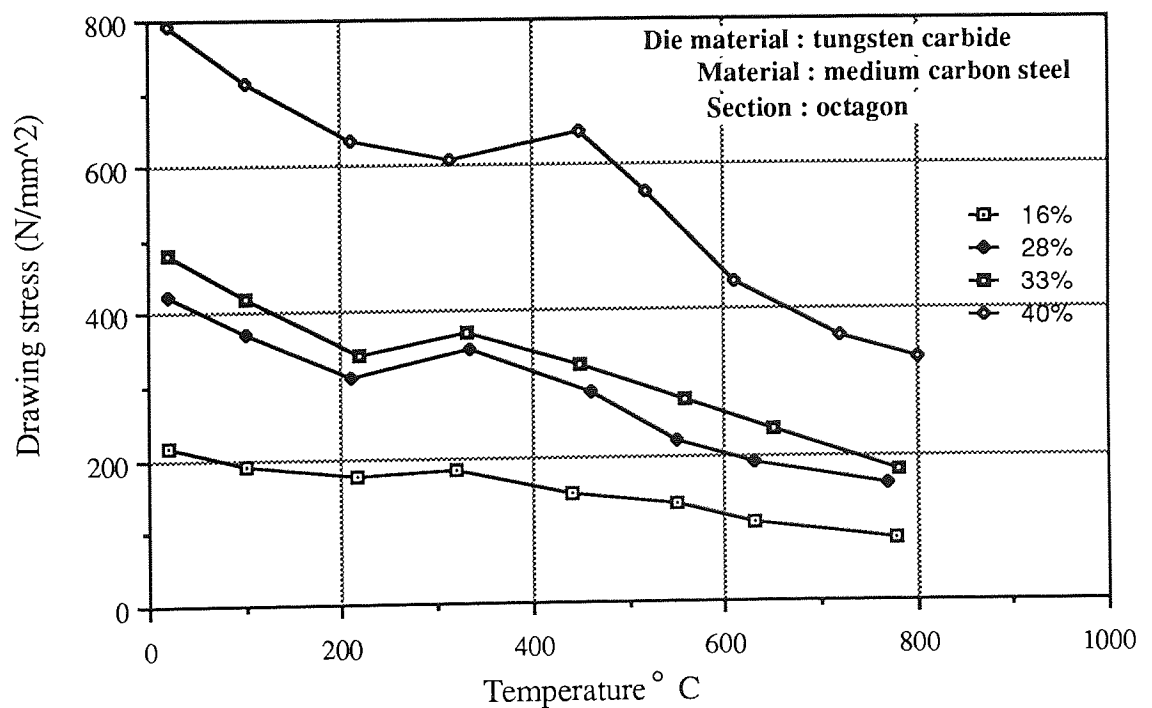
Fig.7.12. Variation of experimental drawing stress with temperature and reduction of area using the modified die design.

189
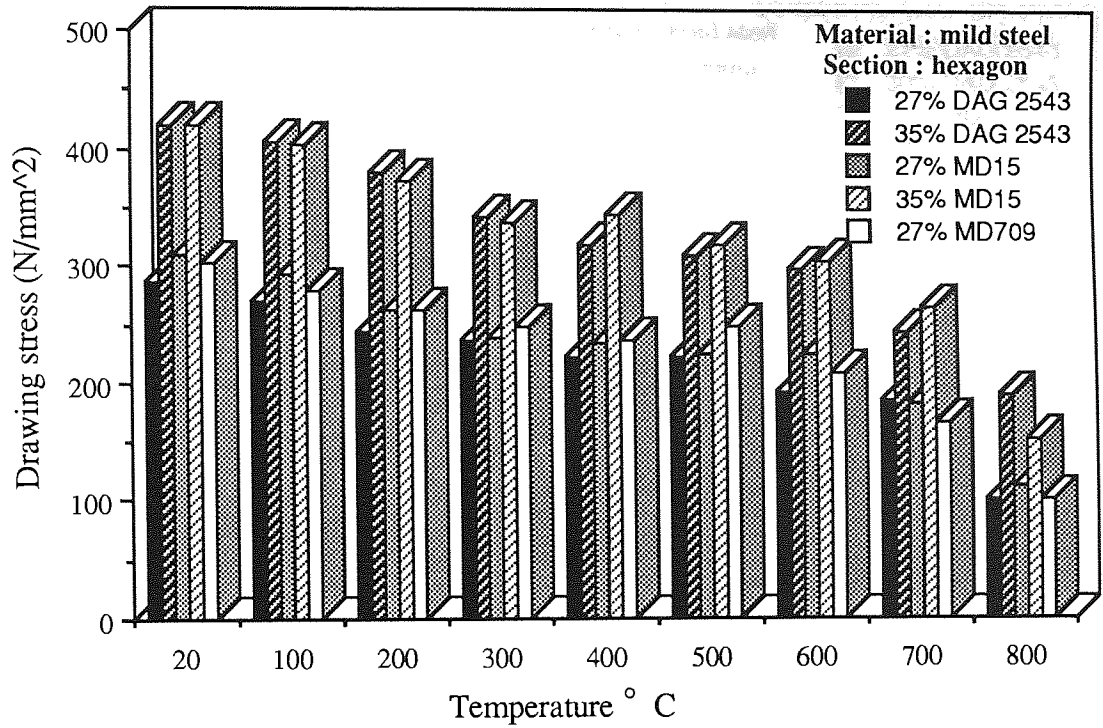
Fig.7.13. Variation of experimental drawing stress with temperature using different lubricants.
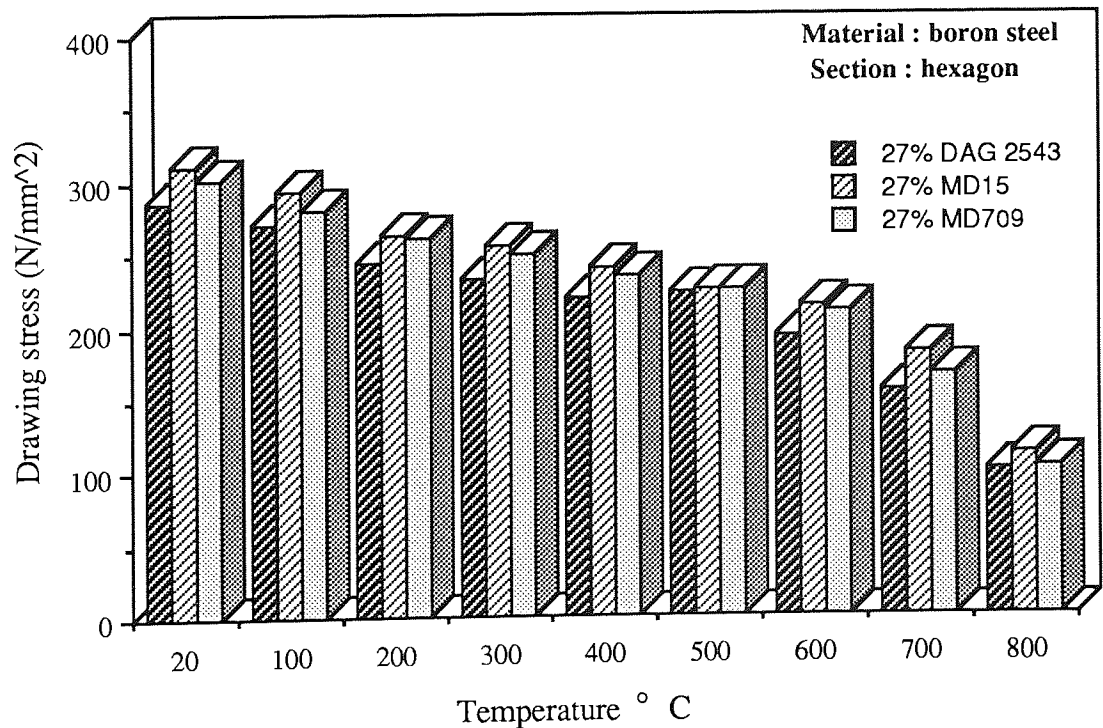
Fig.7.14. Variation of experimental drawing stress with temperature using different lubricants.
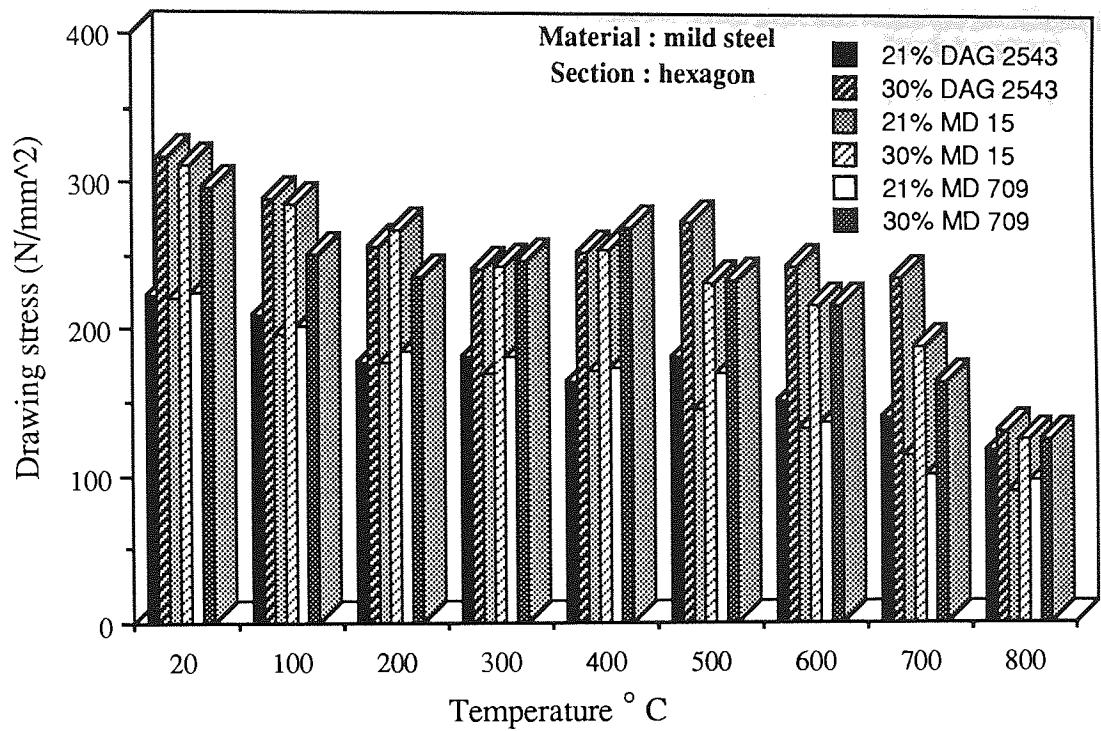
Fig.7.15. Variation of experimental drawing stress with temperature using different lubricants.
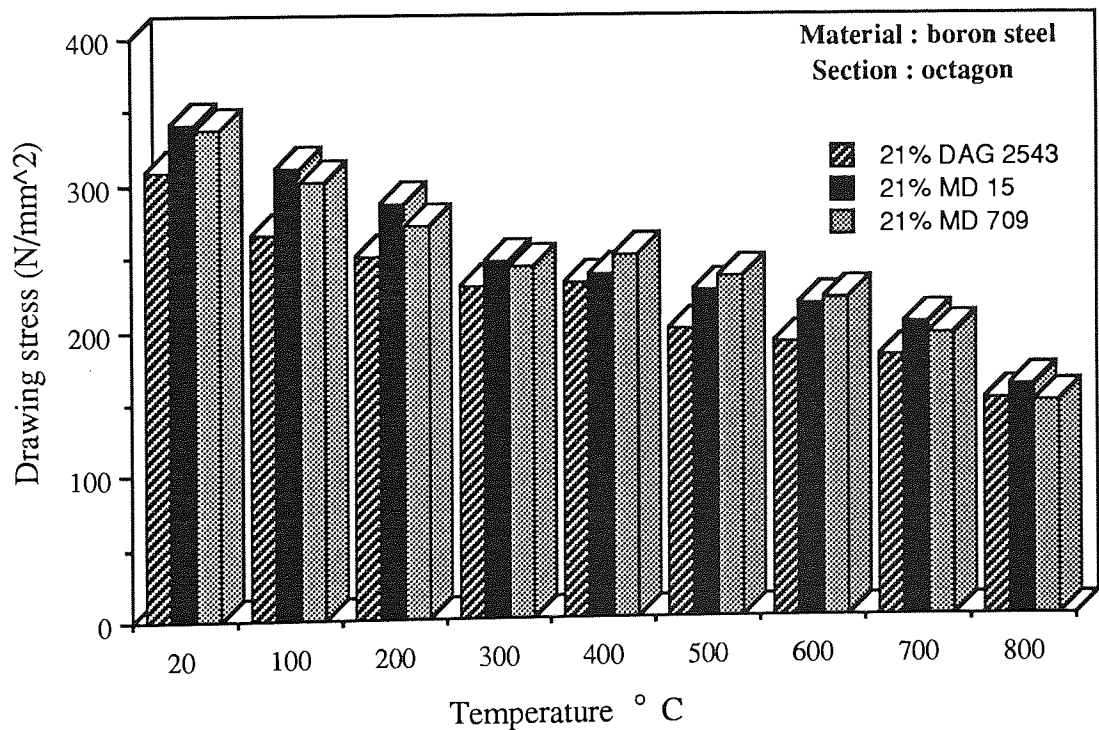
Fig.7.16. Variation of experimental drawing stress with temperature using different lubricants.
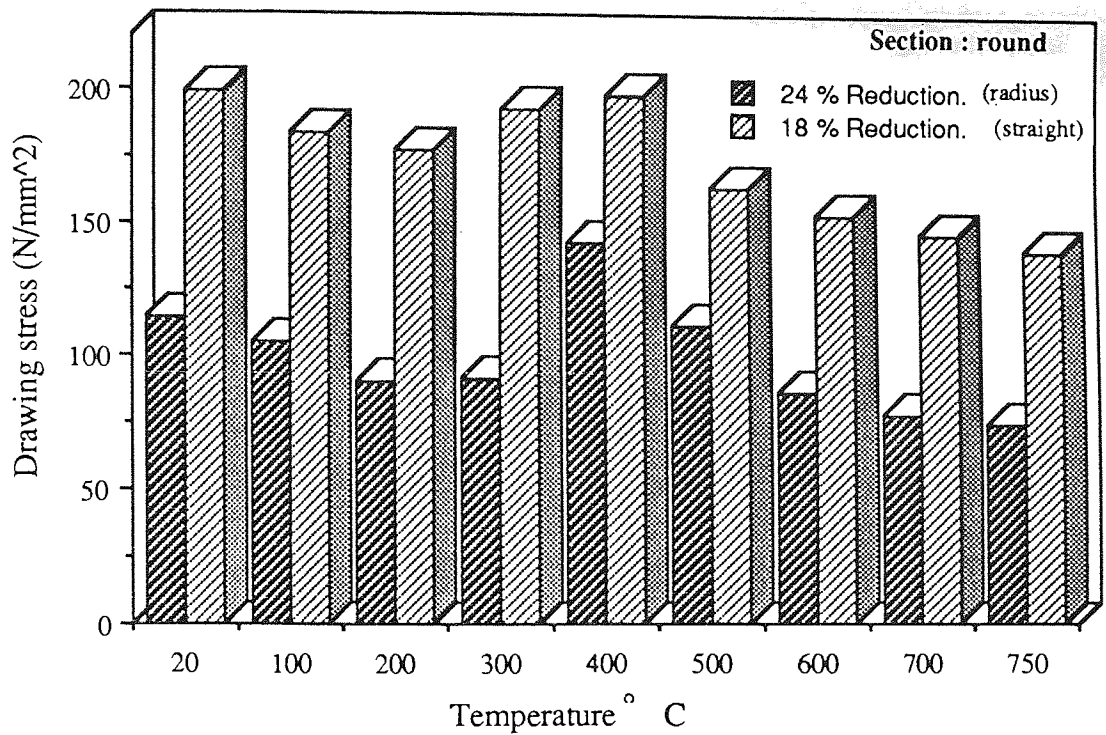
Fig.7.17. A demonstration of the effect of die geometry on drawing stress, dies being used are of straight and radius geometry.
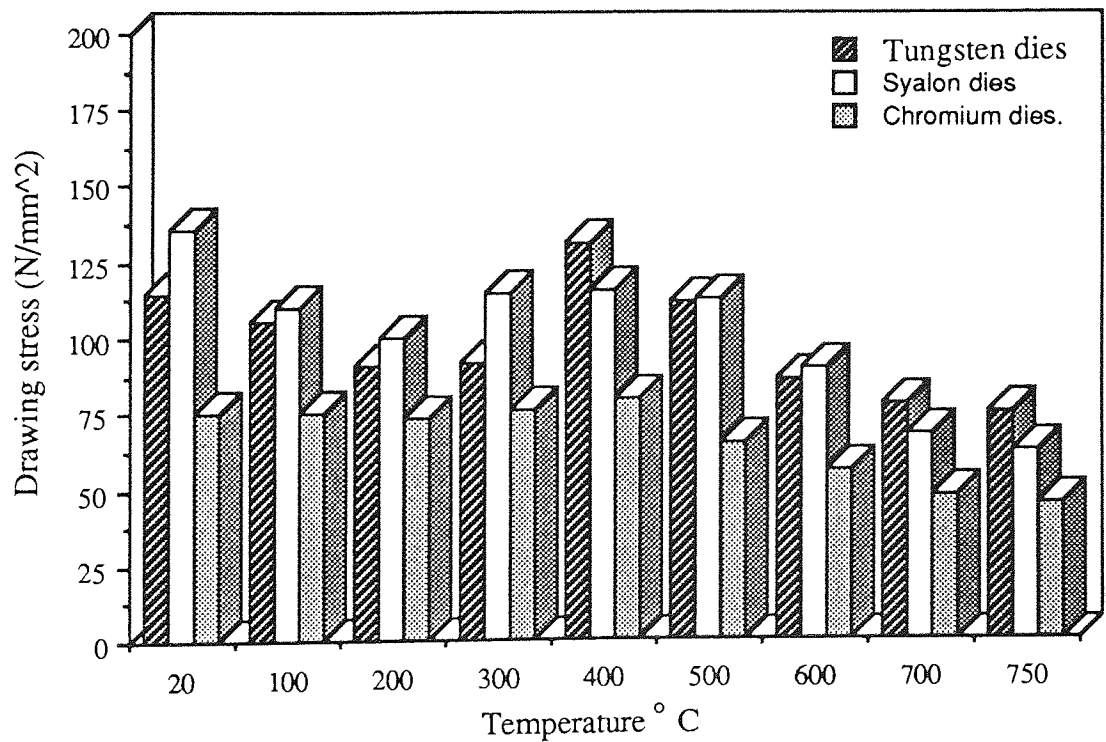
Fig.7.18. The variation of the drawing stress with temperature using three different die materials at 24% reduction of area.

192

Fig.7.19. Variation of experimental drawing stress with temperature and reduction of area using chromium carbide dies.

Fig.7.20. Variation of experimental drawing stress with temperature and reduction of area using syalon dies.

193
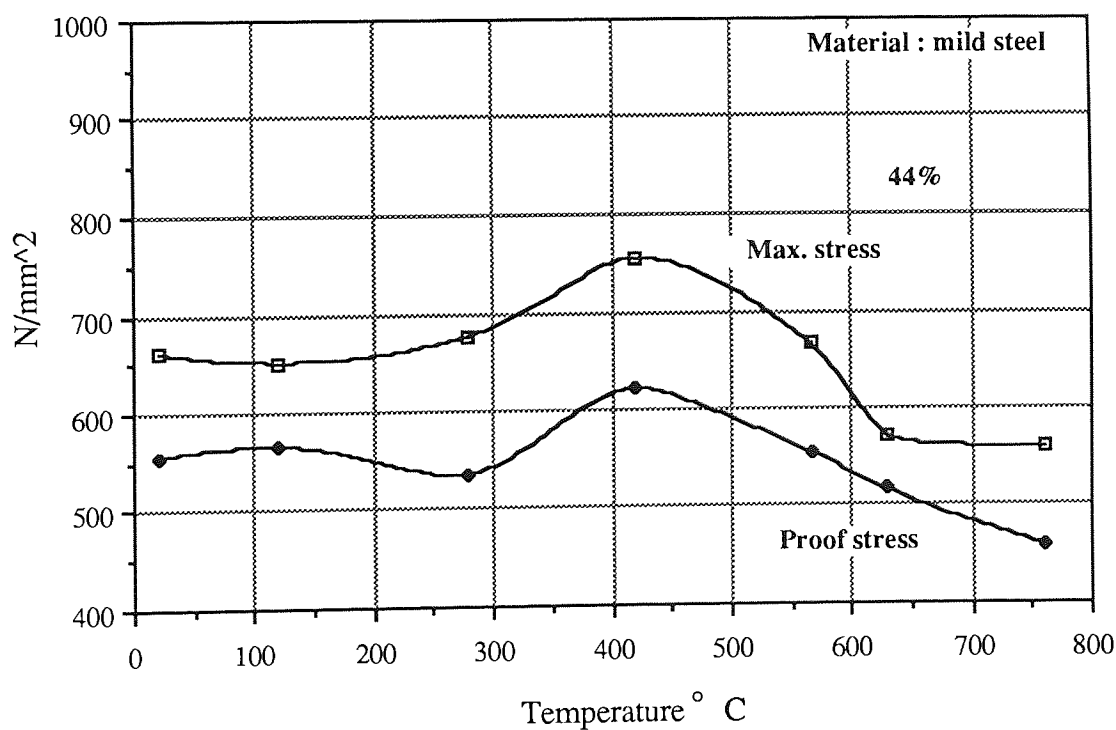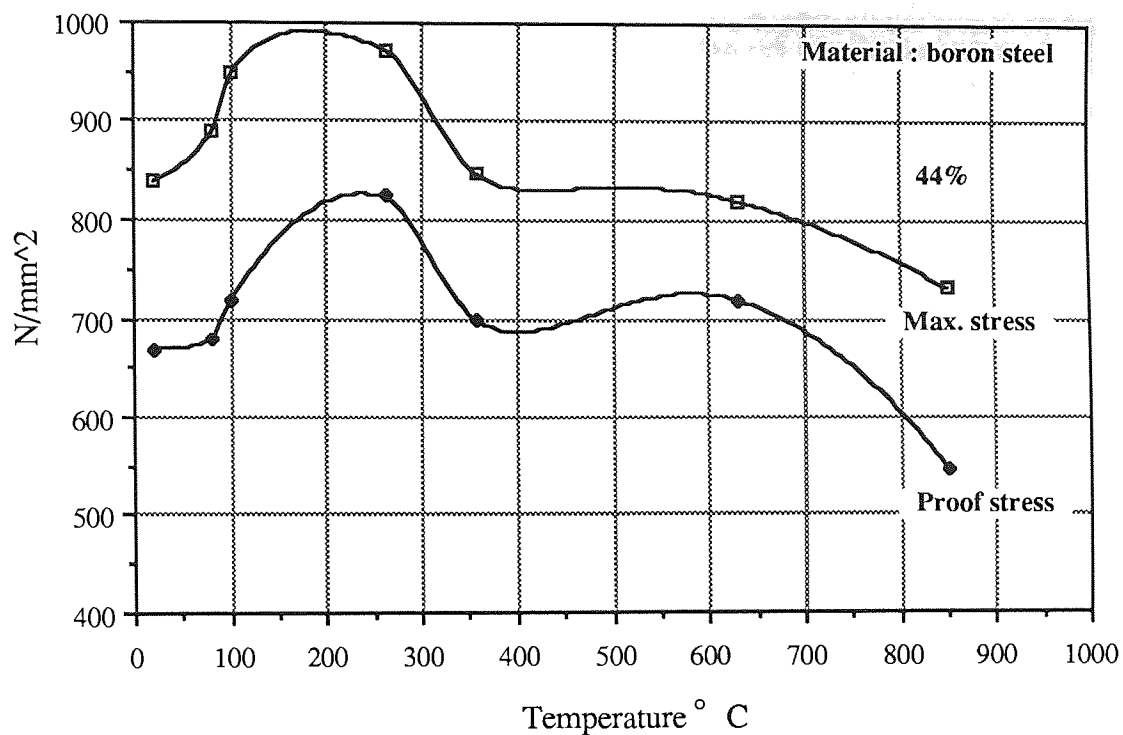
Fig.7.21. Variation of maximum stress and proof stress with temperature for a square section, results obtained by tensile testing.
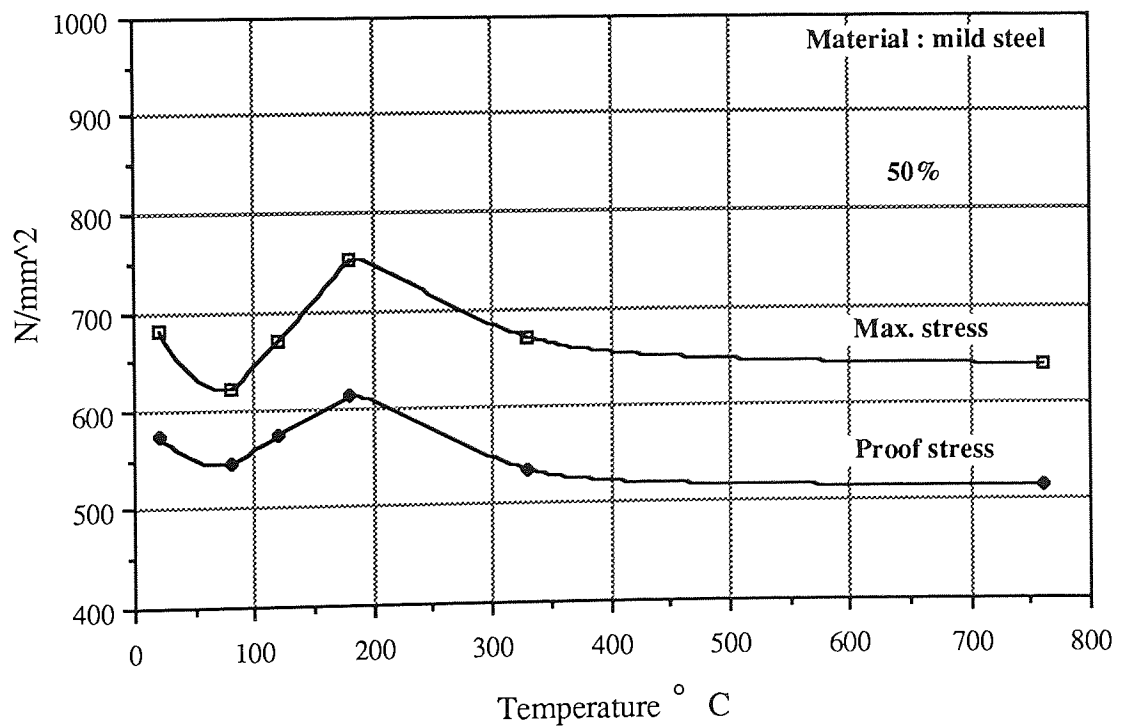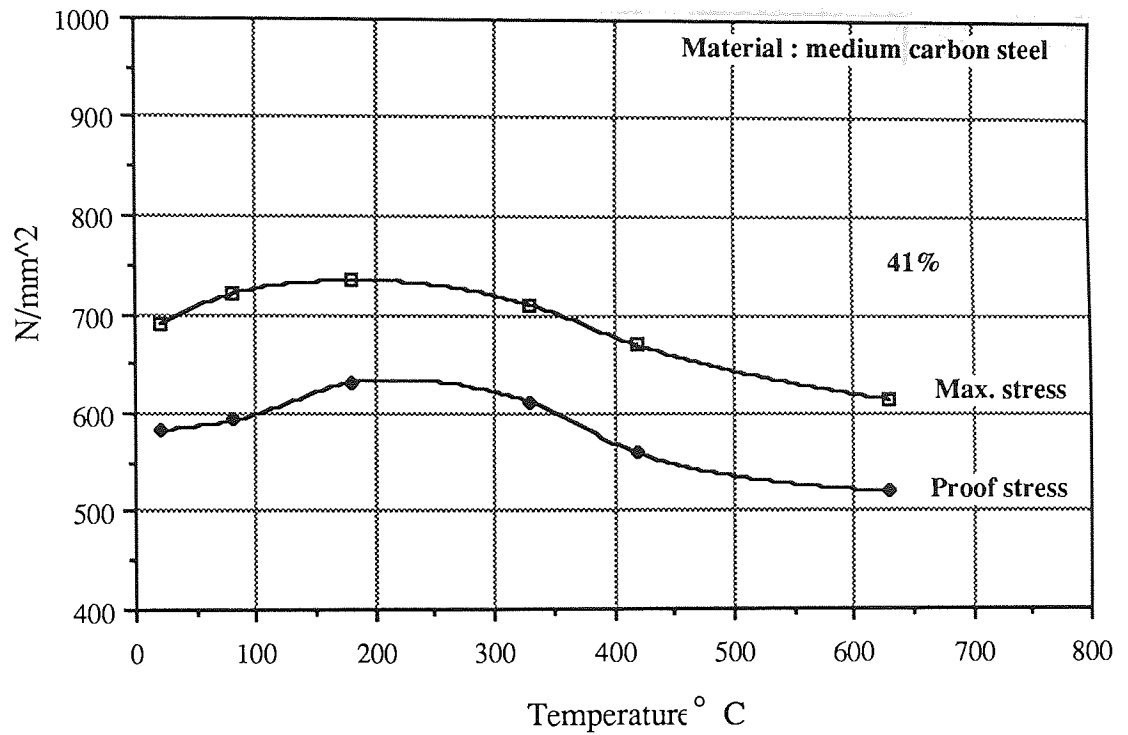
Fig.7.22. Variation of maximum stress and proof stress with temperature
for a square section, results obtained by tensile testing.
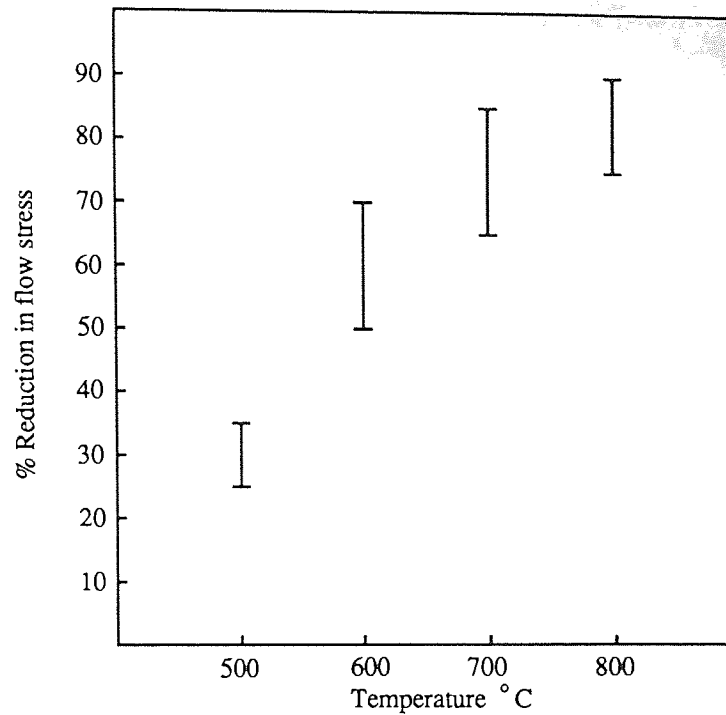
Fig.7.23. Precentage reduction in flow stress, compared with that at room temperature. Results obtained by torsion testing. The scatter band for each temperature covers three different steels, tested at three different strain rates.
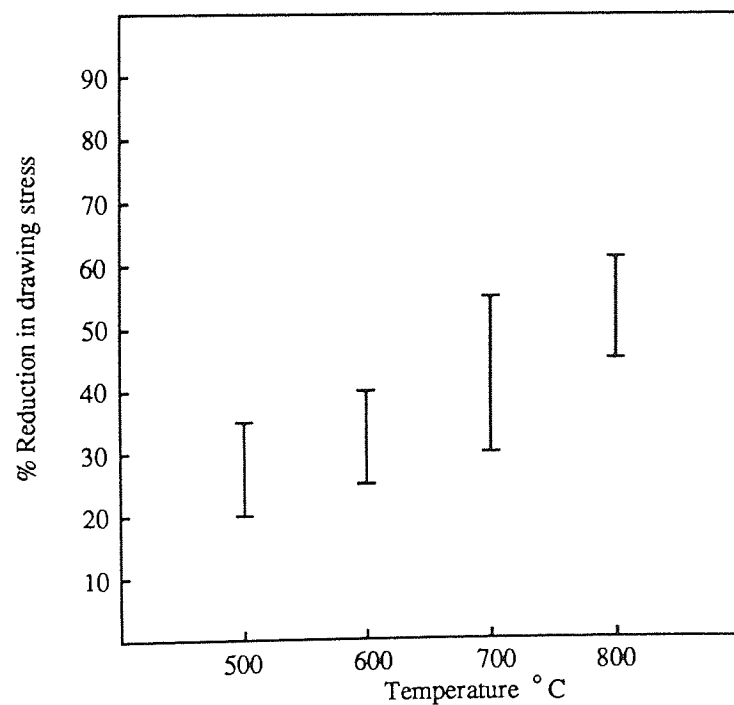
Fig.7.24. Precentage reduction in drawing stress, compared with that at room temperature. Results obtained by polygonal drawing. The scatter band for each temperature covers three different steels, three polygonal sections and three die designs.
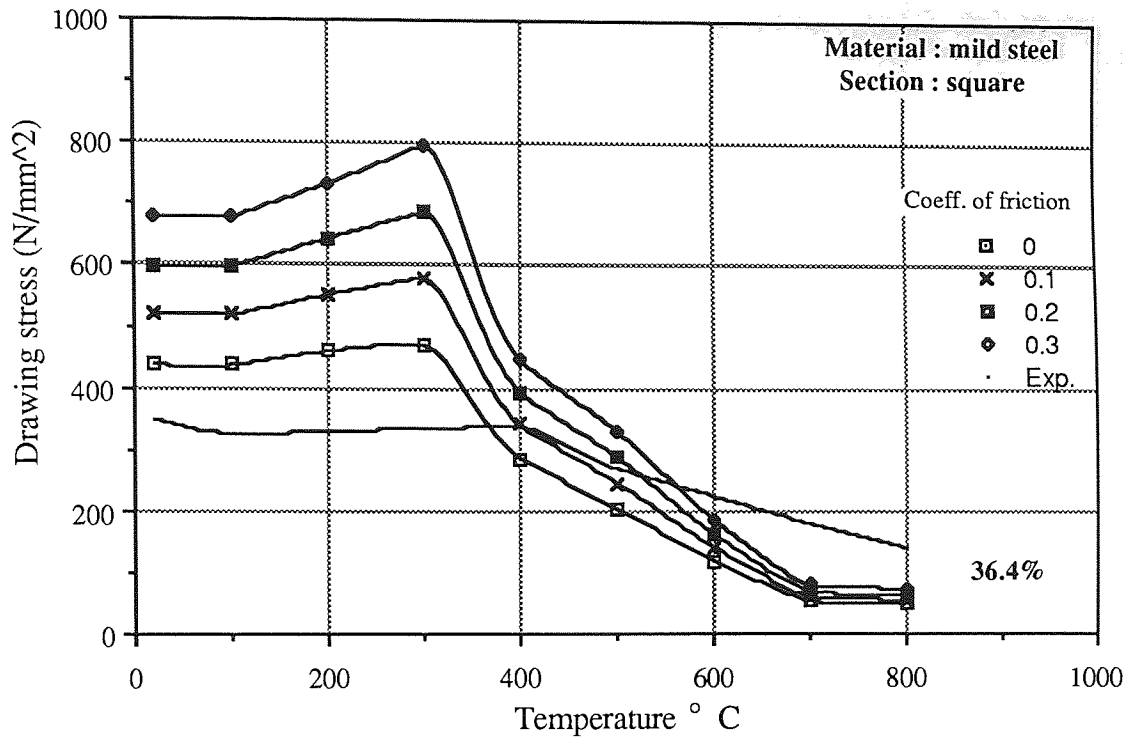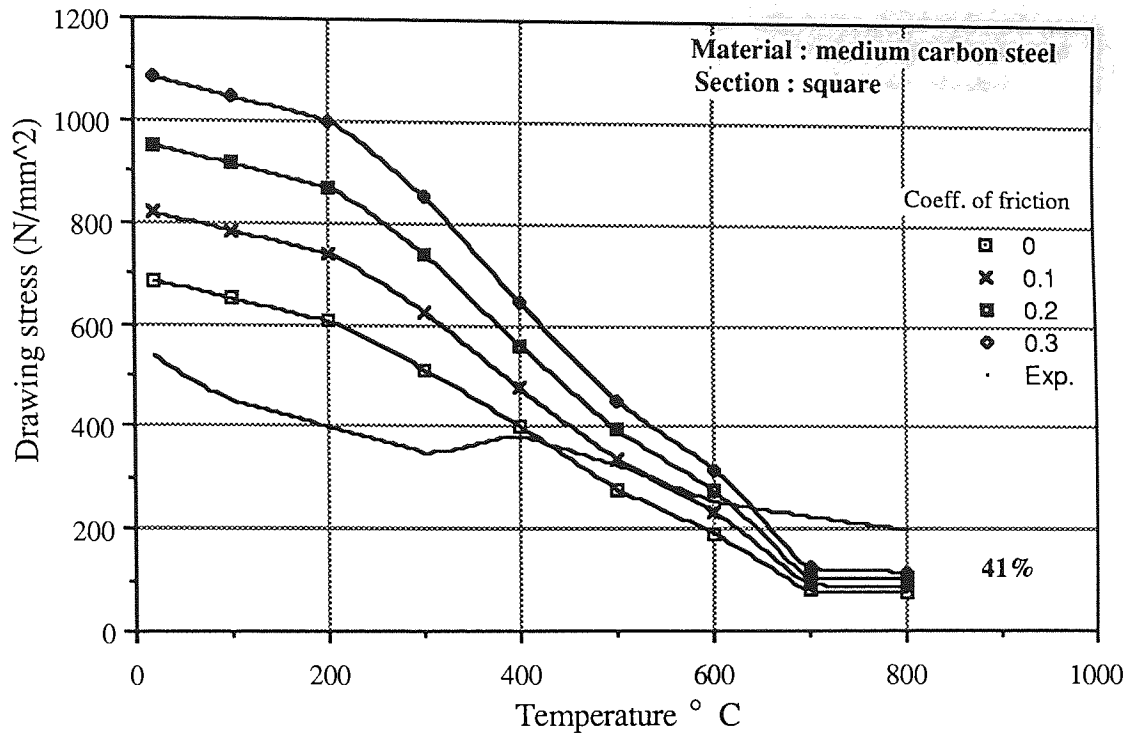
Fig.7.25. Variation of drawing stress with temperature, comparison of experimental and theoretical results for various coefficients of friction.
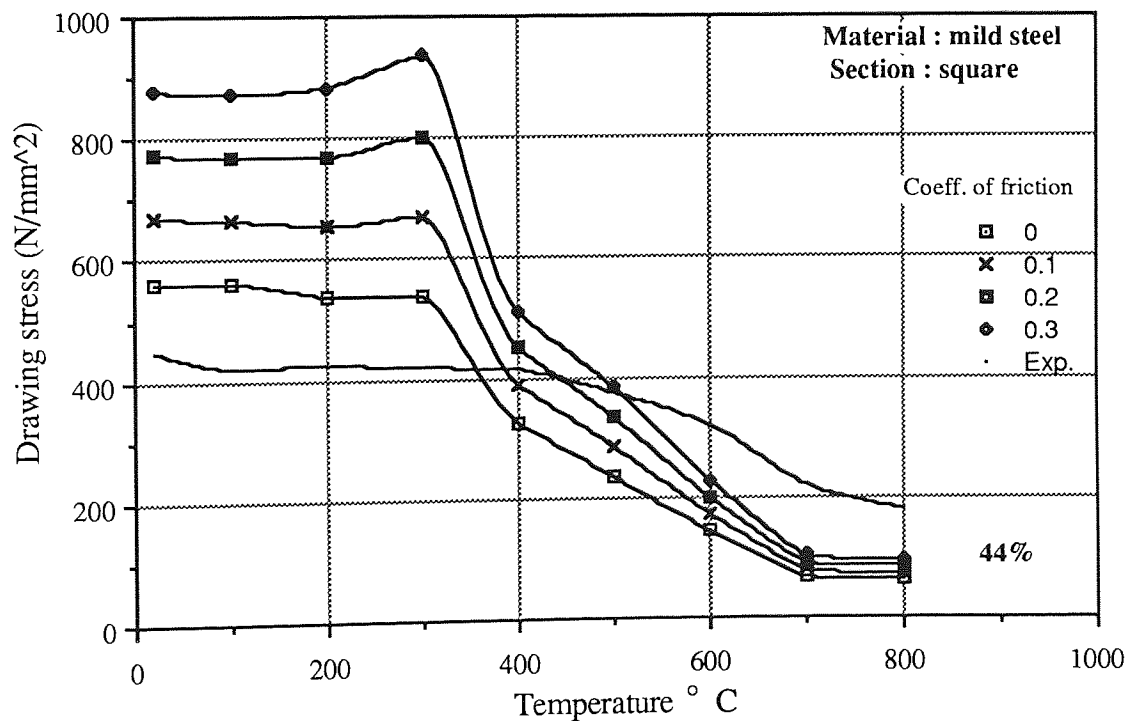
Fig.7.26. Variation of drawing stress with temperature, comparison of experimental and theoretical results for various coefficients of friction.
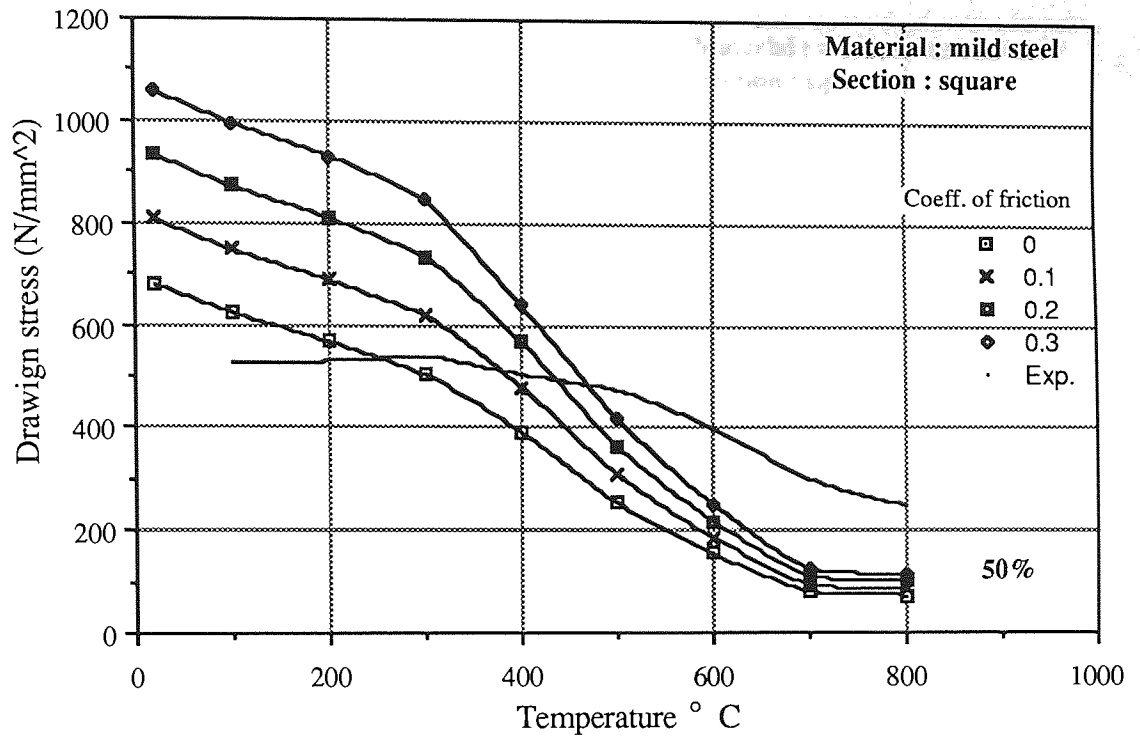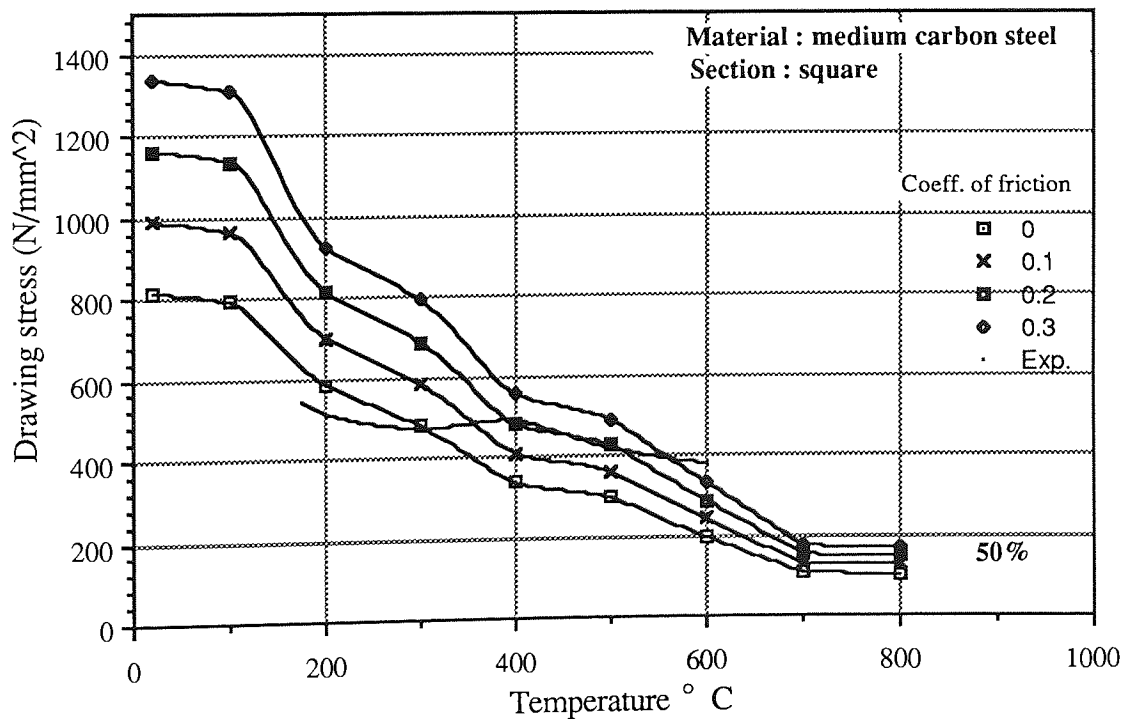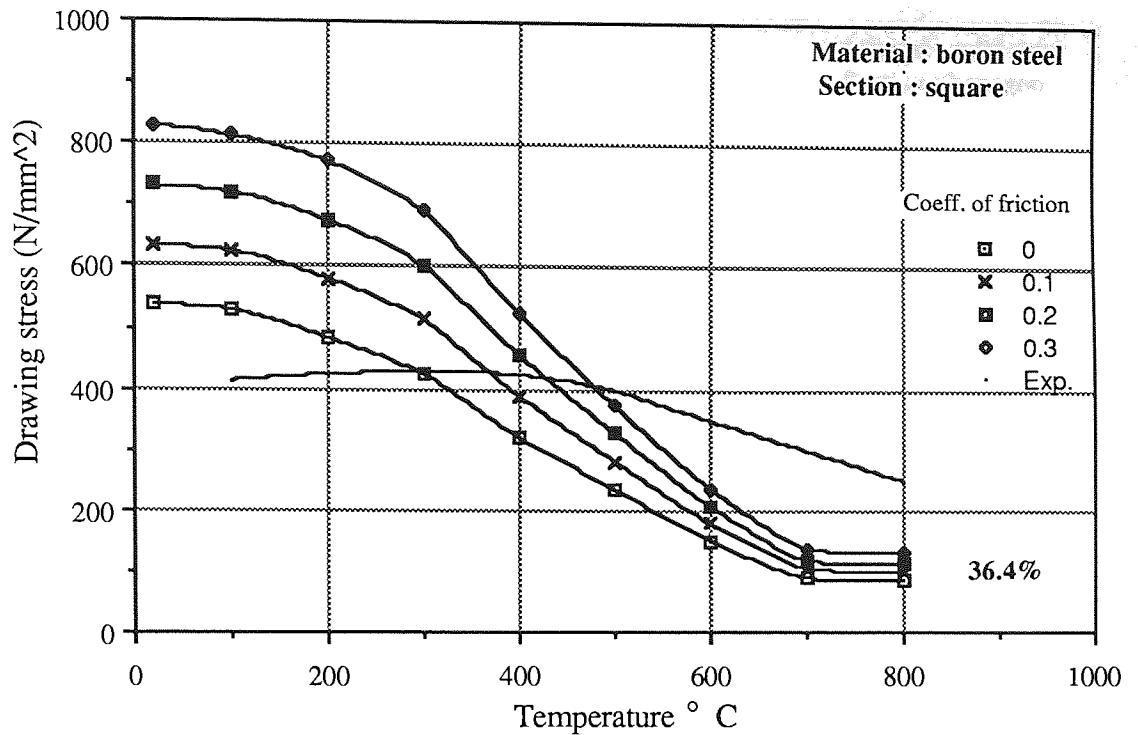
Fig.7.27. Variation of drawing stress with temperature, comparison of experimental and theoretical results for various coefficients of friction.
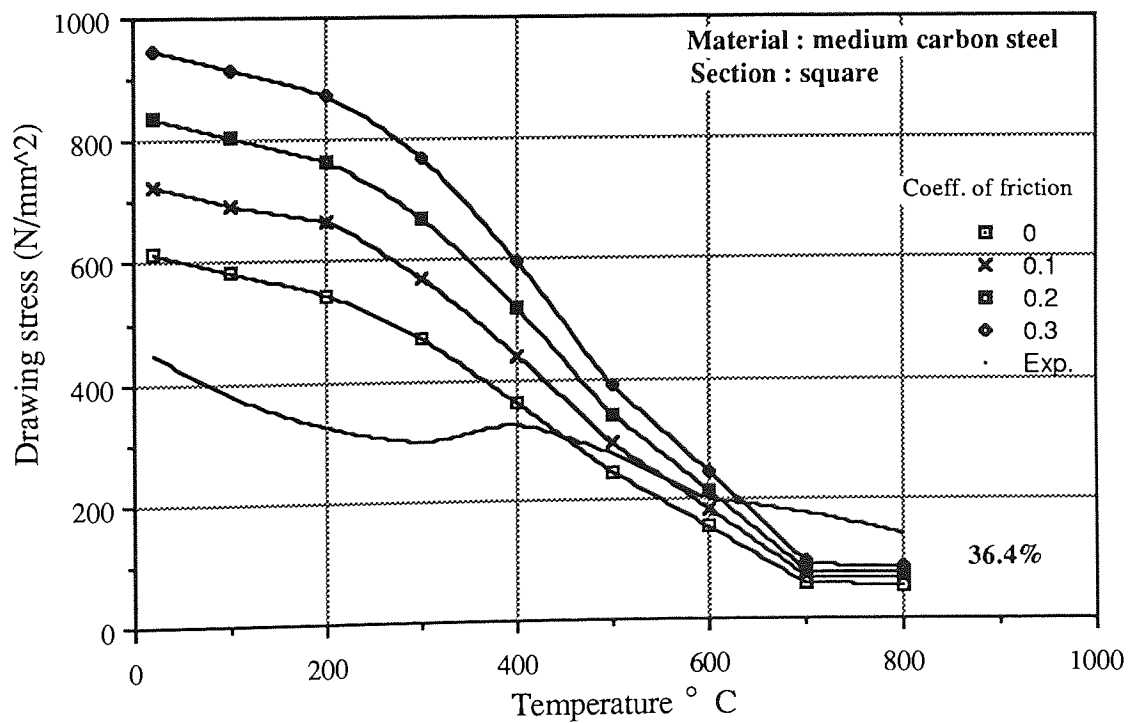
Fig.7.28. Variation of drawing stress with temperature, comparison of experimental and theoretical results for various coefficients of friction.
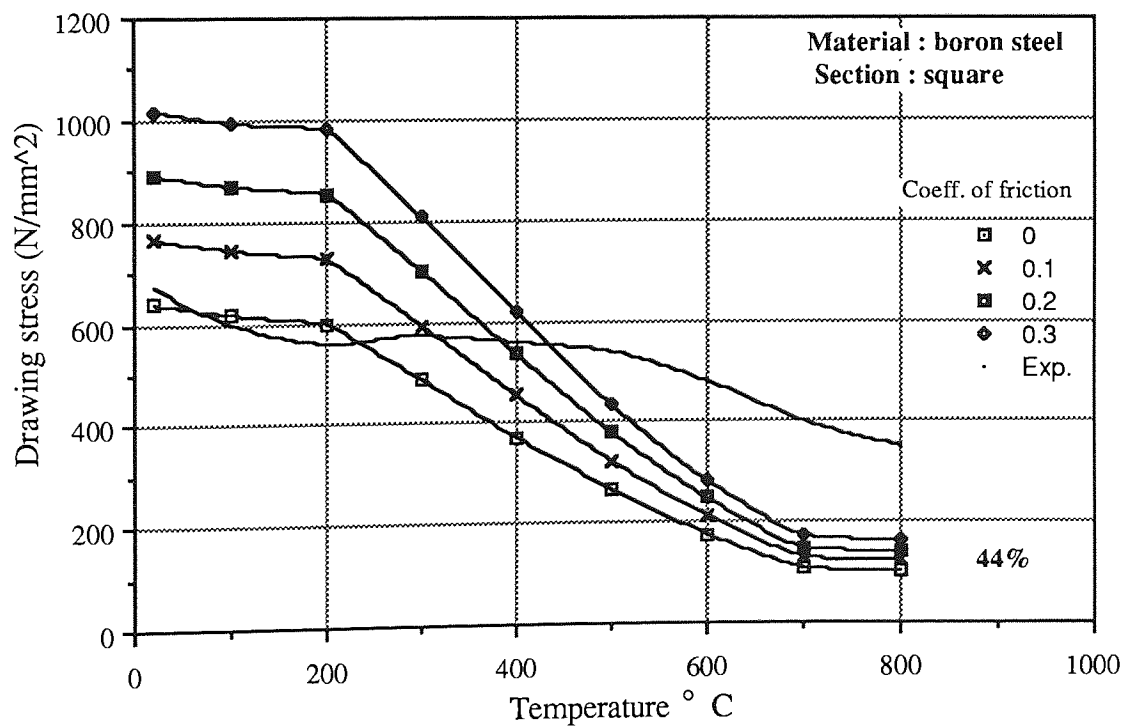
Fig.7.29. Variation of drawing stress with temperature, comparison of experimental and theoretical results for various coefficients of friction.

Fig.7.30. Variation of drawing stress with temperature, comparison of experimental and theoretical results for various coefficients of friction.

Fig.7.31. Variation of drawing stress with temperature, comparison of experimental and theoretical results for various coefficients of friction.

Fig.7.32. Variation of drawing stress with temperature, comparison of experimental and theoretical results for various coefficients of friction.
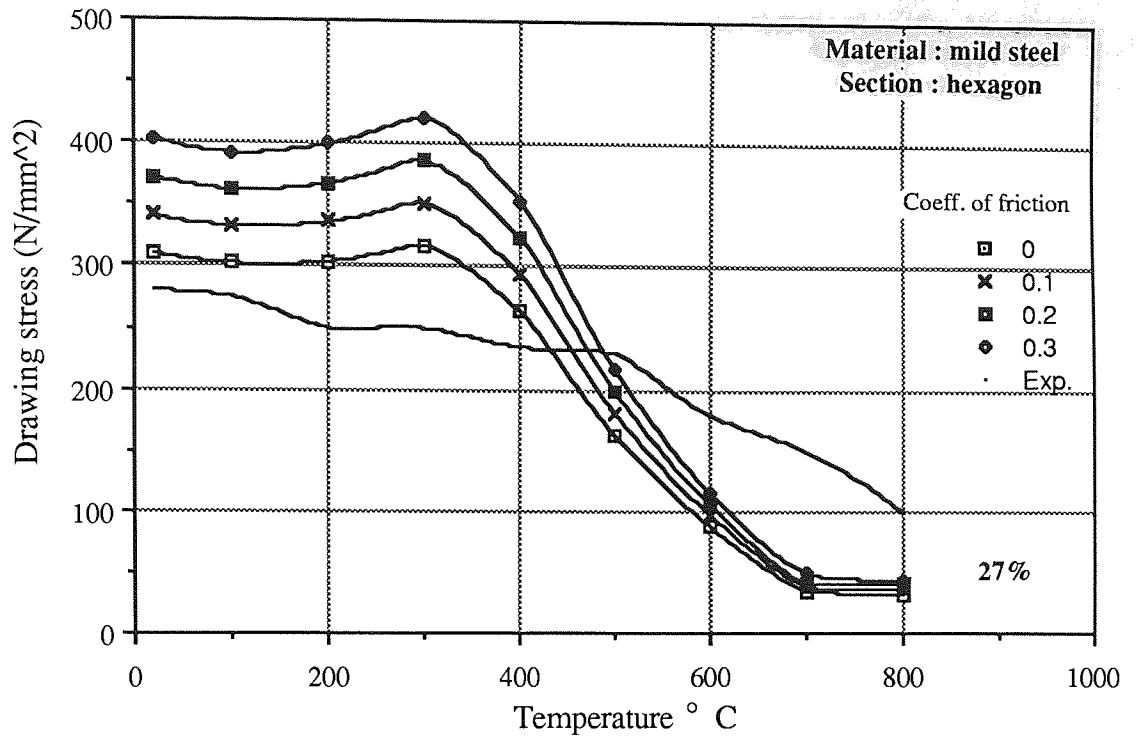
Fig.7.33. Variation of drawing stress with temperature, comparison of experimental and theoretical results for various coefficients of friction.
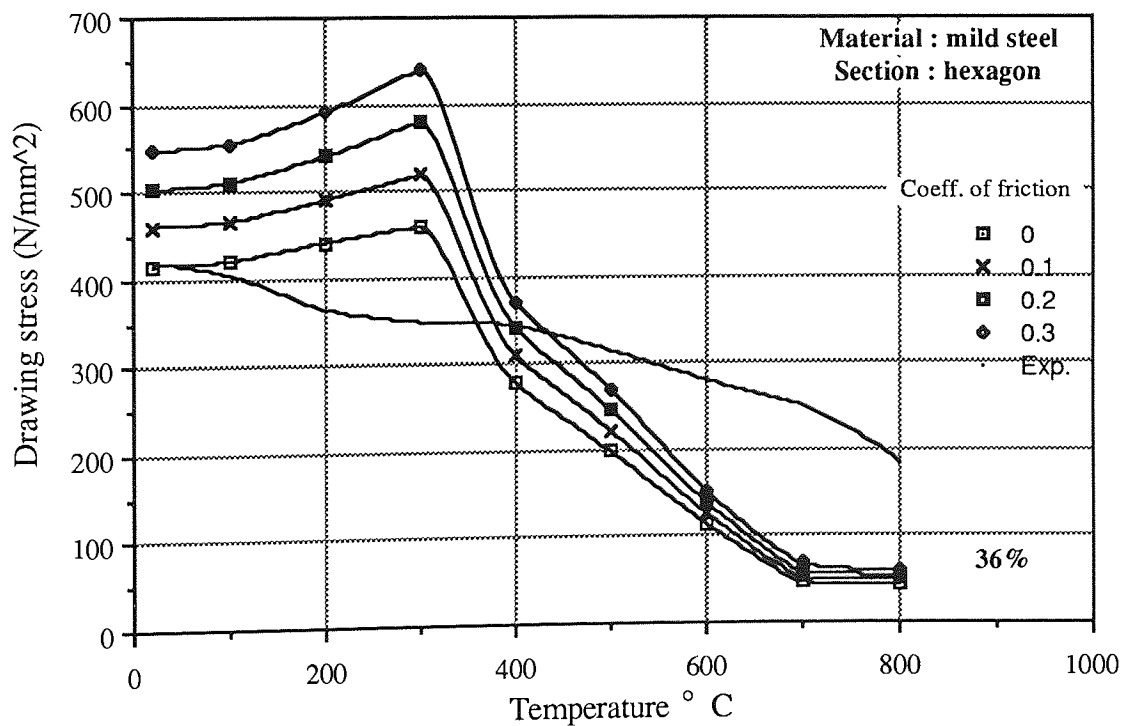

Fig.7.34. Variation of drawing stress with temperature, comparison of experimental and theoretical results for various coefficients of friction.
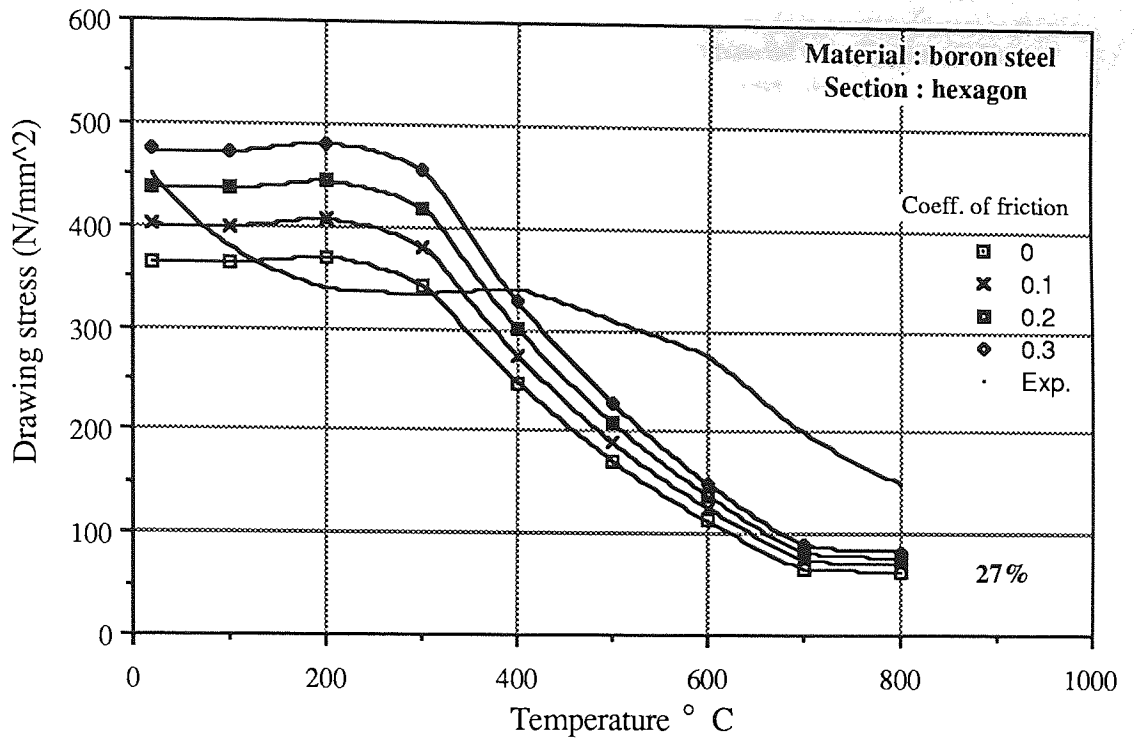
Fig.7.35. Variation of drawing stress with temperature, comparison of experimental
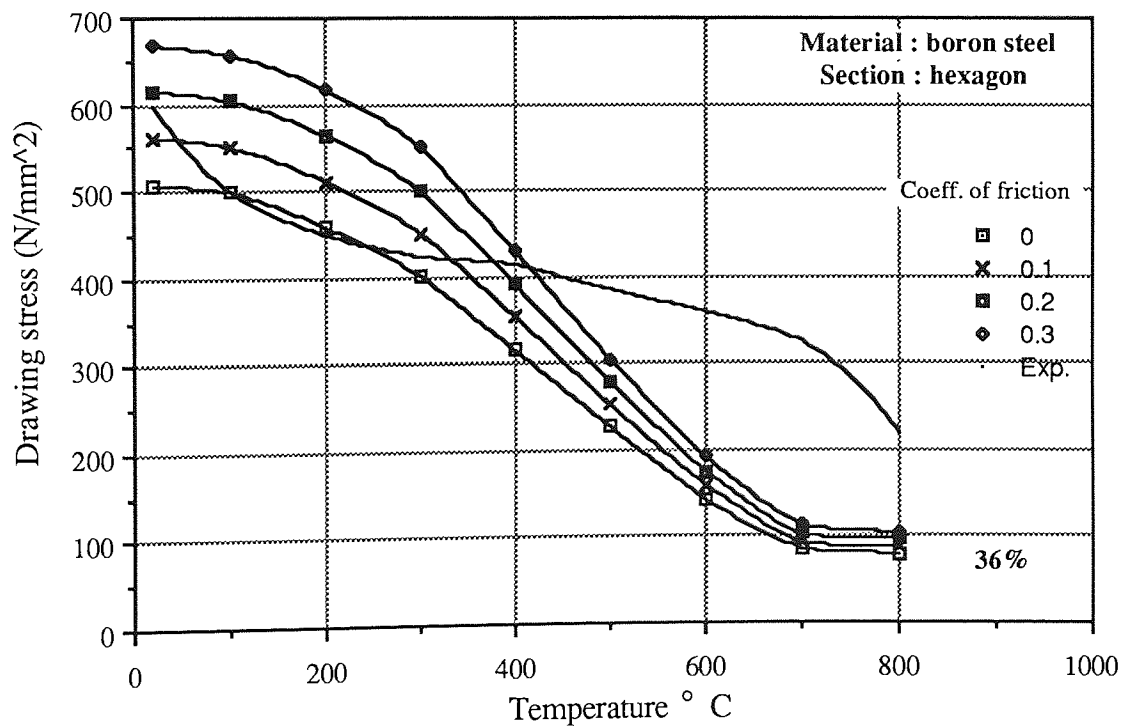and theoretical results for various coefficients of friction.

Fig.7.36. Variation of drawing stress with temperature, comparison of experimental
and theoretical results for various coefficients of friction.

Fig.7.37. Variation of drawing stress with temperature, comparison of experimental and theoretical results for various coefficients of friction.

Fig.7.38. Variation of drawing stress with temperature, comparison of experimental and theoretical results for various coefficients of friction.
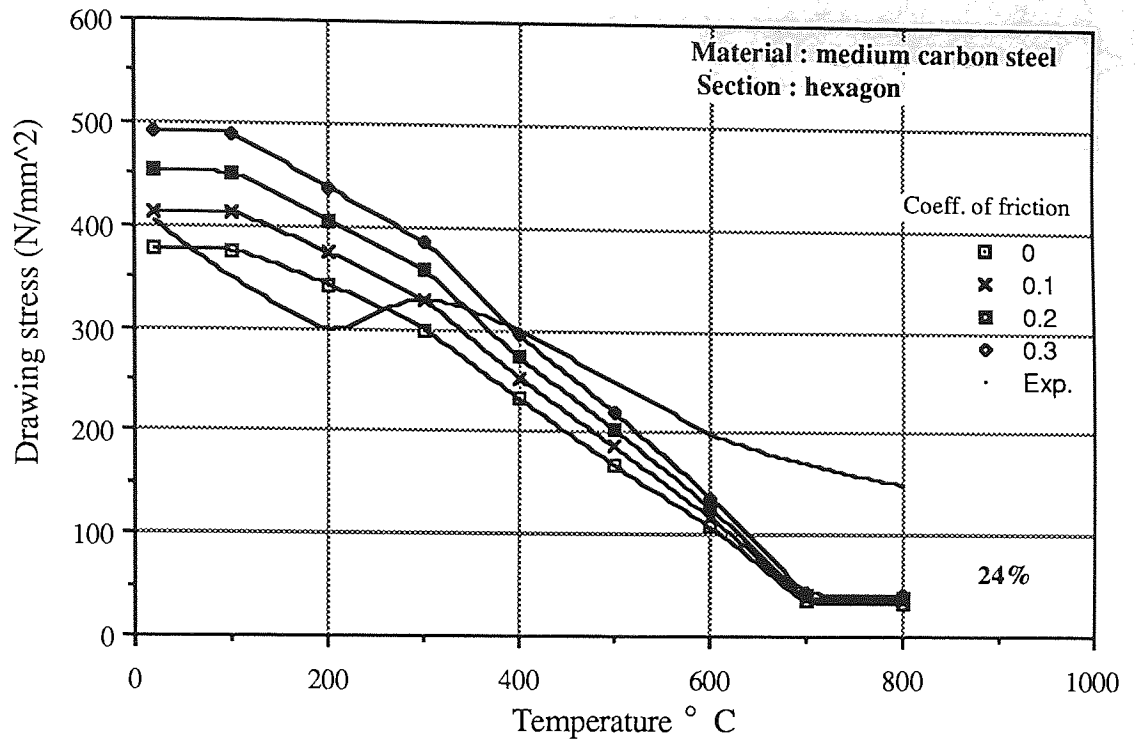
Fig.7.39. Variation of drawing stress with temperature, comparison of experimental and theoretical results for various coefficients of friction.
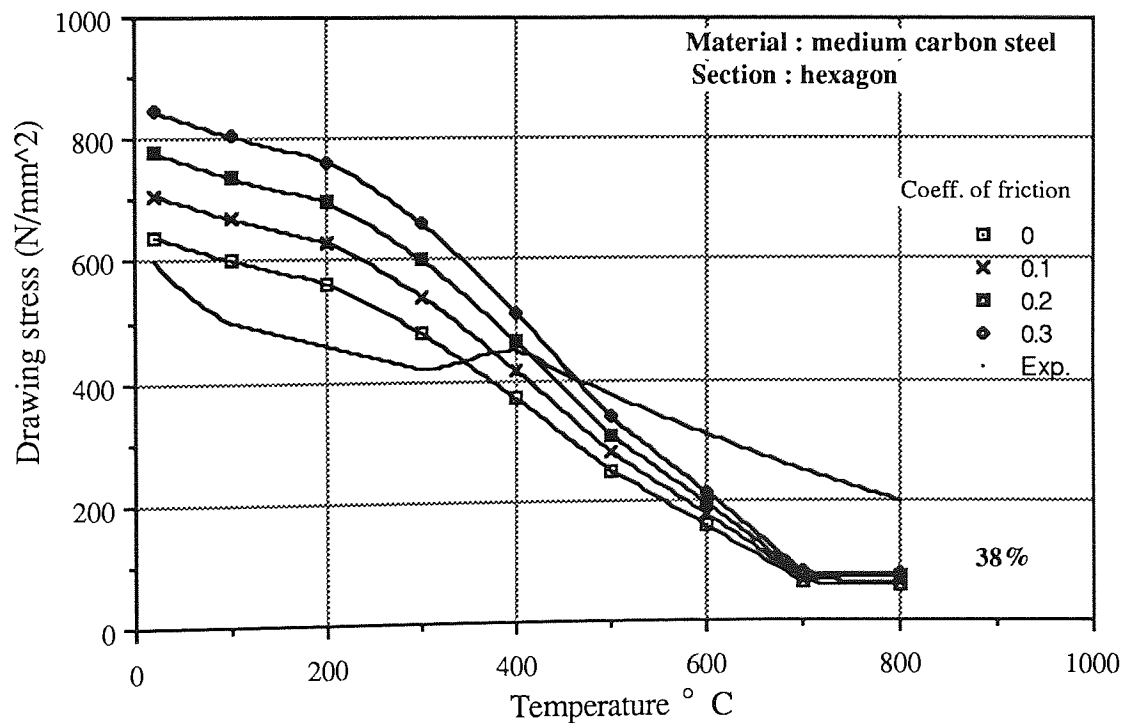

Fig.7.40. Variation of drawing stress with temperature, comparison of experimental and theoretical results for various coefficients of friction.
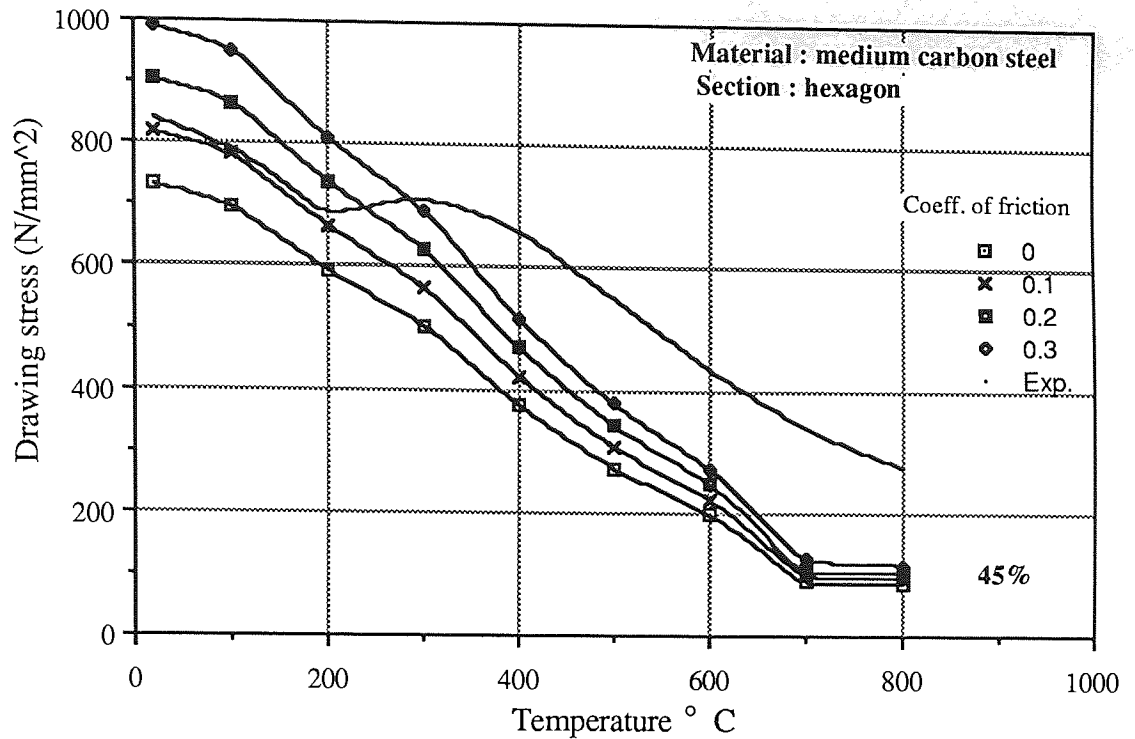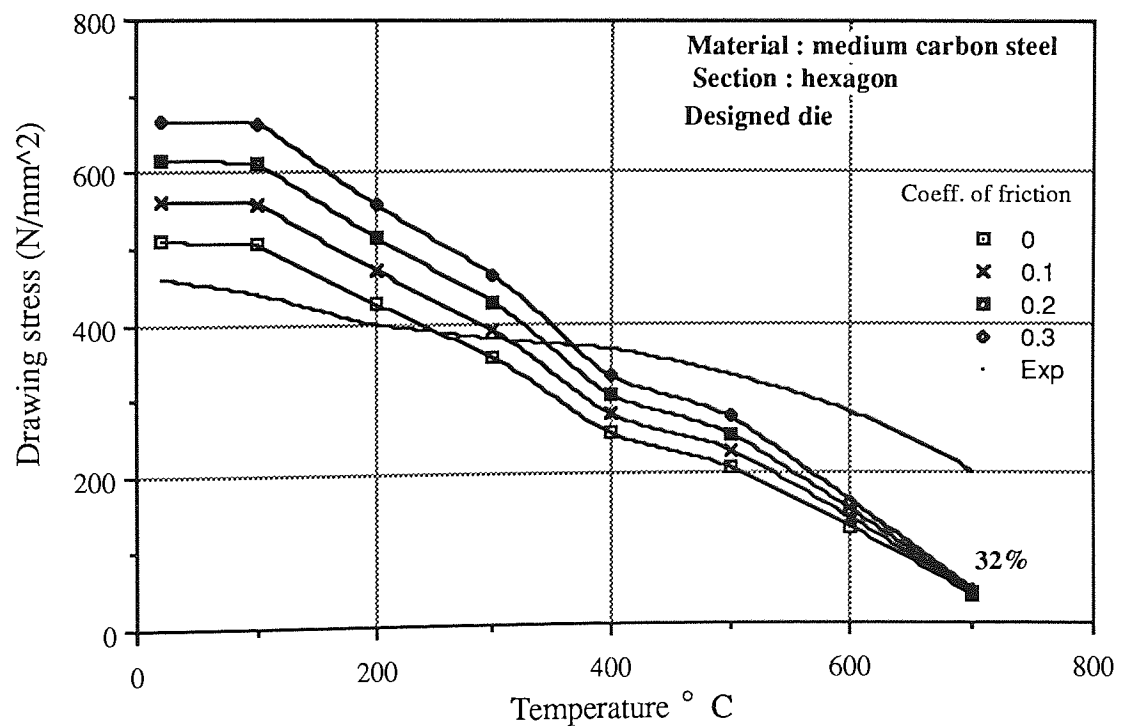
Fig.7.41. Variation of drawing stress with temperature, comparison of experimental and theoretical results for various coefficients of friction.

Fig.7.42. Variation of drawing stress with temperature, comparison of experimental and theoretical results for various coefficients of friction.

Fig.7.43. Variation of drawing stress with reduction of area, comparison of experimental and theoretical results for various coefficients of friction.

Fig.7.44. Variation of drawing stress with reduction of area, comparison of experimental and theoretical results for various coefficients of friction.

Fig.7.45. Variation of drawing stress with reduction of area, comparison of experimental and theoretical results for various coefficients of friction.

Fig.7.46. Variation of drawing stress with reduction of area, comparison of experimental and theoretical results for various coefficients of friction.
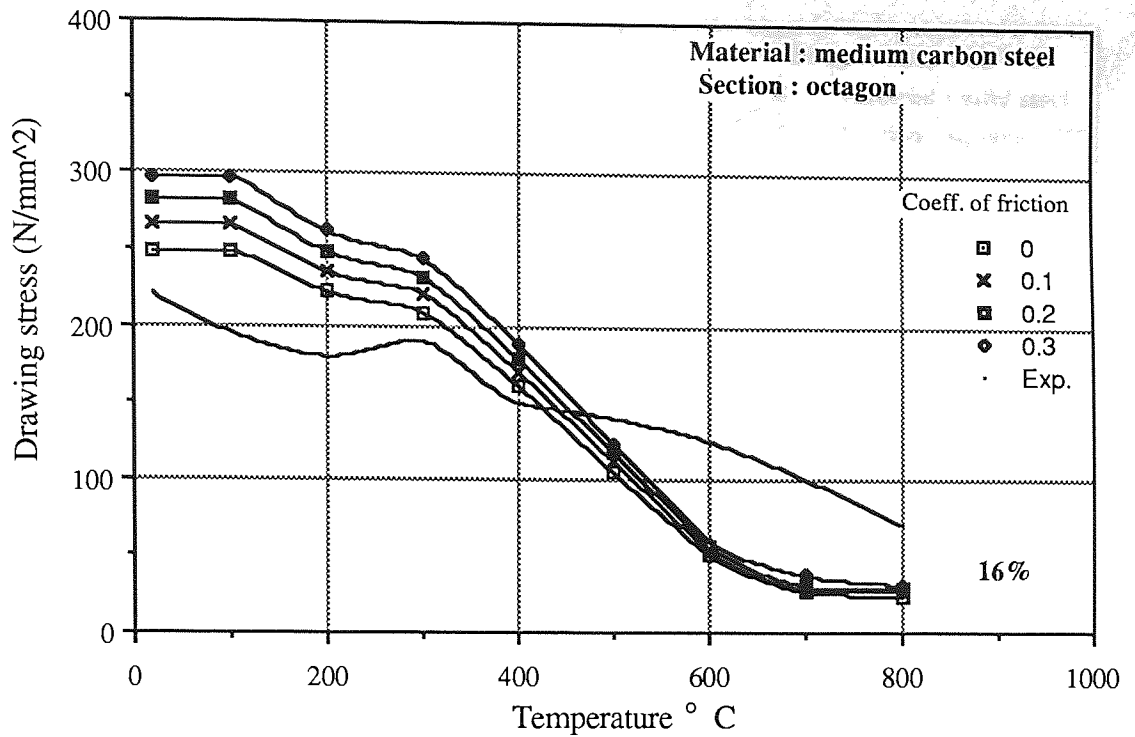
207

Fig.7.47. Variation of drawing stress with reduction of area, comparison of experimental and theoretical results for various coefficients of friction.
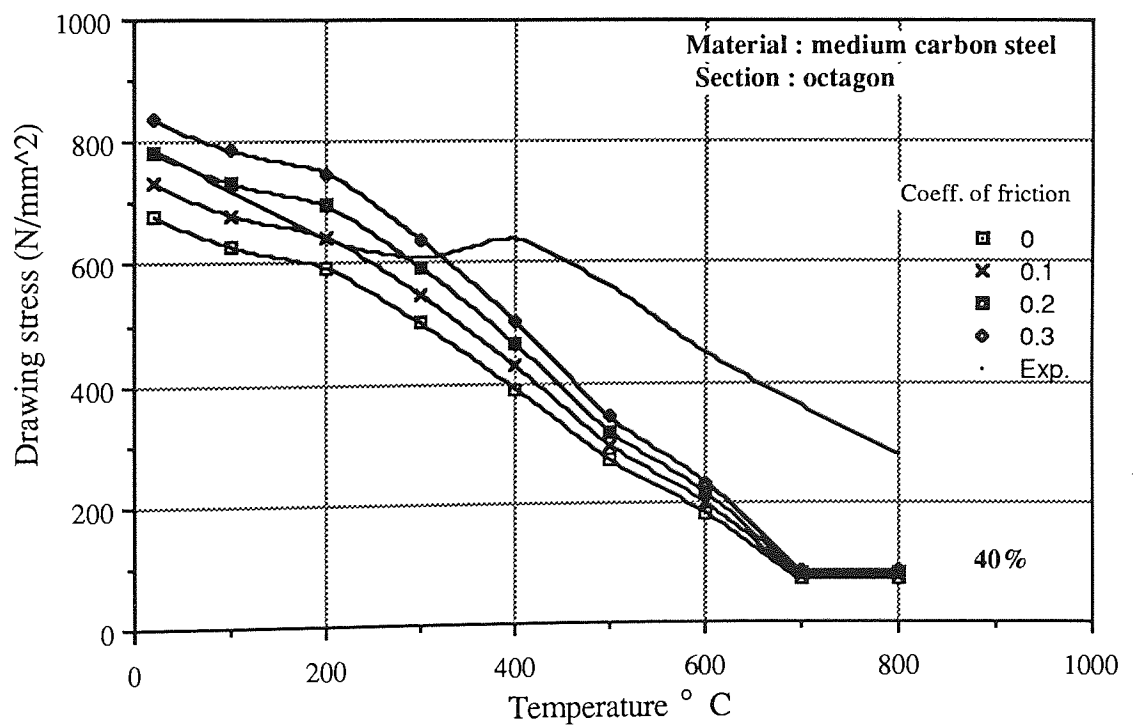

Fig.7.48. Variation of drawing stress with reduction of area, comparison of experimental and theoretical results for various coefficients of friction.

208

Fig.7.49. Variation of drawing stress with reduction of area, comparison of experimental and theoretical results for various coefficients of friction.
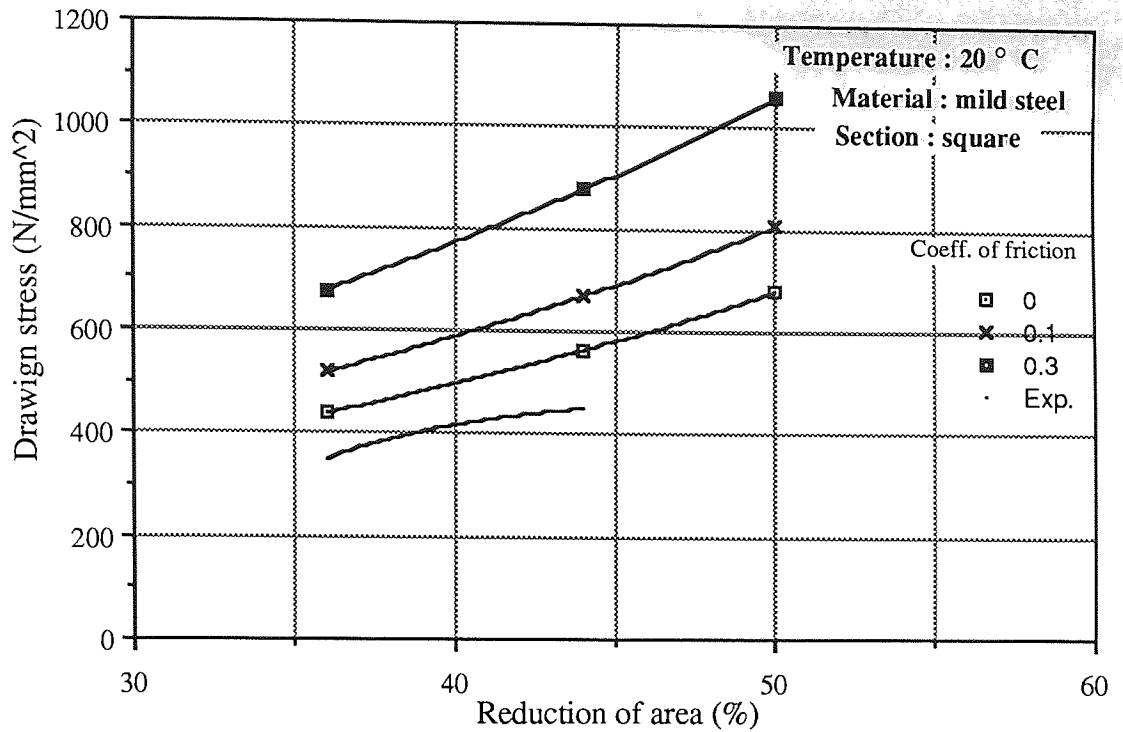

Fig.7.50. Variation of drawing stress with reduction of area, comparison of experimental and theoretical results for various coefficients of friction.
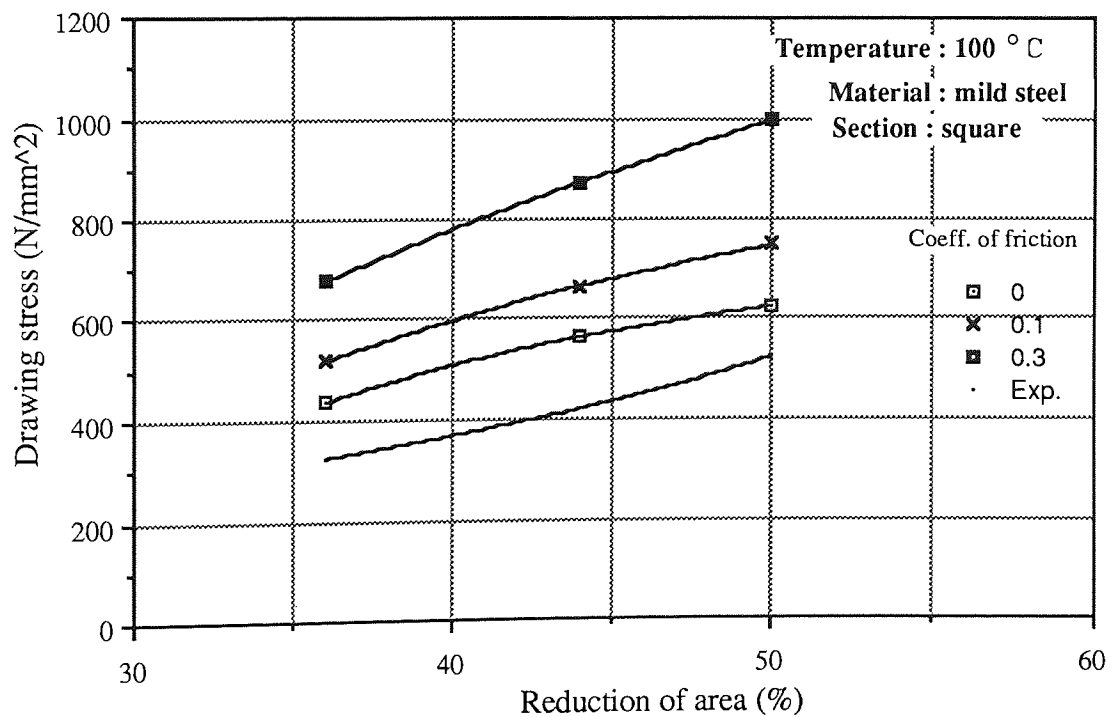
Fig.7.51. Variation of drawing stress with reduction of area, comparison of
experimental and theoretical results for various coefficients of friction.

Fig.7.52. Variation of drawing stress with reduction of area, comparison of
experimental and theoretical results for various coefficients of friction.

210
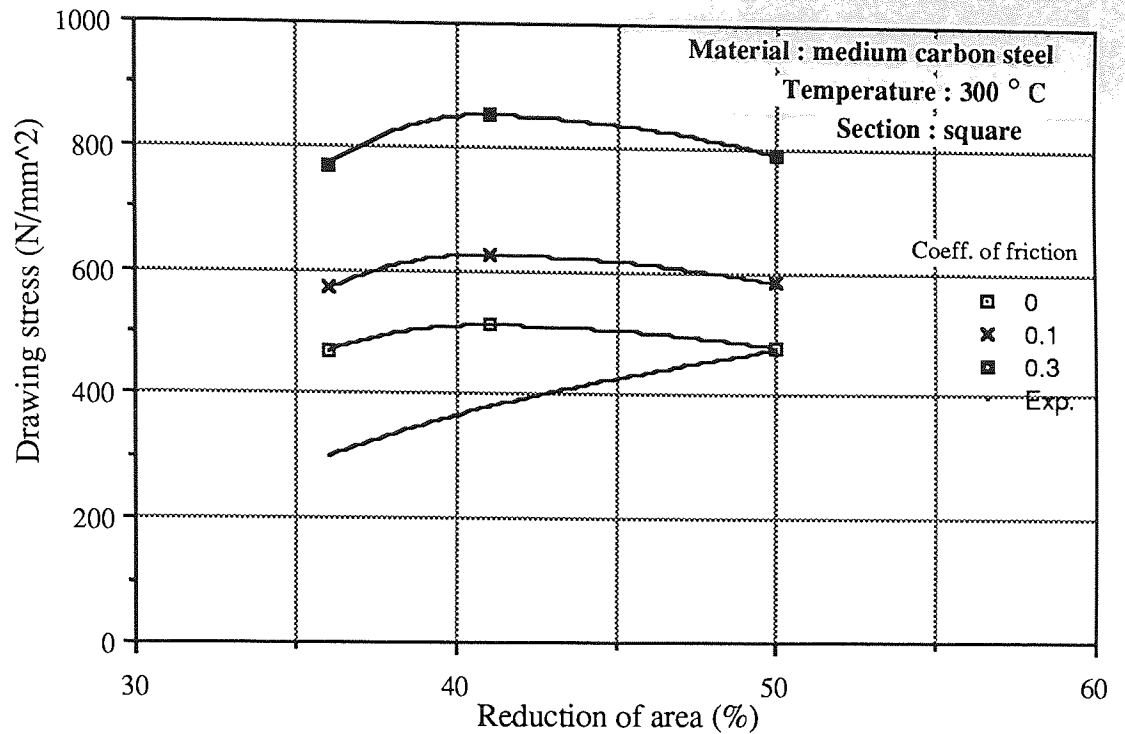
Fig.7.53. Variation of drawing stress with reduction of area, comparison of
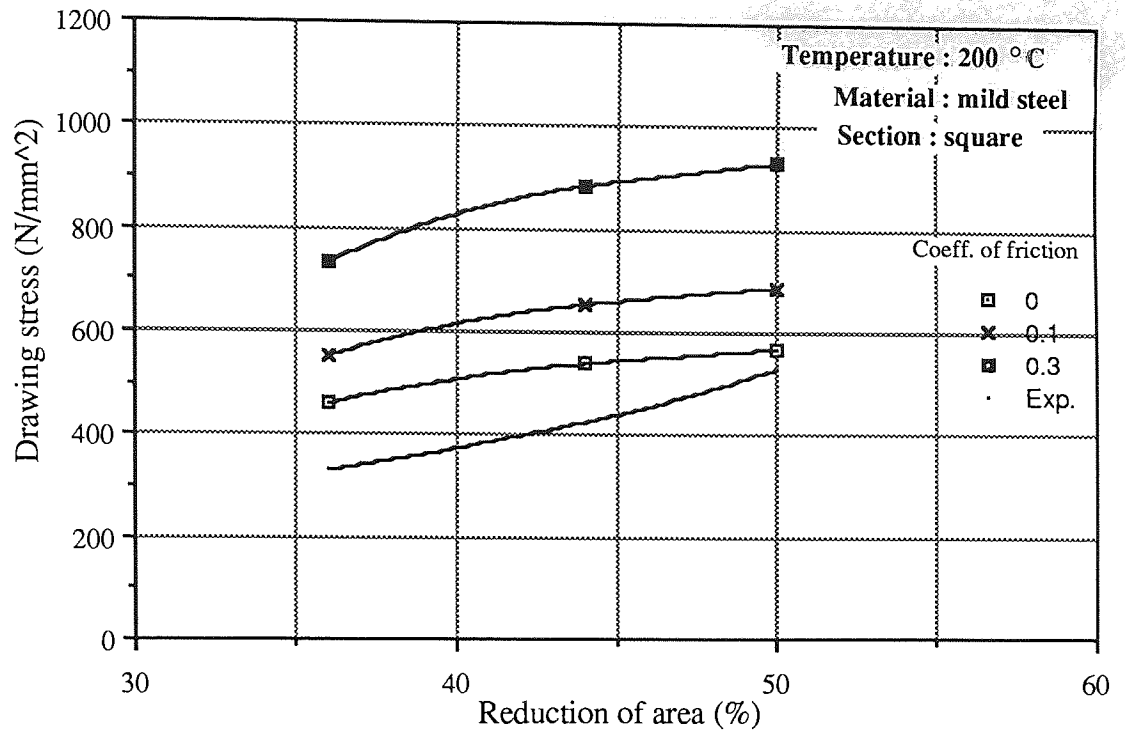experimental and theoretical results for various coefficients of friction.
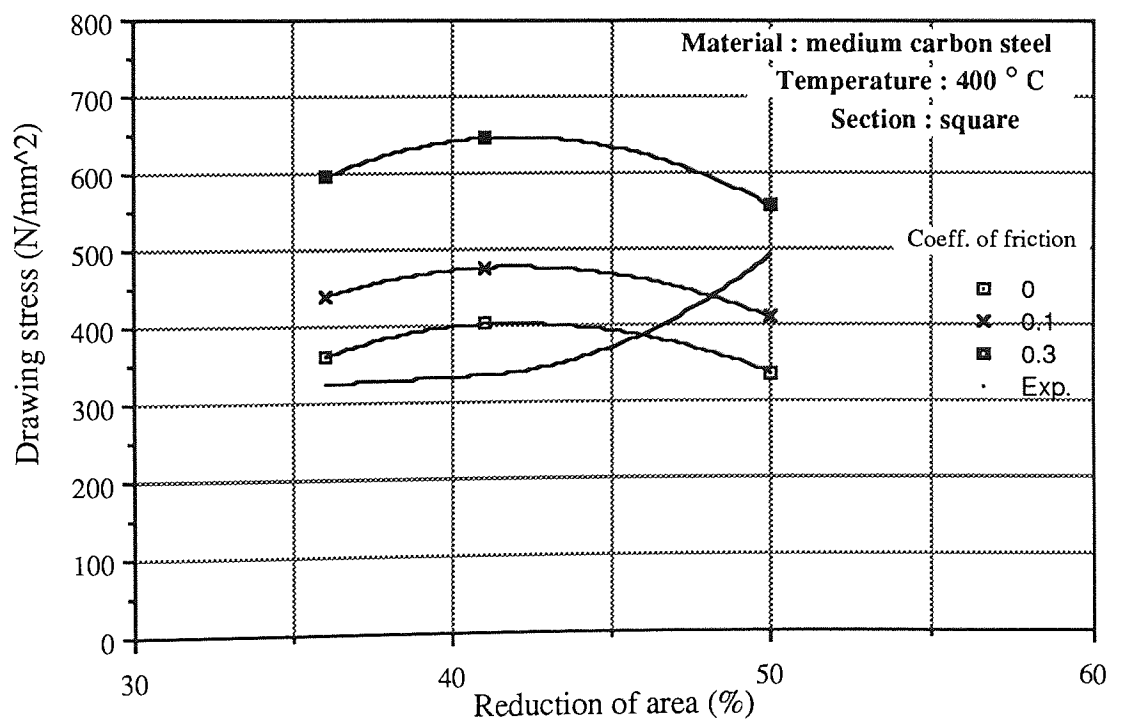
Fig.7.54. Variation of drawing stress with reduction of area, comparison of
experimental and theoretical results for various coefficients of friction.
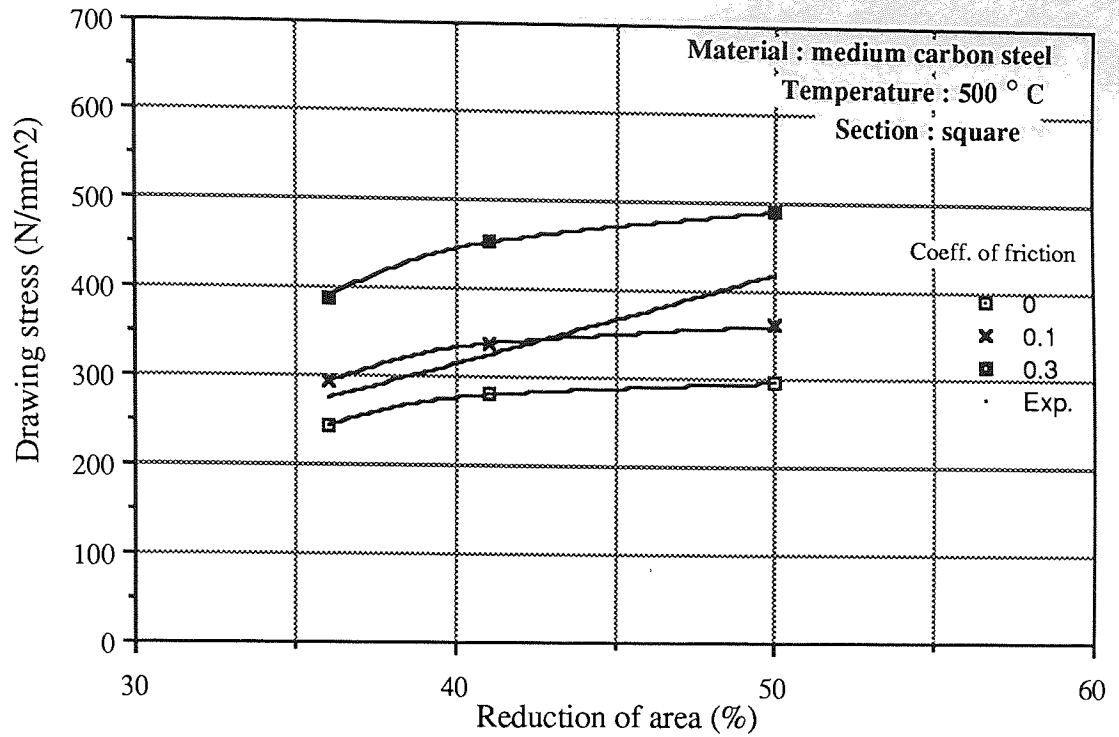
Fig.7.55. Variation of drawing stress with reduction of area, comparison of
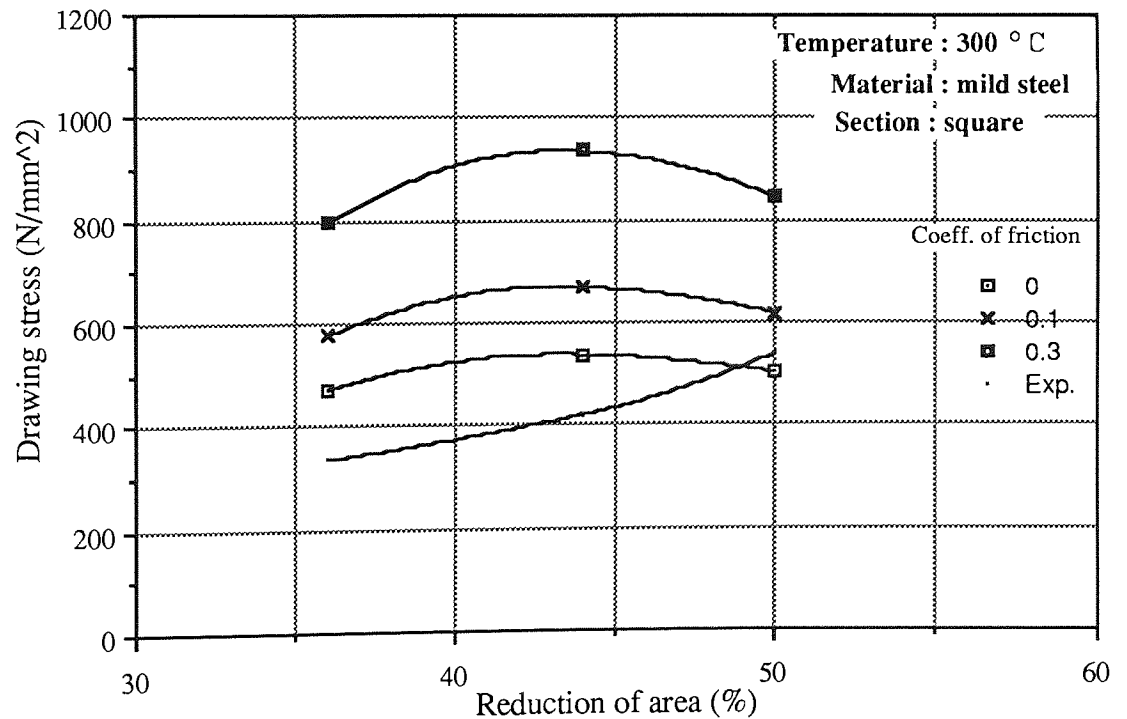experimental and theoretical results for various coefficients of friction.
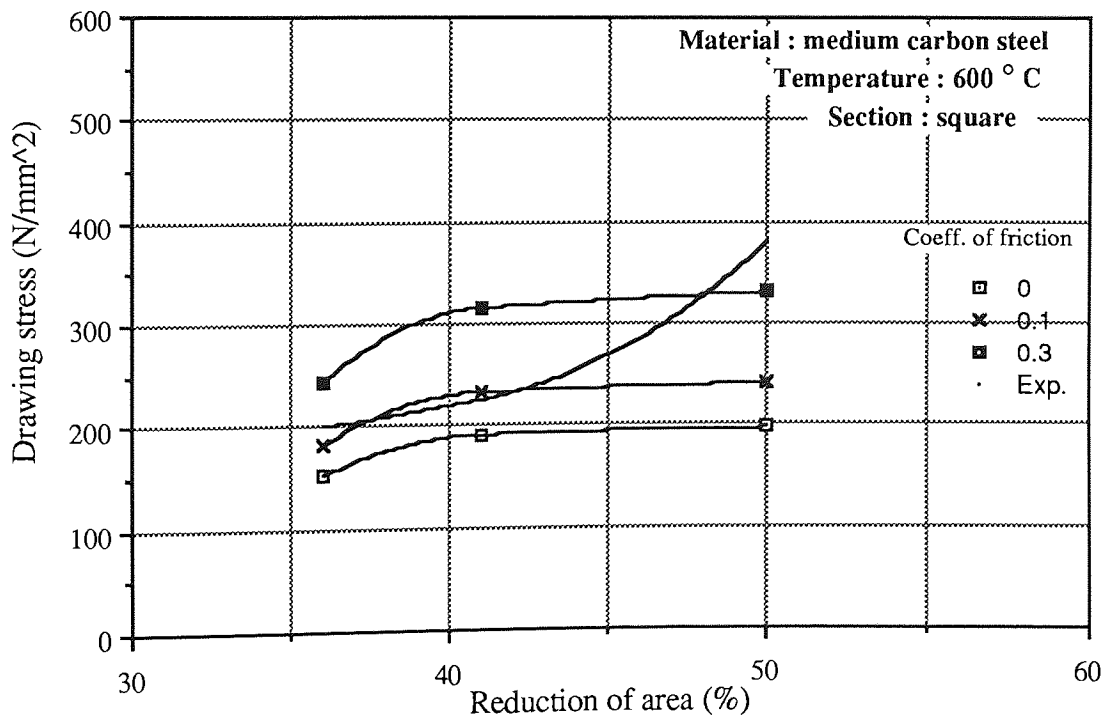
Fig.7.56. Variation of drawing stress with reduction of area, comparison of
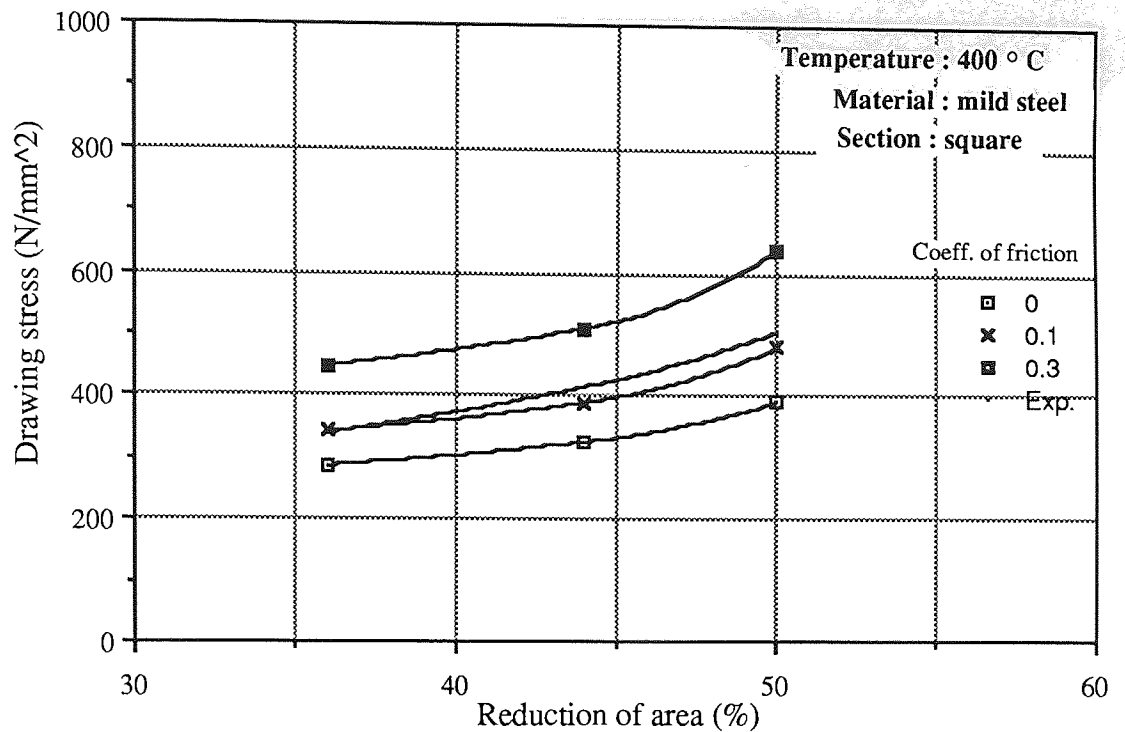experimental and theoretical results for various coefficients of friction.
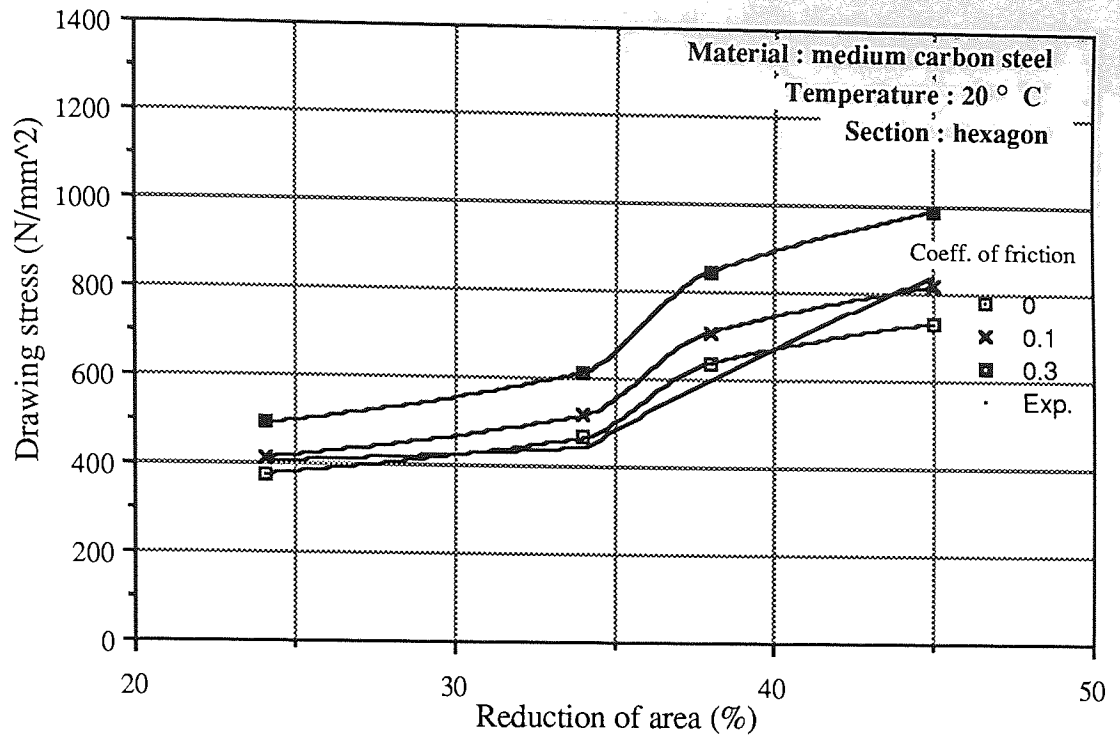
Fig.7.57. Variation of drawing stress with reduction of area, comparison of experimental and theoretical results for various coefficients of friction.
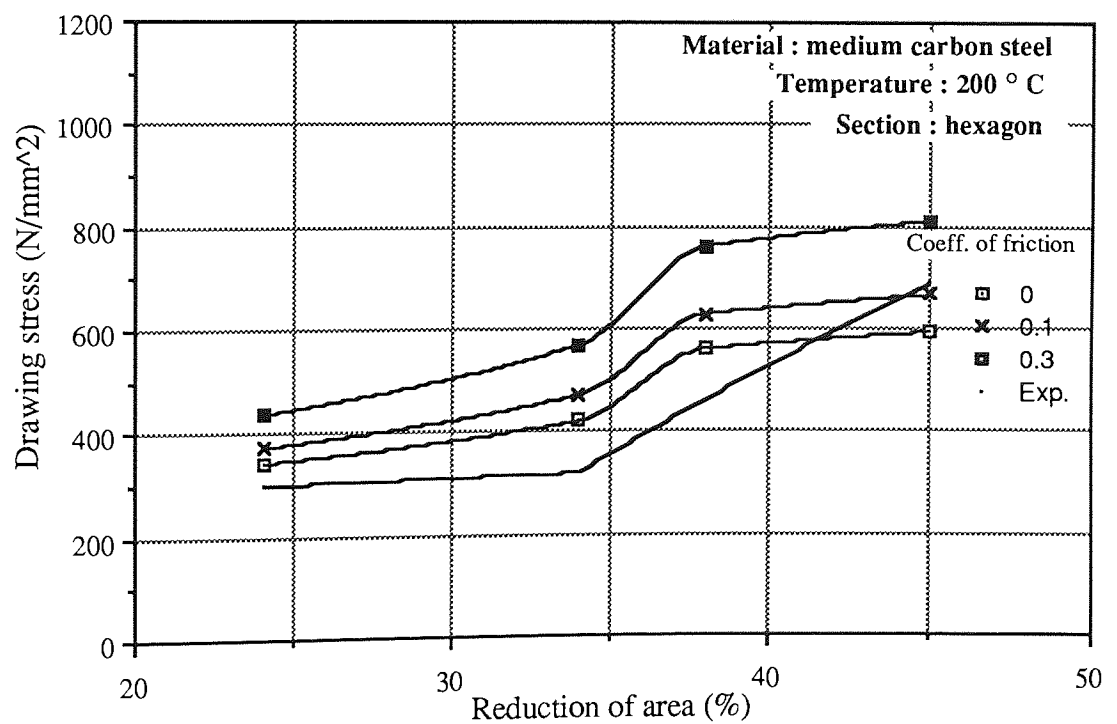
Fig.7.58. Variation of drawing stress with reduction of area, comparison of experimental and theoretical results for various coefficients of friction.

213
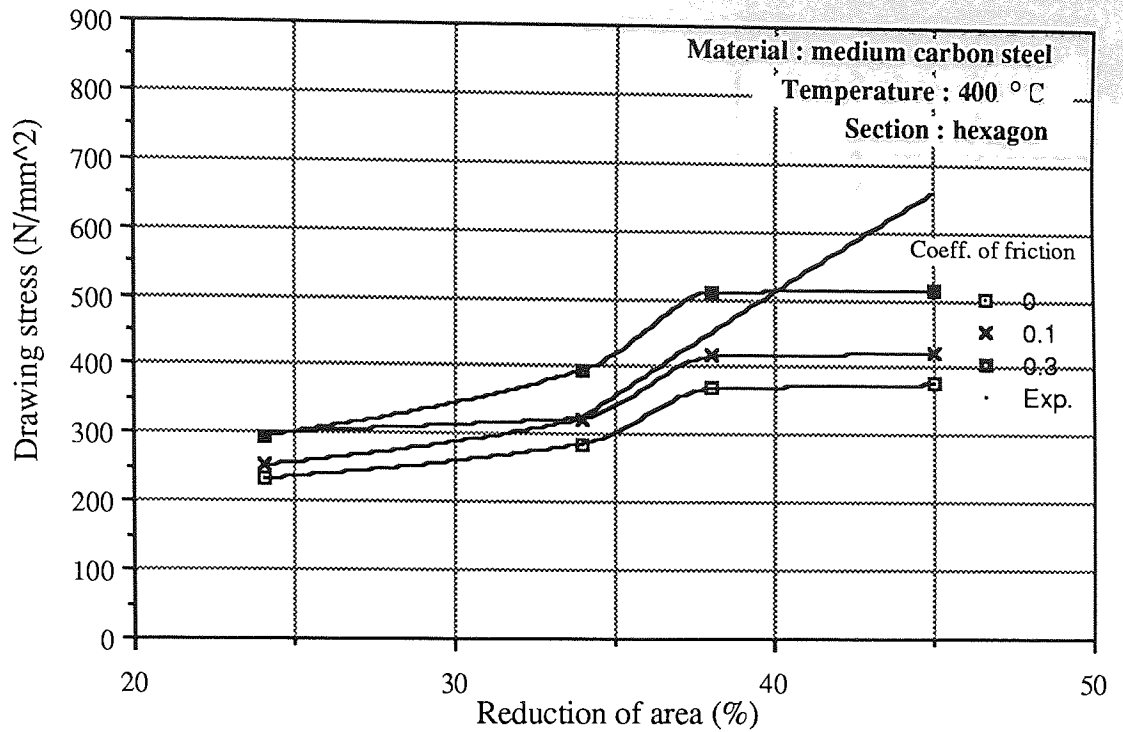
Fig.7.59. Variation of drawing stress with reduction of area, comparison of experimental and theoretical results for various coefficients of friction.
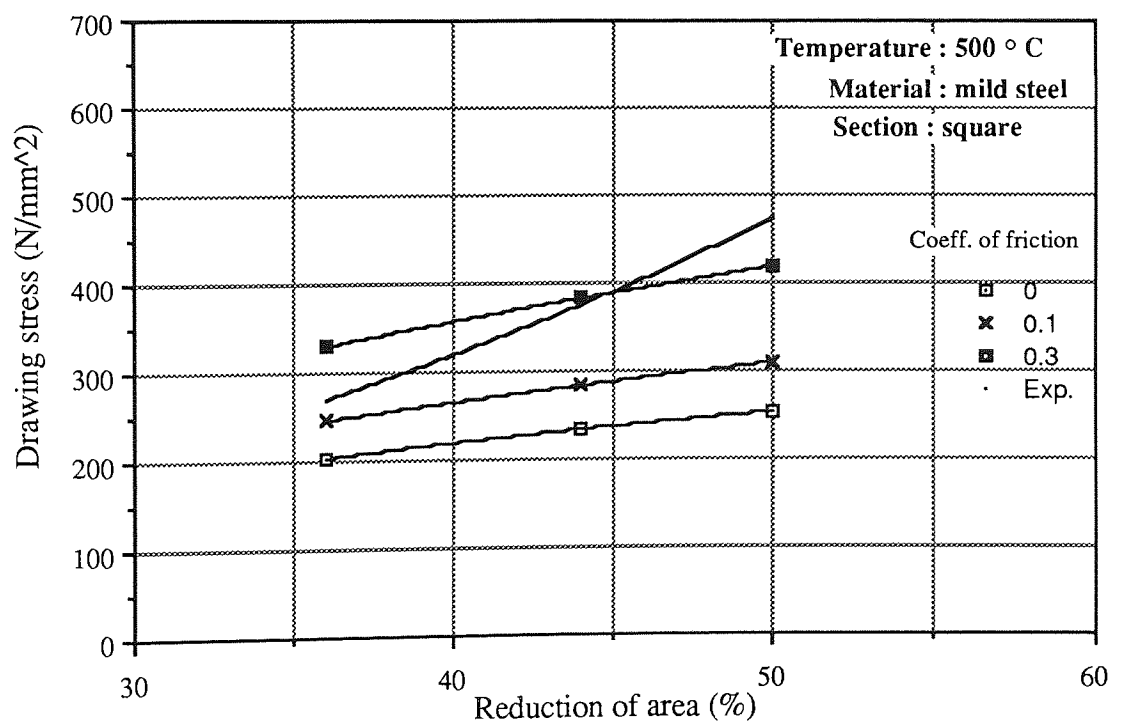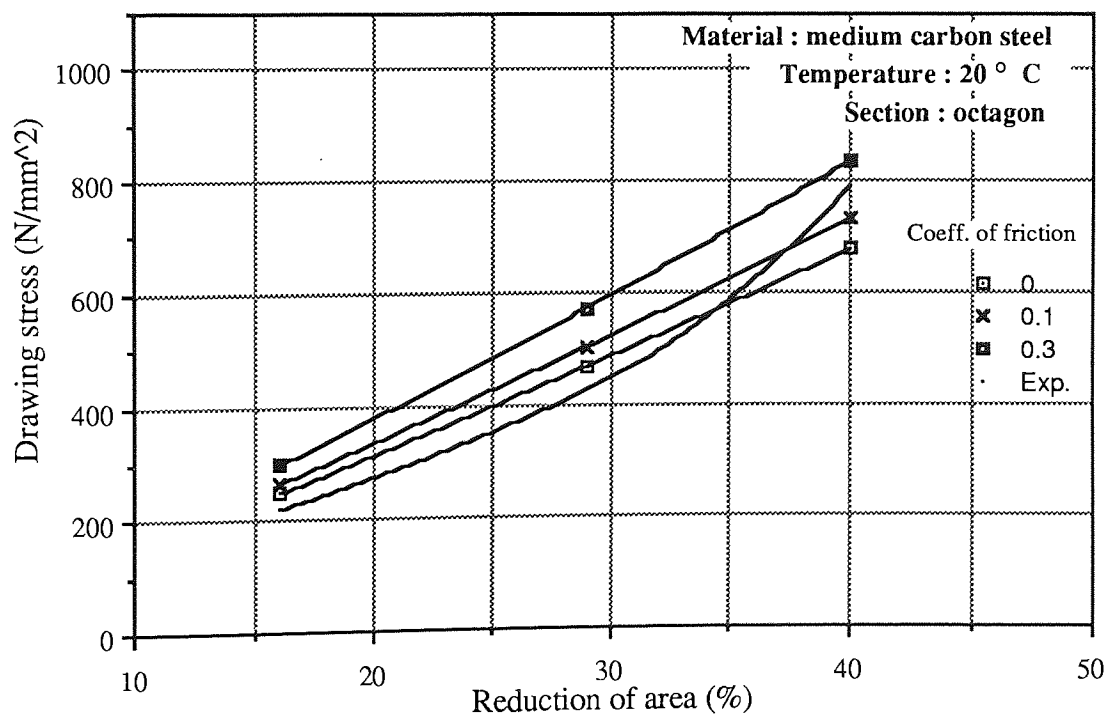

Fig.7.60. Variation of drawing stress with reduction of area, comparison of experimental and theoretical results for various coefficients of friction.
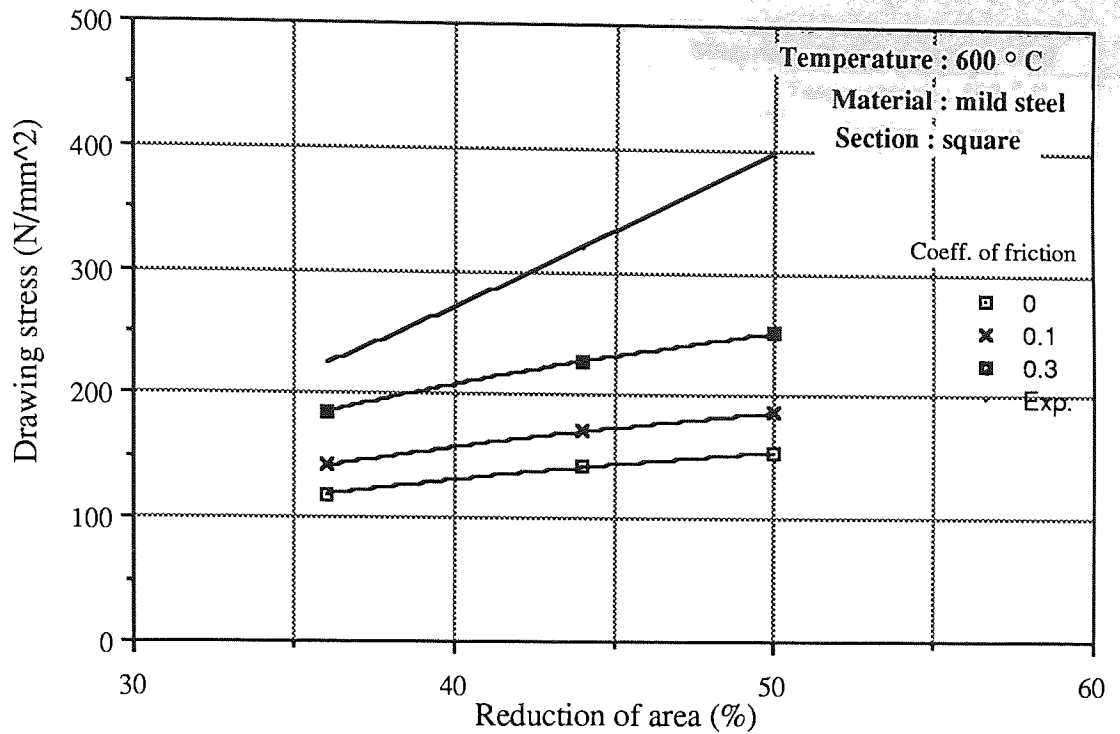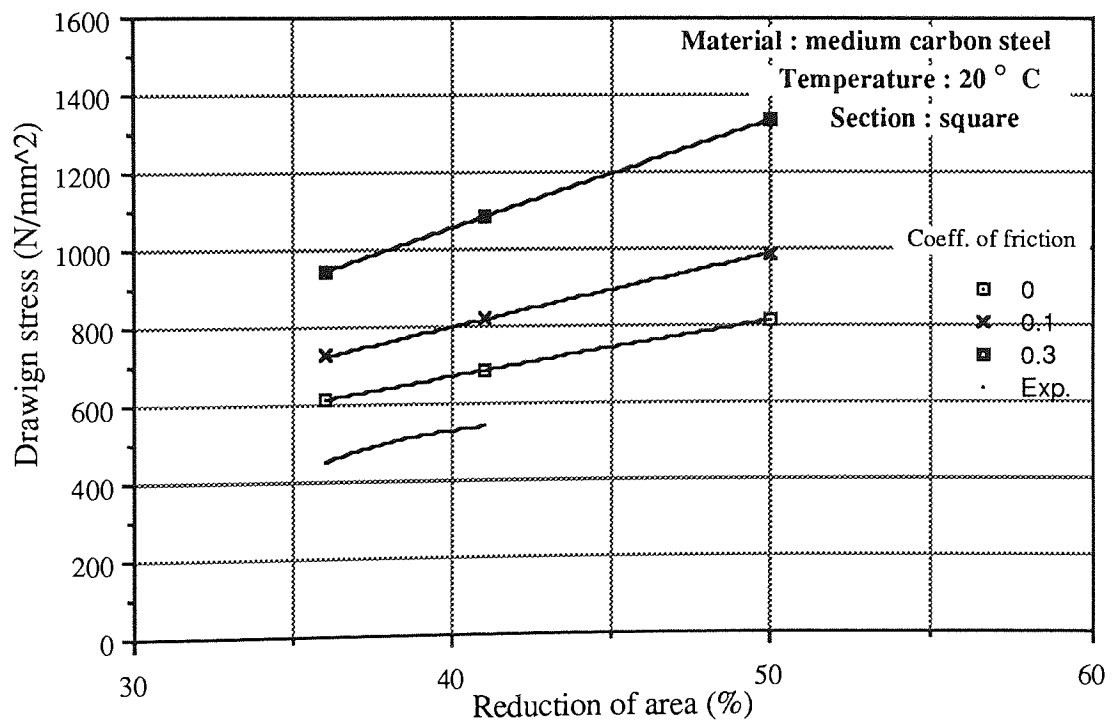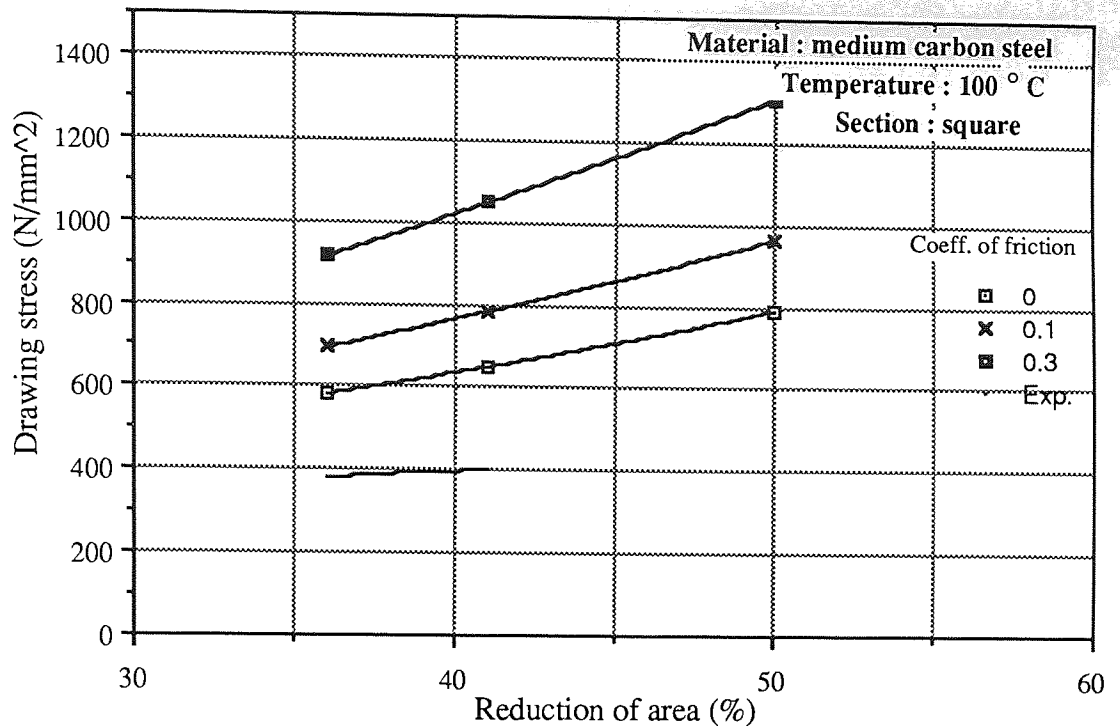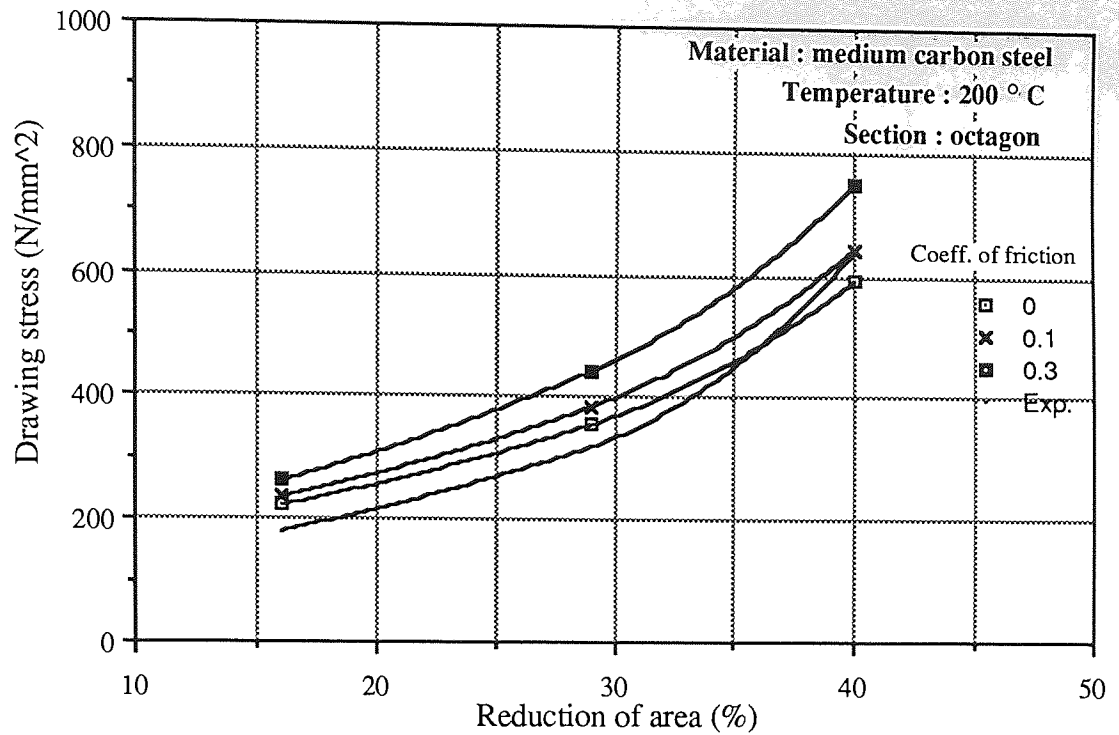
Fig.7.61. Variation of drawing stress with reduction of area, comparison of
experimental and theoretical results for various coefficients of friction.
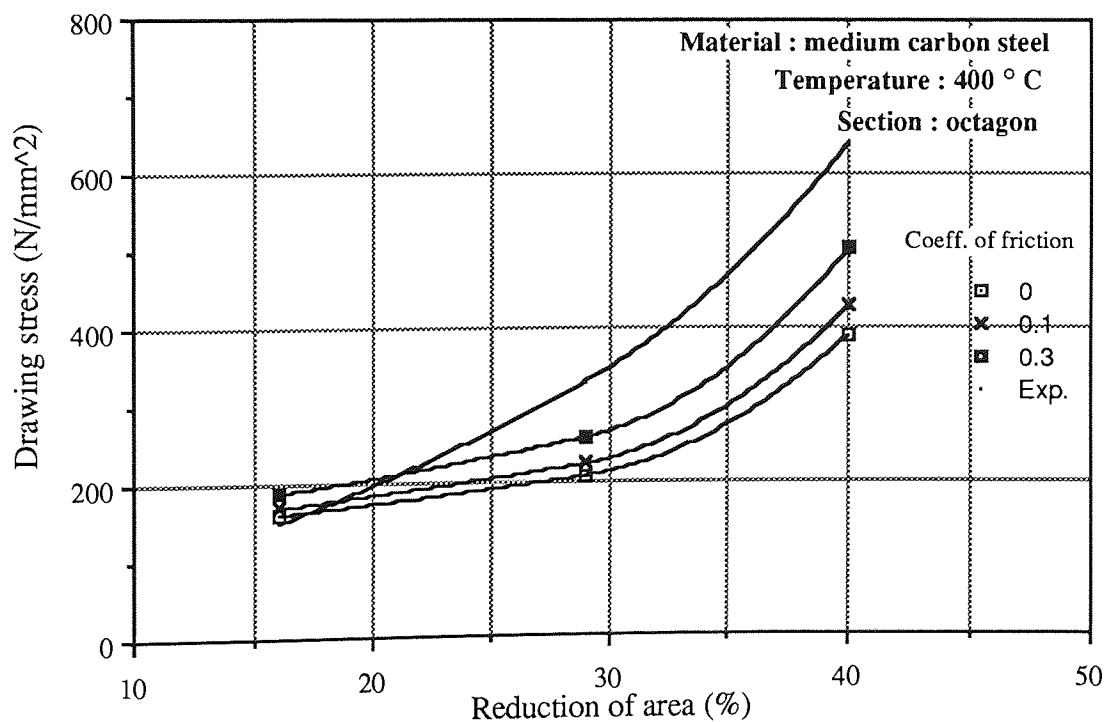
Fig.7.62. Variation of drawing stress with reduction of area, comparison of
experimental and theoretical results for various coefficients of friction.
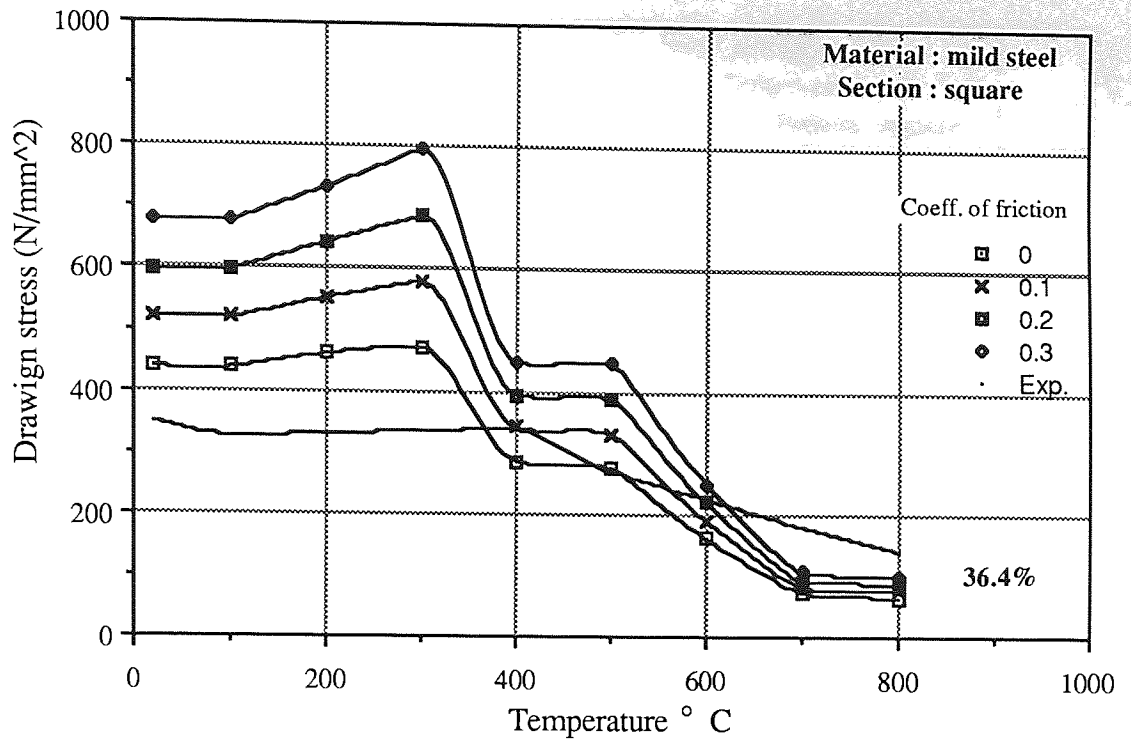
Fig.7.63. Variation of drawing stress with temperature, comparison of experimental and theoretical results for various coefficients of friction, modified results.
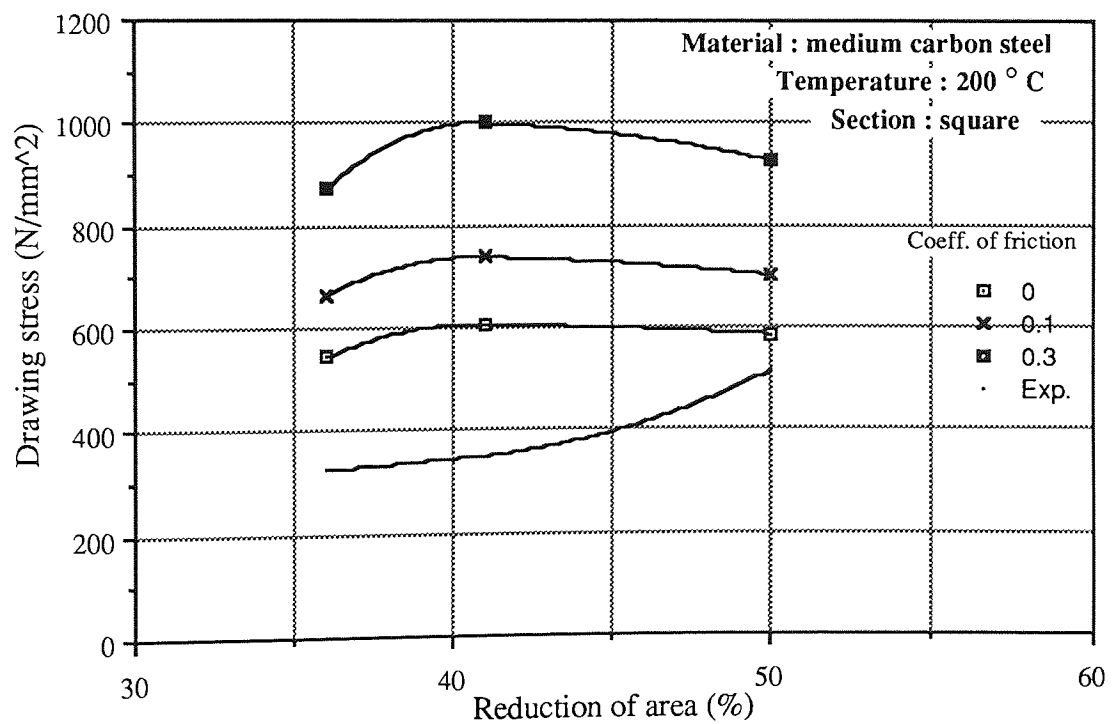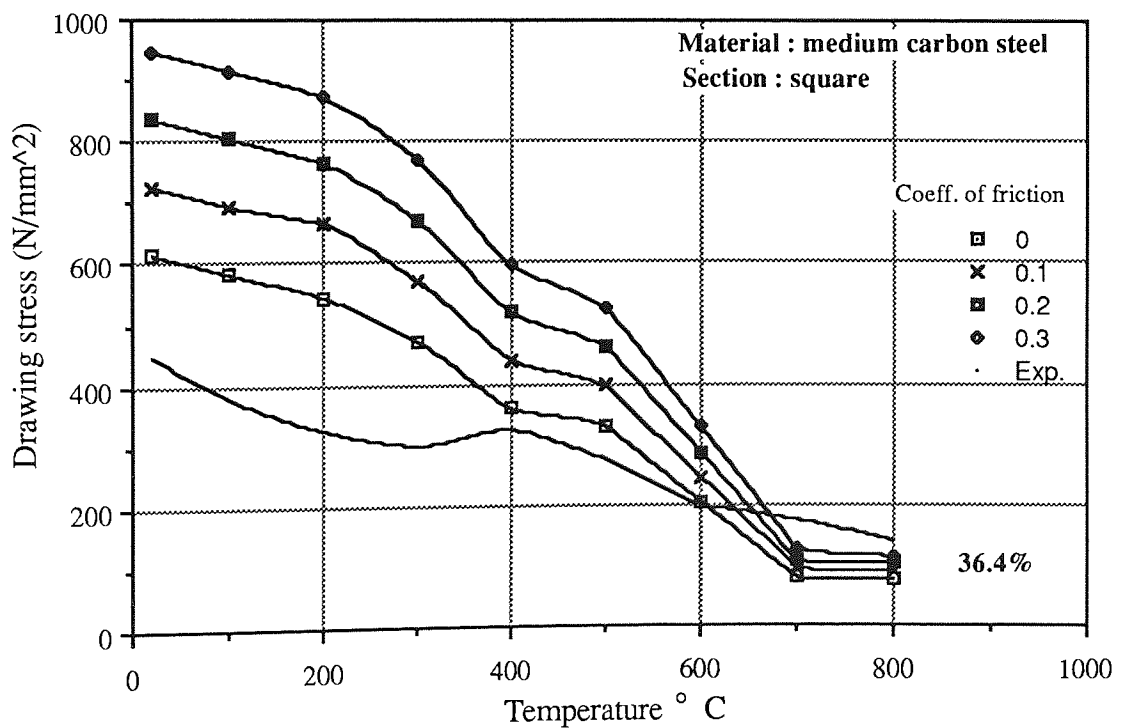

Fig.7.64. Variation of drawing stress with temperature, comparison of experimental and theoretical results for various coefficients of friction, modified results.

216
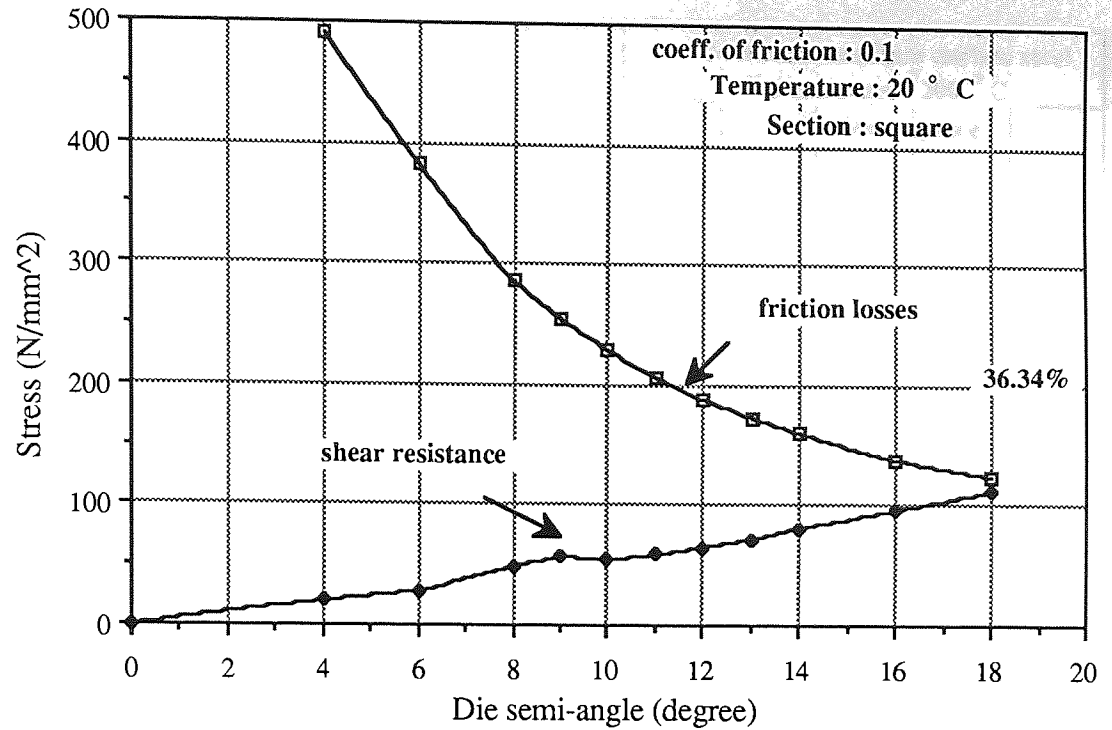
Fig.7.65. Portions of the drawing stress to overcome resistance.
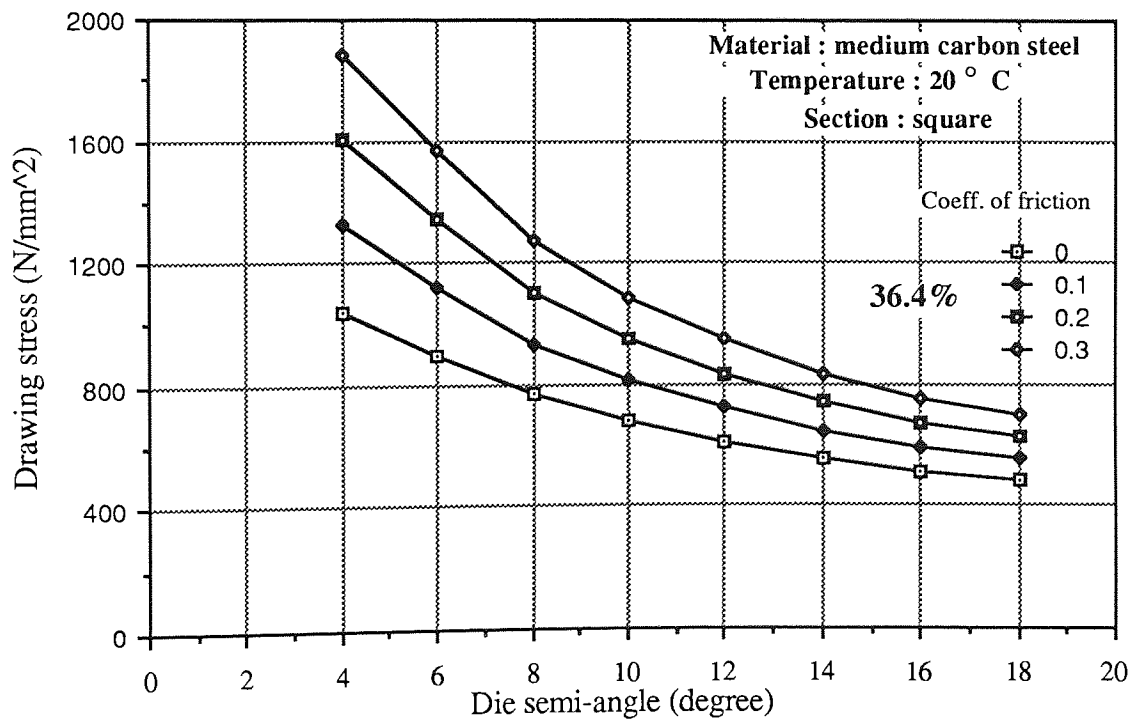
Fig.7.66. Variation of drawing stress against die semi-angle for various
Values of coefficient of friction.
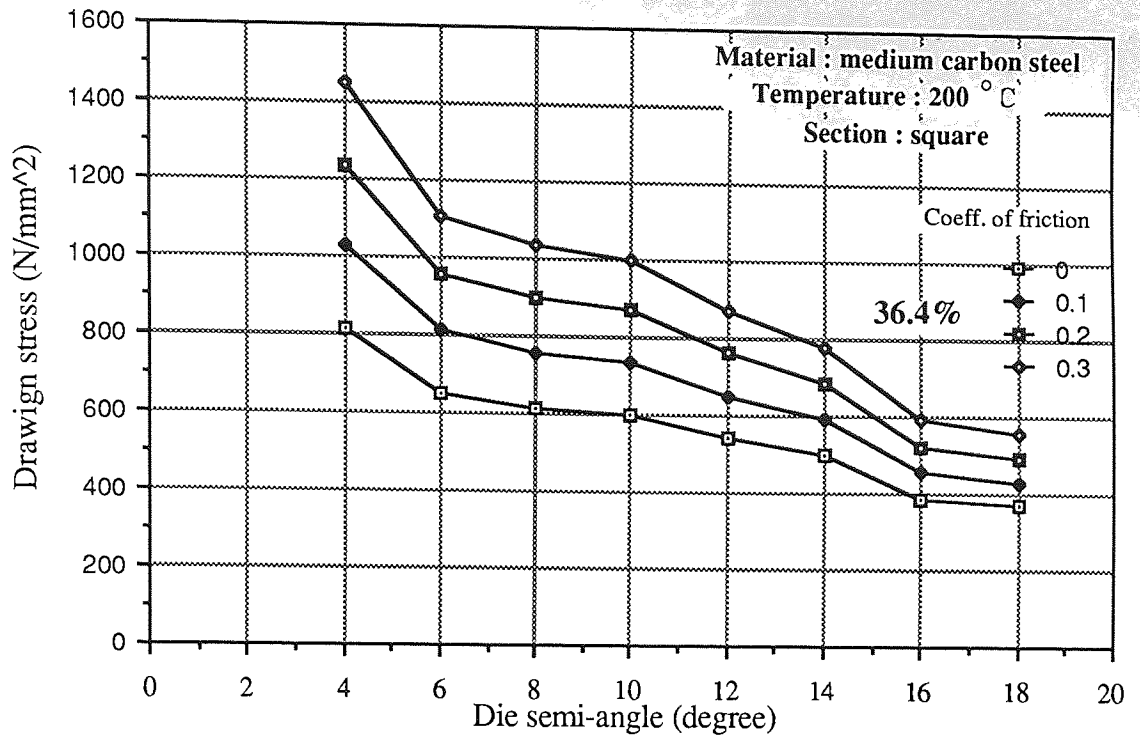
Fig.7.67. Variation of drawing stress against die semi-angle for various
Values of coefficient of friction.
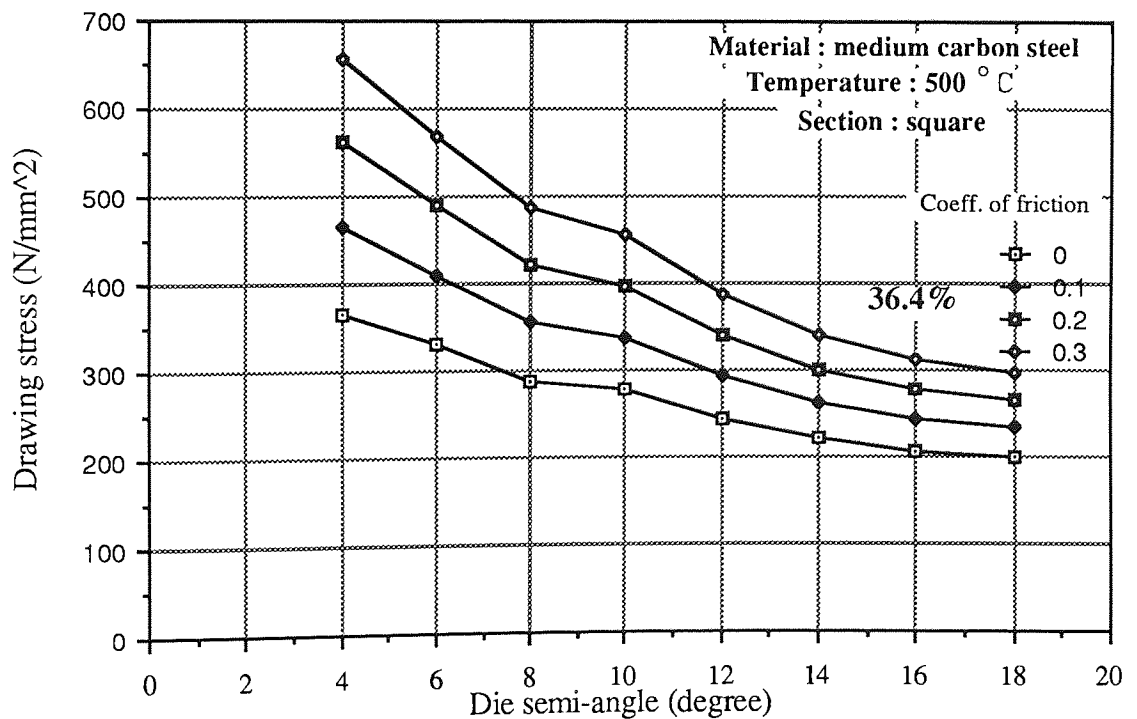
Fig.7.68. Variation of drawing stress against die semi-angle for various
Values of coefficient of friction.
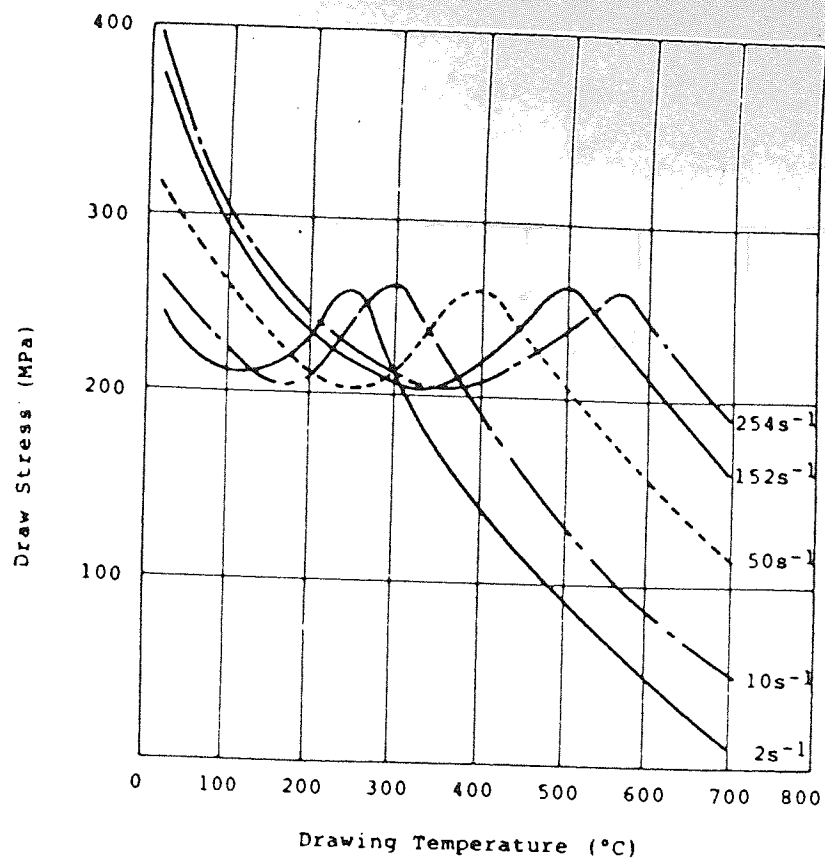
Fig. 7.69.   Theoretical results for various draw speeds and temperatures (20% reduction in area and constant friction factor of 0.1) after Loh (91).

Natural strain
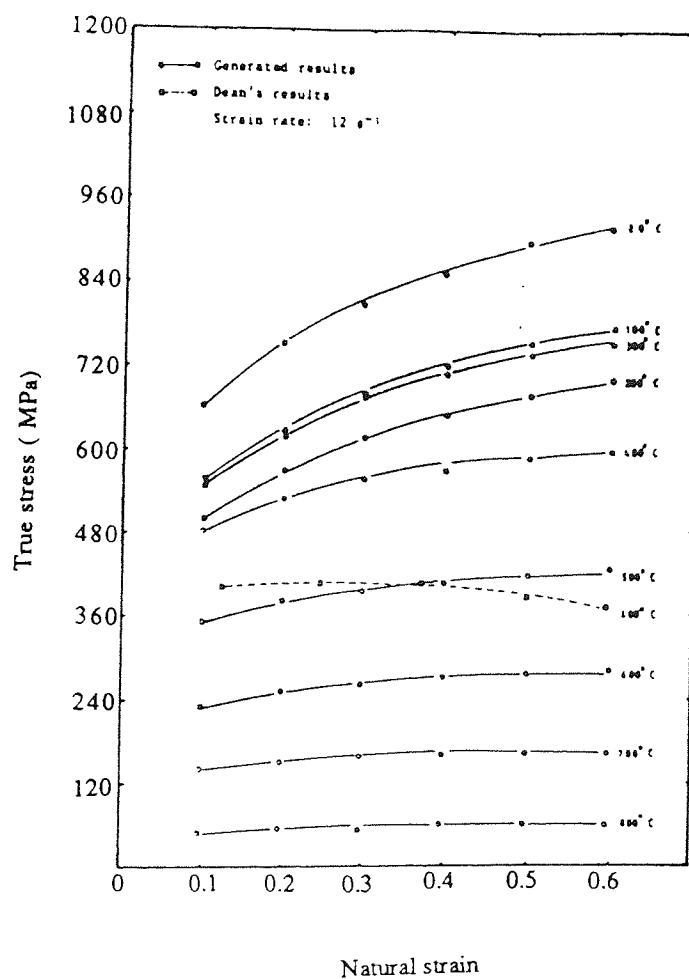
Fig. 7.70.   The generated stress-srain curves for medium carbon steel after Loh (91)

219
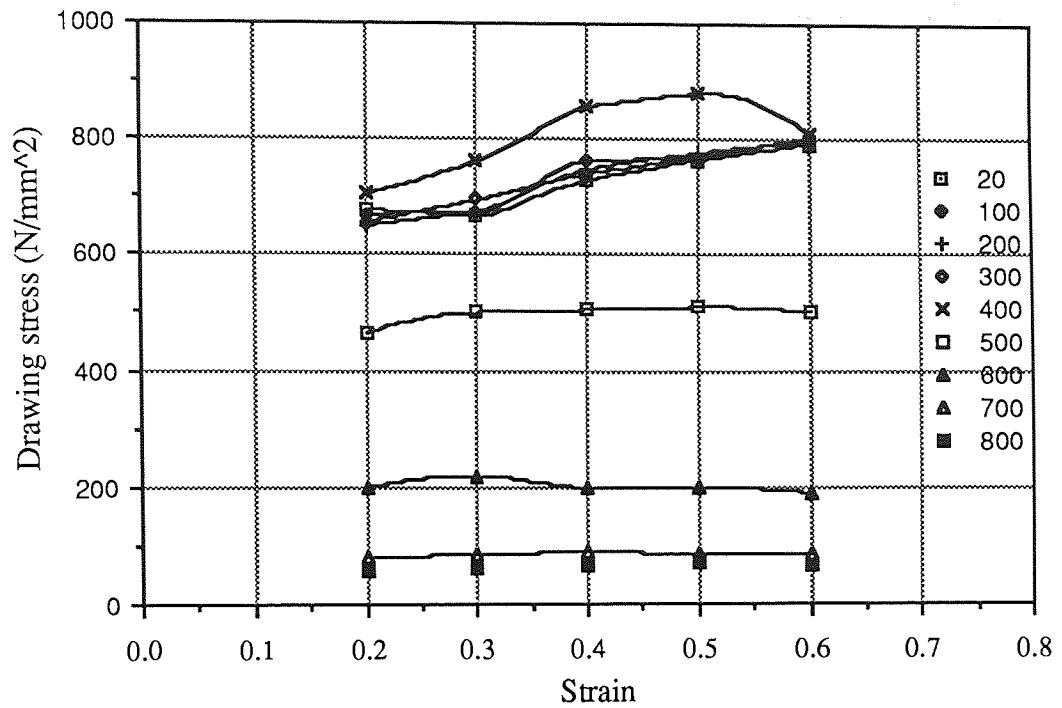
Fig.7.71. Stress-strain curves for medium carbon steel.
for a rate of twist of 90 deg/min.
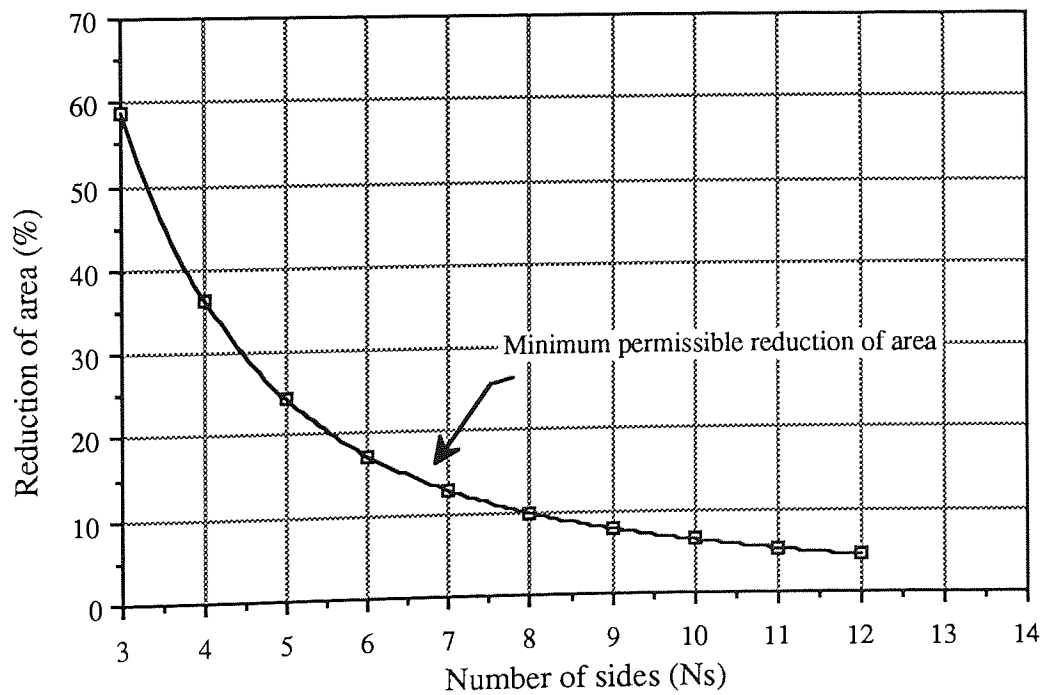
Fig.7.72. The theoretical limits for minimum permissible reductions of area.

Fig.7.73. The three-dimensional modelling of the deformation zone

Test results

Test material   : Mild steel   Test temperature   : 20 deg C

Test speed   : 6 m/s   Coefficent of friction : 0.05

Section   : Square   Reduction of area   : 36.34 %

Die semi-angle :12

Nodal position	Temperature deg. C	Effective strain rate	Effective mean strain	Flow stress N/mm^2
1	20	0	0	-
2	95	1	0.9	599
3	258	1.3	1.85	582
4	429	1.6	2.9	517
5	20	0	0	-
6	95	1	0.9	599
7	259	1.3	1.86	581
8	430	1.6	2.9	516
9	20	0	0	-
10	48	0.43	0.38	524
11	112	0.53	0.79	587
12	186	0.68	1.23	559
13	20	0	0	-
14	55	0.52	0.46	545
15	136	0.65	0.96	587
16	226	0.83	1.5	595
17	20	0	0	-
18	48	0.43	0.38	524
19	113	0.54	0.79	587
20	187	0.69	1.24	558
21	20	0	0	-
22	55	0.52	0.47	545
23	37	0.66	0.97	587
24	227	0.84	1.5	594
25	20	0	0	-
26	39	0.29	0.26	488
27	80	0.37	0.54	582
28	131	0.47	0.85	589
29	20	0	0	-
30	40	0.33	0.29	489
31	87	0.41	0.6	572
32	143	0.52	0.94	584
33	20	0	0	-
34	39	0.29	0.26	489
35	81	0.37	0.55	582
36	133	0.47	0.86	588
37	20	0	0	-
38	41	0.33	0.29	489
39	88	0.41	0.61	572
40	144	0.52	0.95	583

Drawing stress : 440 N/mm^2

Ym = 421 N/mm^2
Yf = 553 N/mm^2

Table. 7.1. Tabulated results of the three dimensinoal modelling

Test results

Test material   : **Mild steel**   Test temperature   : **100 deg C**

Test speed   : **6 m/s**   Coefficent of frictic n : **0.05**

Section   : **Square**   Reduction of area   : **36.34 %**

Die semi-angle :12

Nodal position	Temperature deg. C	Effective strain rate	Effective mean strain	Flow stress N/mm^2
1	100	0	0	-
2	176	1	0.9	566
3	329	1.3	1.85	554
4	492	1.6	2.9	463
5	100	0	0	-
6	176	1	0.9	566
7	330	1.3	1.86	553
8	493	1.6	2.9	458
9	100	0	0	-
10	128	0.43	0.38	515
11	192	0.53	0.79	554
12	261	0.68	1.23	580
13	100	0	0	-
14	136	0.52	0.46	540
15	215	0.65	0.96	599
16	307	0.83	1.5	562
17	100	0	0	-
18	128	0.43	0.38	515
19	193	0.54	0.79	554
20	263	0.69	1.24	580
21	100	0	0	-
22	136	0.52	0.47	539
23	216	0.66	0.97	599
24	308	0.84	1.5	562
25	100	0	0	-
26	119	0.29	0.26	483
27	162	0.37	0.54	631
28	214	0.47	0.85	599
29	100	0	0	-
30	121	0.33	0.29	483
31	167	0.41	0.6	551
32	221	0.52	0.94	597
33	100	0	0	-
34	119	0.29	0.26	483
35	163	0.37	0.55	631
36	215	0.47	0.86	599
37	100	0	0	-
38	121	0.33	0.29	483
39	168	0.41	0.61	551
40	221	0.52	0.95	596

Drawing stress : 433 N/mm^2   Ym = 411 N/mm^2
                                          Yf = 560 N/mm^2

Table. 7.2. Tabulated results of the three dimensional modelling

Test results

Test material   : Mild steel   Test temperature   : 500 deg C

Test speed   : 6 m/s   Coefficent of frictic n : 0.05

Section   : Square   Reduction of area   : 36.34 %

Die semi-angle :12

Nodal position	Temperature deg. C	Effective strain rate	Effective mean strain	Flow stress N/mm^2
1	500	0	0	-
2	555	1	0.9	301
3	637	1.3	1.85	159
4	684	1.6	2.9	110
5	500	0	0	-
6	556	1	0.9	300
7	638	1.3	1.86	158
8	684	1.6	2.9	110
9	500	0	0	-
10	522	0.43	0.38	345
11	564	0.53	0.79	283
12	599	0.68	1.23	216
13	500	0	0	-
14	527	0.52	0.46	345
15	578	0.65	0.96	255
16	617	0.83	1.5	187
17	500	0	0	-
18	522	0.43	0.38	345
19	564	0.54	0.79	282
20	600	0.69	1.24	214
21	500	0	0	-
22	528	0.52	0.47	345
23	578	0.66	0.97	254
24	617	0.84	1.5	187
25	500	0	0	-
26	514	0.29	0.26	323
27	543	0.37	0.54	324
28	571	0.47	0.85	268
29	500	0	0	-
30	515	0.33	0.29	319
31	547	0.41	0.6	320
32	578	0.52	0.94	255
33	500	0	0	-
34	514	0.29	0.26	322
35	543	0.37	0.55	328
36	572	0.47	0.86	266
37	500	0	0	-
38	515	0.33	0.29	319
39	547	0.41	0.61	319
40	578	0.52	0.95	254

Drawing stress : 207 N/mm^2

$Y_m = 188$ N/mm^2
$Y_f = 188$ N/mm^2

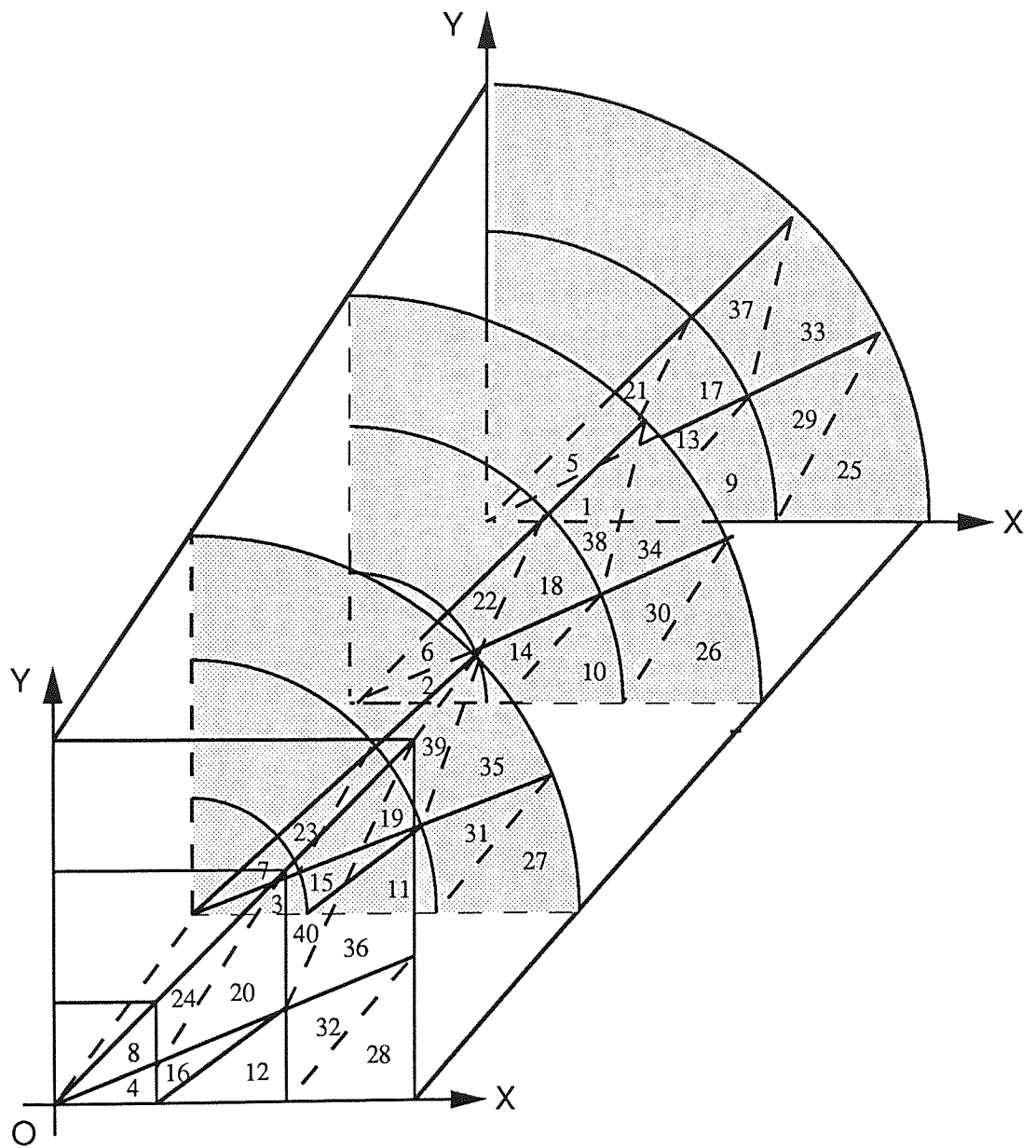Table. 7.3. Tabulated results of the three dimensional modelling

224

Test results

Test material   : Mild steel   Test temperature   : 100 deg C

Test speed   : 6 m/s   Coeffient of friction : 0.05

Section   : Square   Reduction of area   : 50 %

Die semi-angle : 12

Nodal position	Temperature deg. C	Effective strain rate	Effective mean strain	Flow stress N/mm^2
1	100	0	0	-
2	211	o.87	1.32	601
3	461	1.23	2.78	557
4	722	1.81	4.44	63
5	100	0	0	-
6	212	0.88	1.32	600
7	462	1.24	2.8	552
8	722	1.83	4.47	63
9	100	0	0	-
10	147	0.37	0.56	622
11	254	0.52	1.2	583
12	370	0.77	1.9	538
13	100	0	0	-
14	155	0.45	0.68	556
15	278	0.64	1.5	574
16	418	0.94	2.31	521
17	100	0	0	-
18	148	0.37	0.57	623
19	255	0.53	1.19	583
20	373	0.78	1.9	537
21	100	0	0	-
22	156	0.45	0.69	556
23	279	0.64	1.46	573
24	419	0.95	2.3	520
25	100	0	0	-
26	130	0.25	0.38	515
27	197	0.36	0.82	550
28	273	0.53	1.31	576
29	100	0	0	-
30	134	0.28	0.43	540
31	210	0.48	0.91	601
32	302	0.59	1.45	564
33	100	0	0	-
34	130	0.26	0.39	514
35	198	0.36	0.83	549
36	275	0.53	1.32	575
37	100	0	0	-
38	134	0.28	0.43	540
39	211	0.4	0.91	601
40	303	0.59	1.46	564

Drawing stress : 611 N/mm^2   Ym = 377 N/mm^2
                                     Yf = 559 N/mm^2

Table. 7.4. Tabulated results of the three dimensional modelling

225

Test results

Test material : medium carbon steel   Test temperature : 100 deg C

Test speed : 6 m/s   Coefficent of friction : 0.05

Section : Square   Reduction of area : 36.34 %

Die semi-angle :12

Nodal position	Temperature deg. C	Effective strain rate	Effective mean strain	Flow stress N/mm^2
1	100	0	0	-
2	205	1	0.9	810
3	425	1.3	1.85	771
4	651	1.6	2.9	222
5	100	0	0	-
6	205	1	0.9	810
7	426	1.3	1.86	771
8	654	1.6	2.9	220
9	100	0	0	-
10	141	0.43	0.38	768
11	233	0.53	0.79	815
12	335	0.68	1.23	787
13	100	0	0	-
14	151	0.52	0.46	773
15	263	0.65	0.96	800
16	385	0.83	1.5	778
17	100	0	0	-
18	142	0.43	0.38	768
19	234	0.54	0.79	815
20	337	0.69	1.24	787
21	100	0	0	-
22	151	0.52	0.47	773
23	264	0.66	0.97	799
24	386	0.84	1.5	778
25	100	0	0	-
26	126	0.29	0.26	672
27	184	0.37	0.54	798
28	254	0.47	0.85	801
29	100	0	0	-
30	128	0.33	0.29	672
31	194	0.41	0.6	811
32	272	0.52	0.94	798
33	100	0	0	-
34	126	0.29	0.26	762
35	185	0.37	0.55	798
36	256	0.47	0.86	801
37	100	0	0	-
38	128	0.33	0.29	672
39	195	0.41	0.61	811
40	273	0.52	0.95	798

Drawing stress : 569 N/mm^2

Y_m = 534 N/mm^2
Y_f = 762 N/mm^2

Table. 7.5. Tabulated results of the three dimensional modelling

CHAPTER EIGHT

FINITE ELEMENT ANALYSIS OF POLYGONAL DIES

Chapter Eight

8.0 Finite Element Analysis of Polygonal Dies

8.1 Introduction

There are commonly three methods that can be used in analysing the temperature distribution in the deformation zone of a die. These are, experimental, mathematical modelling and finite element techniques. The latter two techniques are considered in the situation where carrying out the analysis by experimental techniques is extremely costly and demanding in skills. In addition the degree of difficulty involved as illustrated by Ranger [96]. Moreover, mathematical modelling and finite element techniques are usually selected as an alternative which can give greater flexibility to analyse the temperature distribution inside a die, as a paper concept.

In this Chapter a finite element numerical analysis is carried out on the various die geometries and die materials used in the drawing of polygonal sections from round at elevated temperatures. Use was therefore made of the Finite Element Method (FEM), which is available as a computer package PAFEC finite element-on the VAX-B cluster main frame system. Interactive graphic analysis is achieved by an accompanying software called PIGS (Pafec Interactive Graphics System).

The aim of analysing the drawing dies numerically is to gain a greater understanding of the behaviour of the various die designs and die materials under the process of elevated temperature drawing, and to establish the temperature distribution, stress concentration and thermal distortions in the deforming zone. The optimum die design and die material to be used for this process can thus be established.

8.2 The finite element method

FEM is a powerful computer-based technique which can be used to accurately analyse the behaviour of a continuum structure, subjected to any complex loads and boundary conditions. This method is basically an extension of the matrix methods of solution for a skeletal structure. As designers and analysts from various disciplines have gained easier access to computers and computer software, FEM has gained widespread recognition and become an indispensable tool.

FEM proceeds to analyse the behaviour of a continuum by artificially dividing it into a finite number of elements, generally known as a mesh. Individual elements are connected together at nodal points as shown in fig.8.1.

Typical nodal
point

Typical rectangular
finite element

Typical triangular
finite element
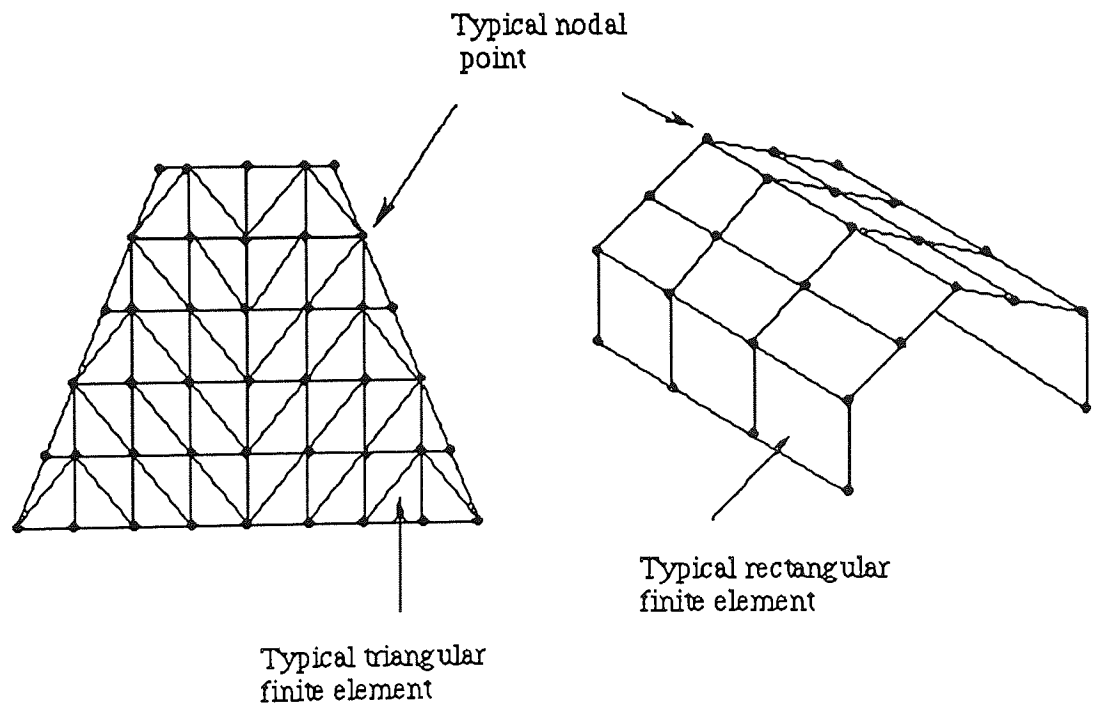
Fig. 8.1. Typical finite element applications.

An assumed approximate function, usually of polynomial form, is chosen to represent the displacement of an element. Continuity of each element is satisfied at the nodal points only, but in most cases the chosen function is such that it is also satisfied along

the common boundaries. The matrix method of analysis is then formulated (usually by the stiffness displacement method) to analyse each element and, in turn, the whole continuum. The repetitive nature of the FEM makes it particularly suited to computer implementation. Thus, complex shapes, which would otherwise have not been possible or too intensive to attempt, can be analysed readily.

8.3 Finite elements

Different shapes and families of elements exist from the simple line, one-dimensional elements to more complex and sophisticated twenty-noded isoparametric three-dimensional elements. However the choice is normally restricted to a few types, depending upon the nature of analysis, degree of accuracy required and the computer working capacity. The most common type of elements used are the rectangular and triangular shaped ones, fig.8.2.
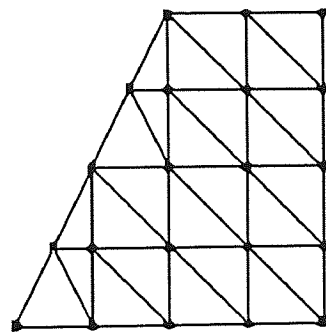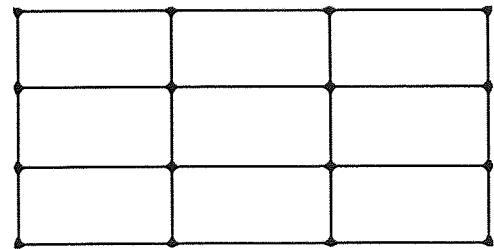
a . triangular elements   b. rectangular elements

Fig.8.2. Typical finite element idealisations

Each shape of element is described by an individual displacement function and each family by a general function. It has been found that certain shapes of elements achieve better results than others Pafec[127]. This is principally due to the accuracy of the assumed displacement function chosen. It is because of this that rectangular shaped

229

elements are preferred to triangular elements. Nevertheless, good results can be achieved by increasing the number of elements in the zone of interest. Also, due to the approximate nature of the displacement functions used, a sufficient number of elements are needed to achieve an acceptable representation of the overall continuum. The term 'sufficient' varies to the particular problem under consideration. The accuracy of the results increases with the number of elements taken, but this requires increased computer capacity and processing time which leads to greater financial outlay requirements. As a general rule, meshes are recommended by Pafec[127] to be more finally graded where sharp changes of stress or temperature are expected i.e. near openings or points of loading as shown in fig.8.3.

Point load
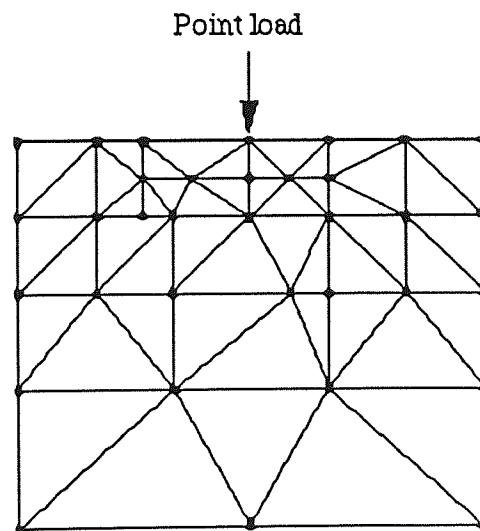
Fig.8.3. Typical example of a graded mesh.

8.4 Finite element computer software.

8.4.1 Program for automatic finite element calculations - PAFEC.

Although designers may resort to writing their own FE computer programmes, it is easier, faster and more accurate to use a comprehensive FE computer package available

today. One such FE package used extensively in industry is PAFEC. It is a large scale, general purpose 2-D or 3-D, linear and non-linear, FE analysis system. A comprehensive element library and system capabilities exists, typical examples of element types available are shown in fig.8.4. The procedures required to operate PAFEC are straight forward. The user inputs data via a data file in a prescribed modular form. The file is then run to process the displacements, stresses or other chosen analysis. All decisions in the formulation of the FE analysis are left to the user. Thus, it is important that the user has some knowledge of the finite elements available and the desired results.

The PAFEC finite element suite consists of ten separate computer programs, which, when executed sequentially, give a complete engineering analysis. Each of these programs is known as a PHASE of PAFEC. A synopsis of operations for each of the PAFEC PHASES is given below

PHASE 1, Read

Data modules are read in, default values are inserted and the modules are placed on to the the backing store. The NODES module is expanded so that all mid-side nodes are included.

PHASE 2, Pafblocks

This is a module in the data file for generating a complicated model mesh by the use of a simple input statement. Any PAFBLOCKS data is replaced by the nodal co-ordinates and topological description of the complete mesh of elements.
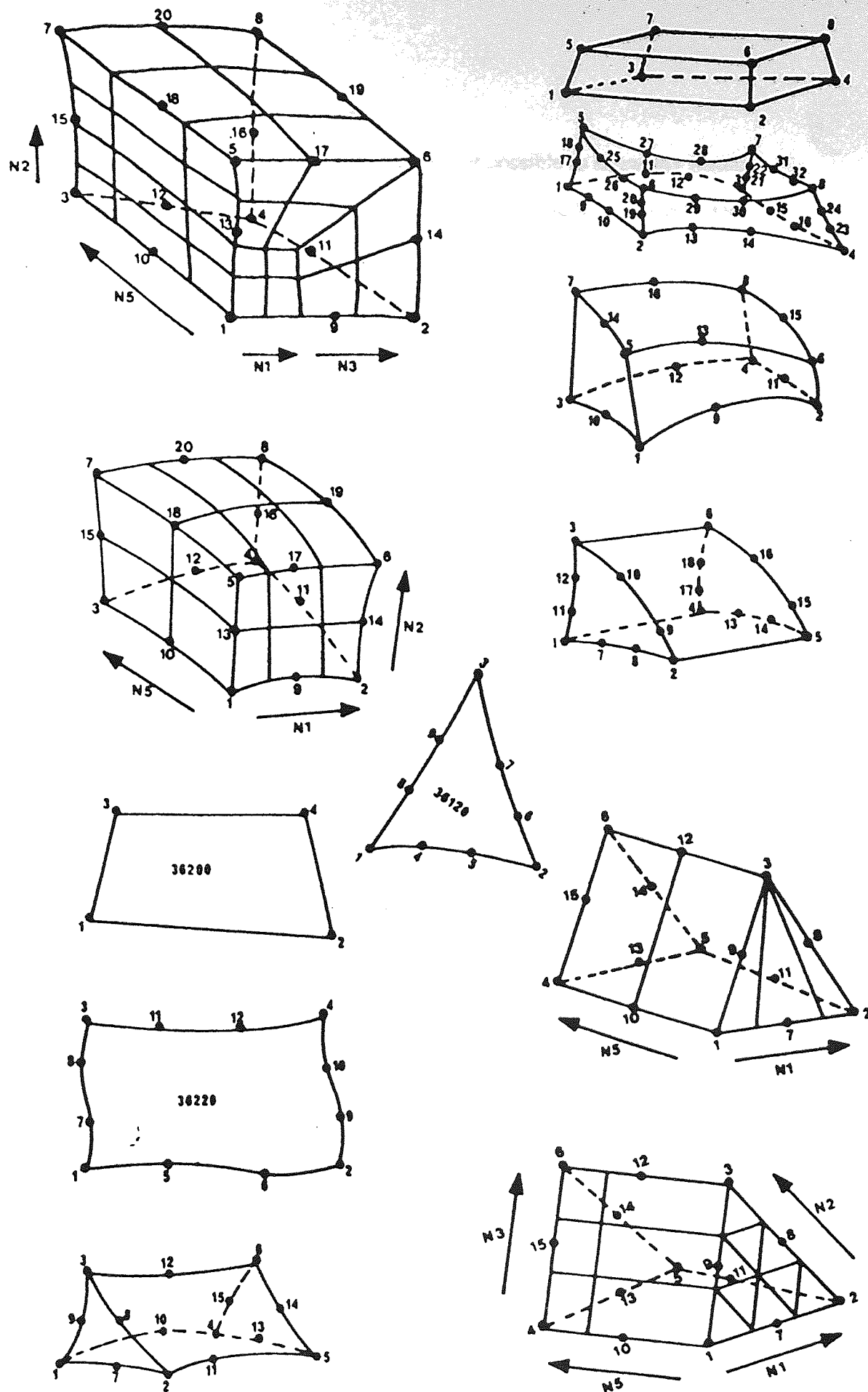
Fig. 8.4. Typical types of finite elements available in PAFEC library.

PHASE 3, IN.DRAW   Structure

The structure itself is drawn. At this stage it is not possible to show any results such as displacements, stresses, or temperatures since these have not yet been evaluated.

PHASE 4, Pre-solution housekeeping

In this phase the constraints on the problem are considered and a numbering system for the degrees of freedom is derived.

PHASE 5, IN.DRAW   Constraints

This phase is very similar to phase 3 except that the constraints, degrees of freedom etc. are drawn.

PHASE 6, Elements

The stiffness (or others such as conductivity, mass, etc.) matrices of the elements are found and put on to a file store.

PHASE 7, Solution

The system equations are solved for displacements, temperatures or whatever are the primary unknowns in the problem being tackled.

PHASE 8, OUT.DRAW   Displacements.

The primary unknowns in the problem (ie displacements or temperature) are drawn.

PHASE 9, STRESS

The stresses are derived.

PHASE 10, OUT.DRAW

Stress contours, stress vector plots etc. are produced.

8.4.2 PAFEC thermal analysis

PAFEC can be used to determine the temperature distributions in complex engineering structures. Often, temperatures are required in order that thermal stresses can be analysed in the components. There are two types of thermal calculations. The most straightforward is a steady state analysis, the other is a transient one in which there is usually a thermal shock and knowledge of how the temperature varies with time is required. However, thermal stresses and corresponding temperatures and mechanical stresses due to loading cannot be found by the solution of a single set of equations. First, a set of equations has to be solved to give temperatures then another set-of equations is solved in which the displacements (and therefore the stresses) are the unknowns.

The usual procedure for carrying out a temperature calculation, and then a thermal stress calculation, is to run two separate jobs. PAFEC will pick up correct temperature information automatically from the data file for the second run involving stress and load applications.

The input data concerning the temperature distribution is obtained from the solutions given by the theoretical process modelling i.e. the numerically solved upper bound theory.

8.4.3 Pafec Interactive Graphics System - PIGS

All results and data from the PAFEC runs can be interactivated on PIGS which is an extremely powerful aid for the user of finite elements. It enables the production of graphical representations of the input or output data interactively. Thus, any wrong data

or choice of analysis can be ironed out without having to supply new data and re-run the program.

The primary facilities on the PIGS software can be itemised as follows.

i) Finite element model generation

ii) Mesh modification

iii) Interactive loads and restraints placement

iv) Pafec file editing

v) Full colour and shading

vi) Stress vector and contour display

vii) Automatic generation of high quality hard copy

viii) Automatic PAFEC data file generation

ix) Graph production

Typical examples of the type of outputs which can be achieved from PIGS can be seen in figs. 8.6 - 8.16.

8.4.4 Finite element analysis of the section dies

A PAFEC input data file is created in order to submit for FE analysis of the section dies used. A typical data file is seen in fig.8.5. Seven system modules are chosen to fully analyse the die for temperature distribution. These modules can be itemised as follows ;

i) Control

ii) Nodes

iii) Pafblocks

iv) Mesh

v) Materials

vi)   Loads

vii)   Temperature

The CONTROL module is used as an aid to guide the process through the various paths within the PAFEC system.

The NODES module is where co-ordinate values of nodes are inserted, to define the problem.

Automatic generation of the mesh is achieved by the use of PAFBLOCKS and MESH modules. The Pafblocks facility is used to reduce the magnitude of data preparation required to create a mesh. A sufficient number of nodes are required to define the layout and shape of each Pafblock. These are then divided into a number of elements by referring to the Mesh module. The advantage to be gained from the use of these two modules is found when re-analysis of a problem, with different mesh densities is required.

The MATERIALS module relates to the properties of the material used. The properties are pre-programmed into the PAFEC software for different materials but may be overwritten by the user. The PLATES and SHELLS module relates to the properties and thickness of the material when using 2-D analysis.

For the LOADS module, the case, location, direction and values of loads are given in a prescribed manner, these loads could be temperatures, pressures etc.

The TEMPERATURE module is used to input known steady state temperatures in a temperature distribution problem.

236

TITLE ROUND TO SQUARE WITH LAND DIE

CONTROL
CALC.STEADY.TEMPS.
CONTROL.END
NODES

NODE.NUMBER	X	Y	Z
1	470	0	0
2	530	110	0
3	0	0	0
4	190	455	0
5	705	230	265
6	705	295	265
7	130	230	265
8	315	680	265
9	495	60	0
10	50	250	0
11	180	475	265
12	640	160	0
13	640	640	0
14	765	295	265
15	765	870	265
16	580	150	0
17	390	595	0
18	515	820	265
19	710	370	440
20	750	485	440
21	225	370	440
22	405	830	440
23	725	440	440
24	270	605	440
25	860	530	440
26	860	1020	440
27	800	520	440
28	615	970	440
29	980	1040	1200
30	1240	1300	1200
31	605	1040	1200
32	1240	1680	1200
33	1055	1220	1200
34	780	1490	1200
35	1005	1145	1200
36	1145	1285	1200
37	1000	1640	1200
38	655	1290	1200
39	650	130	155
40	650	195	155
41	80	130	155
42	265	580	155
43	125	375	155
44	715	195	155
45	715	765	155
46	470	715	155

PAFBLOCK
ELEMENT.TYPE = 39620
PROPERTIES = 1

BLOCK.NUMBER TYPE GROUP.NUMBER N1 N2 N5 TOPOLOGY
1 1 1 1 2 3   1 2 3 4 39 40 41 42 9 0 0 10 0 0 0 0 0 0 0 43
2 1 1 1 2 3   2 12 4 13 40 44 42 45 16 0 0 17 0 0 0 0 0 0 0 46
3 1 1 1 4 3   39 40 41 42 5 6 7 8 0 0 0 43 0 0 0 0 0 0 0 11
4 1 1 1 4 3   40 44 42 45 6 14 8 15 0 0 0 46 0 0 0 0 0 0 0 18
5 1 1 1 5 3   5 6 7 8 19 20 21 22 0 0 0 11 0 0 0 0 23 0 0 24
6 1 1 1 5 3   6 14 8 15 20 25 22 26 0 0 0 18 0 0 0 0 27 0 0 28
7 1 1 1 6 3   19 20 21 22 29 33 31 34 23 0 0 24 0 0 0 0 35 0 0 38
8 1 1 1 6 3   20 25 22 26 33 30 34 32 27 0 0 28 0 0 0 0 36 0 0 37

MESH
REFERENCE   SPACING.LIST
1   2
2   4
3   2
4   2
5   4
6   3

MATERIALS
MATERIALS.NUMBER   K
12   80

TEMPERATURE
LOAD.CASE TEMPERATURE   LIST.OF.NODES
1   25   31 645 637 21 474 466 458 7 319 41 167 159
1   25   710 26 563 557 551 15 365 45 263 257
1   25   151 3 587 589 591 13 579 583 17 4 10
1   500   25 27 20 23 19
1   515   501 499 393 391 389
1   547   495 493 385 383 381
1   578   489 487 377 375 378 14 338 6 286 5 334 332 281
1   578   279 277 40 200 44 77

END.OF.DATA.

Fig. 8.5. Typical PAFEC data input file

238

8.4.5 Three dimensional modelling or modelling for 3D

3-D modelling is used to provide a more realistic representation of the stress and temperature distribution. The type of element used was the 37110, a twenty-noded, iso-parametric, brick element for 3-D stress analysis. This is a general-shaped 3-D element with six curvilinear faces and twelve edges. There are eight- corner nodes and one mid-side node on each of the edges, giving twenty nodes in all. For the 3-D temperature analysis the element type used was the 39620. This is a twenty-noded, brick element for temperature calculations. Reasonable distortion from the basic cubical shape is permitted. If mid-side node numbers are omitted from the TOPOLOGY entry in the ELEMENTS module then corresponding sides are taken as straight.

List of Finite Element Analysis Figures.

Fig. 8.6

241

Fig. 8.7

FA 1 | STEADY STATE THERMAL : PHASE= 7 | X=250 Y=355 Z=335

M>FA8> JOB1.BE FOUND> RETRIEVE THIS FILE (Y/N)= Y> YOUR STRUCTURE CONTAINS 609 NODES,88 ELEMENTS,1
LOADCASE(S)> THE BACKING STORE IS POST PHASE 4> THE STRUCTURE CONTAINS 609 PROCESSING NODES
,ELEMENTS> LOADCASE SET TO ONEM>V55> ENTER DEGREES ABOUT X,Y AND Z AXES= 250,355,335M>FA1M>MD6M>FA1
> FACE SORTING STARTED> COMPLETEDM>

242

8.5 Results from finite element analysis

Temperature distributions in the deforming zone are obtained from the three-dimensional modelling of the process, for test temperatures of 100 and 500°C. It was assumed that the outer surface temperature of the workpiece will be the same as that at the inner surface of the die deforming zone for the purpose of these analyses and that the die was cooled externally and the temperature was kept at 25°C, this was achieved by using thermocouples attached to the outer surface of the dies during drawing to monitor the temperature change. Due to the vast amount of data output from the PAFEC analysis, only a typical example of a data file is given in fig.8.5. Typical examples of the type of outputs which can be achieved from PIGS are shown in figs.8.6 - 8.16.

A three dimensional true scale model of the square, hexagon and round dies used in the experimental work are presented in a finite element structure. The testing temperature of 500°C was chosen to illustrate any differences in the temperature distribution especially when using Syalon dies at higher temperatures. The following observations are made :

1. Temperature distribution in the deforming zone for chromium carbide, Syalon, tungsten carbide and Stellite dies are very similar, and they only differ by a few degrees. Figs.8.8 and 8.9, show the temperature distribution using a round-to-square die geometry at a testing temperature of 500°C, for tungsten carbide and Syalon respectively. Tungsten carbide has slightly higher values than those obtained using Syalon.

2. The heat transfer (conduction) and temperature distribution is uniform across a die, i.e. the temperature distribution across a die is similar using all materials tested, therefore there is no concentration of heat in a particular die material compared with the others. Since the temperature distribution and, therefore, thermal distortions are similar for all materials used, therefore, die wear of a

243

Fig. 8.8. Steady state thermal distribution analysis, using tungsten carbide die without land, at the drawing temperature of 500 deg.C

Fig. 8.9

particular die being higher than the other, is not attributed to the temperature concentration being higher when using this particular material.

3. Figs.8.8 and 8.11, show the temperature distribution using the round-to-square , without land, die designed by Basily and Sansome[53] and also the same die with land. It is clear that the temperature distribution is more uniform when using the latter die and that the temperature concentration at the end of the deforming zone and the beginning of the land portion of the die is distributed uniformally as compared to fig.8.8, therefore, die wear at that area will be reduced by using a die with a suitable land portion.

4. Similar temperature distributions for all dies are obtained at the higher temperature of 500°C.

5. Figs.8.8 to 8.12, show that, the temperature is uniformally distributed round the die, which is kept at 25°C at the outer surface by direct cooling. Therefore, this indicates that die cooling affects the temperature distribution and that a uniform distribution is obtained, which is contradictory to Altan[97], where he concluded that the large temperature gradient in the die used, shows that external cooling of the die is an extremely inefficient way of cooling. It is therefore suggested that the analysis of the thermal distribution in polygonal dies using finite element methods should be used as a fast technique for deciding on or examining the performance of any newly developed die materials, as compared to the well-established one. Further to check and monitor how effective die cooling and the effect of varying the cooling of the dies is on the temperature distribution throughout the die.

Fig. 8.10. Steady state thermal distribution analysis, using tungsten carbide die without land, at the drawing temperature of 100 deg.C.

FA 1 STEADY STATE THERMAL : PHASE= 7

X=250 Y=355 Z=335
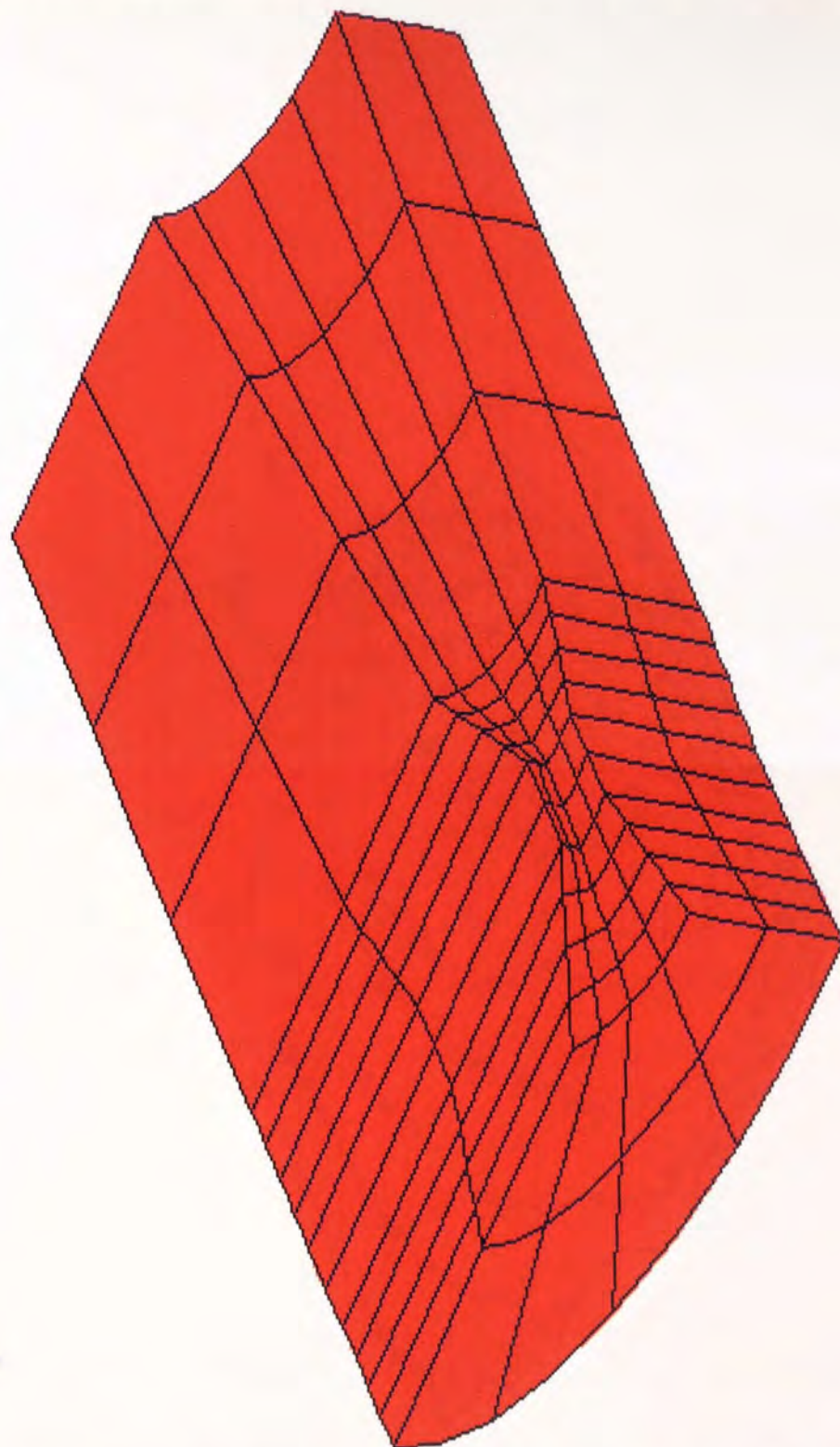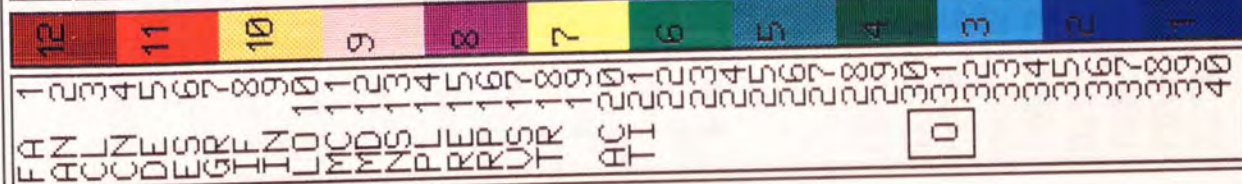
> JOB2.B5 FOUND> RETRIEVE THIS FILE (Y/N)= Y> YOUR STRUCTURE CONTAINS 713 NODES,104 ELEMENT5,1 LOADCASE(5)
> THE BACKING STORE IS POST PHASE 4> THE STRUCTURE CONTAINS 713 FREEDOM5> PROCESSING NODE5,ELEMENT5
> LOADCASE SET TO ONE H>V55> ENTER DEGREES ABOUT X,Y AND Z AXE5= 250,355,335M>MD18M>FA1M>MD6FA1
> NO NUMBER OPTION GIVEM>MD6M>FA1> FACE SORTING STARTED> COMPLETEDM>MD17M>FA1M>MD1M>FA1M>V55
> ENTER DEGREES ABOUT X,Y AND Z AXE5= 250,0,355M>FA1M>MD22M>FA1M>V55> ENTER DEGREES ABOUT X,Y AND Z AXE5=
250,355,335M>MD21M>MD18M>FA1M>MD6M>MD17M>FA1> FACE SORTING STARTED> COMPLETEDM>

Fig. 8.11

STEADY STATE THERMAL : PHASE= 7   X=250 Y=355 Z=335

FA 1
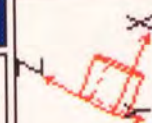
E2

J 5.53
I 4.97
H 4.42
G 3.86
F 3.30
E 2.75
D 2.19
C 1.64
B 1.08
A 0.52

LOAD   1
TEMPS
CLIP   5
MAX TMP
POWER 3
0.58
MIN TMP
POWER 1
2.50
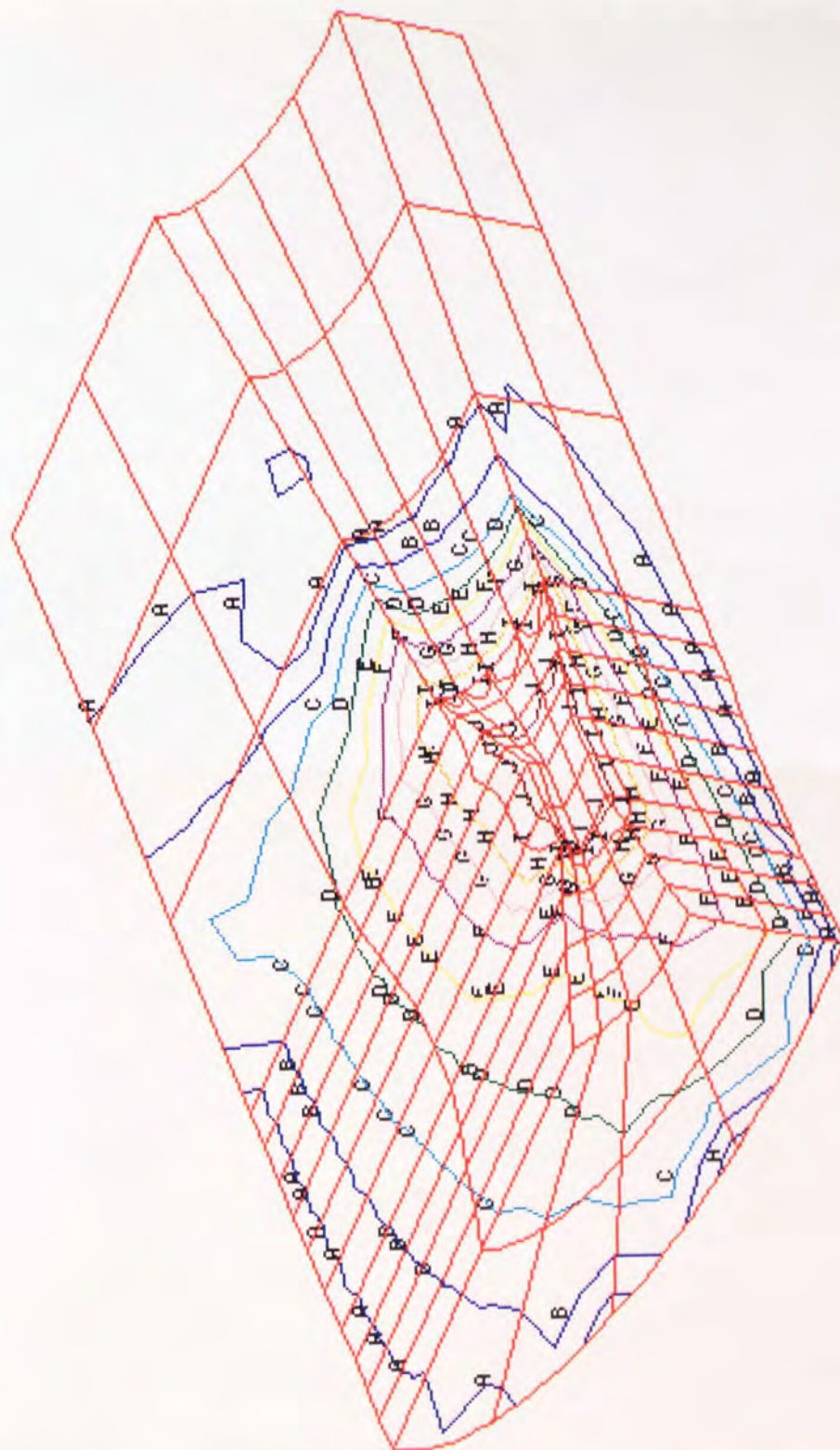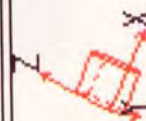
TEMPERATURE PROCESSING BEGUN> TEMPERATURE PROCESSING COMPLETEDM>FA1> TEMPERATURES   > FACE PROCESSING BEGUN
> FACE PROCESSING COMPLETE> M FOR MENU M>
> FACE PROCESSING COMPLETE> M FOR MENU M>V55> ENTER DEGREES ABOUT X,Y AND Z AXES= 250,355,335M>MD18M>FA1M>MD6FA1
> LOADCASE SET TO ONE M>V55> ENTER DEGREES ABOUT X,Y AND Z AXES= 250,355,335M>MD18M>MD17M>FA1M>MD1M>FA1M>V55
> NO NUMBER OPTION GIVEM>MD6M>FA1> FACE SORTING STARTED> COMPLETEDM>MD17M>FA1M>MD22M>FA1M>V55> ENTER DEGREES ABOUT X,Y AND Z AXES=
> ENTER DEGREES ABOUT X,Y AND Z AXES= 250,0,355M>FA1M>MD6M>MD17M>FA1> FACE SORTING STARTED> COMPLETEDM>AN4>
250,355,335M>MD21M>MD18M>FA1M>MD6M>MD6M>FA1> FACE SORTING STARTED> COMPLETEDM>AN4>

Fig. 8.12

Fig. 8.13. Steady state thermal distribution analysis, using Syalon die die with land, at the drawing temperature of 500 deg.C.

STEADY STATE THERMAL : PHASE= 4

X=250 Y=355 Z=335

FA 1
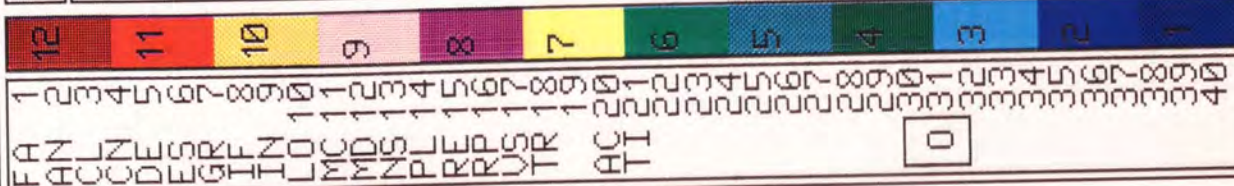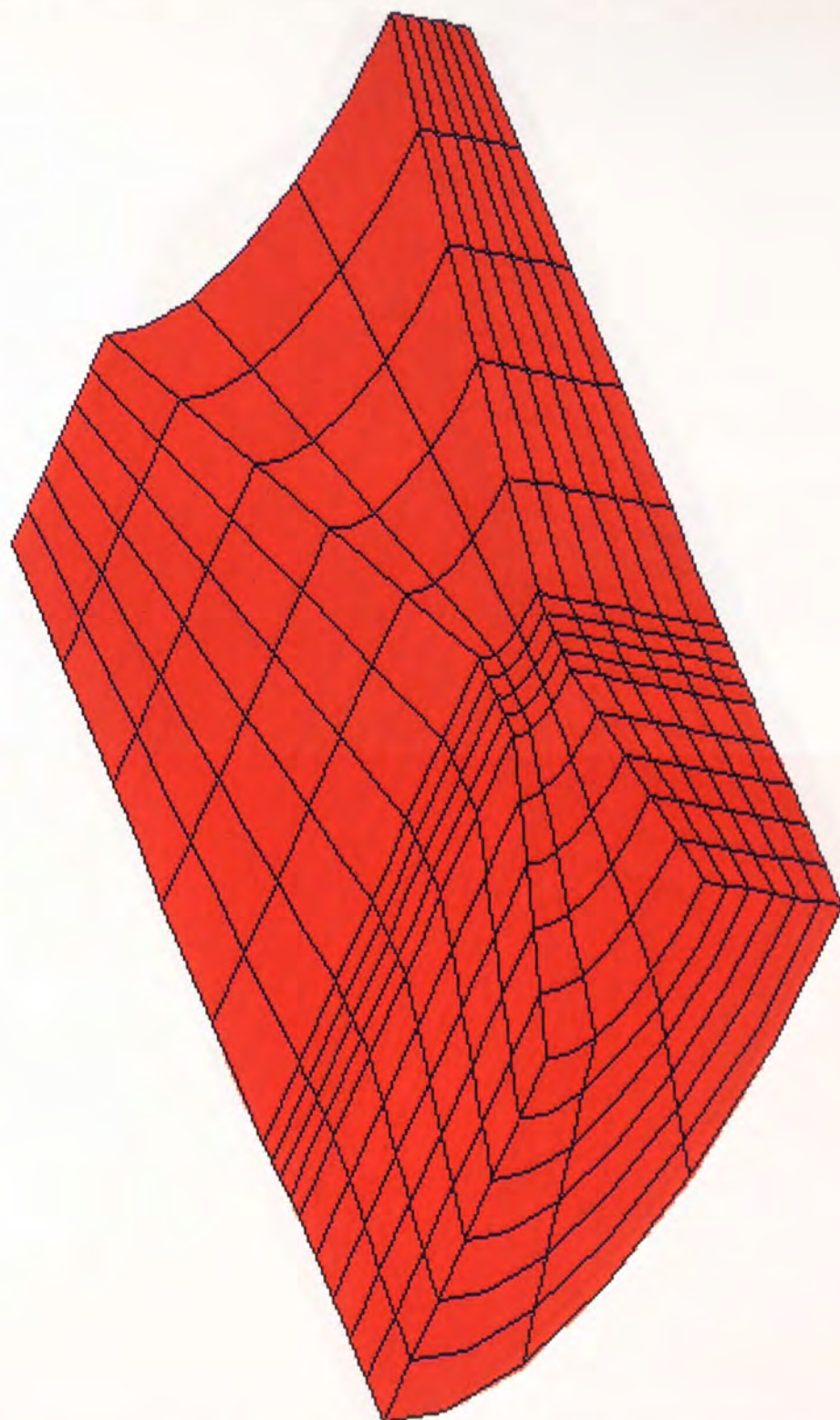
M>FA8> LOH1.BE FOUND> RETRIEVE THIS FILE (Y/N)= Y> YOUR STRUCTURE CONTAINS 1487 NODES,1 LOADCASE(5),
THE HIGHEST NUMBERED ELEMENT IS 252> THE BACKING STORE IS POST PHASE 4> THE STRUCTURE CONTAINS 1487 FREEDOMS
> PROCESSING NODE, ELEMENTS> LOADCASE SET TO ONEM>C55> NO NUMBER OPTION GIVENM>250,355,335> OVERFLOW
> NO NUMBER OPTION GIVENM>V55> ENTER DEGREES ABOUT X,Y AND Z AXES= 250,355,335M>FA1M>MD6M>FA1
> FACE SORTING STARTEC> COMPLETEDM>

251

CHAPTER NINE

OBSERVATIONS AND DISCUSSION

Chapter Nine

9.0   Observations and Discussion of Results

9.1 Introduction

This chapter presents an account of observations and a detailed discussion of results in the study of polygonal drawing from round at elevated temperature. The discussion of results is dealt with under two main headings;

1) Experimental results

- drawing test results

- torsion testing at elevated temperature

- mechanical testing of test specimens

- metallographic examination of samples drawn at various temperatures and reductions of area.

(ii) Theoretical results

- upper bound solution

- finite element analysis of polygonal dies.

The discussion of the results obtained from torsion testing at elevated temperature and the finite element analysis of polygonal dies have been dealt with separately in their respective chapters.

9.2   Discussion of the experimental results

9.2.1   Introduction

The process of drawing polygonal sections from round at elevated temperatures of up to 850°C has been achieved successfully. The technique of drawing mild, medium carbon and boron steel wire into octagonal, hexagonal and square sections from round

at up to 850°C and 50% reduction of area in one pass has been established. The merits and demerits of the range of hot drawing die materials have been investigated.

The effects of drawing temperature, reduction of area, die design and lubrication have also been investigated experimentally. Examples of the experimental results are shown in figs.7.1 - 7.20, showing the variation of drawing stress with temperature for square, hexagonal and round sections, for a number of reductions of area, using four different die materials and five different die geometries, two of these concerning conventional round drawing.

In general, the drawing stress is reduced as the temperature of the wire is increased. However there is an increase in the drawing stress in the temperature range 250-400°C which is attributed to the strain-ageing phenomenon; the range depending on the material properties, the reduction of area and the drawing speed.

Manjoine[71] used mild steel for tension tests conducted at a strain rate of 0.5 /s, and found that the strain-ageing region lies between 150-350 °C. Samanta[62] used a low carbon steel (0.11%), and a strain rate of 0.066 /s, and found that the strain-ageing region lies between 150-300 °C. Recently Loh and Sansome[91], found that for a constant drawing speed of 6 m/min, the strain-ageing region is in the approximate temperature range of 200-400 °C.

9.1.2 Effect of die geometry

Five different die designs were used, these compromise a die designed by Basily and Sansome[53], a modified conventional section-to-section die, a die designed specifically for this work, a conventional round-to-round die 'radius' and finally a conventional round die 'straight'. The total number of dies used in this research work is fourteen.

At the lowest reduction of area possible using the square die, i.e. 36.34%, all dies produced an acceptable square section, the modified design producing a slightly better shape, an improved surface finish and good dimensional stability.

Different die geometries gave different drawing stresses for the same reduction of area. Dies designed by Basily[53] are for a specific incoming wire size so that if a different size is used the deforming passage is changed and therefore a distorted shape is produced, with an increase in the redundant work . These dies, in general, gave higher drawing stresses compared with the other dies. Some tests showed lower drawing stresses using this die, due to the fact that this die was designed without land in order that a comparison will be made with results obtained by Basily[53] figs.7.1-7.6.

Fig.7.2. shows that, when producing a square section with a 44% reduction of area, dies used by Basily[53] generally failed to produce any section above 350°C, only two tests produced an acceptable shape at 450°C, but the majority failed to perform at above 350°C, due to geometry of the die, the instability that takes place as the section leaves the deformation zone and insufficient cooling. Fig.7.6, shows that, when producing a square section with a 41% reduction of area using medium carbon steel, sharp corners are produced, but over 500°C tensile failure is more frequent. Dies used by Basily[53] did produced sharp corners, but with frequent failure during drawing, and at higher temperatures it failed to produce any section.

At 50% reduction of area the modified die failed to produce any shapes when drawn cold, but at 80°C and 150°C when drawing mild steel and medium carbon steel respectively it produced an extremely good shape. Use of the die designed by Basily[53] failed to produce a square section below 270°C, and at over 450°C it was difficult to draw when using medium carbon steel; when using mild steel it failed to produce a square section with 50% reduction of area in one pass even when the temperature was

256

increased, this is probably due to the combination of the higher temperature needed to draw a 50% reduction of area and the instability that takes place at the higher temperatures coupled with the insufficient cooling that may occur at these temperatures e.g. at 44% reduction of area it failed to draw above the temperature of 350°C. Comparing this to the minimum temperature of 270°C needed to draw a successful square with a 50% reduction of area using medium carbon steel i.e this temperature probably would have been enough to draw at, but because of tensile failure and instability the drawing process was never achieved at this reduction of area. It was achieved using medium carbon steel because it is a stronger material with a higher tensile stresses. This is illustrated in fig.7.6, where a square section was drawn with 41% reduction of area and up to 500°C, as compares to the general temperature of 350°C maximum for mild steel at 44% reduction of area.

Fig.7.17, illustrates the effect of die geometry on the drawing stress at various temperatures and reductions of area when using the conventional round-to-round radius and straight taper dies, where the lowest results were obtained by using the radius design.

9.1.3   Effect of die material

Different die materials gave different drawing stresses for the same reduction of area with the lowest values resulting from the use of chromium carbide. Wear rings were clearly visible at the die entry and in the deforming zone of the Syalon dies. This is probably due to the frictional work at the die wire interface being of a considerable magnitude. Crack lines were formed in the chromium carbide dies, probably due to the thermal stresses set up in the die.

Figs.7.7 - 7.12, show that tungsten carbide dies produced slightly lower drawing stresses than Stellite at the lower reduction of area, but as the reduction of area

increased to 38 and 45% it produced slightly higher drawing stresses. At 45% reduction of area, for a hexagon section at room temperature using tungsten carbide dies, the proportion of tensile failure during drawing was high; there were no failures when using Stellite dies at the same temperature. In general, Stellite gave good surface finish and lower drawing stress especially at high reductions of area, which may mean that it performs well under severe conditions; these advantages are gained at the expense of the cost of Stellite dies (almost twice that of tungsten carbide).

Comparing figs.7.9 - 7.11, when producing a hexagonal section with 24% reduction of area at normal temperature, the drawing stress was 300 N/mm^2 using the chromium carbide designed die comparing with 400 and 420 N/mm^2 when using the modified die design with tungsten carbide and Stellite as a die material respectively. Fig.7.18 shows that Syalon dies gave the highest drawing stresses up to 400°C, but as the test temperature increased the results obtained became compatible with those obtained using tungsten carbide dies.

When producing rounds, Loh and Sansome[91] needed to heat medium carbide steel wire to 200°C before producing a 45% reduction of area. In the present work, with the same lubricant and workpiece material, a 45% reduction of area was achieved in the more severe and highly stressed process of producing hexagon section at room temperature. Figs.7.19 - 7.20, show that Syalon dies gave 30-40% higher drawing stresses compared with chromium carbide dies and 20% comparing with tungsten dies. When a material is drawn at 200°C the drawing stress is reduced by 15-25%. Loh[91] compensated for the increase incurred by the use of Syalon dies by using 200°C as the testing temperature i.e. to reduce the drawing stress by at least 15-25%. The reason for being able to achieve a 45% hexagon at room temperature is attributed to the die material.

9.1.4 Effect of the lubricant

Figs.7.13 - 7.16, shows that the use of an appropriately formulated lubricant reduces the drawing stress further. Using MolyDag 709 lubricant with toluene produced relatively low drawing stresses compared with MolyDag 15, but as the test temperature increases, especially above 300°C, it produced unpleasant toxic fumes which are unacceptable. It is considered that MolyDag 709 with toluene is not a suitable lubricant for elevated temperature drawing despite the advantages of the very rapid drying agent so that the lubricant dries before the induction heater is reached, and there is no need for an airwipe system to remove any excess lubricant, or any further help to dry the lubricant before leaving an even coat of graphite-based lubricant.

Generally MolyDag 15 and MolyDag 709 gave higher drawing stresses compared with Dag 2543 when used for hexagonal, octagonal and square sections at high reductions of area; resulting in a very good surface finish compared with the other lubricants.

9.1.5 Mechanical testing

From the tests carried out, it is clear that the process of drawing at elevated temperatures is capable of producing still further increases in tensile and yield strength, with a decrease in ductility values. Fig.7.21, shows a sample of the tests carried out under the same drawing conditions. Both tensile and yield strength rise to a maximum in the range of 250 - 400°C, at which elongation and reduction of area values reach a minimum. Strength for given drawing temperature generally increases with increased reduction of area. In general, the reduction of area produced at room temperature would have to be doubled in order to match the strength developed in drawing at elevated temperature.

Basily and Sansome[53] could not achieve more than 43% reduction of area when drawing mild steel at normal temperature, with frequent tensile failures and die

breakage, even at the lower reduction of area 36.34%. No die breakage was experienced in the present work, this is probably due to;

-      dies were made professionally and no subsequent alteration was made to them unlike the practice of Basily and Sansome[53] where failure took place, possibly as a result of less than satisfactory heat treatment of the die after modifications.

-      some of the dies designed for the work carried out by[53,120,121] having too small die semi-cone angles of 4 and 5 ° which too affected the performance and led to die breakage.

-      the die material used was tool steel which is not as efficient as tungsten carbide or Stellite, it was used because it is readily available, is less expensive and cheaper to machine to different die shapes than tungsten carbide. There are a number of problems associated with the use of the conventional tool steels, the most significant of which are distortion on heat treatment and the non-uniformity of properties throughout the material.

Wire breakage was not very frequent and it only took place at the higher reductions of area of 44% or above. Basily reported many tensile failures and die breakages at 36.34% reduction of area, wire failure is due;

-      the method of swaging adopted contributed to the breakage of samples during testing, using a drawbench did not help, because of the limited stroke length available and the number of swaged stages needed for the higher reductions.

-      the die design, where the die semi-cone angle used was too small coupled with inadequate heat treatment after die modifications.

-      die material and lubrication used, where the effect of friction is highlighted.

9.1.6 Microstructure examinations

A microsection was taken from every test piece after each the drawing operation, these samples where ground polished and etched with a 2% Nital solution, and examined at both low and high magnification (150 x), using an optical metallurgical microscope. A number of examples have been chosen to illustrate the effect of drawing at elevated temperatures on the microstructure and the mechanical properties of the drawn material, when drawing a square section directly from round and are described in the next section. (When viewing the photographs the direction of drawing is from left to right)

Mild steel

Fig.9.1, shows a typical low carbon steel structure in the unstressed annealed undrawn condition. The structure consisting of small lamellar pearlite colonies (dark) a mixture of ferrite and iron carbide $Fe_3 C$ in a ferrite matrix (white) grains, of soft, almost pure iron. Fig.9.2, shows the same structure as above but the grain boundaries are clearly visible. Ferrite grains are elongated in the working direction. Distorted structure, i.e. work hardened, grains being elongated and deformed. Proof stress (P.S.) 489 N/mm^2, Maximum stress (M.S.) 652 N/mm^2 and hardness 260 Hv, the material at this stage starts to loss it is ductility.

Fig.9.3, Pearlite colonies taking on a more granular (dotted) appearance. Ferrite grain boundaries are no longer visible due to higher general stress levels affecting the etch. Etching attacks different positions of the structure differently. It attacks pearlite colonies and highly stressed areas and grain boundaries. This is the start of the temperature range where the material will be in it is most hardened condition, due to the strain-ageing phenomenon where the drawing stress increases as the drawing temperature is increased. P.S. 546, M.S. 696 N/mm^2 and hardness 240 Hv.
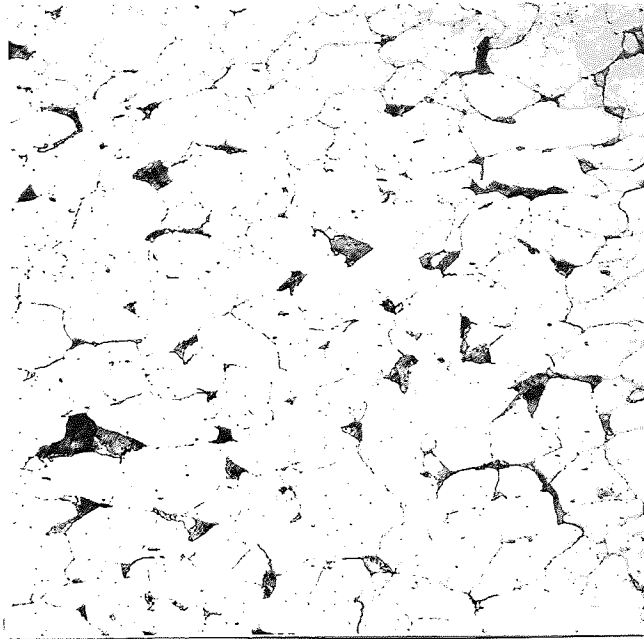
Fig.9.1. Mild steel structure, undrawn.
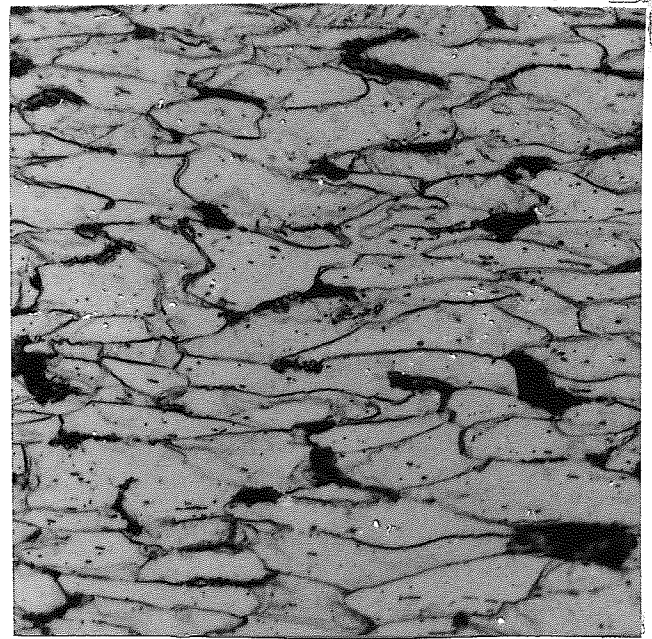
Fig.9.2. Mild steel structure, drawn at 20°C with 44% reduction of area.
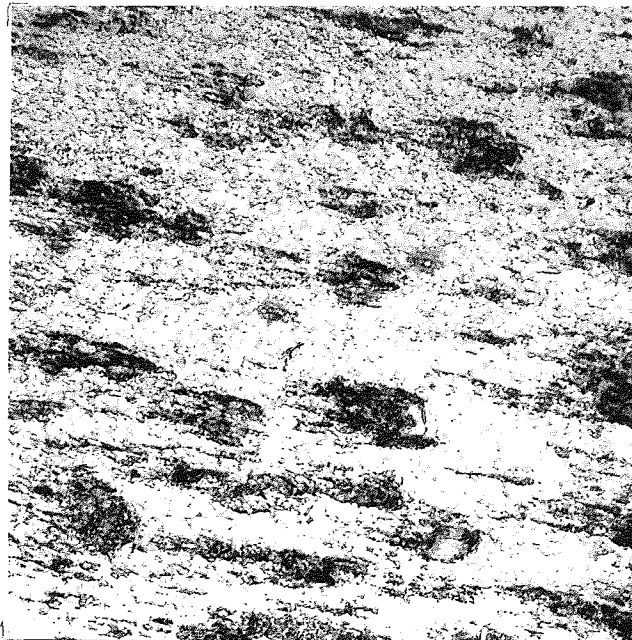
Fig.9.3. Mild steel structure, drawn at 371°C with 44% reduction of area.
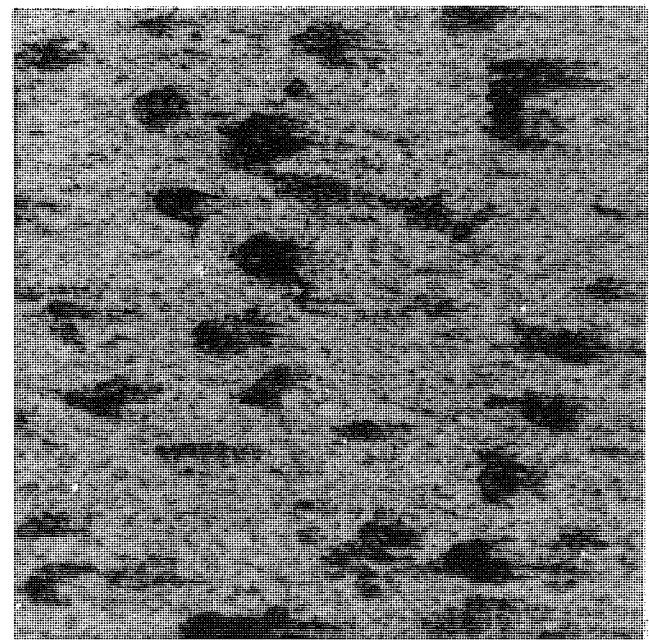
Fig.9.4. Mild steel structure, drawn at 420°C with 44% reduction of area.

Fig.9.4, very similar to the above structure, pearlite colonies slightly smaller, stress relief will start to take place without visible change, because of the extra energy present in the structure which will activate the process of recovery and also because of recrystallisation. At this stage the material has lost ductility and the strength is increased considerably, a situation were the peak of "strain-ageing" phenomenon is experienced. P.S. 623, M.S. 756 N/mm^2 and hardness 239 Hv.

Fig.9.5, Freshly formed pearlite colonies (dark) would appear lamellar at a sufficiently high magnification. Ferrite will be a mixture of old and new grains (α), both ferrite and pearlite start to change on heating above 700°C some ferrite converts to austenite (γ), and pearlite transforms completely in the austenite phase field where a mixture of ferrite and austenite with no pearlite exists at 760°C. When cooling down, fresh ferrite precipitates from the austenite and the carbon content of the remaining austenite increases. All remaining austenite converts to new fresh unstressed lamellar pearlite when the eutectoid temperature is reached i.e. produces a more ductile and unstressed material. All changes above this eutectoid temperature are due to diffusion run processes, below 723°C the new grains remain and a refined structure is finally obtained. At this temperature a ductile material will be obtained were strength and hardness decreases slightly from where it was at the 'strain ageing' region. P.S. 460, M.S. 612 N/mm^2 and hardness 216 Hv.

Fig.9.6, as fig.9.3, but greater reduction of area, recrystallisation and grain growth has occurred quicker than fig.9.3, due to the increase in the drawing energies being available, ferrite grain boundaries visible. P.S. 536, M.S. 671 N/mm^2 and hardness 210 Hv, material very tough, ductility highly reduced.

Fig.9.7, as fig.9.4, but fully annealed to give new equi-axed ferrite grains with no directionality. Pearlite laminations are just visible at this magnification. When
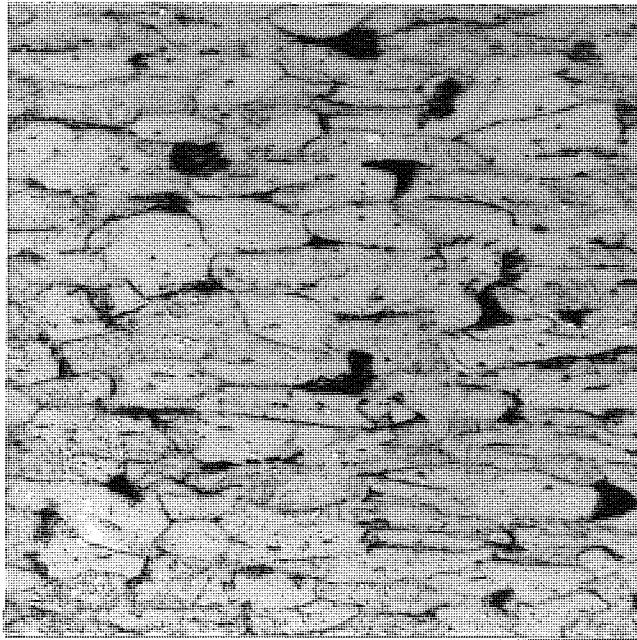
Fig.9.5. Mild steel structure, drawn at 760°C with 44% reduction of area.
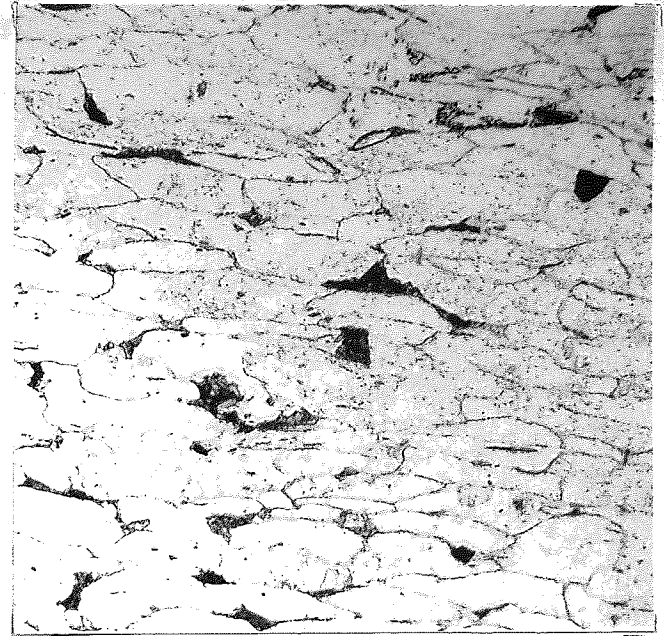
Fig.9.6.Mild steel structure, drawn at 330°C with 50% reduction of area.
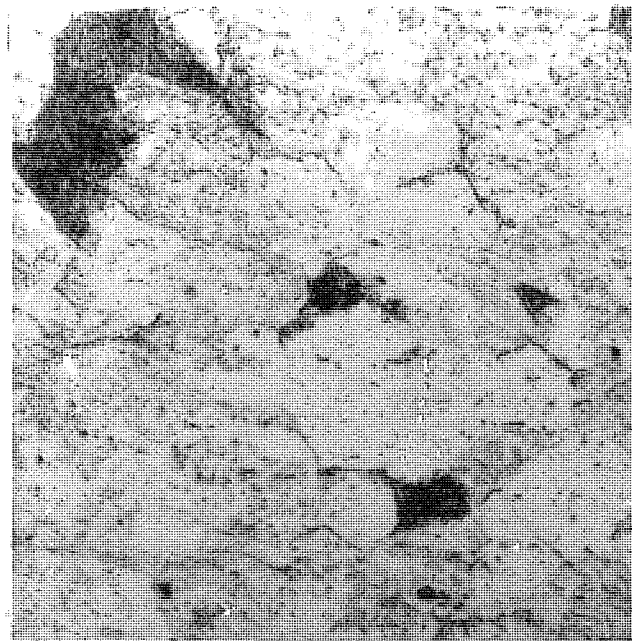
Fig.9.7. Mild steel structure, drawn at 420°C with 44% reduction of area, then annealed.

annealing, large equi-axed grains are formed, in a shorter time if the material was highly stressed i.e. fig.9.4, the new grains will form more quickly than fig.9.5, because there are less stressed grains due to the fact that a stress relieving process takes place during drawing at this temperature. When annealing the material becomes very ductile, losses it is strength. P.S. 188, M.S. 316 N/mm^2 and a very ductile material is obtained.

Boron steel

Figs.9.8-9.11, react similarly to mild steel, but shows more pearlite or iron carbide for any given carbon content, and possible recrystallisation of ferrite or spheroidisation of pearlite at slightly lower temperatures. Full anneal would also occur at a lower temperature i.e eutectoid point would move down and left on the equilibrium diagram.

Fig.9.9   P.S. 699   M.S. 839 N/mm^2 and hardness 244 Hv loss of ductility.

Fig.9.10   P.S. 824   M.S. 973 N/mm^2 and hardness 244 Hv, loss of ductility.

Fig.9.11   P.S. 719   M.S. 820 N/mm^2 and hardness 244 Hv, very ductile.

Medium carbon steel

Fig.9.12, structure consists of ferrite and large amount of pearlite (lamellar). Fig.9.13, elongated ferrite a few grain boundaries and fine carbide particles. P.S. 593 and M.S.721 N/mm^2, because of the localized heating, high reduction and high carbon content, the effect at 100°C appeared similar to the effect at much higher temperature when using mild steel. fig.9.14, the same but carbides are much more uniformly distributed, no grain boundaries visible P.S. 612 and M.S. 711. Fig.9.15, same as fig.9.14, but annealed, fresh ferrite (non-directional equi-axed) and lamellar pearlite, very low Proof stress and Maximum stress comparing with the unannealed test.
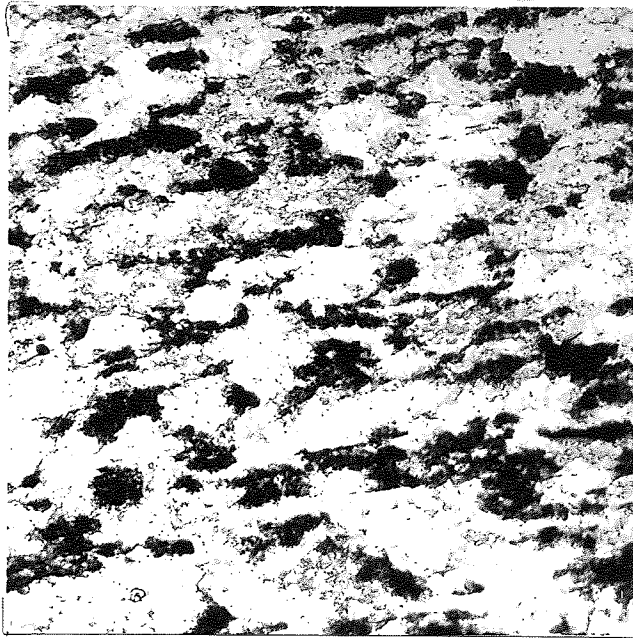
Fig.9.8. Boron steel structure, undrawn.
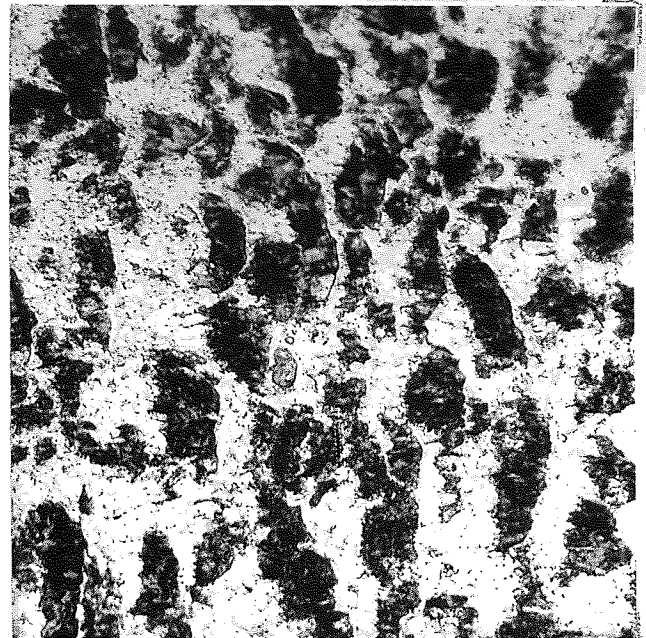
Fig.9.9. Boron steel structure, drawn at 20°C with 44% reduction of area.
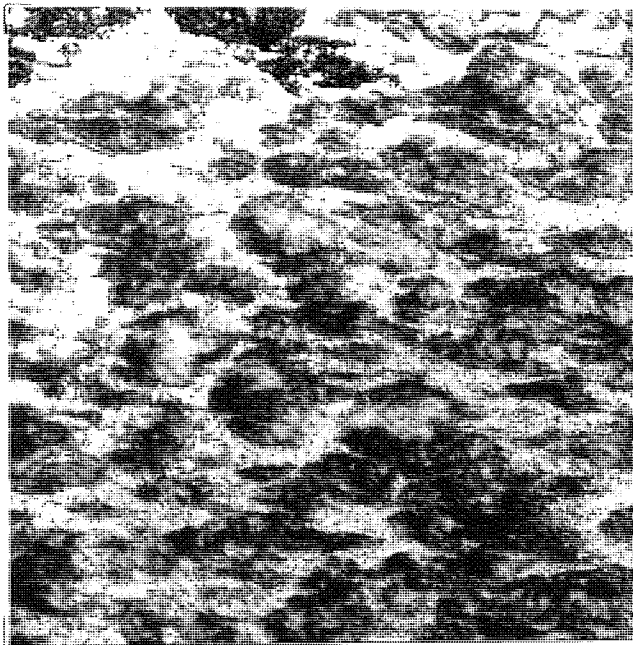
Fig.9.10. Boron steel structure, drawn at 358°C with 44% reduction of area.
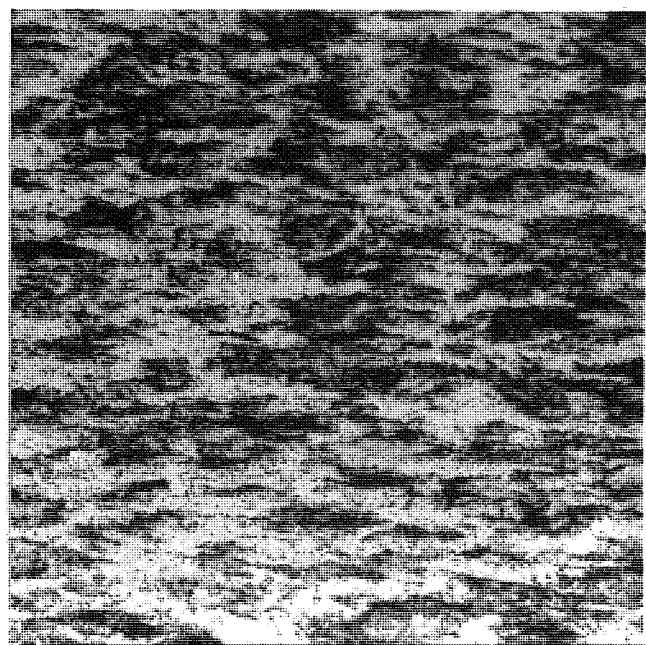
Fig.9.11. Boron steel structure, drawn at 630°C with 44% reduction of area.

266
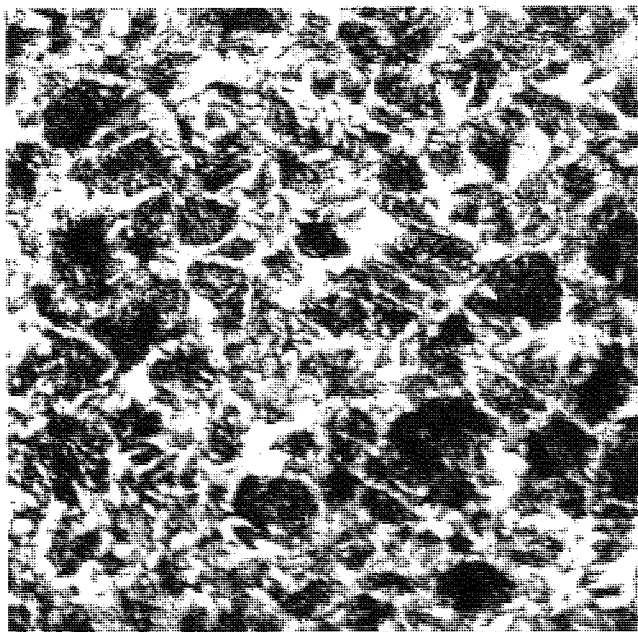
Fig.9.12. Medium carbon steel structure, undrawn.

Fig.9.13. Medium carbon steel structure, drawn at 100°C with 41% reduction of area
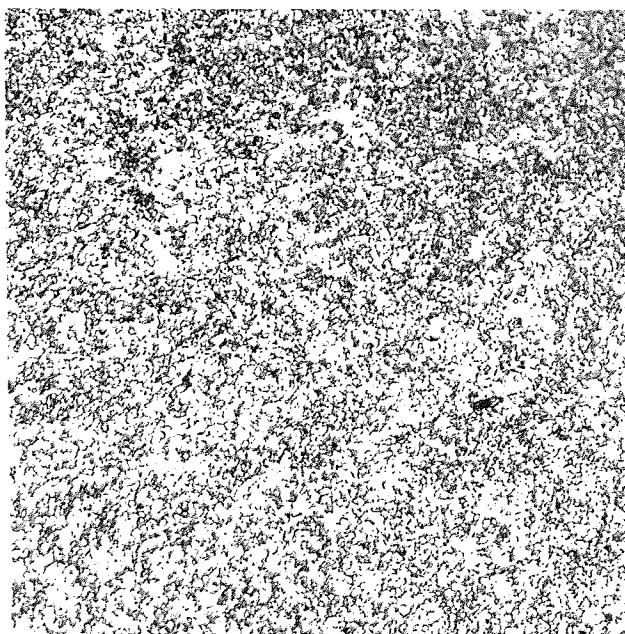
Fig.9.14. Medium carbon steel structure, drawn at 300°C with 41% reduction of area.
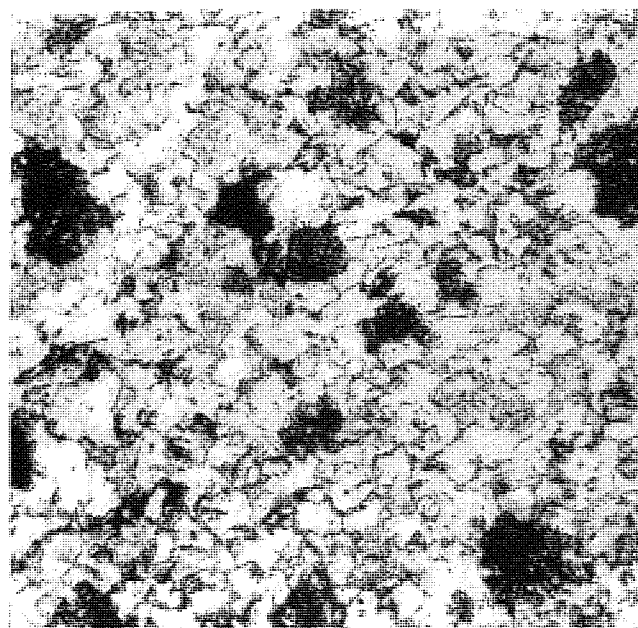
Fig.9.15. Medium carbon steel structure, drawn at 300°C with 41% reduction of area, then annealed.

9.2 Discussion of the theoretical results

The experimental part of the project provided data for establishing the accuracy and reliability of the adopted theoretical method of analysis. In general, the quality of the theoretical results were found to be quite satisfactory and are considered adequate for the purpose of comparison with experimental results.

Due to the fact that, an analytical solution for the polygonal drawing from round at elevated temperature is impracticable, due to the complexity of the die deforming zone, a numerical solution was developed with the aid of the written computer program in "Matlab" computer language.

An upper bound solution was derived in chapter three. It was obtained from a velocity field that minimises the energy required to effect the deformation. The velocity pattern was developed by conformal mapping of triangular elements from the entry plane to the corresponding positions at the exit plane, the solution, therefore accounts for the mode of deformation. However, with slight modification, the solution can be employed for the direct drawing of irregular sections.

The accuracy of the theoretical analysis could be improved by increasing the number of divisions of the inlet and outlet planes. This will be governed by the amount of computer time available for the analysis.

9.2.1 Limitation of achievable reduction of area

In the process of the drawing of polygonal sections from round directly there is a maximum as well as a minimum possible reduction of area per pass. A minimum because the material cannot expand laterally (to fill up corners) and therefore the diagonal of the drawn section is smaller than, or at it is greatest, equal to the diameter of the input stock; a graph showing the minimum permissible reductions of area for a

range of polygonal sections is presented in fig.7.72. As an example, in the case of polygonal drawing of a square from round stock, the minimum possible reduction of area is 36.34% where ;

$$\text{Area at entry} \quad A_1 = \frac{\pi}{4}\, d^2$$

$$\text{Area at exit} \quad A_2 = \frac{d}{\sqrt{2}} \cdot \frac{d}{\sqrt{2}} = \frac{d^2}{2}$$

9.2.2 The effect of temperature, friction and reduction of area on the theoretical drawing stress

The theoretical results for producing square, hexagon and octagon sections from round using mild steel, medium carbon steel and boron steel as a workpiece material are shown in figs.7.25 to 7.68. As expected, the upper bound solution generally predicted a higher value of drawing stress compared with that of the experimental results, which is superimposed onto the theoretical results to facilitate the comparison.

The results from the upper bound solution for a given drawing condition were repeated for different values of the coefficient of friction from 0.0 to 0.3 in order to ;

- Examine the effect of an increase in the coefficient of friction on the drawing stress for a given die semi-angle and a given drawing condition.
- Allow an interpolation of the drawing stress for different coefficients of friction brought about by using different die geometries and different lubricants, while maintaining all the other drawing conditions.

As expected, the upper bound solution predicts a higher value of the drawing stress for an increase in the value of the coefficient of friction for a given die semi-angle. This is simply due to an increase in the frictional work.

All tests are carried out using, drawing speed of 6 m/min and a 12° die semi-angle, unless it is otherwise stated.

It is clear that three regions of workpiece behaviour at various temperatures exist, and these are;

- Steady or gradual softening 100-250 °C.

- Strain-ageing at about 250-400 °C.

- Rapid softening above 450 °C.

This is clearly illustrated in fig.7.23 which shows the percentage reduction in flow stress at elevated temperatures compared with that at room temperature (results obtained by torsion testing), and fig. 7.24 which shows the percentage reduction in the drawing stress, compared with that at room temperature (results obtained from polygonal drawing). At 500 °C, the reduction of flow stress and drawing stress for both cases lies between 20 and 35%; as the temperature increases there is a marked difference between both sets of results. For example at 800 °C, the reduction of flow stress lies between 75 and 90% as compared with that at room temperature, (results obtained using torsion testing), compared with 45 to 63% reduction in drawing stress, (results obtained by polygonal drawing).

In these cases the three regions mentioned earlier do exist; however, at the rapid softening stage, it is noticeable that the values are lower when using torsion testing compared with the results obtained by polygonal drawing. This is probably because, as the temperature increases, the frictional forces increase and, therefore, the drawing stress increases.

Observation of figs.7.25 to 7.42 indicate that the theoretical and experimental data are in reasonable agreement. It is noted, however, that the majority of experimental results

All tests are carried out using, drawing speed of 6 m/min and a 12° die semi-angle, unless it is otherwise stated.

It is clear that three regions of workpiece behaviour at various temperatures exist, and these are;

- Steady or gradual softening 100-250 °C.
- Strain-ageing at about 250-400 °C.
- Rapid softening above 450 °C.

This is clearly illustrated in fig.7.23 which shows the percentage reduction in flow stress at elevated temperatures compared with that at room temperature (results obtained by torsion testing), and fig. 7.24 which shows the percentage reduction in the drawing stress, compared with that at room temperature (results obtained from polygonal drawing). At 500 °C, the reduction of flow stress and drawing stress for both cases lies between 20 and 35%; as the temperature increases there is a marked difference between both sets of results. For example at 800 °C, the reduction of flow stress lies between 75 and 90% as compared with that at room temperature, (results obtained using torsion testing), compared with 45 to 63% reduction in drawing stress, (results obtained by polygonal drawing).

In these cases the three regions mentioned earlier do exist; however, at the rapid softening stage, it is noticeable that the values are lower when using torsion testing compared with the results obtained by polygonal drawing. This is probably because, as the temperature increases, the frictional forces increase and, therefore, the drawing stress increases.

Observation of figs.7.25 to 7.42 indicate that the theoretical and experimental data are in reasonable agreement. It in noted, however, that the majority of experimental results

fall below the theoretical results at temperatures below 400 °C; this may be due to the fact that the upper bound solution over-estimates the deformation loads, and that, the strain-ageing regions do not coincide. This could be attributed to two reasons, firstly, to heat conduction being neglected in the theoretical analysis, thus the theoretical strain-ageing region appears over a lower temperature range than occurs in practice and secondly, the actual temperature increase due to deformation and friction is lower than that predicted by the theoretical analysis, leading to the same effect.

Loh and Sansome[91] made the same observations however they attributed the discrepancies to one or several of the following factors.

- using stress-strain data for 0.15% C in the theoretical analysis, whereas the wire material used in their experiments was a 0.04% C.
- the assumed relationships between B, n and Tm in the power law, dealt with previously .
- the use of velocity-modified temperature concept introduced errors especially at higher values of Tm.
- heat conduction and cooling of the wire were neglected in the theoretical analysis.

Some of the reservations expressed by Loh and Sansome[91] do not apply in this research work, since true stress-strain data for the materials tested were a data bank of the actual results, fed to the theoretical analysis, to estimate the flow stress distribution in the deforming zone, and the modified temperature concept was only used over the temperature of 500°C, which is well above the strain-ageing region, it was felt that the only feasible reason attributed to the above discrepancies are heat conduction being neglected in the theoretical analysis and the temperature rise due to deformation and friction in the theoretical analysis being higher than the actual one.

As the temperature increase from 250 - 450°C, the strain-ageing phenomenon is experienced, where the drawing stress increases as the drawing temperature is increased. At this stage the good fit between the experimental and theoretical results was found for m = 0.2 or 0.3.

As the temperature increases from 500 °C upwards, the rapid softening stage is reached, where the experimental drawing stress due to frictional forces increases, as already explained. However, since the value of flow stress used in the theoretical results will only be effected by the increase in temperature, this will lead to a discrepancy, where the experimental results will be higher than the theoretical. Loh and Sansome[91] commented on the discrepancy on their results as " it is thought that at temperatures of 600°C and above the velocity-modified temperature concept does not hold well, predicting lower flow stresses". The author feels that this is not the case and the real reason is concerned with the increase of the drawing stress due to friction, as compared with the rapid decrease of flow stress as the theoretical drawing temperature is increased.

Flow stress results obtained in this research work using torsion testing at elevated temperature and that used by Loh and Sansome[91], which is obtained from published data by other authors using tests conducted on cam plastometer for medium carbon steel, are similar, an example is presented in figs.7.70 and 7.71. Therefore this proves the capability and the potential of using torsion testing at elevated temperature as a source of obtaining stress-strain data.

Figs. 7.63 and 7.64, show the results previously shown in figs.7.25 and 7.26, with a modified value of the flow stress above the temperature of 500°C, to match the values that probably exist in practice, modified results of flow stress obtained from figs.7.23 and 7.24.

Figs.7.43 to 7.62, show the variation of drawing stress with reduction of area for various coefficients of friction. Generally, as the reduction of area increases the drawing stress increases for a given drawing speed, temperature, die semi-angle and coefficient of friction. Up to the temperature of 400°C, using mild steel and medium carbon steel and producing a square section, the experimental results fall below the theoretical results. However at the temperature of 500°C, using mild steel, a reasonable fit between the experimental and theoretical results was found for the value of m between 0.2 and 0.3, as the temperature increases to 600°C, the value of m exceeds 0.3. A better fit is found when using medium carbon steel; at the temperature of 500°C the fit is found for m to be between 0 and 0.1 whereas at 600°C, the value is between 0.1 and 0.3.

Generally, as the temperature increases, the constant of friction also increases. The increase is more significant for higher reductions of area (50%). Theoretical results obtained by using mild steel to produce a square section at the temperature of 300°C, show that the value of the drawing stress at 50% reduction of area is slightly less than that at 45%. This discrepancy could be explained as follows; at this temperature the material is experiencing a strain-ageing phenomenon at the lower reduction of area, however, at the higher reduction of area of 50%, the temperature increase due to deformation and friction is higher than, say, at 40% reduction of area, therefore the actual temperature of the material being drawn is higher than that being drawn at 40% reduction of area, the middle region of strain-ageing has been passed and the rapid softening stage has been reached. The value of flow stress at these temperatures is much lower than at the previous stage, therefore a lower value of drawing stress is predicted at these high reductions of area due to the increase in temperature, fig.7.46. At the testing temperature of 400°C, fig.7.47, as the reduction of area increases, the drawing stress increases. There is no discrepancy in this range of temperature because

the strain-ageing region has been passed and all values of the flow stress are obtained in one region, which is the rapid softening one.

When using medium carbon steel, which is a stronger material, and the temperature increase due to deformation and friction is higher than that for mild steel for the same drawing conditions, section (9.2.5.1), the discrepancy experienced with respect to mild steel will take place at the lower temperature of 200°C, Fig.7.52.

Results obtained for medium carbon steel when producing hexagonal and octagonal sections figs.7.57 to 7.62, show the same trend as when producing square sections, where up to the temperature of 400°C, the experimental results fall below the theoretical results, especially at the lower reduction of area up to 40%, however as the drawing temperature or the reduction of area are increased the correlation deteriorates, due to the falling value of the flow stress at high temperature and reduction of area due to higher frictional forces i.e, higher temperatures and lower flow stress.

9.2.3 The effect of die semi-angle on the theoretical drawing stress

It has already been emphasised that the upper bound solution takes into account the redundant work and the internal shearing within the material, the general trend of the upper bound curves show an increase in the drawing stress with decreasing die semi-angle, because the frictional force increases due to the large contact area between die and workpiece. Likewise, the drawing stress also increases with increasing die semi-angle, as the redundant work increases. Hence, in the upper bound curves, there in an optimum die semi-angle at which the total drawing stress is a minimum for a given coefficient of friction and reduction of area. It is considered however, that this is an over-generalised statement when dealing with polygonal drawing from round, since die geometry has a predominant effect on the value of drawing stress obtained. This is clearly illustrated on the section dealing with the experimental results (7.4) where

274

satisfactory results were obtained using a 12° as compared to 7° die semi-angle. Basily and Sansome[53] reported and used the optimum die angle of 7° in their research work. It is considered that this part of the analysis is irrelevant unless the theoretical analysis takes into consideration the effect of the variation of die geometry on the drawing stress.

In the present work, an optimisation of the shear surfaces was carried out as discussed in Chapter three, by including parameters at the inlet and outlet shear surfaces to optimise these surfaces and therefore, to minimise the total shear power. Fig.7.65 shows portions of the drawing stress to overcome resistance to deformation; the value of the shear resistance used is the optimised value. In this graph, it can be seen clearly that at certain die semi-angle values, the value of shear resistance increases and then decreases, illustrating that an area of minimum shear resistance exists. Figs.7.66 - 7.68, show the variation of drawing stress against die semi-angle for various values of coefficient of friction at different temperatures.

9.2.4 The effect of strain-rate on the drawing stress

Due to the limited strain-rate range obtained when using the torsion testing machine at elevated temperature, tests at higher strain-rates have not being conducted. However results obtained by Loh and Sansome[91], fig.7.69, Manjoine[71], Samanta[62], and Oyane[93] show that, as the strain-rate increases, the strain-ageing region shifts to higher temperatures. At the lowest speeds the strain-ageing regions were at about 200 to 400°C.

9.2.5 Strain, strain-rate, temperature and flow stress distribution in the deforming zone

The three-dimensional modelling of temperature, strain, strain-rate and flow stress in the deformation zone is shown in fig.7.73 and tables 7.1 - 7.5. The following assumptions are made.

- the test temperature is uniform across a section, i.e. the temperature at the surface of the wire is the same as at the centre.

- the temperature increase due to deformation varies across a section unlike Siebel and Kobitzsch[94] who assumed that the temperature increase due to deformation is uniform across a section.

Studying figs 2.2, 2.5 and 2.6 of Chapter two, it is clear that the amount of distortion i.e. " the angle of twist and deviation" increases as the material moves from the outer surface to the centre of the chosen plane, this, of course, means that the strain and strain-rate values increase accordingly, which in turn causes the value of temperature increase due to deformation to increase as the material moves towards the centre of the plane. Since it was assumed that the test temperature is uniform across a section, therefore the temperature increases inside a plane will be higher than that of the surface. This could be offset by not assuming a uniform test temperature across the incoming wire.

9.2.5.1 The effect of material properties

Tables 7.2 and 7.5 show values of strain, strain-rate, temperature and flow stress distribution in the deforming zone for mild and medium carbon steel. It is clear that the temperature gradient in the deformation zone for medium carbon steel is higher than that of mild steel, due to the higher flow stress values. Higher flow stress will lead to the temperature rise due to deformation and frictional work increasing, resulting in higher

temperature values in the deforming zone. Generally, the mechanical properties of the test material affect the magnitude of the heat generated due to deformation and frictional work. The strain and strain-rate distributions are constant for the same draw conditions.

9.2.5.2 The effect of die semi-angle

The temperature distribution in the deforming zone is greater for the smaller die semi-angle, due to the contact area between die-wire interface increasing causing an increase in temperature due to frictional work.

9.2.5.3 The effect of drawing speed

As the drawing speed increases, the effective strain-rate increases causing the temperature to rise due to frictional and deformation work. The effective strain is not affected by the change in speed.

9.2..5.4 The effect of reduction of area

As the reduction of area increases, the temperature increase due to deformation and frictional work due to the increased contact area increases causing the temperature distribution in the deforming zone to increase, Tables 7.2 and 7.4.

CHAPTER TEN

CONCLUSIONS AND SUGGESTIONS FOR FURTHER WORK

Chapter Ten

10.0 Conclusions and Suggestions for Further Work

10.1 Conclusions

An extensive investigation of the mechanics of the drawing of polygonal sections from round at elevated temperature has be accomplished successfully both theoretically and experimentally to enable the following conclusions to be drawn;

1. The technology of drawing polygonal section from round at elevated temperatures has been successfully developed in the laboratory and, the process has proved to be a technically viable and a successful method of production.

2. The technique of drawing mild, medium carbon and boron steel wire into octagonal, hexagonal and square sections from round at up to 850°C and 50% reduction of area in one pass has been established.

3. The drawing stress can be considerably reduced when tests are carried out at elevated temperature, e.g. by up to 40-50% at 750°C.

4. Medium carbon and boron steel which could not be cold drawn for a 50% reduction of area, were successfully drawn at temperatures starting from 80°C, depending on the die geometry used.

5. The maximum reduction of area in a single pass can be greatly increased.

6. Chromium carbide dies gave the lowest drawing stresses for the same reduction of area.

7. Syalon dies gave the highest drawing stresses up to 400°C, however, as the temperature increased, the results obtained became compatible with those obtained using tungsten carbide dies.

8. The drawing stress and surface finish were noticeably affected by die material, die design and lubricant formulation.

9. The experimental drawing stress decreases as the temperature increases up to about 250°C. In the temperature range of 250-400°C the drawing stress increases with temperature, due to the strain-ageing phenomenon. Above the temperature of 450°C, the drawing stress decreases rapidly with temperature. As the drawing speed increases, the strain-rate increases causing a shift of the strain-ageing region towards the higher temperature. Thus the optimum drawing temperature will not be the same for different drawing speeds.

10. Process time is reduced by eliminating inter-stage annealing.

11. Generally, it is now possible, for a given material, to predict the optimum drawing temperature, reduction of area per pass, die profile and lubricant.

12. Finite element analysis helps in deciding on the optimum die design and die material for a particular process, as well as the effectiveness of die cooling.

13. There is a minimum as well as a maximum reduction of area for the polygonal drawing from round in a single pass, governed by the shape of the section produced.

The theoretical results showed that ;

14. Generally, there is good agreement between the theoretical and experimental values.

15. The upper bound solution indeed predicts a higher value of the drawing stress for an increase in the value of the coefficient of friction.

16. An increase in the coefficient of friction does not affect the strain-ageing region.

17. There was satisfactory agreement between the theoretical and experimental results for drawing temperature below 500°C. At higher temperatures, the coefficient of friction increases causing the experimental drawing stress to increase, whereas the theoretical value of drawing stress decreases due to the decrease of the flow stress at high temperatures. This introduces discrepancy at high temperatures.

18. As the drawing temperature and reduction of area increase a good fit was found between the experimental and theoretical results for higher values of coefficient of friction.

19. The drawing speed affects strain-ageing; as the speed increases the strain-ageing shifts towards the higher temperature. Thus the effects of temperature and strain-rate on the flow stress must be considered together.

20. An increase in the reduction of area or the strength of the material causes the prediction of the temperature in the deforming zone and, therefore, the temperature at the exit to increase.

21. As the coefficient of friction increases, the temperature at the die-wire interface increases, due to frictional work.

In general, the process of elevated temperature section drawing from round was successfully analysed both theoretically and experimentally and there is a good agreement between results obtained using both techniques.

10.2 Suggestion for further work

In the light of the experience and conclusions formulated in this research programme, further work is suggested in the following directions :

-    It will be advantageous to carry out a three-dimensional process modelling using finite element techniques This modelling will include, the die region as well as the workpiece material. A useful comparison could then be made with the experimental and theoretical results obtained in this current research work.

-    It would be valuable to extend the drawing technique to austenitic and stronger ferrous and non-ferrous materials. Non-ferrous materials such as aluminium bronze, nickel alloys, and some brasses which are difficult to cold draw and would require frequent inter-stage annealing. Therefore, it will be advantageous to draw these materials at elevated temperature.

-    An investigation of the polygonal drawing of section tubes from round at elevated temperature should be carried out, since it has great interest from the academic point of view and for industrial application. This process is of great potential since it will facilitate the production of seamless section tubes from a readily available wide range seamless round stock. This will have a considerable application in many engineering fields, such as heat exchangers and nuclear

281

power plants. There are some problems which might arise and could be studied from such work, e.g. the transformation of the inner tube into the required polygonal shape without using a plug and the study of problems arising from the use of a plug.

- Improving the theoretical analysis, by using a different form of conformal mapping, where the transformation will not be for the whole inlet plane into the corresponding outlet plane, but only parts of the outside surface, depending on the reduction of area, where the centre of the deforming material remains undeformed.

- The application of ultrasonic vibration to this process, in which the drawing forces are generally higher than those in the corresponding axisymmetric drawing, because of the higher redundant and frictional effects involved. It is therefore suggested that the application of ultrasonic vibration to the process could reduce the process loads, improve the reduction of area Winsper[125], improving drawing conditions and increases die life.

- The development of a closed loop system consisting of the drawing equipment and the induction heating equipment, where the operation will be a computer controlled data acquisition and control system, to control the power required to heat a certain wire material of a known diameter at a measured drawing speed, to a certain temperature i.e. the computerization of the whole process and the introduction of a computer aided manufacturing process.

- There is a continual demand for polygonal sections possessing a wider range of mechanical properties. Some of these properties, which are unobtainable by cold drawing, can be achieved by drawing at specific temperatures and reductions of

area which give the desired metallurgical properties. A study of the combined effect of controlling and varying the drawing temperature and the rate of cooling is therefore suggested, to yield tensile properties which are not possible with cold drawing alone. It is also suggested that the effect on the microstructure of drawing the first pass as a large one at elevated temperature followed by a light finishing pass at normal temperatures be studied since, this technique will certainly improve the dimensional accuracy.

- A study of the effect of the application of various lubricants at high temperature on the workpiece material microstructure is proposed.

- Further work is required in terms of loadcell design in conjunction with operation in a high temperature environment. The effect of temperature on the loadcell is highlighted when testing at high temperatures and during tests of longer duration. This has been dealt with in section (5.4.1.2). The use of an improved version of the self-temperature-compensated gauges in the loadcell design is therefore suggested.

REFERENCES

REFERENCES

1)   Sachs, G. - Plasticity Problems in Metals, Trans. Faraday Soc., (1928) 24, 84-92.

2)   Hoffman, O. & Sachs, G. - Introduction to the Theory of Plasticity for Engineers, McGraw-Hill Press, New York, (1953).

3)   Davis, E.A. & Dokos, S.J. - The Theory of Wire Drawing. J. Appl. Mech. (1944) 11, A-193 to A-198.

4)   Atkins, A.G. & Caddell, R.M. - The Incorporation of Work Hardening and Redundant work in Rod Drawing Analysis. Int. J. Mech. Sci. (1968) 10, 15-28.

5)   Johnson, R.W. & Rowe,G.W. - Redundant Work in Drawing Cylindrical Stock. J. Inst. Met. (1968) 96, 97-105.

6)   Siebel, E. - Stahal und Eisen (Iron and Steel), (1947), 66-67, 171-180

7)   Korber, F. & Eichinger - Die Grundlagen der bildsamen Verformung, Mitt KW Inst. Eisenforschung, (1940), 22, 57.

8)   MacLellan, G.D.S. - A Critical Survey of Wire Drawing Theory. J. Iron and Steel Inst. (1948), 158, 347-356.

9)   Wistreich, J.G. - The Fundamentals of Wire Drawing. Met. Rev. (1958), 3 (10), 97-142.

10)   Wistreich, J.G. - Investigation of the Mechanics of Wire Drawing. Proc. Inst. Mech. Engrs. (1955), 169, 654-665.

11)   Whitton, P.W. - J. Inst. Metals, (1957-58) 86, 417.

12)   Sachs, G. & van Horn, K. R. - Practical Metallurgy, American Society of Metals, (1955).

13)   Shield, R.T.- J. Mech. Phy. Sol, (1955) 3, 246-258.

14)   Avitzur, B. - Analysis of Wire Drawing and Extrusion Through Conical Dies of Small Cone Angle. J. Eng. Ind. Trans. ASME, Series B, (1963) 85, 89-96.

15)   Avitzur, B. - Analysis of Wire Drawing and Extrusion Through Conical Dies of Large Cone Angle J. Eng. Ind. Trans. ASME, Series B, (1964) 86, 305-316.

16)   Ford, H. & Alexander, J.M. - Advanced Mechanics of Materials, Longman, (1972).

17)   Johnson, w. - Plane-Strain Slip-Line Fields: Theory and Bibliography London: Edward Arnold. (1970).

18)   Hill, R. - Mathematical Theory of Plasticity, Clarenden Press, (1950).

19)   Halling, J. - Engineer, (1959) 207, 250-256.

20)   Prager,W. & Hodge, P.G - Theory of Perfectly Plastic Solids. Wiley, (1951). Chapter 8.

21)   Drucker, D.C. & Providence, R.L. - Coulomb Friction, Plasticity and Limit Loads. J. Appl. Mech. (1954) 21, 71-74.

22)   Hill, R.- On the State of Stress in a Plastic-Rigid Body at the Yield Point. Phil. Mag. (1951) 42, 868

23)   Johnson, W. & Mellor, P.B.- Engineering Plasticity. van Nostrand, (1973), Chapter 13.

24)   Kudo, H. - An Upper Bound Approach to Plane-Strain Forging and Extrusion. Int. J. Mech. Sci. (1960) 1, 57-83.

25)   Avitzur, B. & Pachla. W. - The Upper Bound Approach to Plain Problems using Linear and Rotational Velocity Fields-II: Applications. J. of Eng. for Ind. Nov.(1986) 108 , 307-316.

26)   Alexander, J.M. - Proc. Inst. Mech. Engrs. (1959) 173, 85-91.

27) **Kudo, H.** - Some Analytical and Experimental Studies of Axisymmetric Cold Forging and Extrusion-I. Int. J. Mech. Sci.(1960) $\underline{2}$, 102-127.

28) **Kobayashi, S.** - Upper Bound Solutions of Axisymmetric Forming Problems. Trans. ASME Nov. (1963) 326-332

29) **Kobayashi, S. & Thomsen, E.G.** - Upper Bound and Lower Bound Solutions to Axisymmetric Compression and Extrusion Problems, Int. J. Mech. Sci. (1965) $\underline{7}$, 127-143.

30) **Thomsen, E.G., Yang, C.T, & Kobayashi, S.**- Mechanics of plastic deformation in metal processing. MacMillan Press, (1965).

31) **Pugh, H.D.** - J. Mech. Eng. Sci. (1964) $\underline{6}$, 362.

32) **Avitzur, B et al.** - Limit Analysis of Flow Through Conical Converging Dies. J. of the FraNklin Inst. (1975) $\underline{299}$, 339-358.

33) **Avitzur, B.** - Metal Forming. McGraw-Hill, New York (1968).

34) **Thompson, P.J., Fogg, B. and Chishlom, A.W.J.** - A Cam-plastometer for Investigations into the Cold and Warm Working Characteristics of Alloy Steel. Int. J. Mech. Tool Des. Res., (1969) 9th Conf, 97-116.

35) **Frisch, J. & Thomsen, E.G.** - Experimental Study of Metal Extrusion at Various Strain Rates. Trans. ASME (1954) $\underline{76}$, 599-606.

36) **Thomsen, E.G.** - A New Approach to Metal Forming Problems-Experimental Stress Analysis for a Tubular Extrusion. Trans. ASME (1955), $\underline{77}$, 515-522.

37) **Shabaik, A.H. & Thomsen, E.G.**- Computer Application to Visioplasticity Method. Trans. ASME Series B (1967) $\underline{89}$, 339-349.

38) **Clough, R.W.** - The Finite Element in Plane Stress, Proc. 2nd, A.S.C.E. Conf. on Electronic computation, Pittsburg, Pa. (1960).

39) **Lee, C.H & Kobayashi, S.C.** - New Solution to Rigid-Plastic Deformation Problems using Matrix Method, J. Eng. Ind. (1973) 95, 865.

40) **Kobayashi, S.** - Rigid-Plastic Finite Element Analysis of Axisymmetric Metal Forming Processes, Numerical Modelling of Manufacturing Processes.ASME, PVP-PB-025 (1977) 49-68.

41) **Lee, C.H & Kobayashi, S** - Elastoplastic Analysis of Plane Strain and Axisymmetric Flat punch Indentation by the Finite Element Method. Int. J. Mech. Sci.,(1970) 12 (4), 349-370.

42) **Zienkiewicz, O.C. &Godbole, P.N.** - Flow of Plastic and Vios-plastic Solids with Special Reference to Extrusion and Forming Processes. Int. J. Num. Meth. Engrg. (1974) 8, 3-16.

43) **Hartely, P., Sturgess, C.E.N & Rowe, G.W.** - Friction in Finite Element Analyses of Metal Forming Processes. Int. J. Mech. Sci. (1979) 21, 301-311.

44) **Lee, E.H.** - Some Comments on Elastic-plastic Analysis, Int. J. Solids and Structures, (1981) 17, 859-872.

45) **Rothman, D.**- Ph.D Thesis, University of Aston in Birmingham, (1970).

46) **Linicus, W. & Sachs, G.** - Mitt. Dt. Mater. Anst. 'Spanlose formung der metalle', (1931) 16, 36-67.

47) **Nishihara, T. & Kakuzen, M.** - Tech. Rep. Eng. Inst. Kyoto University, (1955) 5, Rep No. 22, 75.

48) **Rothman, D. & Sansome, D.H.** - An Investigation of Rod Drawing with Die Rotation. Inst. J. MTDR. (1970) 10, 179-192.

49) **MacLellan, G.D.S.**- Critical Survey of Wire Industry. J. Iron steel Inst. (1948) 158, 347-356.

50) **Wistreich, J.G.** - Investigation of the Mechanics of Wire Drawing. Proc. Inst. Mech. Engrgs. (1955) 169, 654-665.

51)   MacLellan, G.D.S.- Some Friction Effects in Wire Drawing. J. Inst. Met. (1952-53) 81, 1-13.

52)   Lancaster, P.R. & Rowe, G.W. - Proc. Inst. Mech. Engrgs, (1963 - 64), 178, 69 - 89.

53)   Basily, B.B - The Mechanics of Section Drawing. Ph.D, Thesis, University of Aston in Birmingham, (1976).

54)   Torzera, T.A. - On Non-Homogeneous Work for Wire Drawing. Trans. ASM, (1964) 57, 309-323.

55)   Atkins, A.G. & Caddell, R. M. - The Influence of Redundant Work when Drawing Rods Through Conical Dies. Trans. ASME series B, (1968), 90, 411-418.

56)   Basily, B.B. & Sansome, D.H. - Determination of the Mean Coefficient of Friction in the Drawing of Section Rods from Round bars. Proc. 17th Int. MTDR. Conf. (1976) 475-481.

57)   Thompson, P.J. & Sansome, D.H.- Apparent Strain Method for Analysis of Steady State Metal Working Operations. Metals Technology (1976), 497-502.

58)   Jonas, J.J., Sellars. C. M & Tegart. W. McG.- Metall. Rev. (1969) 14, 1-24.

59)   Hirschvogel. M. - J. Mech. Work. Tech. (1979) 4 (2), 317-332.

60)   Mamalis. A.G, Johnson. W & Marczinski -: A current State Review of the Warm-Working of Metals. Proc. 18th Int. M.T.D.R.Conf.,1977, MacMillan, London, (1978), 173-182

61)   Hosford, F.W & Caddell, M.R. - Metal Forming, Mechanics and Metallurgy. Englewood Cliffs London: Prentice - Hall 1983

62) **Samanta, S.K.** - Resistance of dynamic Compression of Low Carbon Steel and Alloy Steels at Elevated Temperatures and High Strain-rates. Int. J. Mech. Sci. (1968) 10, 613-636.

63) **Hawkins, D.N** - Met. Sci., (1976) 10, 113-121.

64) **Hawkins, D.N** - Warm Working of Steel, J. Mech. Work. Tech, (1985) 11 5-21.

65) **Cruden, A.K. &Thomson. J.F.** - Extrusion Pressures, Press loads and Tool stresses for the warm Extrusion of steel, NEL Rep. NO. 456, 1970.

66) **Yuasa, K.** - Metall. and Met. Form., (1974) 41 (6), 76-79.

67) **Nadai, A & Manjoine. M.J.** - High-speed Tension Tests at Elevated Temperatures, J. Appl. Mec.(1941) 8 , A77

68) **Osakada. K, Oyane. M, & Tanak. H.** - In: Proc. 13th Int. Mach. Tool Des. Res.Conf. (1972), MacMillan London, (1973), 357-362.

69) **Alder, J. F & Phillips, V.A.** - The Effect of Strain Rate and Temperature on the Resistance of Aluminium, Copper, and Steel to Compression. J. Inst. Metals.(1954-55) 83, 80-86.

70) **Cook, P.M.** - True Stress-strain Curves for Steel in Compression at High Temperature and Strain Rates, for Application to the Calculation of Load and Torque in Hot Rolling. Proceedings of Conf. on Properties of Materials at High Rates of Strain. (1957), 86-97.

71) **Manjoine, M.J.** - Influence of Rate of Strain and Temperature on Yield Stresses of Mild Steel. J. Appl. Mech, (1944), A211-A218.

72) **Doraivelu, S.M & Gopinathan. V.**- Development of a Tool Set-up for Studying the Influence of Temperature on Compressive Flow Strength under Dynamic Conditions. Proc. 18th Int MTDR. conf. (1977), 37-42.

73) **Thomason, P.F, Fogg. B & Chisholm, A.W.J** - : Proc 14th Int. MTDR. Conf.,1973, MacMillan, London, (1974), pp. 791-797.

74) **Thomason, P.F.** - Proc. Instn. Mech. Engrgs, (1969-70) 184,885.

75) **Belgian 'Cold Forging Group'** - Cam plastometer Tests, Presented at Stuttgart Meeting of Int. cold Forging Group., May (1977).

76) **Eleiche, A.S** - 'A literature Survey of the Combined Effects of Strain Rate and Elevated Temperature on the Mechanical Properties of metals'. Brown. Univ. AFML-TR-72-1308, (1972).

77) **Dean, T.A** - In: Proc. 11th Int. MTDR. Conf., 1970, vol. B, (1971), 779-801.

78) **MacGregor, C.W & Fisher. J.C** - 'Tension Tests at Constant True Strain Rates' J. Appl. Mech, (1945), A217-A227.

79) **Sellars, C.M & Tegart. W.J.McG.** - 'Hot Workability'. Int. Met. Reviews, (1972) 17, 1-24.

80) **Sellars, C.M & Davies. G.J** - Hot Working and Forming Processes. Sheffield (1979), 17-20 July. The Metal Society, London.

81) **Singer, A.R.E & Evans. R.W.**- New Technique for Rapid Measurement of High Temperature Flow Stress. Hot Working and Forming Processes. Sheffield (1977) 77-79.

82) **Ludwik, P** - 'Elements der techonologischen Mechanik', (1909): Berlin (Springer).

83) **Hodierne, F. A.**- A Torsion Test for use in Metal-working Studies. J. Inst. Metals. (1962-63), 91, 267-273.

84) **Johnson, W & Mellor .P.B** - Engineering Plasticity. van Nostrand Reinhold Company. London, (1987).

85) **Samanta, S** - Effect of Strain Rate on Comperessive Strength of Tool Steel Deformation under Hot Working Conditions, (1966) 122-130.

86) **Zener, C & Hollomon. J.** - J. Appl. Phys., (1944) 39, 163.

87) **Jonas, J.J, Sellers .C.M & Tegart. W.J.McG.** - Met. Rev. 14 p. 1 (1969).

88) **MacGregor, C.W. & Fisher, J.C.** - ' A velocity-modified Temperature for the Plastic Flow of Metals ' J. Appl. Mech. (1946), A11-A16.

89) **Inoue, K** - J. of Iron and Steel Inst of Japan, (1955) 41, 593-601.

90) **Nakayama, K** - ' Studies on the Mechanism of Metal Cutting' Bulletin of the Faculty of Engineering. Yokohama National univ., (1959) 8, 1-25.

91) **Loh, N.H** - The Mechanics of Drawing Wire at Elevated Temperature. Ph.D Thesis, (1983). Univ. of Aston in Birmingham.

92) **Oxley, P.L.E** - ' allowing for strain rate effects in the analysis of metal working processes' . Conf. series no. 21. The Inst of physics, (1974) 359-381.

93) **Oyane, M, Takashima. F, Osakada. K. & Tanaka. H** - 'The Behaviour of some Steels under Dynamic Compression'. 10 th Japan congress on testing Materials, (1967), 72.

94) **Siebel, E. & Kobitzsch, R.** - Temperature Increase in Material in Wire Drawing, Stahl und Eisen, (1943) 63, 110

95) **Kopp, R.** - Investigations of the Temperature Fields in Drawing Round Bars, Dissertation, Technical University, Claushal, Germany (1968).

96) **Ranger, A.E,** " An Electrical Analogue for Estimating Die Temperatures During Wire Drawing, " J. Iron and Steel Inst. (1958) 383

97) **Altan, T.** - Heat Generation and Temperature in Wire and Rod Drawing.Wire Journal (1970) 3, 54-59.

98) **Johnson, W. & Kudo, H.** - The upper-bound Solutions for the Determination of Temperature Distribution in Fast Rolling and Axisymmetric Extrusion Processes. Int. J. Mech. Sci. (1960) 1, 175-191.

99) **Tay, O.A, Farmer, L.E and Oxley, P.L.B.**- A numerical Method for Calculating Temperature Distribution in Metal Working Processes. Int. J. Mech. Sci. (1980) 22, 41-57.

100) **Bishop, W.F.J.** - "An Approximate Method for Determining the Temperature Reached in Steady Motion Problems of Plane Plastic Strain. J. of Mech. and Applied Maths. (1956) 9 , pt 2, 237-246.

101) **Altan, T.& Kobayashi. S** - A Numerical Method for Estimating the Temperature Distribution in Extrusion Through Conical Dies. J. of Engrg. for Ind. (1968) 107-118.

102) **Lahoti, G, & Altan, T.** - Prediction of Temperature Distribution in Axisymmetric Compression and Torsion. J. Engng. Materials Tech. Trans. ASME, (1975), 97, 113.

103) **Lahoti, G.D, et al.** - Computer-Aided Prediction of Metal flow, Temperature and Forming Load in Selected Metal-forming Processes. ASME AMD, 28, APPL. of Numerical Methods of forming Processes, ASME Winter Annual. Meet. San Franscisco, Calif., Dec 10-15 (1978).183-195.

104) **Avitzur, B.**- Analysis of Metal Flow Through Conical Converging Dies as an Adiabatic Process. 'Fourth N.A. metal working Res. Conf. Berttelle, 1976

105) **Juneja, B.L. & Prakash, R.** - An Analysis for drawing and extrusion of polygonal sections. Int. J. M.T.D.R (1975) 15, 1-30.

106) **Prakash, B.L. & Khan, Q.M.** - An Analysis of Plastic Flow through Polygonal Converging Dies with Generalised Boundaries of Zone of Plastic Deformation. Int. J. M.T.D.R.(1979) 19, 1-19.

107) **Basily, B.B. & Sansome, D.H.** - Some Theoretical Considerations for the Direct Drawing of Section Rod from Round Bar. Int. J. Mech. Sci., (1976) 18, 201-205, Pergamon Press.

108) **Dong-Yol Yan & Choong-Hong Lee.** - Analysis of Three- dimensional Extrusion of Sections through Curved Dies by Conformal Transformation. Int. J. Mech. Sci. (1978) 20, 541-552.

109) **Boer, C.R., Avitzur, B., Schneider, W.R. and Eliasson, B** - An Upper Bound Approach for the Direct Drawing of Square Section Rod from Round Bar. 20th M.T.D.R., Conf., (1979) 149-156.

110) **Nagpal, V. & Altan, T.** - Analysis of the Three-dimensional Metal Flow in Extrusion of Shapes with the use of Dual Stream Functions. Proc. Third N.Am. Metal Res. Conf. Pittsburgh, Pa. (1975). 26-40

111) **Yang, D.Y, Kim, M.V & Lee, C.H.**- A New Approach for Generalized three-Dimensional Extrusion of Sections from Round Billets by Conformal Transformation. IUTAM Symposium on Metal Forming Plasticity, Germany, (1979) 204-211.

112) **Hoshino, S. & Cunasekera, S.J.** - An Upper Bound Solution for the Extrusion of Square Section from Round Bar through Converging Dies. 21st M.T.D.R. Conf., (1980)97-105.

113) **Gunasekera, S.J. & Hosihino, S.** - Analysis of Extrusion and Drawing of Polygonal Sections through Straightly converging dies. J. Eng. Ind. Trans. ASME,, (1982) 104, 38-45.

114) **Kiuchi, M. et al** - Study on Non-symmetric Extrusion and Drawing. 22nd M.T.D.R., Conf., (1981) 523-532.

115) **Jornaz, M.I, Crane, L.W & Cole, I.M.**- The Drawing of Polygonal Sections from Round at Elevated Temperature. 28th M.T.D.R., Conf., (1990) 425-430.

116) **Kiuchi, M.**- Overall Analysis of Non-axisymmetric Extrusion and Drawing. Proc. 12th NAMRC. Conf., (1984) 111-119.

117) **Gunasekera, S.J. & Hosihino, S.** - Analysis of extrusion of polygonal sections through streamlined dies. J. of Engrg. for Ind. Aug. (1985) 107, 229-232.

118) **Hang, C.H, Yang, D.Y. & Kiuchi, M.** - A New Formulation for Three-dimensional Extrusion and its Application to Extrusion of Clover Sections. Int. J. Mech. Sci., (1986) 28, No.4, 201-218.

119) **Chitkara, N.R. & Abrinia, K.**- A General Upper Bound Solution for Three-dimensional Extrusion of Shaped Sections using CAD-CAM Bilinear Surface Dies. 28th M.T.D.R., Conf., (1990) 417-424.

120) **Kariyawasam, V.P.** - The Mechanics of Drawing Polygonal Tube from Round on a Plug. Ph.D Thesis (1980). Univ. of Aston in Birmingham.

121) **Muriuki, M.WA.** - The Mechanics of Drawing Polygonal Tubes from Round on a Cylindrical Plug. Ph.D Thesis (1981). Univ. of Aston in Birmingham.

122) **Kiuchi, M. & Kimura, T.** - Computer Simulation of Extrusion and Drawing of Tubular Products having Square Cross-sections with Round Inner Holes.25th M.T.D.R., Conf., (1985) 561-569.

123) **Webster, W & Davis, R** - Finite Element Analysis of Round to Square Extrusion Processes. Man. Eng. Trans, Proc. NAMRC (1978).

124) **Boer, R.C. &Webster, D.W.Jr.** - Direct Upper Bound Solution and Finite Element Approach to Round-to-square Drawing. Trans. of. the ASME 107 Aug (1985) 254-260.

125) **Winsper, C.E.** - An Investigation of the Mechanics of Wire Drawing with the Super-position of an Oscillatory Drawing Stress. Ph.D, (1966), Univ. of Aston in Birmingham.

126) **Williams, J.D.** - Advanced Tool Materials in the Drawing of Metals. Proc. of the Int. Conf. on Dev. in the Drawing of Metals. Book No. 301 London (1983) 264-271.

127) **Henshell, R.D.** - " PAFEC Theory, Results". PAFEC limited, Strelly Hall, Nottingham, England.

BIBLIOGRAPHY

1) **Blazynski, T.Z.** - Metal Forming: Tool Profile and Flow. MacMillan Press Ltd., 1976

2) Strain Gauge Technology - Edited by   **A. L. Window and G.S. Holister** Applied Science Publishers Ltd 1982

3) Design of Tool for Deformation Processes - Edited by **T.Z. Blazynski.** Elsevier Applied Science Publishers 1986

APPENDIX A1

GEOMETRICAL RELATIONS

_____
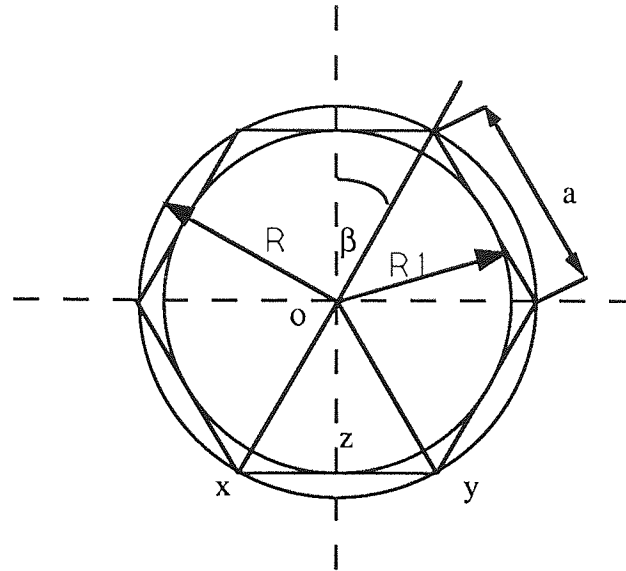
b = Included angle of symmetric portion   R = Radius of the outer circle

R_1= Radius of the inner enclosed circle   a = Side length of the section rod

A = Cross-section area of the section rod D_1= 2 R_1

N_s= Number of sides   D = 2 R

$$\beta = \frac{180}{N_s}$$

$$a = 2\left(R^2 - R_1^2\right)^{0.5}$$

$$R = \frac{a}{2\ \sin\beta}$$
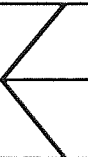
$$R_1 = \frac{a}{2\ \tan\beta}$$

$$A = \frac{1}{4}\ N_s\ a^2\ \cot\beta$$

$$= \frac{1}{2}\ N_s\ R^2\ \sin\beta$$

$$= \ N_s\ R_1^2\ \tan\beta$$

Table (A1.1). Geometrical relations of a section of 4.5 mm including circular diameter

NO.OF SIDES	SECTION NAME	Φ	a	D1	A
3	Triangular	60	3.897	2.249	6.57
4	Square	45	3.182	3.182	10.125
5	Pentagon	36	2.645	3.641	12.037
6	Hexegon	30	2.25	3.898	13.153
7	Heptagon	25.71	1.952	4.055	13.851
8	Octagon	22.5	1.722	4.157	14.319
9	Nonagon	20	1.539	4.229	14.644
10	Decagon	18	1.391	4.280	14.878
11	Unidecagon	16.36	1.268	4.318	15.050
12	Duodecagon	15	1.165	4.347	15.188
∞	Circular	0.0	0.0	4.5	

Appendix (A1.2) The evaluation of area ratio A_r

The diagonal length of the die $= dL_d$

The area of asymmetrical section of a regular polygonal die

$$A_S = \frac{1}{2} \cdot OZ \cdot XY$$

$$= \frac{1}{2} \frac{dL_d}{2} \cos\beta \cdot 2 \frac{dL_d}{2} \sin\beta$$

$\therefore$ Total area bounded by the regular polygonal die

$$A_{ST} = A_S \cdot \text{number of sides}$$

$$= \frac{dL_d^2 \sin 2\beta}{8} N_S$$

Total inlet area of the circular bar $= \pi OR^2$

where

OR is radius of the inlet bar

$$\therefore \text{Area ratio } A_r = \frac{\text{inlet area}}{\text{exit area}}$$

$$\therefore A_r = \frac{8 \pi OR^2}{N_S dL_d^2 \sin 2\beta}$$

$$\text{Reduction of area } R = \frac{A_1 - A_2}{A_1} 100$$

INLET BAR DIAMETER	Bar area	Triangle 6.576	Square 10.125	Pentagon 12.037	Hexagon 13.153	Heptagon 13.851	Octagon 14.319	Nonagon 14.644	Decagon 14.878	Unidecagon 15.050	Duodecagon 15.188	Circular 15.904
4.5	15.904	58.65	36.34	24.31	17.30	12.91	9.970	7.920	6.450	5.360	4.50	0.0
4.8	18.096	63.60	44.04	33.48	27.32	23.46	20.87	19.08	17.78	16.83	16.07	12.11
5.0	19.635	–	48.43	38.70	33.01	29.46	27.07	25.42	24.23	23.35	22.65	19.00
5.2	21.237	–	52.32	43.32	38.07	34.78	32.58	31.04	29.94	26.04	28.48	25.11
5.5	23.758	–	57.38	49.33	44.64	41.70	39.73	38.36	37.38	36.65	36.07	33.06
5.8	26.421	–	61.67	54.44	50.22	47.58	45.80	44.57	43.69	43.04	42.52	39.81
6.0	28.274	–	–	57.40	53.48	51.01	49.36	48.21	47.38	46.77	46.28	43.75
6.5	33.183	–	–	63.70	60.36	58.26	56.85	55.87	55.16	54.65	54.23	52.07
7.0	38.480	–	–	–	–	64.00	62.79	61.94	61.34	60.89	60.53	58.67

Table.(A1.2) Reductions Of Area For Different Section Rods Drawn From Round Stock

299

(b) Die geomerty

(a) Square drawing die

(c) Axisymmetric drawing die
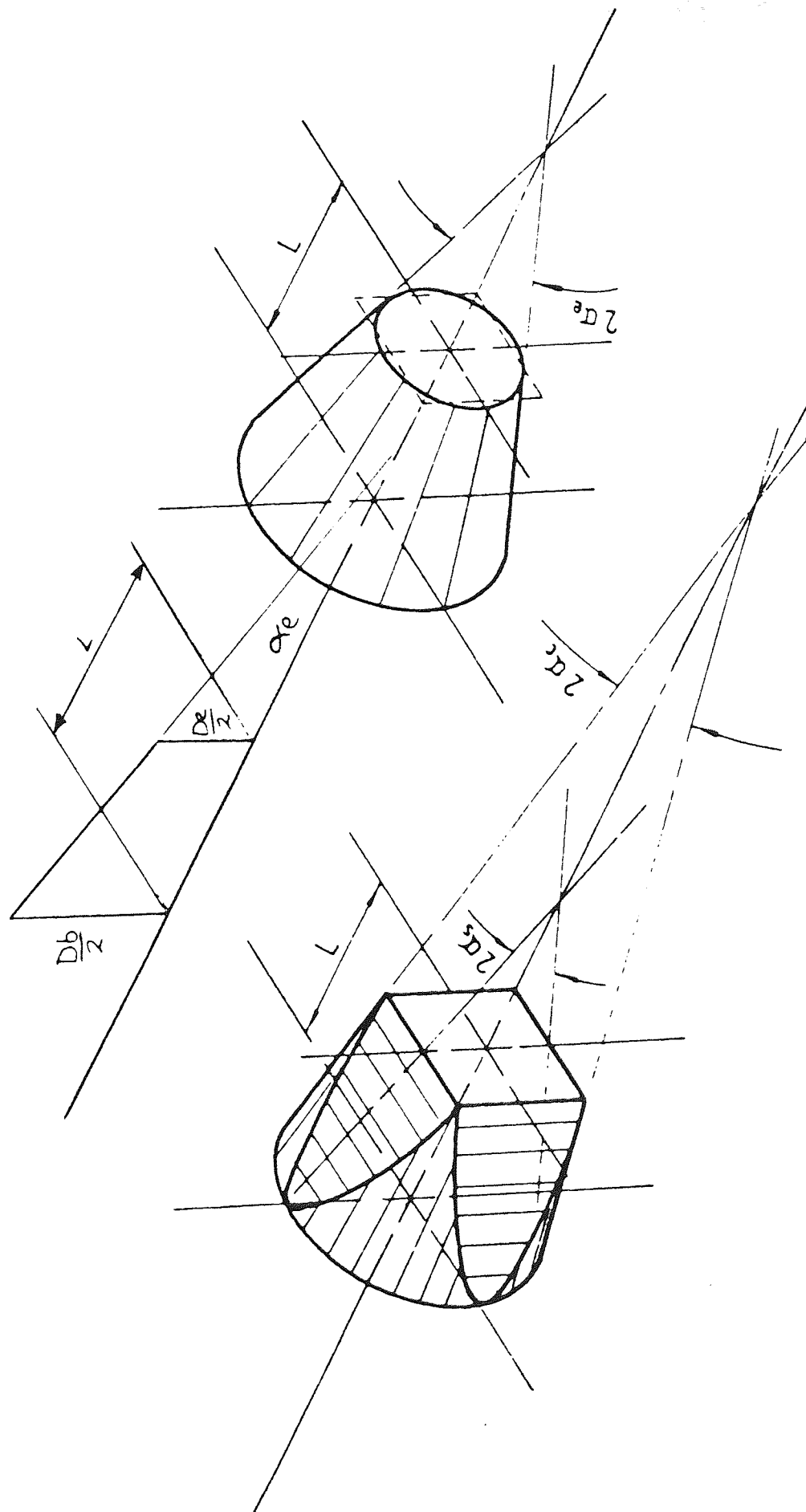
Appendix (A1.3) Isommetric drawing of the square and the corresponding axisymmetric drawing dies

300

APPENDIX A2

SUPPLEMENTARY PROOFS

Appendix(A2.1) Derivation of the co-ordinates of the elemental triangles on the inlet plane.

The equation of a circle having a radius R_i, is given by;

$$X^2 + Y^2 = R_i^2 \qquad (1)$$

The equation of a straight line is given by ;

$$Y = m X \qquad (2)$$

The co-ordinates of any point can be determined from the intersection of the circle and the straight line, by solving equations (1), (2) for X and Y, gives;

$$X_i = \pm R_i \sqrt{\frac{1}{1+m^2}} \qquad (3)$$

where $\qquad m = TAN\theta$

$\qquad\qquad$ T = Thickness of a circular band

$\qquad R_i = (I.T) \qquad I = 1$ to (CB-1)

The positive sine was chosen.

substituting equation (3) in equation (2) yields

$$Y_i = \pm m R_i \sqrt{\frac{1}{1+m^2}}$$

The above procedure was repeated to determine the co-ordinates for each triangle.

Appendix (A2.2) Supplementry proofs

Derivation of Strain Rates in Terms of Velocity Components

1) To find

$$\dot{\varepsilon}_\rho = \frac{d\dot{U}_\rho}{d\rho}$$

Differentiating equation (2.7) with respect to r, gives;

$$= -2 V_1 \frac{\rho_1^2}{\rho^3} \frac{\cos(t\theta)}{\cos(\theta - t\theta)} \tag{1}$$

2) To find

$$\dot{\varepsilon}_\theta = \frac{1}{\rho} \frac{\delta \dot{U}_\theta}{\delta\theta} + \frac{\dot{U}_\rho}{\rho} \tag{2}$$

differentating equation (2.8) with respect to θ, gives;

$$= V_1 \left(\frac{\rho_1}{\rho}\right)^2 \tan\psi \left(\frac{\cos(\theta-t\theta)\left(-t\,\sin(t\theta)\right) - \cos(t\theta)\,(1-t)\left(-\sin(\theta-t\theta)\right)}{\cos^2(\theta-t\theta)}\right)$$

$$= V_1 \left(\frac{\rho_1}{\rho}\right)^2 \frac{\tan\psi}{\cos(\theta-t\theta)} \left(\cos(t\theta)\,(1-t)\,\tan(\theta-t\theta) - t\,\sin(t\theta)\right) \tag{3}$$

∴ substituting equation (3) and (2.7) in equation (2) gives;

$$\dot{\varepsilon}_\theta = V_1 \frac{1}{\rho} \left(\frac{\rho_1}{\rho}\right)^2 \frac{\tan\psi}{\cos(\theta-t\theta)} \left(\cos(t\theta)\,(1-t)\,\tan(\theta-t\theta) - t\,\sin(t\theta)\right) + \frac{1}{\rho} V_1 \frac{1}{\rho} \left(\frac{\rho_1}{\rho}\right)^2 \frac{\cos(t\theta)}{\cos(\theta-t\theta)}$$

$$\dot{\varepsilon}_\theta = V_1 \frac{\rho_1^2}{\rho^3} \frac{\cos(t\theta)}{\cos(\theta-t\theta)} \left[1 + \tan\psi\left((1-t)\,\tan(\theta-t\theta) - t\,\tan(t\theta)\right)\right]$$

3) To find

$$\dot{\varepsilon}_\phi = \frac{1}{\rho \sin\theta} \frac{\delta \dot{U}_\phi}{\delta\phi} + \frac{\dot{U}_\rho}{\rho} + \frac{\dot{U}_\theta}{\rho} \cot(\theta) \tag{4}$$

302

$$\frac{\delta \dot{U}_\phi}{\delta \phi} = 0 \tag{5}$$

substituting equations (5), (2.7) and (2.8) in equation (4), gives ;

$$\dot{\varepsilon}_\phi = V_1 \frac{\rho_1^2}{\rho^3} \frac{\cos(t\theta)}{\cos(\theta - t\theta)} \left(1 + \tan\psi \cot\theta\right) \tag{6}$$

4) To find

$$\dot{\gamma}_{\rho\theta} = \frac{1}{2} \left(\frac{\delta \dot{U}_\theta}{\delta \rho} - \frac{\dot{U}_\theta}{\rho} + \frac{1}{\rho} \frac{\delta \dot{U}_\rho}{\delta \theta} \right) \tag{7}$$

Differentiating equation (2.8) with respect to ρ, gives;

$$\frac{\delta \dot{U}_\theta}{\delta \rho} = -2 V_1 \frac{\rho_1^2}{\rho^3} \frac{\cos(t\theta)}{\cos(\theta - t\theta)} \tan\psi \tag{8}$$

Differentiating equation (2.7) with respect to θ, gives;

$$\frac{\delta \dot{U}_\rho}{\delta \theta} = V_1 \left(\frac{\rho_1}{\rho}\right)^2 \frac{\cos(\theta - t\theta)\left(-t \sin(t\theta)\right) - \cos(t\theta)(1-t)\left(-\sin(\theta - t\theta)\right)}{\cos^2(\theta - t\theta)}$$

$$= V_1 \left(\frac{\rho_1}{\rho}\right)^2 \frac{\cos(t\theta)}{\cos(\theta - t\theta)} \left[(1-t) \tan(\theta - t\theta) - t \tan(t\theta)\right] \tag{9}$$

substituting equations (8), (2.8) and (9) into equation (7), gives;

$$\dot{\gamma}_{\rho\theta} = \frac{1}{2} \left\{ \begin{array}{l} -2 V_1 \dfrac{\rho_1^2}{\rho^3} \dfrac{\cos(t\theta)}{\cos(\theta - t\theta)} \tan\psi - \dfrac{1}{\rho} V_1 \left(\dfrac{\rho_1}{\rho}\right)^2 \dfrac{\cos(t\theta)}{\cos(\theta - t\theta)} \tan\psi \\[4mm] + \dfrac{1}{\rho} V_1 \left(\dfrac{\rho_1}{\rho}\right)^2 \dfrac{\cos(t\theta)}{\cos(\theta - t\theta)} \left[(1-t) \tan(\theta - t\theta) - t \tan(t\theta)\right] \end{array} \right\}$$

$$\dot{\gamma}_{\rho\theta} = \frac{V_1}{2} \frac{\rho_1^2}{\rho^3} \frac{\cos(t\theta)}{\cos(\theta - t\theta)} \left[-3\tan\psi + (1-t) \tan(\theta - t\theta) - t \tan(t\theta)\right] \tag{10}$$

5) To find

$$\dot{\gamma}_{\rho\theta} = \frac{1}{2}\left(\frac{1}{\rho\sin\theta}\frac{\delta\dot{U}_\theta}{\delta\phi} + \frac{1}{\rho}\frac{\delta\dot{U}_\phi}{\delta\theta} - \frac{\cot\theta}{\rho}\dot{U}_\phi \right) \qquad (11)$$

$$\frac{\delta\dot{U}_\theta}{d\phi} = 0 \qquad (12)$$

differentiating equation (2.9) with respect to θ, gives;

$$\frac{\delta\dot{U}_\phi}{\delta\theta} = V_1\left(\frac{\rho_1}{\rho}\right)^2 \frac{\tan\eta}{\cos\psi}\left(\frac{\cos(\theta-t\theta)\,t(-\sin(t\theta)) - \cos(t\theta)(1-t)(-\sin(\theta-t\theta))}{\cos^2(\theta-t\theta)} \right)$$

$$\frac{\delta\dot{U}_\phi}{\delta\theta} = V_1\left(\frac{\rho_1}{\rho}\right)^2 \frac{\tan\eta\,\cos(t\theta)}{\cos\psi\,\cos(\theta-t\theta)}\left((1-t)\tan(\theta-t\theta) - t\tan(t\theta)\right) \qquad (13)$$

substituting equations (12), (13) and (2.9) into equation (11) gives;

$$\dot{\gamma}_{\theta\phi} = \frac{V_1}{2}\frac{\rho_1^2}{\rho^3}\frac{\cos(t\theta)\tan\eta}{\cos(\theta-t\theta)\cos\psi}\left[(1-t)\tan(\theta-t\theta) - t\tan(t\theta) - \cot\theta\right] \qquad (14)$$

6) To find

$$\dot{\gamma}_{\phi\rho} = \frac{1}{2}\left(\frac{\delta\dot{U}_\phi}{\delta\rho} - \frac{\dot{U}_\phi}{\rho} + \frac{1}{\rho\sin\theta}\frac{\delta\dot{U}_\rho}{\delta\phi} \right) \qquad (15)$$

$$\frac{\delta\dot{U}_\rho}{\delta\phi} = 0 \qquad (16)$$

Differentiating equation (2.9) with respect to ρ, gives;

$$\frac{\delta\dot{U}_\phi}{\delta\rho} = -2V_1\frac{\rho_1^2}{\rho^3}\frac{\cos(t\theta)\tan\eta}{\cos(\theta-t\theta)\cos\psi} \qquad (17)$$

substituting equations (16), (17) and into equation (15), gives;

$$\dot{\gamma}_{\phi\rho} = \frac{-3V_1}{2}\frac{\rho_1^2}{\rho^3}\frac{\cos(t\theta)\tan\eta}{\cos(\theta-t\theta)\cos\psi} \qquad (18)$$

APPENDIX A3

COMPUTER PROGRAMS AND RESULTS

```
%                    *** Appendix (A3.1) Main program ***

                 ------*Using  Matlab  Computer  language*-----
% Write variables such as Number of Bands (CB-1), Number of Sectors (ES-1)
% Number of Sides of polygon (Ns), Diagonal length of die (DL) and
% the Radius of inlet bar, Exit velocity(V222), and Number of divisions
% of the deforming zone (inc)
clear;

%                              ***************
x(1,1)=0;y(1,1)=0;
% As **(An example)** CB =3; ES =3; Ns=4; DL=4.5; R=2.25;V2=6/60;inc=3;
CCB = input('The number of circulr bands ');
EES = input('The number of sectors ');
Ns  = input('Number of sides of polygon ');
DL  = input('Diagonal length of die ');
R   = input('Radius of inlet bar ');
V222 = input ('Exit velocity in m/min ');
ES = EES+1;
CB = CCB+1;
V2 = V222/60;
CM=450;JM=1;RM=7860;
b(1:6)=zeros(1:6);ALT1(1:50)=zeros(1:50);AST1(1:50)=zeros(1:50);
BA(1:50)=zeros(1:50);SA(1:50)=zeros(1:50);AST2(1:50)=zeros(1:50);
ALT2(1:50)=zeros(1:50);EQBA(1:50)=zeros(1:50);EQSA(1:50)=zeros(1:50);
ART(1:50)=zeros(1:50);g(1:4)=zeros(1:4);
for i=1:8
x(i,1:8)=zeros(1:8);y(i,1:8)=zeros(1:8);
xa(i,1:8)=zeros(1:8);
ya(i,1:8)=zeros(1:8);
XLT2(i,1:8)=zeros(1:8);YLT2(i,1:8)=zeros(1:8);
XST2(i,1:8)=zeros(1:8);YST2(i,1:8)=zeros(1:8);
xb(i,1:8)=zeros(1:8);yb(i,1:8)=zeros(1:8);end;
e(1:4)=zeros(1:4);
xi(i,1:8)=zeros(1:8);yi(i,1:8)=zeros(1:8);
XLT1(i,1:8)=zeros(1:8);YLT1(i,1:8)=zeros(1:8);
XST1(i,1:8)=zeros(1:8);YST1(i,1:8)=zeros(1:8);
%                    ********************************

str=0; OSIG=0; RO1=0;  DT=0; DF=0;Tstr(1)=0;OSIG(1)=0;
%
Beta = pi/Ns;L=0;
% To find the Across flat length of die
AFL = DL* cos(Beta);

% Polygon section area (A2)
A2 = .125* Ns*(DL^2)*sin(2*Beta);

% Dividing circular inlet bar into (CB-1) Bands of equal thichness (t)
t = R/(CB-1);
A1 = pi*(R^2);
Rd = ((A1-A2)/A1)*100;
Ar = A1/A2;
disp(' A1 ,   A2  ,   Rd  ,    Ar')
disp('    ')
a(1)= A1;a(2)= A2;a(3)= Rd;a(4)= Ar;
disp(a);
```

```matlab
disp(' ')
% disp('   k,      ALT2,    AST2,   EQ band,  EQ sector,  ')
disp(' ')
V1=V2/Ar;

for k=1:(CB-1)
  % To find area of inlet bands Band area(BA)
      BA(k) = pi*(t*k)^2/(2*Ns);
    if k==1;
      BA(k)=BA(k);
    else
      BA(k) = BA(k)-sum(BA(1:k-1));
    end;

  % Division of band area into (SE-1) sector area (SA)
      SA(k) = BA(k)/(ES-1);
  % Division of sector into large & small triangles
      B = (t*(k));

    ALT1(k) = (SA(k)*B)/((2*B)-t);
      if k==1;
          AST1(k) = 0;
        else
          AST1(k) = (SA(k)*(B-t))/((2*B)-t);
        end;

  % Refering areas of triangles into exit
      ALT2(k) = ALT1(k)/Ar;
      AST2(k) = AST1(k)/Ar;
      EQBA(k) = BA(k)/Ar;
      EQSA(k) = SA(k)/Ar;
      b(1)= k;b(2)= ALT2(k);b(3)=AST2(k);
      b(4)=EQBA(k);b(5)=EQSA(k);
      % disp(b);
 end;

% To establish the x and y co-ordinates along Across flats lengths
% disp(' ')
% disp('   k    , j  ,  x(k,1) ,  y(k,1) ')
% disp(' ')
for k=1:(CB)
    j=1;

    if k==1;
        x(k,j)=0;
    else
        if k==2;
          EQBA(k-1)= EQBA(k-1);
        else
          EQBA(k-1)= EQBA(k-1)+EQBA(k-2);
        end;
        x(k,1)=sqrt(2*EQBA(k-1)/tan(Beta));
    end;

    y(k,1)=0;
    c(1)=k;c(2)=j;c(3)=x(k,j);c(4)=y(k,j);
    % disp(c);
 end;
```

306

```
% To establish the co-ordinates along diagonal length
% disp(' ')
% disp('   k,        ES,   x(k,ES),   y(k,ES)')
% disp(' ')

 for k=2:CB
     y(k,ES)=x(k,1)*tan(Beta);
     x(k,ES)=x(k,1);
     d(1)=k; d(2)=ES; d(3)=x(k,ES); d(4)=y(k,ES);
     % disp(d);
 end;

% Mapping of the deformation zone

 for i=2:CB;
     for j=2:ES;

         ia=i; ja=j; ib=i-1; jb=j;
         y(i,j)=(2*ALT2(i-1))/(x(i,1)-x(i-1,1));
         x(i,j)=x(i,1);
         y(i,j)=y(i,j)+y(i,j-1);
         xa(ia,ja)=x(i,j);
         ya(ia,ja)=y(i,j);

         if ya(ia,ja) > y(i,ES);
             ya(ia,ja)=y(i,ES);
             xa(ia,ja)=x(i,ES);
             y(i-1,j)= (2*AST2(i-1))/(x(i,1)-x(i-1,1));
             x(i-1,j)=x(i-1,1);
             y(i-1,j)=y(i-1,j)+y(i-1,j-1);
             xb(ib,jb)=x(i-1,j);
             yb(ib,jb)=y(i-1,j);
             yb(ib,jb)=y(i-1,ES);
             xb(ib,jb)=x(i-1,ES);

         else
             y(i-1,j)= (2*AST2(i-1))/(x(i,1)-x(i-1,1));
             x(i-1,j)=x(i-1,1);
             y(i-1,j)=y(i-1,j)+y(i-1,j-1);
             xb(ib,jb)=x(i-1,j);
             yb(ib,jb)=y(i-1,j);
         end;
     end;
   end;

% calculating the mean co-ordinates.
for k=3:(CB-1);
    for j=2:ES;
        xm=(xa(k,j)+xb(k,j))/2;
        ym=(ya(k,j)+yb(k,j))/2;
        x(k,j)=xm;
        y(k,j)=ym;
    end;
 end;
for j=2:ES
    y(2,j)= yb(2,j);
    x(2,j)= xb(2,j);
    y(CB,j)= ya(CB,j);
```

```
        x(CB,j)= xa(CB,j);
    end;


% At this stage every co-ordinate in the deforming
% zone is established.Next stage is to print all
% the co-ordinates
% disp(' ');
% disp('        i,  j ,  x(i,j),   y(i,j)  ');
% disp(' ');
for i=2:CB;
    for j=1:ES;
      e(1)=i;
      e(2)=j;
      e(3)=x(i,j);
      e(4)=y(i,j);
      %disp(e);
    end;
 end;
% Now every thing is ready for the calculation of the centroid of the large and %
small triangles at the exit.
% disp(' ')
% disp(' Band , Sector, Centroid XLT2,   YLT2 ,  XST2,  YST2 ' )
% disp(' ')
 for i=2:CB;
    for j=2:ES;
       m=i-1; k=j-1;
       XLT2(i-1,j-1) = (x(i-1,j-1)+x(i,j-1)+x(i,j))/3;
       YLT2(i-1,j-1) = (y(i-1,j-1)+y(i,j-1)+y(i,j))/3;

       if i==2,
         XST2(i-1,j-1)=0;
         YST2(i-1,j-1)=0;
       else
         XST2(i-1,j-1) = (x(i-1,j-1)+x(i,j)+x(i-1,j))/3;
         YST2(i-1,j-1) = (y(i-1,j-1)+y(i,j)+y(i-1,j))/3;
       end;
       f(1)=m;f(2)=k;f(3)=XLT2(i-1,j-1);f(4)=YLT2(i-1,j-1);
       f(5)=XST2(i-1,j-1);f(6)=YST2(i-1,j-1);
       % disp(f);
    end;
  end;


% calculation of triangular co-ordinates at inlet
xi(1,1)=0 ; yi(1,1)=0;
disp(' ')
% disp('     i,   j,    inlet x(i,j),   inlet y(i,j),   ')
disp(' ');
 for i=2:CB;
    for j=1:ES;
       R1= t*(i-1);
         if j==1;
           Teta = 0;
         else
           Teta = (Beta*(j-1))/(ES-1);
         end;
       gra = tan(Teta);
       xi(i,j)= abs(sqrt(R1^2/(1+ gra^2)));
       yi(i,j)=gra*xi(i,j);
```

308

```
         g(1)=i;g(2)=j ;g(3)=xi(i,j); g(4)= yi(i,j);
         % disp(g);
      end;
  end;

% Calculation of cetre of gravity of large and small triangles at the inlet
% disp(' ')
% disp(' Band , Sector, Centroid XLT1,   YLT1 ,   XST1,   YST1 ' )
% disp(' ')
 for i=2:CB;
    for j=2:ES;
       m=i-1; k=j-1;
       XLT1(i-1,j-1) = (xi(i-1,j-1)+xi(i,j-1)+xi(i,j))/3;
       YLT1(i-1,j-1) = (yi(i-1,j-1)+yi(i,j-1)+yi(i,j))/3;

       if i==2,
          XST1(i-1,j-1)=0;
          YST1(i-1,j-1)=0;
       else
          XST1(i-1,j-1) = (xi(i-1,j-1)+xi(i,j)+xi(i-1,j))/3;
          YST1(i-1,j-1) = (yi(i-1,j-1)+yi(i,j)+yi(i-1,j))/3;
       end;

       g(1)=m;g(2)=k;g(3)=XLT1(i-1,j-1);g(4)=YLT1(i-1,j-1);
       g(5)=XST1(i-1,j-1);g(6)=YST1(i-1,j-1);
       % disp(g);
    end;
  end;

for TTt=200:100:200;
disp('Test Temperature');TTt
disp(' EQ    FR    def    shear    friction    draw stress ');

% To generate draw parameters for different equivalent die semi-cone angle and  %
  coefficient of friction.
% Varying the equivalent die semi-angle by 2 degree increments.
% varying the coefficient of friction by 0.05 increments.

 for EQ = 9:2:13
    EQA = EQ*(pi/180);
  for FR = 0:0.1:0.3
% disp('Equivalent die semi angle (deg)');EQ
% disp('Mean coefficient of friction');FR
    EqR2 = sqrt(A2/pi);
    Ldie = (R1-EqR2)/tan(EQA);
% disp(' T     shear factor ');
disp(' ');
    for T=0.1:0.1:1
       TP=1-T; WST=0;
% Radius of the shear surface at the inlet
  RO=(Ldie*R1)/(cos(EQA)*(R1-EqR2));
  RO2= EqR2/sin(EQA);
% calculations of flow parameters for the inlet and outlet triangles.

    for i=1:CB-1
       for j=2:ES
          if i==1
```

309

```
                    WS1=0; WS2=0;
                    E=XLT1(i,j-1);
                    F=YLT1(i,j-1);
                    XE=XLT2(i,j-1);
                    XF=YLT2(i,j-1);
                    G=ALT1(i);

% call subroutine to find the optimal conditions

        Minshear;

            else

                for cont=1:2
                WS1=0; WS2=0;

                if cont==1

                E=XLT1(i,j-1);
                F=YLT1(i,j-1);
                XE=XLT2(i,j-1);
                XF=YLT2(i,j-1);
                G=ALT1(i);

            else

                E=XST1(i,j-1);
                F=YST1(i,j-1);
                XE=XST2(i,j-1);
                XF=YST2(i,j-1);
                G=AST1(i);

            end;

%call subroutine to find the optimal conditions

        Minshear;

    end;
   end;
  end;
 end;
% h(1)=T;h(2)=WST
% disp(h)
  WSG=WST;
    if T==0.1
      WSM=WSG;
      Tm=T;
    else
      if WSG<WSM
        WSM=WSG;
        Tm=T;
      else
      end;
    end;
 end;
% disp(' Optimal T, Minimum Shear factor' );
 p(1)=Tm; p(2)=WSM;
```

310

```
% disp(p);

% To calculate shape factor and power of deformation using optimal conditions.
T=Tm;
WST=WSM;
TP=1-T;SLT=0;Rt=0;SLT1=0;AVYm=0;TOYm=0;
  for i=1:CB-1
      for j=2:E

        if i==1;

            Ffac=0; TSS1=0;
            E=XLT1(i,j-1);
            F=YLT1(i,j-1);
            XE=XLT2(i,j-1);
            XF=YLT2(i,j-1);
            G=ALT1(i);
% call defsub program to calculate the deformation parameters

            defsub;

% call latest program to calculate the flow stress.
            latest;

          AVYm=MM;
          ttoy(i,j-1)= sum(AVYm);
          TSS1= TL*jj*DAL1;
          SLT1= TSS1+SLT1;

        else

          toym(cont)=0;
          for cont=1:2
          Ffac=0; TSS=0;
        if cont==1
          cont;
          E=XLT1(i,j-1);
          F=YLT1(i,j-1);
          XE=XLT2(i,j-1);
          XF=YLT2(i,j-1);
          G=ALT1(i);

        else
          cont;
          E=XST1(i,j-1);
          F=YST1(i,j-1);
          XE=XST2(i,j-1);
          XF=YST2(i,j-1);
          G=AST1(i);

        end;
% call program defsub.
  defsub;

% call latest program to calculate the flow stress.
  latest;

  TOYm=MM;
```

```
        toym(cont)=sum(TOYm);
        TSS= TL*jj*DAL1;
        SLT= SLT+TSS;

    end;

        AVYm=(sum(toym))/2;
        ttoy(i,j-1)= sum(AVYm);
      if i==CB-1
        ffoy(i,j-1)=ttoy(i,j-1);
      end
    end;
    end;
end;
      if CB==3;
        nn=4; mm=2;
      else if CB==4;
            nn=12; mm=3;
      else if CB==5;
            nn=24; mm=4;
      end;end;end;

  ttoy1=sum(ttoy);
  Ym=sum(ttoy1)/nn;
  ffoy1=sum(ffoy);
  Yf=sum(ffoy1)/mm;

  PA = 2*Ns/(4*sqrt(3)*(R1^2));
  fs = PA*(SLT+SLT1);
  DDT= Ym*V1*((2*R1)^2);
  WSH=WST*2*Ns*Ym*V1;

% Power loss due to shear
% disp(' Power loss due to shear');
% disp(WSH)

% Total power of deformation.
% disp(' Internal power of deformation ');
  ToPW = abs(DDT*log((2*R1)/(2*EqR2))*fs);
% disp(ToPW)

% Power loss due to friction in the conical part.
% disp(' Power losses due to friction in the conical part');
    FD = FR*Yf*V1/sqrt(3);
    MD = (R1^2)/sin(EQA);
    FRco = abs(2*FD*MD*log(R1/EqR2)*Rt*tan(pi/Ns));
% disp(FRco)

% Power loss due to friction in land portion of die.
% disp(' Power loss due to friction in land');
    FRL = abs(FR*Yf*V2*(EqR2*2)*L*Ns*tan(Beta));
% disp(FRL)
% Total frctional power loss.
% disp(' Total friction power loss');
    TOFR = abs(FRco+FRL);
% disp(TOFR)

% Total power.
```

```
% disp(' Total power');
 Tpor= ToPW+TOFR+WSH;
% disp(Tpor)

% Minimum draw stress.
% disp('Minimum draw stress');
 Ds= 0.6*(Tpor/(V2*pi*(EqR2^2)));
% disp(Ds)

QQ(1)=EQ;QQ(2)=FR;QQ(3)=ToPW;QQ(4)=WSH;QQ(5)=TOFR;QQ(6)=Ds;
disp (QQ);
ttoy=0;ffoy=0;
   end;
  end;
 end;
end
```

%   -------*** END OF MAIN PROGRAM ***---------

*** SUB. latest ***

% To find the experimental mean-strain rate using Atkins formula.

```
%                     *******************
     str(1:50)=zeros(1:50);OSIG(1:50)=zeros(1:50);RO1(1:50)=zeros(1:50);
 DT(1:50)=zeros(1:50);DF(1:50)=zeros(1:50);Tstt(1:50)=zeros(1:50);
 Tstr(1:50)=zeros(1:50);NT(1:50)=zeros(1:50);SIGMA(1:50)=zeros(1:50);
 TTT(1:50)=zeros(1:50);TT=TTt;MAT=1;tstr(1:50)=zeros(1:50);
 Str(1:50)=zeros(1:50);
%                     *******************

 Mst=(V2*tan(EQA)*((1-Rd*0.01)+sqrt(1-Rd*0.01)))/EqR2;

disp('Mean Experimental strain rate');Mst
TOYm=0;AVYm=0;TTOY=0;
```

% To divide the distance between RO and RO2 into increments and subt. from RO
to
% obtain RO1
```
 disp('Test temperature is ');TT

for ii =3:inc+2;

 AM=0;BM=0;
 Dst=RO-RO2;
 INC=Dst/inc;
 R01(ii-1)=RO-(INC*(ii-2));
 Ff=R01(ii-1)^3;
 V6=(V1*(RO^3)*cos(T*Te)*jj);
 V7=sqrt(3)*Ff*cos(TP*Te);
 V9=V6/V7;
```

```matlab
% computing the theoretical mean strain rate.
%disp('Theortical mean strain rate')
  Tstt=V9;
% computing the theoretical mean strain.

        Ff1=R01(ii-1);
        T1= log(RO/Ff1);
        T2= jj*cos(Zeta)*cos(FiT);
        T3=T1*T2/sqrt(3);
%disp('theoretical mean strain')
  Tstr(ii-1)= ((1*log(RO/Ff1))*(jj*cos(Zeta)*cos(FiT)))/sqrt(3);
  tstr=Tstr(ii-1);
  str(ii-1)= Tstr(ii-1)-Tstr(ii-2);
  Str=str(ii-1);
% call subroutine to decide on which material to used.

  DATA1;

% Temperature rise due to deformation.
%  disp('flow stress');
%  CM= specific heat in J/kg k;
%  RM= density in kg/m^3;
%  JM= conversion factor between mechanical and thermal energies (=1);

DT(ii-1)= (0.5*(OSIG(ii-1)+OSIG(ii-2))*1000000*str(ii-1))/(CM*JM*RM);

% Temperature increase due to friction. assuming that the centroids
% of the outer band acts as a point of contact between workpiece and die;to reduce
% calculations.then

if i==CB-1;

  EQA1=EQA-(EQA/(CB-1));
  Df1=3*FR*0.5*(OSIG(ii-1)-OSIG(ii-2))*1000000*sin(EQA)*tan(pi/Ns);
  Df2=(RO^2-RO1(ii-1)^2)*INC;
  Df3=4*pi*sqrt(3)*CM*JM*RM*(cos(EQA1)-cos(EQA));
  Df4=(RO^3-RO1(ii-1)^3);

  DF(ii-1)=(Df1*Df2)/(Df3*Df4);

      % if DF(ii-1)<0;
  %           DF=0;
  % else end;

  NT(ii-1)=DT(ii-1)+DF(ii-1)+TT;
  TTT(ii-1)=DT(ii-1)+DF(ii-1);
  TT=NT(ii-1);

  else

% The new temperature taking into consideration deformation temperature rise due
to.

  NT(ii-1)=DT(ii-1)+TT;
  TT=NT(ii-1);

  end;
```

% The new temperature taking into consideration temperature rise due todeformation % and friction.

```
 TT=NT(ii-1);
```

% To find the new flow stress with the increased temperature

```
  DATA1;

  SIGMA(ii-1)= OSIG(ii-1);
  TT=NT(ii-1);
% disp('new flow stress')
  Ym= SIGMA(ii-1);
  BM(ii-1)=SIGMA(ii-1);
% TOYm= TOYm+BM
% disp('Ym');Ym;
end;
```

% call subroutine integration.

```
 Integration1;
```

%   *** SUB. defsub ***

% subroutine to calculate the deformation parameters;

```
        R11=sqrt(E^2+F^2);
        R22=sqrt(XE^2+XF^2);;
        Tet1=asin(R11/RO);
        DA=RO*(1-cos(EQA));
        Dth1=RO*(cos(Tet1)-cos(EQA));
        Fi2=atan(XE/XF);
        Bet2=2*Beta;

           if Fi2>Beta
              Dth2=DA*(DL/(2*cos(Bet2-Fi2))-R22)/R22;
           else
              Dth2=DA*(DL/(2*cos(Fi2))-R22)/R22;
           end;

        Fi1=atan(E/F);
        FiT=Fi1-Fi2;
        Zs=Ldie+Dth1-Dth2;
% The length of the path of flow in die zone.

        Zts=sqrt((E-XE)^2+(F-XF)^2+Zs^2);
        ZR=sqrt((R11-(R22*cos(FiT)))^2+Zs^2);
        Zeta=atan((R22*sin(FiT))/ZR);
        Tet2=atan((R11-(R22*cos(FiT)))/Zs);
        DAL1=G/cos(T*Tet1);
        cki=abs(Tet2-Tet1);
        Te=Tet1;
        TL=cos(T*Te)/cos(TP*Te);
% To find R(t) for the friction calcuations.

        Ffac=cos(T*Te)/(cos(Zeta)*cos(cki)*cos(TP*Te));
```

315

```
      Rt=Rt+Ffac;
   aa = 8;
   ab = (TP*tan(TP*Te)-T*tan(T*Te));
   bb = 2*(1+(tan(cki)*(ab^2)));
   bc = 1+tan(cki)*(1/tan(Te));
   cc = 2*(bc^2);
   dd = ((TP*tan(TP*Te)-3*tan(cki)-T*tan(T*Te))^2);
   ee = ((TP*tan(TP*Te)-T*tan(T*Te)-(1/tan(Te)))^2);
   ff = 3*((tan(Zeta))^2)*(1/(cos(cki))^2);
   gg = abs(aa+bb+cc+dd+ee-ff);
   jj = sqrt(gg);
```

```
%                                              *** SUB. Mishear ***
```

```
% This subroutine to find the minimum shear factor.
   R11=sqrt(E^2+F^2);
   R22=sqrt(XE^2+XF^2);
   Tet1=asin(R11/RO);
   DA=RO*(1-cos(EQA));
   Dth1=RO*(cos(Tet1)-cos(EQA));
   Fi2=atan(XE/XF);
   Bet2=2*Beta;

     if Fi2>Beta
        Dth2=DA*(DL/(2*cos(Bet2-Fi2))-R22)/R22;
     else
        Dth2=DA*(DL/(2*cos(Fi2))-R22)/R22;
     end;

   Fi1=atan(E/F);
   FiT=(Fi1)-(Fi2);
   Zs=((Ldie)+(Dth1)-(Dth2));
% The length of the path of flow in die zone.

   Zts=sqrt((E-XE)^2+(F-XF)^2+Zs^2);
   ZR=sqrt((R11-(R22*cos(FiT)))^2+Zs^2);
   Zeta=atan((R22*sin(FiT))/ZR);
   Tet2=atan((R11-(R22*cos(FiT)))/Zs);
   DAL1=G/cos(T*Tet1);
   cki=abs(Tet2-Tet1);
   ws1=(cos(T*Tet1)*tan(Zeta)/(cos(TP*Tet1)*cos(cki)))^2;
   ws2=(cos(T*Tet1)*tan(cki)-sin(T*Tet1)+cos(T*Tet1)*tan(TP-Tet1))^2;
   WS1=sqrt(ws1+ws2);
   WS2=WS1*DAL1*2/sqrt(3);
   WST=WST+WS2;
```

```
%                                          *** SUBROUTINE  DATA1 ***
```

```
% Subroutine to choose which material to be used
% finding the flow stress.

if MAT==1;
   MILD1;
else if MAT==2;
   BORON1;
else if MAT==3;
   MEDIUM1;
end;
```

```
         end;end;

%                              *** SUB. Integration1 ***

% to the value of the flow stress.
MM=0;
for ii=3:inc+2
   (Tstr(ii-1));
    (str(ii-1));
    (OSIG(ii-1));
  end;

Tstr(inc+1);
 for ii=3:inc+2
   mm=0;
    mm = (OSIG(ii-1)*str(ii-1))/Tstr(inc+1);
    MM = mm+MM;
end;

AVYM=MM;


%                    *** DATA FILE FOR BORON STEEL***

% This is the data file for boron steel with temperature below 200.
   ii=ii-1;
   if TT<= 200
% disp('Temperature is 200 degs or less');

if Tstr(ii) <= 0.2;
   OSIG(ii) = 413+(.63*TT)-(6*0.0001*TT^2);
  else if Tstr(ii) <= 0.3;
   OSIG(ii) = 583+(0.4*TT)-(0.002*TT^2);
  else if Tstr(ii) <= 0.4;
   OSIG(ii) = 622+(0.4*TT)-(0.002*TT^2);
  else if Tstr(ii) <= 0.5;
   OSIG(ii) = 659+(0.1*TT)-(9.03*0.0001*TT^2);
  else if Tstr(ii) <= 0.6;
   OSIG(ii) = 656+(0.5*TT)-(0.003*TT^2);
  else if Tstr(ii) <= 0.7;
  OSIG(ii) = 664+(0.6*TT)-(0.003*TT^2);
  else if Tstr(ii) <= 0.8;
   OSIG(ii) = 693+(0.2*TT)-(0.002*TT^2);
  else if Tstr(ii) <= 0.9;
  OSIG(ii) = 704+(0.3*TT)-(0.002*TT^2);
  else if Tstr(ii) > 0.9;
  OSIG(ii) = 717+(0.6*TT)-(0.003*TT^2);

end;
 end;end;end;end;end;end;end;end;

% disp('flow stress');OSIG(ii)
  ii=ii+1;
% This is the data file for boron steel with temperature above 700 degs.

  else if TT> 700
% disp('Temperature is above 700 degs ');
```

317

```
if Tstr(ii) <= 0.2;
  OSIG(ii) = 380-0.4*TT;
  else if Tstr(ii) <= 0.3;
  OSIG(ii) = 2961-(7.6*TT)+(0.005*TT^2);
  else if Tstr(ii) <= 0.4;
  OSIG(ii) = 150-0.1*TT;
  else if Tstr(ii) <= 0.5;
  OSIG(ii) = 731-0.85*TT;
  else if Tstr(ii) <= 0.6;
  OSIG(ii) = 731-0.85*TT;
  else if Tstr(ii) > 0.6;
  OSIG(ii) = 731-0.85*TT;

end;
 end;end;end;end;end;
% disp('flow stress');OSIG(ii)
 ii=ii+1;


% This is the data file for boron steel with temperature above 450 degs.

 else if TT> 450
% disp('Temperature is above 450 degs ');

if Tstr(ii) <= 0.2;
  OSIG(ii) = 1023-1.3*TT;
  else if Tstr(ii) <= 0.3;
  OSIG(ii) = 2961-(7.6*TT)+(0.005*TT^2);
  else if Tstr(ii) <= 0.4;
  OSIG(ii) = 4225-(11.4*TT)+(0.0078*TT^2);
  else if Tstr(ii) <= 0.5;
  OSIG(ii) = 731-0.85*TT;
  else if Tstr(ii) <= 0.6;
  OSIG(ii) = 1111-1.4*TT;
  else if Tstr(ii) > 0.6;
  OSIG(ii) = 1111-1.4*TT;
end;
 end;end;end;end;end;

% disp('flow stress');OSIG(ii)
 ii=ii+1;

 else if TT> 200
% disp('Temperature is above 200 degs and less than 450 degs');

if Tstr(ii) <= 0.2;
  OSIG(ii) = 413+(.63*TT)-(6*0.0001*TT^2);
  else if Tstr(ii) <= 0.3;
  OSIG(ii) = 447+(0.85*TT)-(0.001*TT^2);
  else if Tstr(ii) <= 0.4;
  OSIG(ii) = 467+(0.97*TT)-(0.001*TT^2);
  else if Tstr(ii) <= 0.5;
  OSIG(ii) = 572+(0.5*TT)-(5.5*0.0001*TT^2);
  else if Tstr(ii) <= 0.6;
  OSIG(ii) = 489+(1.1*TT)-(0.002*TT^2);
  else if Tstr(ii) <= 0.7;
  OSIG(ii) = 494+(1.1*TT)-(0.0015*TT^2);
```

```
  else if Tstr(ii) <= 0.8;
   OSIG(ii) = 510+(1.1*TT)-(0.0016*TT^2);
  else if Tstr(ii) <= 0.9;
   OSIG(ii) = 524+(1.1*TT)-(0.0016*TT^2);
  else if Tstr(ii) > 0.9;
   OSIG(ii) = 524+(1.1*TT)-(0.0016*TT^2);

end;
 end;end;end;end;end;end;end;end;end;

% disp('flow stress');OSIG(ii)
 ii=ii+1;
end;end;end;
```

%   *** DATA FILE FOR MEDIUM CARBON STEEL***

```
% This is the data file for medium steel with temperature below 200.
 ii=ii-1;
 if TT<= 200
 %disp('Temperature is 200 degs or less');

if Tstr(ii) <= 0.2;
  OSIG(ii) = 697-(0.03*TT)-(5.6*0.0001*TT^2);
 else if Tstr(ii) <= 0.3;
  OSIG(ii) = 664+(0.1*TT)-(3.2*0.0001*TT^2);
 else if Tstr(ii) <= 0.4;
  OSIG(ii) = 715+(0.8*TT)-(0.003*TT^2);
 else if Tstr(ii) <= 0.5;
  OSIG(ii) = 762+(0.08*TT)-(2.8*0.00001*TT^2);
 else if Tstr(ii) <= 0.6;
  OSIG(ii) = 792+(0.06*TT)-(1.5*0.0001*TT^2);
 else if Tstr(ii) <= 0.7;
 OSIG(ii) = 804+(0.08*TT)-(2.2*0.0001*TT^2);
 else if Tstr(ii) <= 0.8;
  OSIG(ii) = 829-(0.03*TT)-(1.3*0.0001*TT^2);
 else if Tstr(ii) <= 0.9;
 OSIG(ii) = 848*10^(-9.7*0.00001*TT);
 else if Tstr(ii) > 0.9;
 OSIG(ii) = 848*10^(-9.7*0.00001*TT);

end;
 end;end;end;end;end;end;end;end;

% disp('flow stress');OSIG(ii),
 ii=ii+1;

% This is the data file for medium steel with temperature above 700 degs.

 else if TT> 700

% disp('Temperature is above 700 degs ');

if Tstr(ii) <= 0.2;
  OSIG(ii) = 255-0.26*TT;
 else if Tstr(ii) <= 0.3;
  OSIG(ii) = 682-0.82*TT;
 else if Tstr(ii) <= 0.4;
```

```
 OSIG(ii) = 591-0.69*TT;
 else if Tstr(ii) <= 0.5;
 OSIG(ii) = 574-0.6*TT;
 else if Tstr(ii) <= 0.6;
 OSIG(ii) = 204-0.17*TT;
 else if Tstr(ii) > 0.6;
 OSIG(ii) = 204-0.17*TT;

end;
 end;end;end;end;end;
% disp('flow stress');OSIG(ii)
 ii=ii+1;


% This is the data file for medium steel with temperature above 450 degs.

 else if TT> 450

% disp('Temperature is above 450 degs ');

if Tstr(ii) <= 0.2;
 OSIG(ii) = 255-(0.26*TT);
 else if Tstr(ii) <= 0.3;
 OSIG(ii) = 3541-(9.5*TT)+(0.006*TT^2);
 else if Tstr(ii) <= 0.4;
 OSIG(ii) = 4018-(10.9*TT)+(0.008*TT^2);
 else if Tstr(ii) <= 0.5;
 OSIG(ii) = 4176-(11.4*TT)+(0.008*TT^2);
 else if Tstr(ii) <= 0.6;
 OSIG(ii) = 3766-(10*TT)+(0.007*TT^2);
 else if Tstr(ii) > 0.6;
 OSIG(ii) = 3766-(10*TT)+(0.007*TT^2);

end;
 end;end;end;end;end;
% disp('flow stress');OSIG(ii)
 ii=ii+1;

 else if TT> 200
% disp('Temperature is above 200 degs and less than 450 degs');

if Tstr(ii) <= 0.2;
 OSIG(ii) = 764-(0.99*TT)+(0.002*TT^2);
 else if Tstr(ii) <= 0.3;
 OSIG(ii) = 782-(1.01*TT)+(0.002*TT^2);
 else if Tstr(ii) <= 0.4;
 OSIG(ii) = 1142-(3*TT)+(0.006*TT^2);
 else if Tstr(ii) <= 0.5;
 OSIG(ii) = 1142-(2.9*TT)-(0.0059*TT^2);
 else if Tstr(ii) <= 0.6;
 OSIG(ii) = 780+(0.095*TT)-(5*0.00001*TT^2);
 else if Tstr(ii) <= 0.7;
 OSIG(ii) = 804+(0.03*TT);
 else if Tstr(ii) <= 0.8;
 OSIG(ii) = 829-(0.03*TT)-(1.3*0.0001*TT^2);
 else if Tstr(ii) <= 0.9;
 OSIG(ii) = 848*10^(-9.7*0.00001*TT);
 else if Tstr(ii) > 0.9;
```

```
      OSIG(ii) = 848*10^(-9.7*0.00001*TT);

end;
 end;end;end;end;end;end;end;end;end;

% disp('flow stress');OSIG(ii),
  ii=ii+1;
end;end;end;
```

%   *** DATA FILE FOR MILD STEEL***

```
% This is the data file for mild steel with temperature below 200.
  ii=ii-1;
  if TT<= 200
% disp('Temperature is 200 degs or less');

if Tstr(ii) <= 0.2;
  OSIG(ii) = 454+(0.04*TT)-(7.8*0.0001*TT^2);
 else if Tstr(ii) <= 0.3;
  OSIG(ii) = 478+(0.4*TT)-(0.003*TT^2);
 else if Tstr(ii) <= 0.4;
  OSIG(ii) = 504+(0.6*TT)-(0.004*TT^2);
 else if Tstr(ii) <= 0.5;
  OSIG(ii) = 527+(0.5*TT)-(0.003*TT^2);
 else if Tstr(ii) <= 0.6;
  OSIG(ii) = 528+(0.7*TT)-(0.0004*TT^2);
 else if Tstr(ii) <= 0.7;
 OSIG(ii) = 551+(0.5*TT)-(0.003*TT^2);
 else if Tstr(ii) <= 0.8;
  OSIG(ii) = 569+(0.5*TT)-(0.003*TT^2);
 else if Tstr(ii) <= 0.9;
 OSIG(ii) = 588+(0.4*TT)-(0.003*TT^2);
 else if Tstr(ii) > 0.9;
 OSIG(ii) = 588+(0.4*TT)-(0.003*TT^2);

end;
 end;end;end;end;end;end;end;end;

% disp('flow stress');OSIG(ii),
  ii=ii+1;
% This is the data file for mild steel with temperature above 700 degs.

  else if TT> 700
% disp('Temperature is above 700 degs ');


if Tstr(ii) <= 0.2;
  OSIG(ii) = 80-0.051*TT;
 else if Tstr(ii) <= 0.3;
  OSIG(ii) = 85-0.051*TT;
 else if Tstr(ii) <= 0.4;
  OSIG(ii) = 90-0.051*TT;
 else if Tstr(ii) <= 0.5;
  OSIG(ii) = 95-0.051*TT;
 else if Tstr(ii) <= 0.6;
  OSIG(ii) = 100-0.051*TT;
 else if Tstr(ii) > 0.6;
```

```
    OSIG(ii) = 100-0.051*TT;

end;
 end;end;end;end;end;
% disp('flow stress');OSIG(ii)
 ii=ii+1;


% This is the data file for mild steel with temperature above 450 degs.
 else if TT> 450
% disp('Temperature is above 450 degs ');

if Tstr(ii) <= 0.2;
  OSIG(ii) = 2882-(7.49*TT)+(0.0049*TT^2);
 else if Tstr(ii) <= 0.3;
  OSIG(ii) = 2934-(7.6*TT)+(0.0049*TT^2);
 else if Tstr(ii) <= 0.4;
  OSIG(ii) = 3001-(7.7*TT)+(0.005*TT^2);
 else if Tstr(ii) <= 0.5;
  OSIG(ii) = 3193-(8.3*TT)+(0.0055*TT^2);
 else if Tstr(ii) <= 0.6;
  OSIG(ii) = 3214-(8.3*TT)+(0.0055*TT^2);
 else if Tstr(ii) > 0.6;
  OSIG(ii) = 3214-(8.3*TT)+(0.0055*TT^2);

end;
 end;end;end;end;end;
% disp('flow stress');OSIG(ii)
 ii=ii+1;

else if TT> 200
% disp('Temperature is above 200 degs and less than 450 degs');

if Tstr(ii) <= 0.2;
  OSIG(ii) = 365*10^(4.48*0.0001*TT);
 else if Tstr(ii) <= 0.3;
  OSIG(ii) = -139+(4.2*TT)-(0.006*TT^2);
 else if Tstr(ii) <= 0.4;
  OSIG(ii) = -88+(3.9*TT)+(0.005*TT^2);
 else if Tstr(ii) <= 0.5;
  OSIG(ii) = -45+(3.8*TT)-(0.005*TT^2);
 else if Tstr(ii) <= 0.6;
  OSIG(ii) = -35+(3.8*TT)-(0.005*TT^2);
 else if Tstr(ii) <= 0.7;
 OSIG(ii) = 495*10^(2.4*0.0001*TT);
 else if Tstr(ii) <= 0.8;
  OSIG(ii) = 678*10^(-3*0.0001*TT);
 else if Tstr(ii) <= 0.9;
 OSIG(ii) = 695*10^(-3*0.0001*TT);
 else if Tstr(ii) > 0.9;
  OSIG(ii) = 695*10^(-3*0.0001*TT);
end;
 end;end;end;end;end;end;end;end;
% disp('flow stress');OSIG(ii),
 ii=ii+1;
end;end;end;

%                              END
```

```
10  REM "SECTION"
20  *FX16,3
30  REM *FX7,7
40  PRINT" INSTRUMENTATIN , DATA ACQUISITION "
50  PRINT"BY M.JORNAZ"
60  @%=&020205
70  X=0:Y=0:Z=0:W=0
80  REM-------------------------------------------------------------------
90  REM  SET UP A TABLE FOR VALUES FROM ANALOUGE TO DIGITAL
      CONVERTER TO TEST
100 REM  THE READINGS BEFORE THE ACTUAL TEST
110 REM-------------------------------------------------------------------
120 PRINT"-------------------------------------------------------------------"
130 PRINT"|"TAB(4)"K1"TAB(15)"TIME"TAB(27)"SPEED"TAB(41)"TEMPERATURE"
      TAB(58)" LOAD"TAB(72)":"
140 PRINT"|"TAB(72)"|"
150 PRINT"|"TAB(15)"Sec"TAB(28)"m/min"TAB(45)"deg"TAB(58)"kN"TAB(72)"|"
160 PRINT"-------------------------------------------------------------------"
170 TIME=0 : K1 = 1 : MX= 1.8/63250
180 X=ADVAL(1)*MX   : Y=ADVAL(2)*MX*1005 : Z=ADVAL(3)*MX
190PRINT"|"TAB(2)K1;TAB(9)"|"TAB(13)TIME/100;TAB(23)"|"TAB(25)X;TAB(39)"|"T
      AB(41)Y;TAB(55)"|"TAB(57)Z;TAB(72)"|"
200 delaytime=TIME+50
210 REPEAT
220 REM WAIT FOR 30 SECONDS
230 UNTIL TIME >=delaytime
240 K1=K1+1
250 IF TIME<1000 THEN GOTO 180
260 PRINT"-------------------------------------------------------------------"
270 INPUT"WOULD YOU LIKE TO REPEAT THAT AGAIN (Y/N) ";U$
280 IF U$="Y" GOTO 120
290 REM-------------------------------------------------------------------
300 REM  REAL TIME TESTING WILL START NOW.
310 REM-------------------------------------------------------------------
320 PRINT"
330 INPUT"FOR REAL TIME GRAPHICAL REPERASENTATION WITHOUT
      PRINTING   DATA (Y/N)" ;Q$
340 IF Q$="Y"   GOTO 2370
350 PRINT"'
360 INPUT"WOULD YOU LIKE TO START THE TEST NOW  (Y/N) ";A$
370 IF A$="N" THEN :PRINT":PRINT "UP DATING VALUES ":PRINT": GOTO 120
380 CLS
390 INPUT "ENTER TEST NUMBER ";TN : PRINT
400 INPUT  "* AMPLIFIER GAIN USED *";G
410 IF G= 100   THEN M= 14.4099
420 IF G= 200   THEN M= 7.5699
430 IF G= 500   THEN M= 2.8731
440 IF G= 1000  THEN M = 1.4361
450 TEMPG = 1005  : TACG = 4.59
460 PRINT
470 INPUT " IS THE BRIDGE BALLANCED ( Y/N )";J$
480 IF J$="N" THEN GOTO 460
490 REM***-------------------------------------------------------***
500 REM TEST RESULTES WILL BE RECORDED AFTER FIVE SECONDS FROM
      THE START
510 REM OF THE TESTING SO THAT STEADY STATE WILL BE REACHED.
520 REM***-------------------------------------------------------***
```

```
530 X=0:Y=0:Z=0:K1=1:X1=0:Y1=0:Z1=0
540 PROCLBL
550 HI=0: LOW=999999 : SLOW =LOW : CLOW =LOW :HIM=0:HIP=0 :SY=5
560 TIME=0   : MX=1.8/63250
570 REM IF TIME<500 GOTO 560
580 SOUND 1,-15,77,3
590 SOUND 1,-15,97,5
600 X=ADVAL(1)*MX*TACG
610 Y=ADVAL(2)*MX*TEMPG
620 Z=ADVAL(3)*MX*M
630  X1=X1+X : Y1=Y1+Y  :Z1=Z1+Z
640 REM NOW PRINT VALUES IN THE SCREEN
650 IF HI>X GOTO 670
660 HI= X
670 IF HIM>Y GOTO 690
680 HIM = Y
690 IF HIP>Z GOTO 710
700 HIP = Z
710 PROCSCROL
720 delaytime=TIME+50
730 REPEAT
740 REM WAIT FOR 30 SECONDS
750 UNTIL TIME >=delaytime
760 IF LOW<X GOTO 780
770 LOW = X
780 IF SLOW<Y GOTO 800
790 SLOW = Y
800 IF CLOW<Z GOTO 820
810 CLOW = Z
820 K1=K1+1  : SY=SY+1 : CY=CY+1
830 IF K1=18 OR K1=36 OR K1=52 THEN SY=5:PROCLBL:GOTO 600
840 IF TIME<1500 THEN GOTO 600
850
860 PRINT"-------------------------------------------------------------------------"
870 PRINT TAB(23)"HI  =",HI, :PRINT TAB(23)"LOW =",LOW
880 PRINT TAB(39) "HI  =",HIM, :PRINT TAB(39)"LOW =",SLOW
890 PRINT TAB(55)"HI  =" ,HIP , :PRINT TAB(55)"LOW =",CLOW
900 PRINT "K1";K1
910 PRINT"'
920 VEL=(X1/(K1-1))
930 LOD=(Z1/(K1-1))
940 TEM=(Y1/(K1-1))
950 VDU2
960 PRINT "           *** TEST NUMBER *** ",TN  :PRINT"
970 PRINT "The highest ,and lowest SPEED values recorded are  = "HI " , ";LOW
980 PRINT "The highest ,and lowest TEMP values recorded are = "HIM " , ";SLOW
990 PRINT "the highest, and lowest LOAD values recorded are = "HIP*1000 " , ";
    CLOW*1000
1000 PRINT
1010 PRINT"THE AVERAGE VALUE OF THE LOAD       = ";LOD*1000
1020 PRINT
1030 PRINT"THE AVERAGE VALUE OF THE SPEED      = ";VEL
1040 PRINT
1050 PRINT"THE AVERAGE VALUE OF THE TEMPREATURE  = ";TEM
1060  PRINT"'
1070 VDU3
1080  REM *****END OF DATA ACQUISITION AND EXPERIMENT*****
1090 REM *** READY TO PRINT DATA ON THE SCREEN ***
1100 REM ****** PRINTING OF DATA ON SCREEN ******
```

```
1110 PRINT'"
1120 INPUT"DO YOU WISH TO HAVE DATA PRINTED ON THE SCREEN (Y/N) ";A$
1130 IF A$="N"THEN  2210
1140 CLS
1150 PRINT
1160 PRINT"************INPUT THE FOLLOWING INFORMATION
     ************"
1170 PRINT
1180 REM ** THIS INFORMATION WILL INCLUDE ,MATERIAL USED,DIE
     MATERIAL&CODE,
1190 REM ** LUBRICANTE ,AND ALL OTHER PROCESS VARIABLES **
1200 INPUT  "* INPUT DATE OF TEST *"; DT  :  PRINT
1210 INPUT  "* WIRE MATERIAL TESTED *";W$  :  PRINT
1220 INPUT  "* LUBRICATION USED *"; LUB$  :  PRINT
1230 INPUT  "* REFERENCE No *"; RE$ : PRINT
1240 INPUT  "* DIE MATERIAL USED *";D$    :  PRINT
1250 INPUT  "* DIE SEMI-ANGLE (deg) *";DS  :  PRINT
1260 INPUT  "* BRIDGE SUPPLY TO LOAD CELL(v) *";B    :  PRINT
1270 INPUT  "* INITIAL DIAMETER OF WIRE (mm) *";D1   :  PRINT
1280 INPUT  "* IS IT SECTION DRAWING (Y/N) ", S$ : PRINT
1290 IF S$ ="Y" GOTO 1880
1300 INPUT  "* FINAL DIAMETER OF WIRE (mm) *";D2    :  PRINT
1310 CLS
1320 REM *** TO PRINT TEST DATA ***
1330 VDU2
1340 PRINT"            **** TEST DATD ****           " :PRINT"
1350 PRINT" DATE OF TEST IS---------------------------",DT
1360 PRINT
1370 PRINT" WIRE MATERIAL TESTED IS------------------",W$
1380 PRINT
1390 PRINT" LUBRICATION USED IS ---------------------",LUB$
1400 PRINT
1410 PRINT " REFERENCE No IS -------------------------",RE$
1420 PRINT
1430 PRINT" DIE MATERIAL USED IS --------------------",D$
1440 PRINT
1450 PRINT" DIE SEMI-ANGLE IS------------------------",DS " deg"
1460 PRINT
1470 PRINT" BRIDGE SUPPLY TO LOAD CELL IS ------------",B " v"
1480 PRINT
1490 PRINT" AMPLIEFIER SPAN USED IS ------------------",G
1500 PRINT
1510 PRINT" INITIAL DIAMETER OF WIRE IS --------------",D1 " mm"
1520 PRINT
1530 IF S$ = "Y" GOTO 1560
1540 PRINT" FINAL DIAMETER OF WIRE IS ---------------",D2 " mm"
1550 GOTO 1620
1560 PRINT " DIAGONAL LENGTH OF DIE ------------------",D3 " mm"
1570 PRINT
1580 PRINT " NUMBER OF SIDES IS ---------------------",NS
1590 PRINT
1600 VDU3
1610 GOTO 1920
1620 PRINT'"
1630 VDU3
1640 REM *** CALCULATING PARAMETERS ***
1650 PRINT
1660 REM R1,R2    I- INITIAL&FINAL RADII.
1670 REM RED      I- REDUCTION OF AREA.
```

325

```
1680 REM V1,V0    I- INLET&OUTLET VELOCITIES IN METERS PER MINUTE.
1690 REM ANG      I- THE DIE-SEMI ANGLE IN RADIANS.
1700 REM LOD,DST  I- THE DRAWING LOAD &THE DRAWING STRESS.
1710 REM STRR     I- THE STRNIN-RATE CALCULATED BY 'ATKINS FORMULA.
1720 REM TEM      I- THE DRAWING TEMPERATURE.
1730 REM TACG     I- TACHO-METER GRADIANT.
1740 REM TEMPG    I- TEMPRATURE GRANIANT.
1750 R1=D1/2 :  R2=D2/2
1760 RED =(R1^2-R2^2)/R1^2
1770 ANG =PI*DS/180
1780 REM *** TO CALCULATE THE VELOCITY THE AVERAGE VOLTAGE VALUE
     WILL BE ***
1790 REM *** MULTIPLIED BY A FACTOR WHICH IS THE GRADIANT OF THE
     TACHO- ***
1800 REM *** METER CALIBRATION GRAPH IN ORDER TO CONVERT TO m/s.
1810 V1=(R2/R1)^2*VEL
1820 REM *** TO CALCULATE THE DRAWING LOAD & HENCE THE DRAWING
     STRESS THE ***
1830 REM *** THE AVERAGE VOLTAGE VALUE IS CONVERTED TO KN &
     KN/mm^2 RESPT.***
1840 DST  = LOD/(R2^2*PI)
1850 STRR=VEL*TAN(ANG)*(1-RED*0.01+(1-RED*0.01)^0.5)/R2
1860 REM *** THE STRAIN-RATE IS CALCULATED USING ATKINS FORMULA
     ***
1870 GOTO 2000
1880 INPUT "* DIAGONAL LENGTH OF DIE IN (mm) IS *";D3 : PRINT
1890 INPUT "* NUMBER OF SIDES IS *";NS  : PRINT
1900 GOTO 1310
1910  PRINT"'
1920 B = PI/NS
1930 A1 = (PI*D1^2)/4
1940 A2 =(( D3^2* SIN(2*B))/8)*NS
1950 RED = (A1-A2)/A1
1960 ANG = PI*DS/180
1970 V1 = (A2/A1)*VEL
1980 DST = LOD/A2
1990 REM *** THE SAME PROCEDURE FOR THE DRAWING TEMPERATURE ***
2000 CLS
2010 PRINT"*** PRESS "Y" AND RETURN FOR SUBSEQUENT VALUES ***"
2020 INPUT A$
2030 IF A$="" THEN GOTO 2030
2040 CLS
2050 VDU2
2060 PRINT"     *** HOT WIRE DRAWING TEST RESULTS ***" : PRINT"
2070 PRINT "THE INLET VELOCITY -----------------------",V1," m/min"
2080 PRINT
2090 PRINT "THE OUTLET VELOCITY----------------------",VEL," m/min"
2100 PRINT
2110 PRINT "THE REDUCTION IN AREA---------------------",RED*100," %"
2120 PRINT
2130 PRINT "THE DRAWING TEMPERATURE IS----------------",TEM," deg c"
2140 PRINT
2150 PRINT "THE DRAWING LOAD IS----------------------",LOD*1000,"N"
2160 PRINT
2170 PRINT "THE DRAWING STRESS IS---------------------",DST*1000," N/mm^2"
2180 PRINT
2190 IF S$="Y" GOTO 2210
2200 PRINT "THE MEAN STRAIN RATE IS-------------------",STRR/60," SEC^-1"
2210 PRINT
```

```
2220 VDU3 : GOTO 2520
2230 DEF PROCSCROL
2240 PRINT"l"TAB(2,SY)K1;TAB(9,SY)"l"TAB(13,SY)TIME/100;TAB(23,SY)"l"TAB
     (25,SY) X;TAB(39,SY)"l"TAB(41,SY)Y;TAB(55,SY)"l"TAB(57,SY)Z;TAB(72,SY)"l"
2250 ENDPROC
2260 DEF PROCLBL
2270 CLS
2280 VDU 28,0,31,79,5
2290 CLG:VDU 24,0;896;1270;1000;
2300 VDU5:MOVE10,1000:PRINT"---------------------------------------------------------------
     ---------"
2310 PRINT":"TAB(4)"K1"TAB(15)"TIME"TAB(27)"SPEED"TAB(41)"TEMPERATURE
     "TAB(60)"LOAD"TAB(72)":"
2320 PRINT":"TAB(72)":"
2330 PRINT":"TAB(15)"sec"TAB(28)"m/min"TAB(45)"deg"TAB(60)"kN"TAB(72)":"
2340 PRINT"------------------------------------------------------------------------"
2350 VDU4
2360 ENDPROC
2370 CLS
2380 REM ------- RLT MONITORING -------
2390 CLS:SC=400/65520 : FLAG=0 :KK=0 :TIME0=TIME
2400 DUR=50
2410 MODE4 : PROCAXIS
2420 TIMER=TIME+DUR:MI=0:TI=0:C2=0
2430 C2=C2+1:MI=MI+ADVAL(1):TI=TI+ADVAL(2)
2440 IF TIME<TIMER THEN GOTO 2440
2450 MI=MI/C2 : TI=TI/C2   :ABT=(TIME-TIME0)/100 :RLT=INT(ABT)
2460 IF FLAG=0 THEN SMT=RLT  ELSE SMT=RLT-60*KK
2470 XM=SMT*20+10 : XT=SMT*20+10 : YM=INT(MI*SC)+130 :
     YT=INT(TI*SC)+580
2480 VDU 5 : IF SMT<=1 THEN MOVE 10,YM
2490 DRAW XM,YM : MOVE XT-20,YT : DRAW XT,YT : MOVE XM,YM : VDU4
2500 IF XT>=1200 AND XM>=1200 THEN PROCAXIS:FLAG=1:KK=KK+1
2510 Q$=INKEY$(0) : IF Q$<>"Q" THEN GOTO 2420
2520 MODE3:CLS
2530 INPUT" WOULD YOU LIKE TO START AGAIN (Y/N) ";A$
2540 IF A$="Y" CLS : GOTO 120
2550 *FX3,4
2560 MODE3:CLS:END
2570 DEF PROCAXIS
2580 CLG:VDU 28,0,31,79,29:VDU 24,0;123;1279;1023;
2590 MOVE 10,130:DRAW 1250,130:MOVE 10,130:DRAW 10,550
2600 MOVE 10,580:DRAW 1250,580:MOVE 10,580:DRAW 10,1020:MOVE
     10,580:VDU 5
2610 MOVE 15,520:PRINT " SPEED M/MIN ":MOVE 950,170:PRINT"TIME (sec)"
2620 MOVE 15,1000:PRINT"LOAD (kN)" :MOVE 950,620:PRINT"TIME (sec)":VDU4
2630 ENDPROC
2640 END
>
```

END

Section : Hexagon

Material   mild steel   Die material   Tungsten carbide
Die semi cone angle : 12   Diagonal length of die : 4.5 mm
Drawing speed : 6 m/min

Lubrication : DAG 2543

Reduction of Area	Drawing Temperature deg	Drawing Load kN	Drawing Stress N/mm^2	Yield Stress N/mm^2	Maximum Stress N/mm^2	Remarks
	20	3.772	287	524	612	
	100	3.563	271	524	589	
	200	3.223	245	531	601	
	316	3.112	237	546	642	
27	400	2.813	214	583	692	
	500	2.928	223	561	669	
	595	2.542	193	487	608	
	700	1.91	144	480	608	
	800	1.326	101	472	608	
	20	5.544	421	479	612	
	100	5.345	406	494	614	
	271	4.449	338	494	644	
	311	4.51	342	524	669	
35	430	4.209	320	583	709	
	570	3.906	297	436	654	
	680	3.201	243	390	580	
	730	2.85	216	340	520	
	800	2.5	190	221	426	

Lubrication : MD 15

Reduction of Area	Drawing Temperature deg	Drawing Load kN	Drawing Stress N/mm^2	Yield Stress N/mm^2	Maximum Stress N/mm^2	Remarks
	20	4.078	310	516	590	
	100	3.85	293	536	598	
	200	3.46	263	554	620	
	374	3.157	240	590	693	
27	490	2.801	213	520	660	
	595	2.96	225	480	635	
	650	2.403	182	410	603	
	710	2.007	152	385	554	
	800	1.476	112	317	465	

Section : **Octagon**

Material : mild steel   Die material : Tungsten carbide
Die semi cone angle : 12   Diagonal length of die : 4.5 mm
Drawing speed : 6 m/min

Lubrication : DAG 2543

Reduction of Area	Drawing Temperature deg	Drawing Load kN	Drawing Stress N/mm^2	Yield Stress N/mm^2	Maximum Stress N/mm^2	Remarks
	20	3.21	224	495	576	
	80	3.026	211	473	570	
	162	2.559	179	454	566	
	238	2.619	183	481	580	
21	299	2.359	165	495	608	
	364	2.814	197	593	712	
	501	2.605	182	522	608	
	623	2.189	153	420	545	
	786	1.688	118	332	440	
	20	4.544	317	488	594	
	125	4.078	289	488	618	
	172	3.689	258	488	608	
	238	3.47	242	468	586	
29	370	3.626	253	590	695	
	453	3.943	275	529	663	
	520	3.498	244	508	622	
	587	3.376	236	440	559	
	726	1.879	131	305	440	

Lubrication : MD 15

	20	3.168	221	501	576	
	120	2.822	197	488	562	
	200	2.561	179	522	596	
	338	2.438	170	549	644	
21	441	2.478	173	542	650	
	540	2.1	147	490	590	
	615	1.902	133	406	569	
	780	1.288	90	352	501	

Section : Square

Material : mild steel   Die material : Tungsten carbide
Die semi cone angle : 12   Diagonal length of die : 4.5 mm
Drawing speed : 6 m/min   Conventional die

Lubrication : DAG 2543

Reduction of Area	Drawing Temperature deg	Drawing Load kN	Drawing Stress N/mm^2	Yield Stress N/mm^2	Maximum Stress N/mm^2	comment
36.34	20	3.428	338	-	-	
	100	3.35	330	-	-	
	200	3.226	318	-	-	
	280	3.142	310	-	-	
	400	3.136	309	-	-	
	500	2.7	266	-	-	
	570	2.615	258	-	-	
	630	2.465	243	-	-	
	760	1.385	137	-	-	
44	20	4.571	451	566	662	
	120	4.409	435	566	652	
	200	4.3	424	550	660	
	278	4.246	419	536	677	
	419	4.181	413	624	756	
	566	3.487	344	556	667	
	630	3.287	323	517	573	
	760	1.849	182	460	560	
	800					
50	20	-	-			
	90	5.006	494	546	622	
	120	5.336	527	570	650	
	180	4.127	408	613	751	
	250	4.35	430	580	701	
	330	4.763	470	536	671	
	480					
	560					
	750					

Appendix (A3.4)

Program for data acquision for torsion testing at elevated temperature

```
2 REM " TORSION "
3 MODE 3
5 DIM XTORQUE(1000),ANGLEZ(1000),ZTIME(1000)
10 REM HOT TORSION CONTROL PROGRAM
20 CLS
30 INPUT "DATE.";DATE$
40 PRINT
50 INPUT "EXPERIMENT No.";EPNO$
60 PRINT
70 PRINT "MATERIAL-1. MILD"
80 PRINT "       2. MED"
90 PRINT "       3. BORON"
100 MATERIAL$=GET$
110 A=ASC(MATERIAL$)
120 IF A<49 OR A > 52 THEN 100
140 GOSUB 3200
150 PRINT "STRAINRATE (DEGREES/MIN)"
160 PRINT "1. 3.5     3. 30"
170 PRINT "2. 10      4. 90"
180 STRAINRATE$=GET$
190 B=ASC(STRAINRATE$)
200 IF B<49 OR B>53 THEN 180
220 GOSUB 3300
230 INPUT "TEMPERATURE (CELSIUS)";TEMP$
240 PRINT "TEMP IS ";TEMP$;" DO YOU WISH TO RETYPE IT"
250 C$=GET$
260 IF C$="Y" THEN230
270 IF C$="N" THEN 290
280 GOTO 250
290 GOSUB 3000
300 PRINT "DO YOU WISH TO REDO THESE RESULTS"
310 B$=GET$
320 IF B$="Y" THEN 20
330 IF B$="N" THEN 345
340 GOTO 310
345 XREADING=ADVAL(1)
350 PRINT "THE TIME BETWEEN READINGS IS 10 SECONDS, DO YOU WISH TO
     ALTER THIS"
360 A$=GET$
370 IF A$="Y" THEN GOSUB 3400
380 IF A$="N" THEN ITERVAL=10.0
390 IF A$<>"Y" AND A$<>"N" THEN 360
400 CLS
410 PRINT "HIT A KEY TO START RECORDING RESULTS"
420 G$=GET$
430 GOSUB 2000
440 PRINT "TEST COMPLETED"
450 PRINT" HIT A KEY TO PRINT OUT RESULTS"
460 H$=GET$
470 CLS
480 GOSUB 6000
490 PRINT:PRINT
500 PRINT "DO YOU WISH TO CARRY OUT ANOTHER EXPERIMENT"
510 K$=GET$
```

```
520 IF K$="Y" THEN 50
530 IF K$="N" THEN 550
540 GOTO 510
550 END
2000 REM SUBROUTINE TO RECORD RESULTS FROM A/D CONVERTORS
2010 ANGLEZ=0:ANGLE=0:ANGLEX=0:ANGLEY=0
2015 R=0
2020 M=0
2025 VITERVAL=ITERVAL
2030 XTIME=TIME
2040 GOSUB 4500
2045 CLS
2047 PRINT"READING","TIME","TORQUE","ANGLE"
2050 M=M+1
2052 A=M-1
2053 ITERVAL=VITERVAL
2055 IF M<30 THEN ITERVAL=2.0
2060 XTORQUE=((ADVAL(1)-XREADING)/39.4652)*0.113
2070 XTORQUE(M)=XTORQUE
2080 ZTIME(M)=(TIME-XTIME)/100
2090 ANGLEZ(M)=ANGLE
2091 GOSUB 2500
2092 IF M<30 THEN 2098
2094 IF XTORQUE =0 THEN 2098
2096 IF XTORQUE < (XTORQUE(A)/10) THEN 2140
2097 IF M>70 AND XTORQUE<0.2 THEN 2140
2098 IF M=1000 THEN 2130
2100 IF N=1 THEN GOSUB 5000
2110 IF N=0 THEN GOSUB 5200
2120 GOTO 2050
2130 PRINT "OUT OF ARRAY"
2140 RETURN
2500 REM SUBRUOTINE TO PRINT RESULTS ON THE SCREEN
2510 PRINT M,ZTIME(M)," ",XTORQUE(M),ANGLEZ(M)
2520 RETURN
3000 CLS
3010 PRINT "DATE ";DATE$
3020 PRINT "EXPERIMENT No. ";EPNO$
3030 PRINT "MATERIAL ";MAT$
3040 PRINT "STRAINRATE ";RATE
3050 PRINT "TEMPERATURE ";TEMP$
3060 RETURN
3200 IF MATERIAL$="1" THEN MAT$="MILD"
3210 IF MATERIAL$="2" THEN MAT$="MED"
3220 IF MATERIAL$="3" THEN MAT$="BORON"
3230 RETURN
3300 IF STRAINRATE$="1" THEN RATE=3.5
3310 IF STRAINRATE$="2" THEN RATE=10
3320 IF STRAINRATE$="3" THEN RATE=30
3330 IF STRAINRATE$="4" THEN RATE=90
3340 RETURN
3400 INPUT "WHAT INTERVAL DO YOU REQUIRE IN SECONDS"; ITERVAL$
3410 INPUT "REPEAT INTERVAL";ITERVALX$
3420 IF ITERVAL$=ITERVALX$ THEN 3450
3430 PRINT "TWO DO NOT MATCH"
3440 GOTO 3400
3450 CHOP$=ITERVAL$
3460 GOSUB 4000
3470 IF F=1 THEN 3400
```
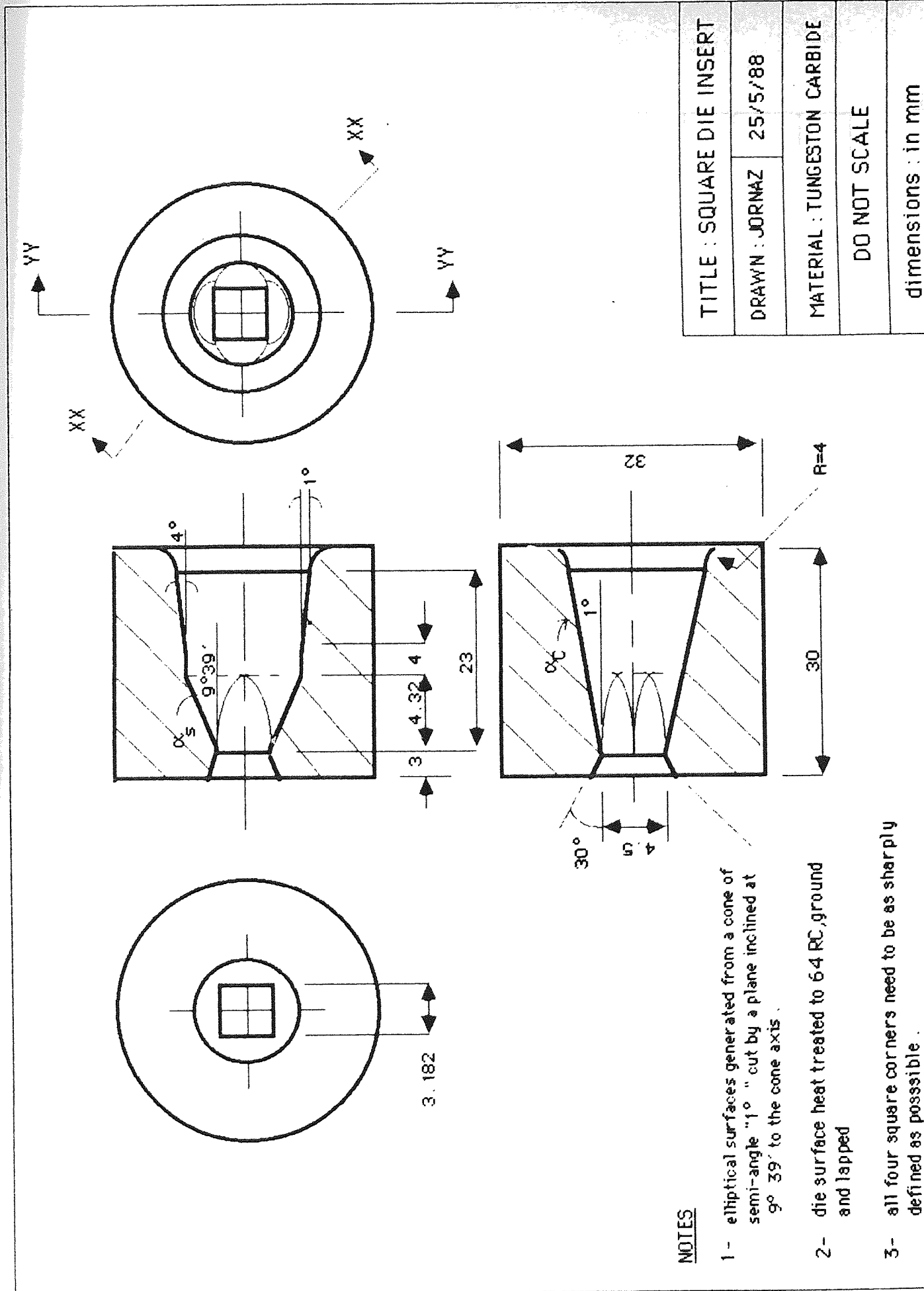
```
3480 ITERVALY$= "+"+ITERVAL$
3490 ITERVAL=VAL(ITERVALY$)
3500 RETURN
4000  D=LEN(CHOP$)
4010F=0
4020 FOR V= 1 TO D
4030 E$=MID$(CHOP$,V,1)
4040 E=ASC(E$)
4050 IF E<48 OR E>57 THEN F=1
4060 NEXT V
4070 IF F<>1 THEN 4080
4080 PRINT "INCORRECT, USE JUST NUMBERS"
4090 RETURN
4500 REM SUBROUTINE TO SET INITIAL POSITION OF ANGLE TRANSDUCER
4510 ANGLEX=ADVAL(2)
4520 IF ANGLEX<1000 THEN N=0
4530 IF ANGLEX>59000 THEN N=1
4535 IF ANGLEX>1000 AND ANGLEX<59000 THEN 4540
4538 GOTO 4573
4540 ANGLEY=ADVAL(2)
4550 IF ANGLEY=ANGLEX THEN 4540
4560 IF ANGLEY>ANGLEX THEN N=1
4570 IF ANGLEY<ANGLEX THEN N=0
4573 IF N=1 THEN ANGLEL=59000
4576 IF N=0 THEN ANGLEL=0
4580 RETURN
5000 ANGLEX=ADVAL(2)
5005 S=0
5008 IF ANGLEL<1000 THEN 5040
5010 IF ANGLEX<1000 THEN 5030
5015 GOSUB 5400
5018 IF S=1 THEN 5065
5020 GOTO 5000
5030 ANGLE=ANGLE+2
5040ANGLEX=ADVAL(2)
5045 ANGLEL=60000
5050IF ANGLEX>59000 THEN 5000
5055 GOSUB 5400
5058 IF S=1 THEN 5065
5060 GOTO 5240
5065 ANGLEL=ANGLEX
5070 RETURN
5200 ANGLEX=ADVAL(2)
5205 S=0
5208 IF ANGLEL>59000 THEN 5240
5210IF ANGLEX>59000THEN 5230
5215 GOSUB 5400
5218 IF S=1 THEN 5265
5220 GOTO 5200
5230 ANGLE=ANGLE+2
5240 ANGLEX=ADVAL(2)
5245 ANGLEL=0
5250 IF ANGLEX<1000THEN 5200
5255 GOSUB 5400
5258 IF S=1 THEN 5265
5260 GOTO 5240
5265 ANGLEL=ANGLEX
5270 RETURN
5400 IF M<30THEN 5450
```
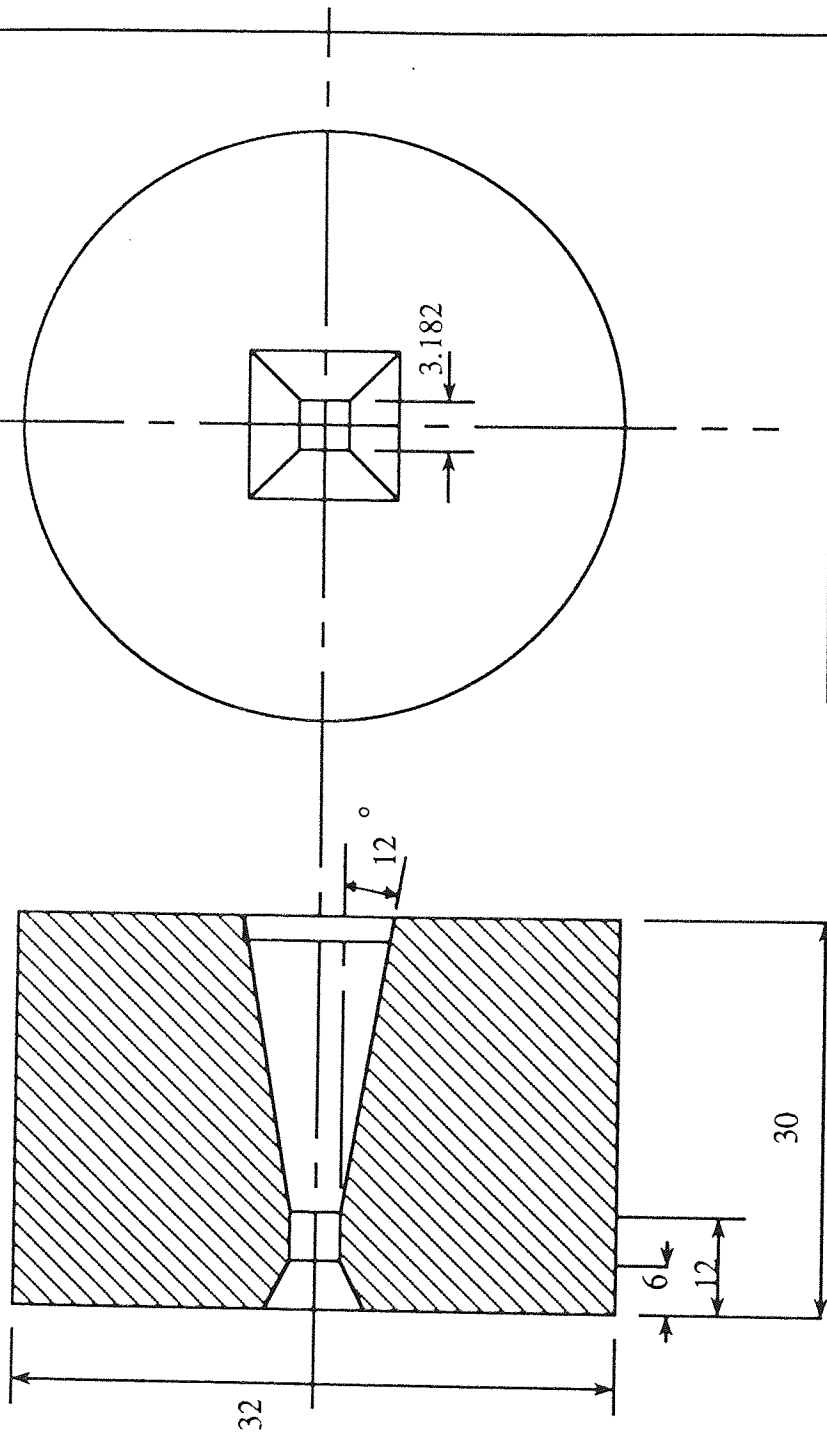
```
5410 X=((60+((M-29)*ITERVAL))/ITERVAL)
5420 R=((TIME-XTIME)/ITERVAL)/100
5430 IF R>X THEN S=1
5440 GOTO 5470
5450 R=((TIME-XTIME)/ITERVAL)/100
5460 IF R>M THEN S=1
5470 RETURN
6000 REM SUBROUTINE TO PRINT OUT RESULTS
6010 VDU2
6020 PRINT DATE$,,"EXP. No ";EPNO$
6030 PRINT "MATERIAL ";MAT$,,"STRAINRATE ";RATE
6040 PRINT "TEMPERATURE ";TEMP$
6050 PRINT:PRINT:PRINT
6060 PRINT "READING","TIME","TORQUE","ANGLE"
6070 FOR I = 1 TO M
6080 PRINT I,ZTIME(I)," ",XTORQUE(I),ANGLEZ(I)
6090 NEXT I
6100 VDU3
6110 RETURN
6120 END
>
```

APPENDIX A4

TECHNICAL DRAWINGS AND DRAW
PROCESS MATERIALS

NOTES

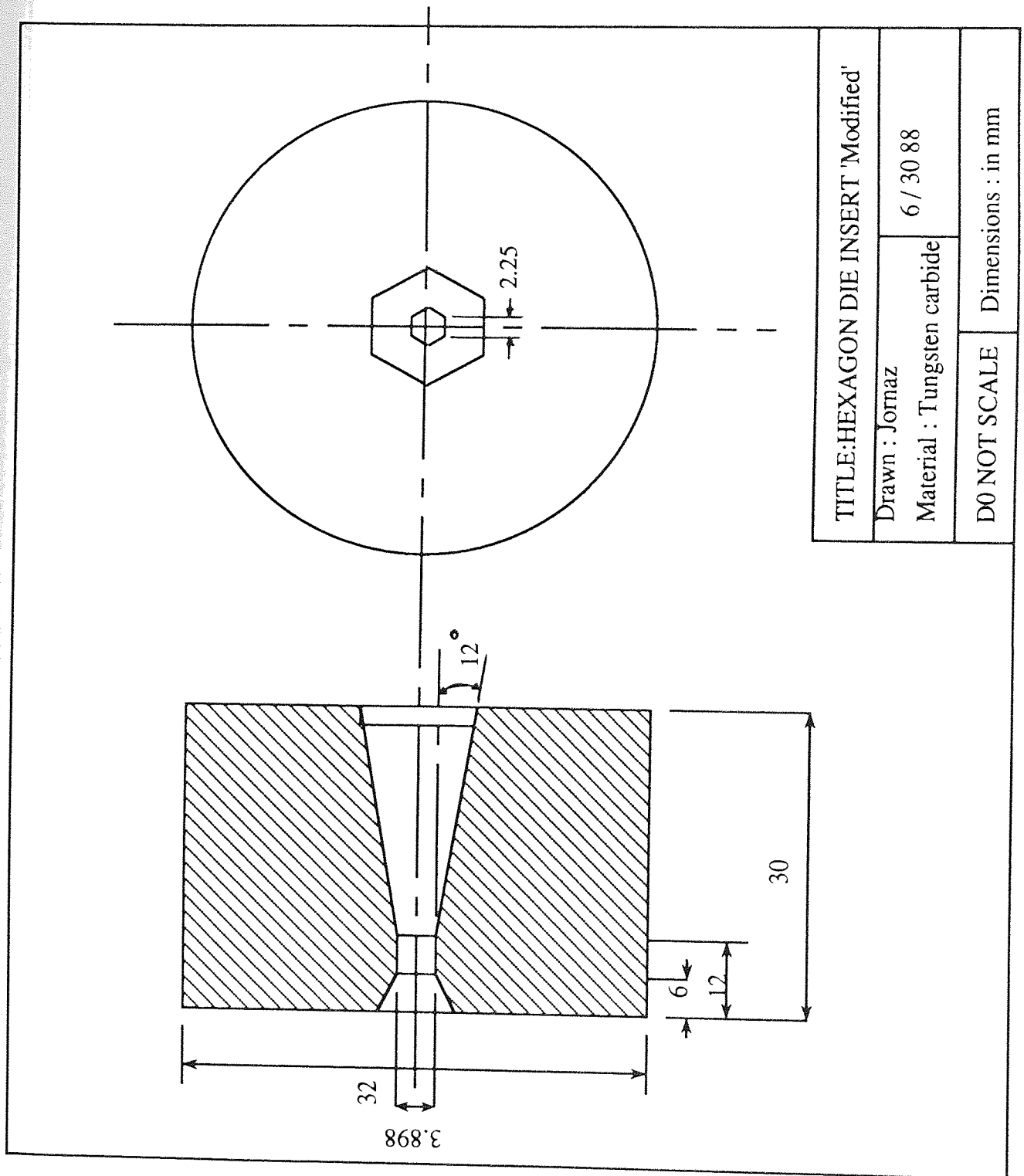1- elliptical surfaces generated from a cone of
   semi-angle "1°" cut by a plane inclined at
   9° 39' to the cone axis.

2- die surface heat treated to 64 RC, ground
   and lapped

3- all four square corners need to be as sharply
   defined as posssible.

335

TITLE : SQUARE DIE INSERT ' Modified'

Drawn : Jomaz | 6 / 30 88

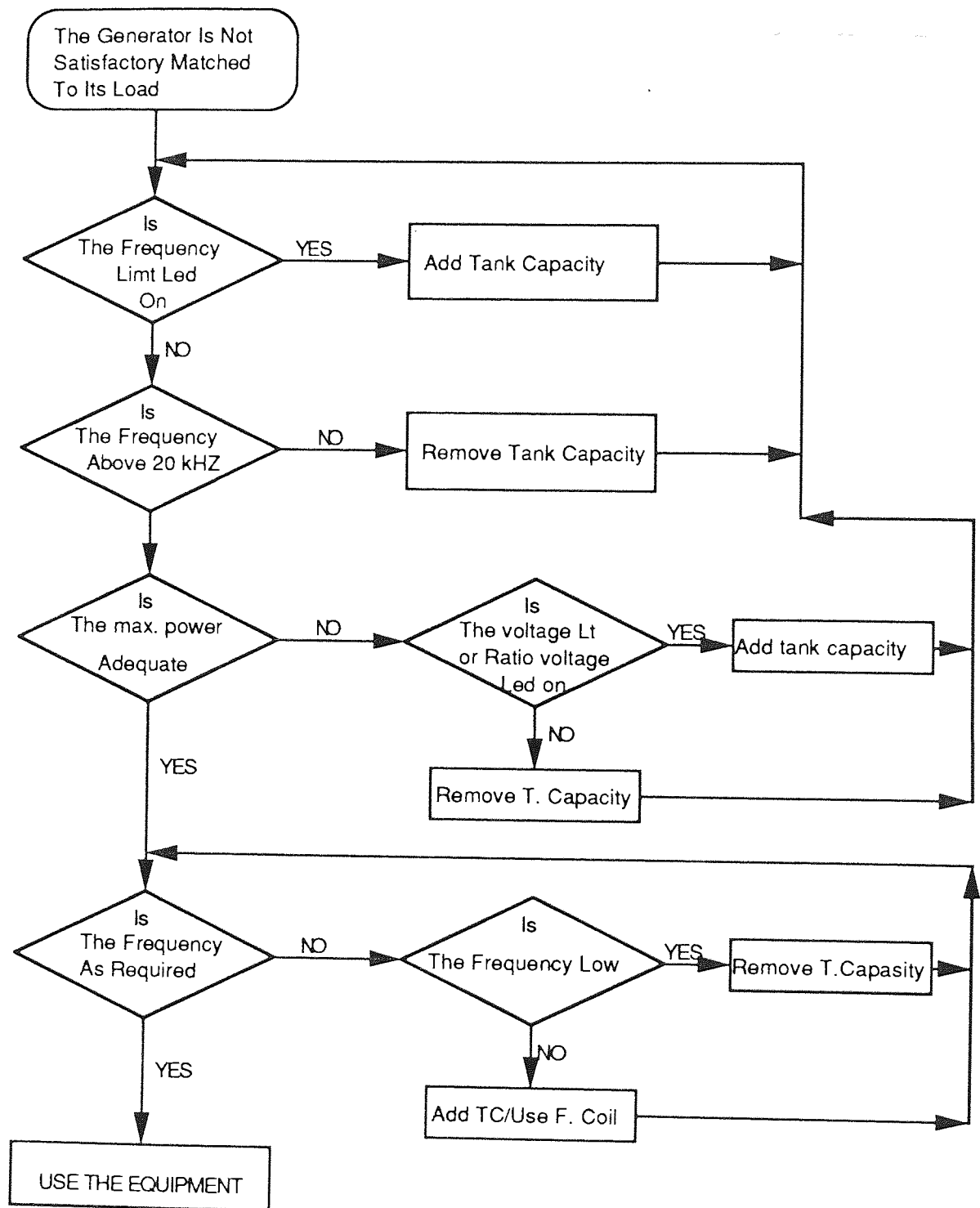Material : Tungsten carbide

DO NOT SCALE | Dimensions : in mm

3.182

12 °

32

30

12

6

3.182

12°

30

6
12

3.182
32

TITLE : SQUARE DIE INSERT 'Designed'

Drawn : Jornaz   9 / 30 88

Material : Tungsten carbide

DO NOT SCALE   Dimensions : in mm

337

TITLE:HEXAGON DIE INSERT 'Modified'

Drawn : Jornaz | 6 / 30 88

Material : Tungsten carbide

DO NOT SCALE | Dimensions : in mm

2.25

12°

30

6

12

32

3.898

2.25

12°

30

6

12

32

3.898

TITLE:HEXAGON DIE INSERT' Designed'

Drawn : Jornaz

Material:chromium carbide

6 / 30 88

Dimensions : in mm

DO NOT SCALE

Fig. A4.1. Flow diagram for matching the induction heater load.
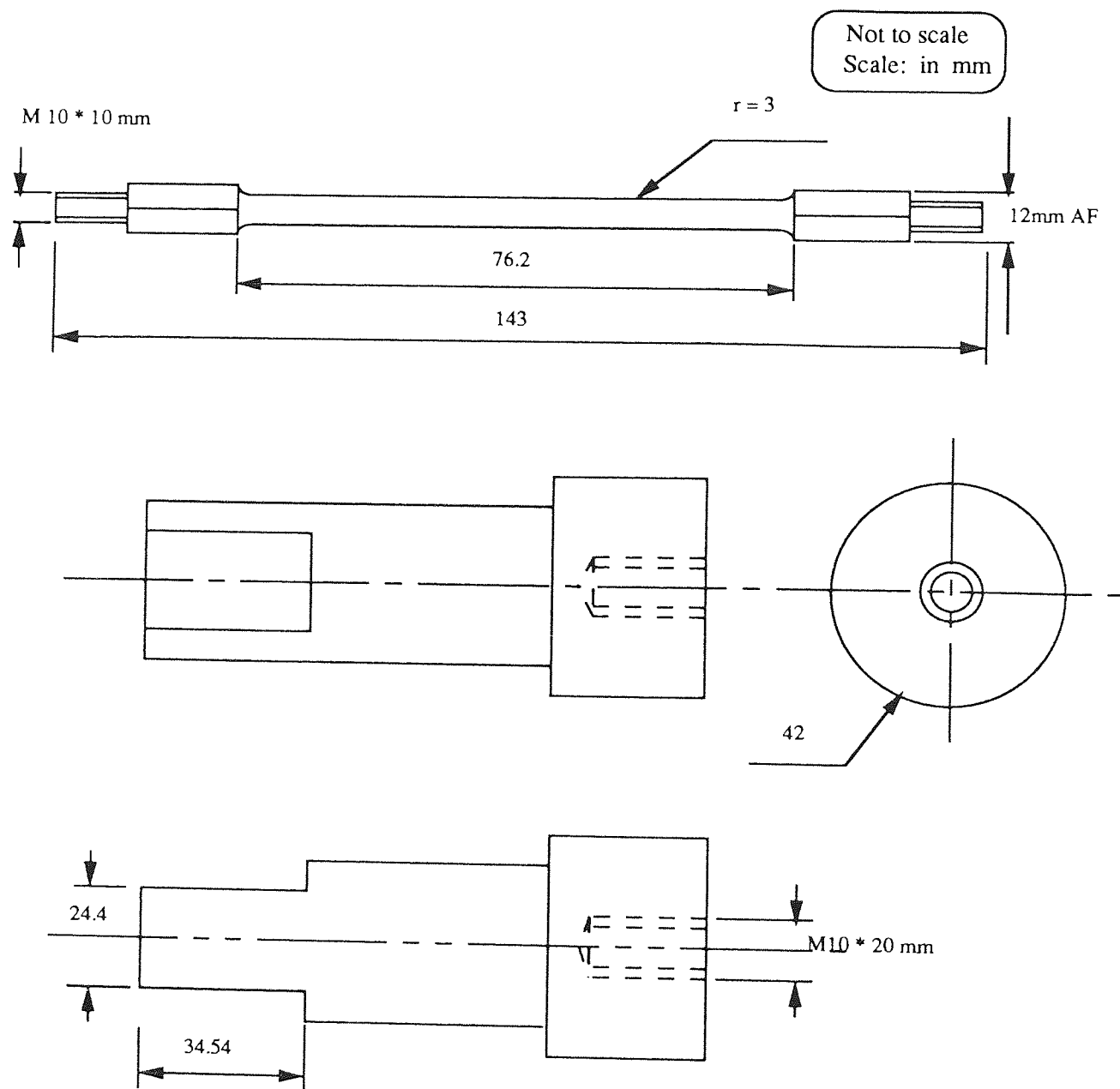
Fig. A4.2. Drawing of specimen and clamps used in torsion testing

LUBRICATION

- ## DAG 2543

Dispersion of graphite and inorganic salts in water which produces a dry coating capable of use at temperatures over 900°C, is clean and fume free in operation.

Physical Properties	Solid content	35%
	Viscocity	1000-1300 cps
	Density	1200 kg/m^3
	Carrier	Water
	Diluent	Water

- ## Moly Dag 15

Water-based MoS$_2$ lubricant for cold and semi-warm forming of alloy and non-alloy steels as well as titanium.

Product Data	Lubricating solid	MoS$_2$
	Soild content	32% by weight
	Carrier	Water
	Diluent	Water

- ## Moly Dag 709

Dry lubricant coating system giving adherent films of bonded molybdenum disulphide on metal surfaces

Product Data	Solids	50%
	Specific gravity	1.3
	Diluents	Xylene, toluene, white spirit, carbon tetrachloride.

DIE MATERIALS

- ## Syalon

is a member of the ceramic family and consists essentially of aluminium nitride, alumina and silicon nitride.

- ## Stellite 7

Co	Cr	WC	C
Bal	26	6	0.4

- ## Tungsten carbide

Co	WC
2.5-6.5	Bal

- ## Chromium carbide

Co	Cr	tungsten + molybdenum	C
Bal	25-32	4-25	1-3

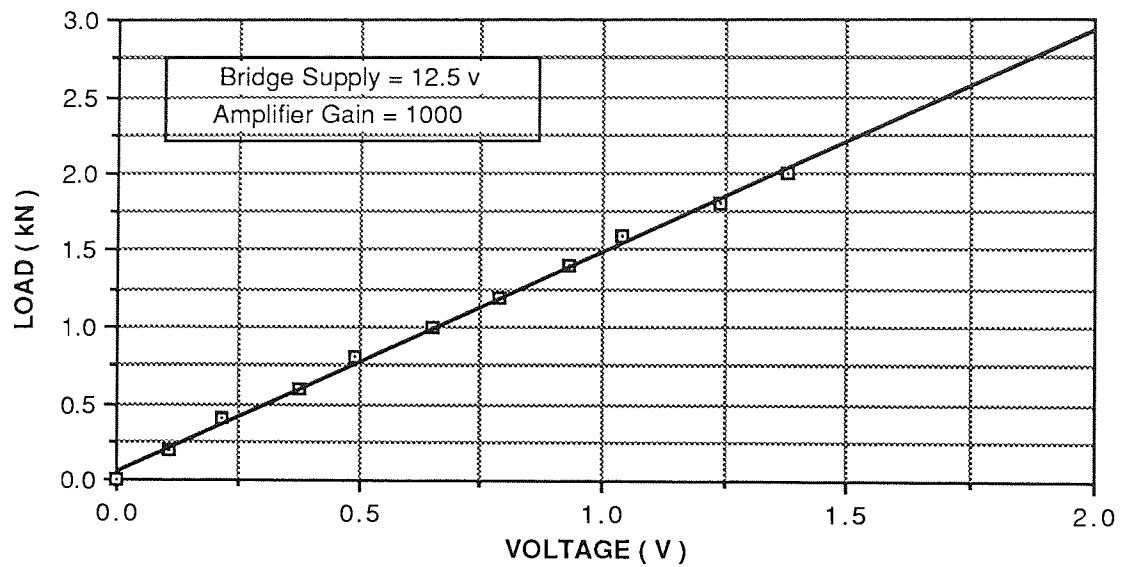# APPENDIX A5

CALIBRATION GRAPHS

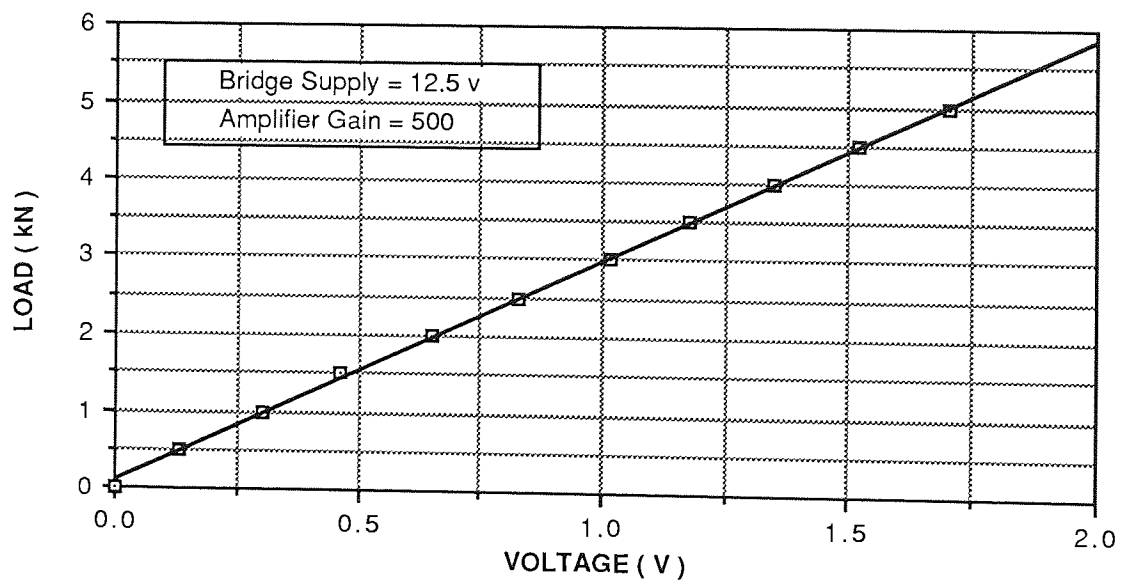Fig.A5.1. Calibration graph for loadcell (load range 0 -2 kN)

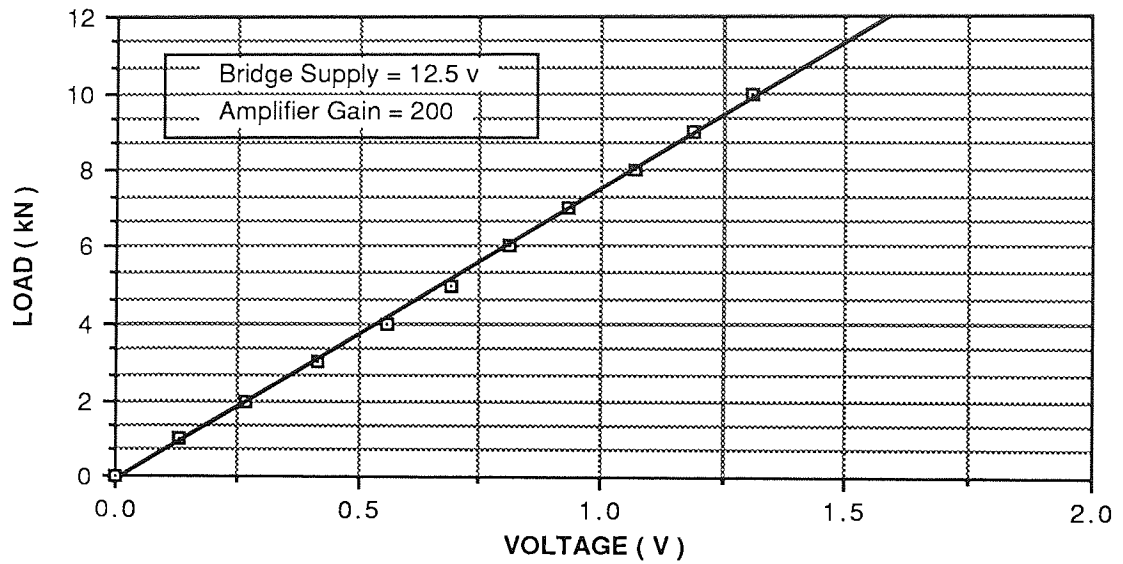Fig.A5.2. Calibration graph for loadcell (load range 0 -5 kN)

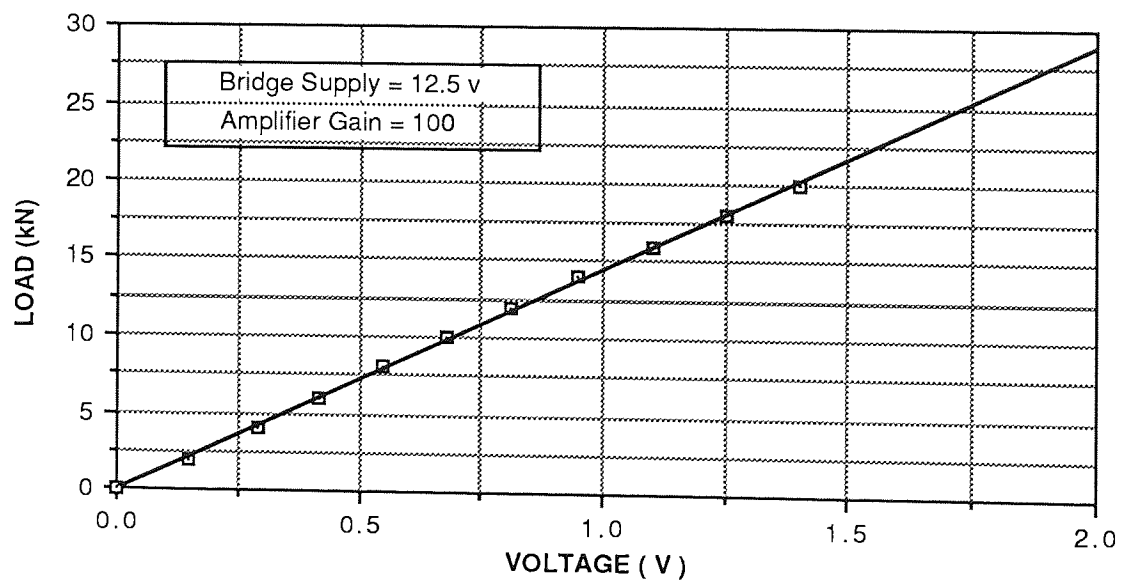Fig.A5.3. Calibration graph for loadcell (load range 0 -10 kN)

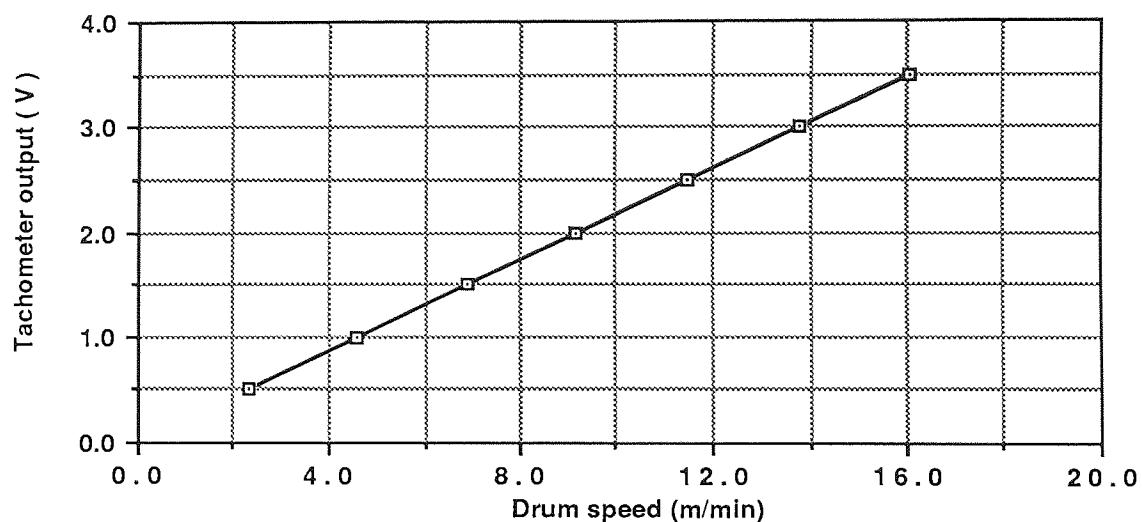Fig.A5.4. Calibration graph for loadcell (load range 0 - 20kN)

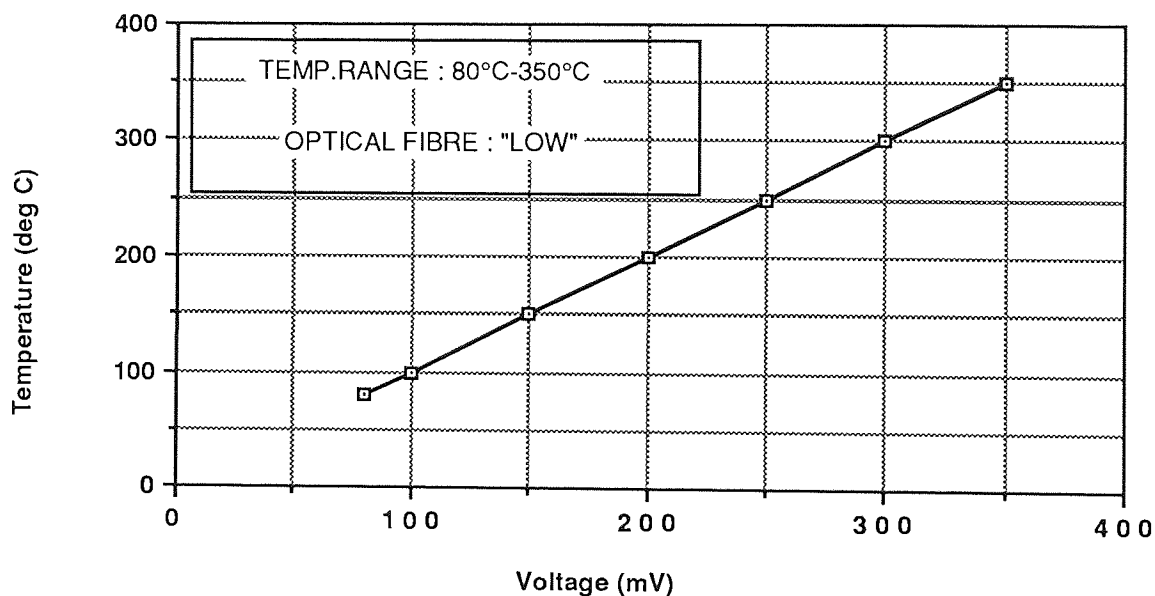Fig. A5.5. Calibration graph of draw speed against tachometer output

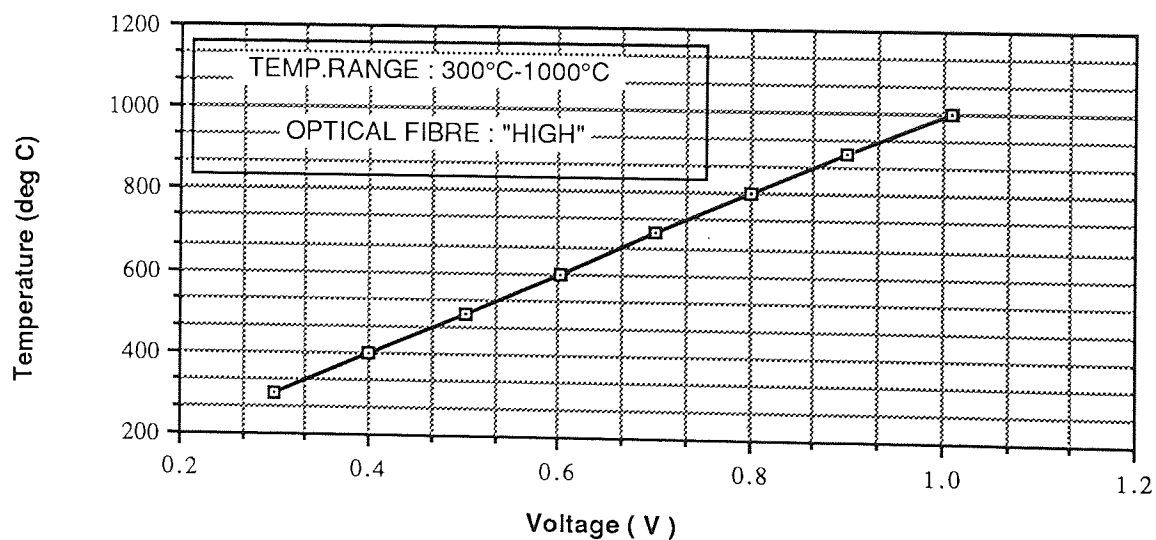Fig. A5.6. Calibration graph of the infra-red thermal monitor using the Low optical fibre

Fig. A5.7. Calibration graph of the infra-red thermal monitor using the High optical fibre